Reservoir Characterization of the Middle Miocene Jeribe Formation from Selected Oil Wells in Kurdistan Region/Northern Iraq

A Thesis

Submitted to the Council of

the College of Science, University of Sulaimani

in partial fulfillment of the Requirements for the Degree of

Master of Science in Geology

(Petroleum Geology)

By

Asos Sdik Abdolla

B.Sc. Geology (2008), University of Sulaimani

Supervised by

Dr. Dler Hussein Baban

Assistant Professor

March, 2017 Rashame, 2716

Supervisor Certification

I certify that the preparation of thesis titled "**Reservoir Characterization of the Middle Miocene Jeribe Formation from Selected Oil Wells in Kurdistan Region/Northern Iraq**" accomplished by (**Asos Sdik Abdolla**), was prepared under my supervision in the college of Science, at the University of Sulaimani, as partial fulfillment of the requirements for the degree of Master of Science in (Geology).

Signature:
Name: Dr. Dler Hussein Baban
Title: Assistant Professor
Date: 06/ 11/ 2016

In view of the available recommendation, I forward this thesis for debate by the examining committee.

Signature:
Name: Dr. Diary Ali Mohammad Ameen
Title: Head of Geology Department
Date: 06/ 11/ 2016

Linguistic Evaluation Certification

I herby certify that this thesis titled "**Reservoir Characterization of the Middle Miocene Jeribe Formation in Selected Oil Wells in Kurdistan Region/Northern Iraq**" prepared by (**Asos Sdik Abdolla**), has been read and checked and after indicating all the grammatical and spelling mistakes; the thesis was given again to the candidate to make the adequate corrections. After the second reading, I found that the candidate corrected the indicated mistakes. Therefore, I certify that this thesis is free from mistakes.

Signature:

Name: Bekhal Abubakir Hussein

Position: English Department College of Languages, University of Sulaimani

Date: 11/ 12/ 2016

Examining Committee Certification

We certify that we have read this thesis entitled **" Reservoir Characterization of the Middle Miocene Jeribe Formation from Selected Oil Wells in Kurdistan Region/Northern Iraq** " prepared by (**Asos Sdik Abdolla**), and as examining Committee, examined the student in its content and in what is connected with it, and in our opinion it meets the basic requirements toward the degree of Master of Science in geology "**Petroleum Geology**"

Signature:
Name: **Dr. Basim Al-Qayim**
Title: Professor
Date: 12/03/ 2017
(Chairman)

Signature:
Name: **Dr. Diar M. Ibrahim**
Title: Lecturer
Date: 12/03/ 2017
(Member)

Signature:
Name: **Dr. Hiwa M. Siddiq**
Title: Lecturer
Date: 12/03/ 2017
(Member)

Signature:
Name: **Dr.Dler H.Baban**
Title: Assistant Professor
Date: 12/03/ 2017
(Supervisor-Member)

Approved by the Dean of the College of Science

Signature:
Name: Dr. Bakhtiar Q. Aziz
Title: Professor
Date: / /2017

Dedication

To my family

Acknowledgements

First of all, I would like to thank the University of Sulaimani for giving me this opportunity to persue my Master Degree at the Department of Geology. Second of all, I would like to thank my supervisor, Dr. Dler Hussein Baban, for all his continuous supporting supervision and patience throughout the years that was working on my Master Degree. Special thanks go to Dr. Diary Ali Mohammed, the Chairman of Geology Department for his great help during my study. Many thanks to Dr. Fadhil Lawa, Geology Department for his assistance in facilitating and obtaining samples from Oil Search Company.

My unlimited thanks to both North Oil Company (NOC) in Kirkuk, and the Australian Oil Search Company for their kind agreement in releasing the used data and samples for this study, Finally, I would like to extend my thanks to Hussein Suad, University of Salahaddin, my fellow graduate student, for his help during my study.

Finally, I would like to thank my family for all the encouragement and generous support they have given over the years.

ABSTRACT

The Middle Miocene Jeribe Formation was studied to determine the reservoir characterizations in the two selected wells, Ja-49 and Taza-2, in the two Jambour and Taza, fields' oil. In this study, the used data include cutting rock samples, different types of conventional and modern logs, and core test data are re-evaluated to accomplish the goals for this study. The thickness of the formation attains 55m in Ja-49, and while it attains 44m in Taza-2, and the lithology of Jeribe Formation appeared to be composed mainly of dolostone, calcareous dolostone, and of dolomitic limestone with amalgamated thin layer of anhydrites. Jeribe Carbonate is mostly consisted of Wackstone and Mudstone Microfacies, with less contribution of Packstone and Grainstone Microfacies. Lithologically most parts of the formation constituency is comprised of, shale with less than 35%. Reservoir characterization revealed that Jeribe Formation has less than 15% primary porosity. However, few horizons have more than 20%, and about 2-3% of the units have secondary porosities such as fractures and vugs.

Permeability was Calculates for Jeribe Formation, using multilinear regression method and suggesting poor to moderate permeability (less than 20md).

Three reservoir units were distinguished depending on the shaleness, porosity, and permeability. The reservoir unit RU-C in the upper part of the formation, has the maximum thickness and of the best reservoir properties among the three units.

The total thickness of Jeribe Formation is impregnated with the to be containing hydrocarbons with different levels of hydrocarbon saturations, and capability to movement. The test of bulk volume water experiment revealed that production from the formation will be accompanied by decent volume of water in most of Jeribe Formations stratigraphic level. Four flow zone indicators, representing four unique hydraulic flow units have distinguished within Jeribe Formation.

Calculations were made for the N/G reservoir, pay, and production ratios, suggesting that the formation in Ja-49 well is more likely has 61%, 22%, rang between 09% respectively, while in Taza-2 well the formation has 62%, 23.5%, and 16.6% respectively.

Contents

Chapter One: Introduction

Chapter Two: Lithological Aspect and Shale Content

Chapter Three: Porosity, Permeability, and Reservoir Units

Chapter Four: Saturation and Reservoir Characterization

Chapter Five: Conclusions and Recommendations

List of Figures

List of Tables

CHAPTER ONE

Introduction

1.1 Preface

The Miocene Carbonate Jeribe Formation in Kurdistan has been recognized for its good quality reservoir properties in most of the discovered oil fields. The porous and permeable nature of the formation which may be enhanced by secondary fracturing or vugging make the formation act as a very attractive target in the exploration plans of most of the petroleum companies in the region. The recently discovered or developing oil fields in Kurdistan Region (ex. Sarqala Oil Field spuded over 9,000sП3/ day from the Jeribe Formation).This indicates the importance of Jeribe as a reservoir formation in all the places where the depositional environment of the formation extended to. Therefore, studying the characteristics of the Jeribe Formation in different areas will improve our understanding to the variations in its reservoir properties and the heterogeneities might occur vertically or laterally to the formation.

Reservoir characterization plays a crucial role in evaluating the economic success of reservoir management and development methods (Beiranvand and Kamali, 2004). The estimation of petrophysical parameters from well log data are an interesting part of the investigation and production processes in the oil and gas industries. It helps to recognize and evaluate hydrocarbon reservoirs from the subsurface (Khan et al., 2013).

1.2 Studied Fields

The studied area covers two separate fields which located in Garmian area of Kurdistan Region namely Jambour and newly discovered Taza Oil Field.

1.2.1 Jambour Field

Jambour Oil Field locates southeast of Kirkuk City. The field located on the same axis of Bai Hassan and Khabbaz structures (Fig.1.1). First exploration well in this field was drilled in 1927. The field which classified by Al-Mehaidi (2009) as giant field represents a long narrow asymmetrical anticline, about 30km long and 4km wide. With the being rock beds in the southwest limb is steeper than those of northeast limb (Amin, 1989). Tectonically the field is located in the Foot Hill Zone (Hamrin –Makhul Subzone), the Folded Zone of the Unstable Shelf (Buday and Jassim, 1987).

1.2.2 Taza Field

Taza structure lies on structural trend with the giant producing Jambur Field to the northwest and Sarqala Field to the southeast. The first well (Taza-1) was drilled back in 2013, operated by the PNG Oil Search Company from which the company announced a proven discovery of 38°API oil, with associated gas in Jeribe/Dhiban and Euphrates/Kirkuk Group formations.

Taza-2 is located 10 km north-west of the Taza-1 discovery well (Fig.1.2) and drilled in 2014 to appraise the hydrocarbon-bearing intervals discovered by Taza-1. Additionally, the well drilled also to

explore deeper Tertiary and Cretaceous targets, including the Cretaceous Shiranish Formation (Oil Search, 2014).

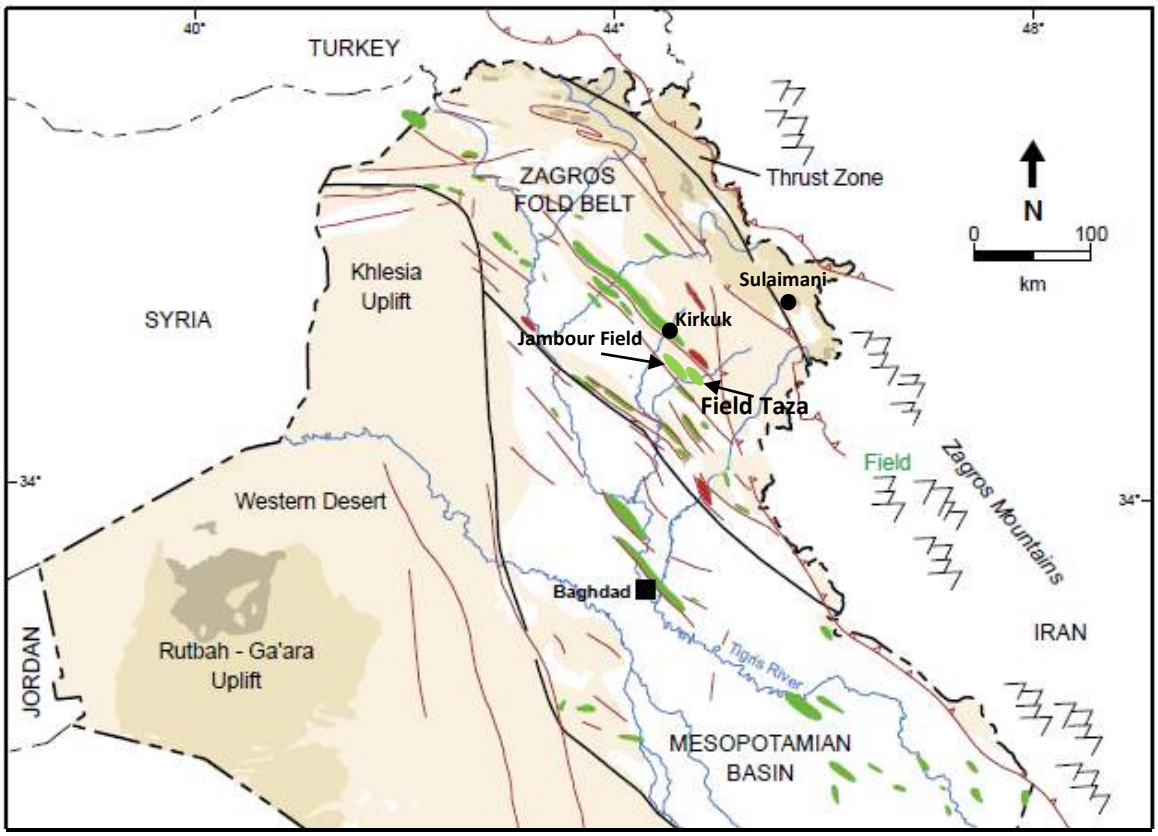

Figure 1.1: Location of the studied fields of Jambour and Taza (the map is after Pitman et al. 2004 with modifications from Aqrawi, 1998)

1.3 Jeribe Formation

The Middle Miocene Sequence was deposited in broad basin following a marine transgression during a phase of strong subsidence that overlapped the margins of the former Oligocene-Early Miocene basin, especially in NE of Iraq. The sequence consists of a shallow water carbonate (Jeribe Formation) overlies by thick evaporates,

carbonate and marls of the (Lower Fars) Formation in the intra-shelf area (Jassim and Buday, 2006).

The Jeribe Formation was first desrcibed by Bellen in 1957 (Bellen et al., 1959) of the type locality near Jaddala Village in the Sinjar anticline in Foothills Zone.

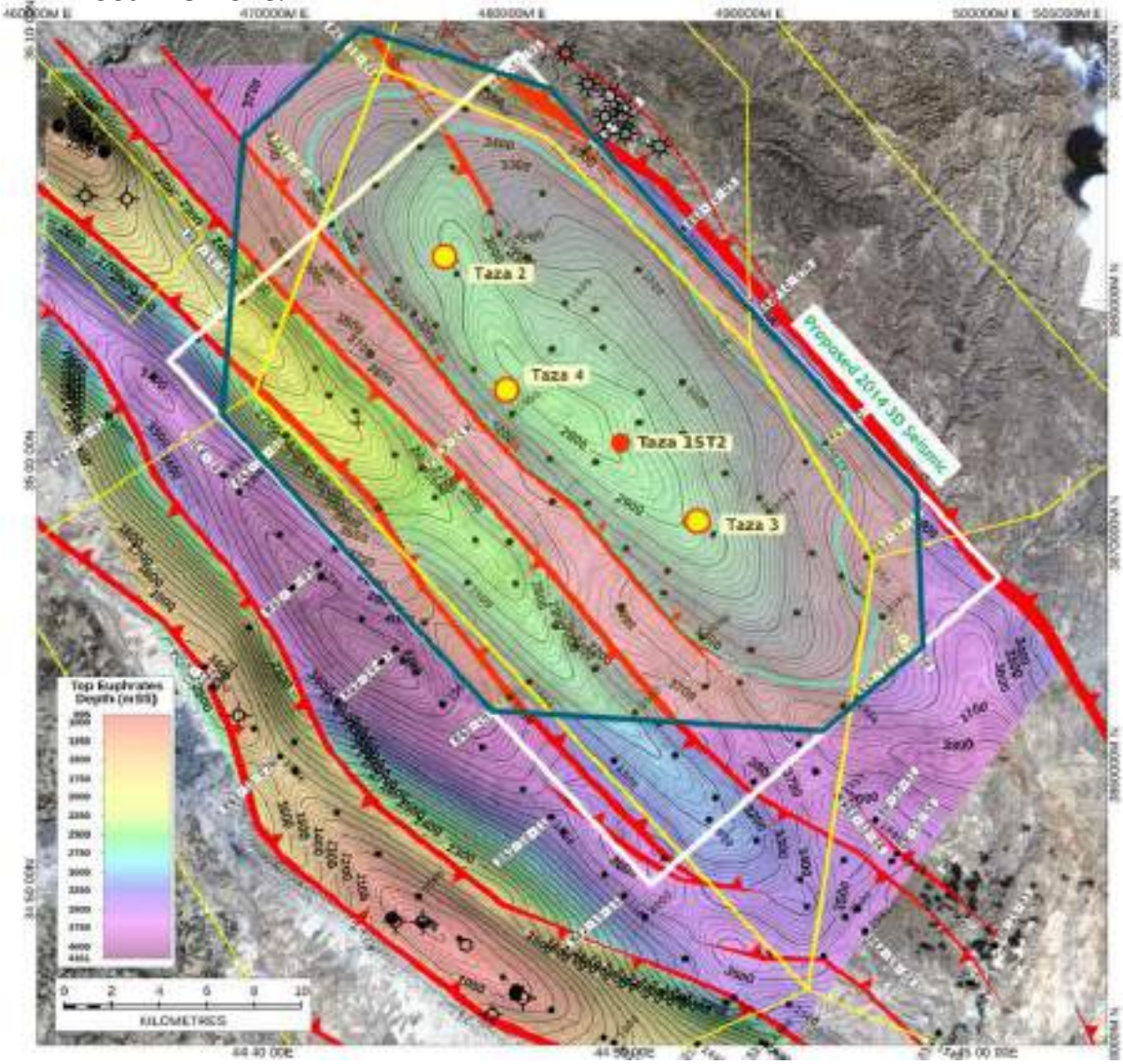

Figure 1.2: Structure contour map on top of Euphrates Formation and location of the studied Taza-2 well, Taza Oil Field (after Oil Search, 2014).

The formation was supposed to be part of Early Miocene age but later included in the Middle Miocene age due to existence of the *Orbulina* datum near the base of the Jeribe Formation (Parzak, 1974).

The thickness of the formation is about 70m (230 ft.) of recrystallized and dolomitized, mostly massive limestones; in beds 1-2 m thick (Bellen et al., 1959). The formation's lithology is relatively uniform consisting mainly of different facies of limestone. Some marly limestone and anhydrite sections were also mentioned by Johnson (1961; in Buday, 1980).

The Jerbie formation was deposited in lagoonal (back-reef and reef environment, with sign of more offshore facies, too. Reef and back reef are predominant according to Bellen et al. (1959). The formation probably represents a shallowing upward carbonate ramp sequence as it was deposited relatively throughout the basin (Aqrawi et al., 2010). The transgressive character is showed by the presence of conglomeratic bed at the bottom of the unit. They probably represent transgressive and high stand systems land deposition related to Ng10 and Ng20 maximum flooding event of Sharland et al., (2001).

The thick evaporites, carbonate and marls of the Lower Fars (Fatha) overlying the last Burdiglian unit (Jeribe Formation) (Jassim and Buday, 2006) (Fig. 1.3). Jeribe Formation is unconformable underlying with Serikangi Formation in the absence of Dhiban Formation as the case in the type locality (Buday 1980). The formation in NE Iraq, over steps the Euphrates Formation in Kirkuk Embayment but in the southern desert is absent (Fig. 1.4). Jeribe Formation in age is equivalent to Govanda

Formation in NE Iraq. It is also recognized in Jezira basin of Syria according to Ponikarov et al. (1967; in Buday 1980). The Kalhur limestones and part of the upper Asmari in Iran are equivalent to Jeribe Formation as mentioned by Jassim and Buday (2006).

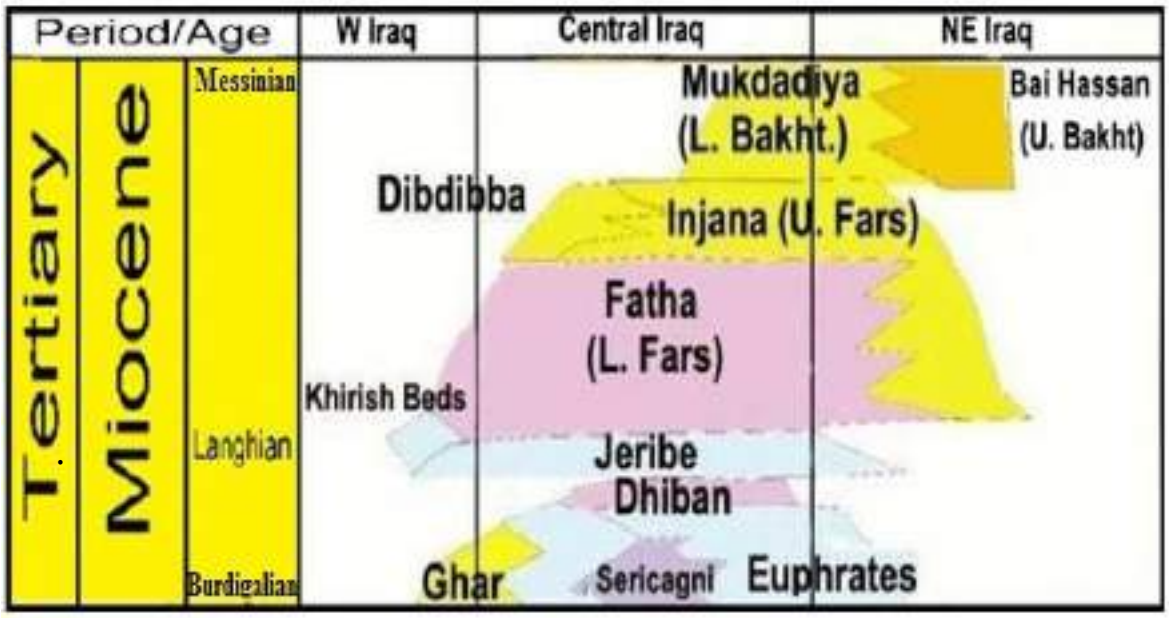

Figure 1.3: A simplified stratigraphic correlation of Miocene formations (after Jassim and Buday, 2006) slightly modified by Al –Dabbas et al., 2012)

1.4 Aims of the study

This study tends to achieve the following targets:

1. Determining the petrographic properties of Jeribe Formation in the studied wells.
2. Evaluating the formation from reservoir potentiality stand point.
3. Determining the fluid types within the reservoir rocks and their saturations.
4. Calculating net to gross reservoir and pay ratios of the formation in the studied wells.
5. Identification of reservoir units.

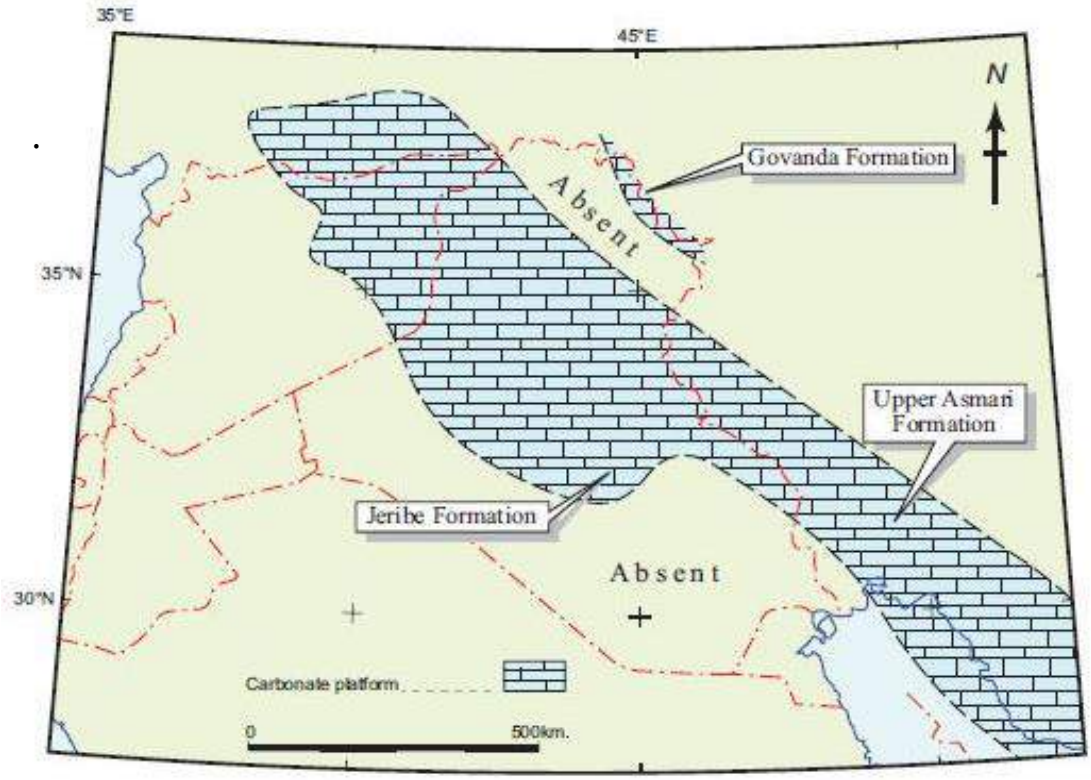

Figure 1.4: Palaeogeographic setting of the Jeribe Formation (after Aqrawi et al., 2010, modified from Goff et al., 1995)

1.5 Sampling and Methodology:

The collected data for this study are mainly obtained from the two drilled wells of Ja-49 (Jambour Field) and Taza-2 (Taza Field). The collected data can be classified into three main groups:

1- Cutting rock samples:

Twenty cutting rock samples from Jeribe Formation in the Ja-49 well have been selected from which thin sections were prepared for petrographic studies including microfacies, diagenesis, and porosity type determination. No rock samples obtained from well Taza-2 due to the regulations of Oil Search Company.

2- Wireline log data:

Most of the available log data for Jeribe Formation in both studied wells have been obtained, and shown in table 1.1.

Table 1.1: The studied wells, their coordinates and elevations, and the used logging tools

Field	Well	Coordinates UTM	Elevation from KB (m)	Type of logs
Jambour	Ja-49	443 755.72 E 3904 537.23 N	294.3	Caliper, Sp, Gamma ray, Sonic, Density, Neutron, Resistivity
Taza	Taza-2	477 456.81 E 3881 593.55 N	504.3	Caliper, Sp, Gamma ray, Sonic, Density, Neutron, Resistivity, Image, NMR

3- Core analysis data:

Core analysis data including porosity and permeability measurements were obtained for the cored interval were between depths 3255m and 3237m (18m thickness with 92.2% recovery) from Oil Search Company for well Taza-2.

The core data were essentially helpful in calibrating the analyzed log data, permeability measurements for non-cored intervals, and cutoff measurements.

Software suchas; Getdata digitizer, Logplot, Adobe Photoshop, Adobe Illustrator, in addition to the micosoft softwares of Excel and

Grapher all have been used in digitizing, plotting, and directing the content of this study.

1.6 Previous Studies

Bellen et al. (1959) have described the formation in the type locality and assigned Jeribe Formation is of Middle Miocene age; composed of recrystallized, detrital limestone.

Lawa (1989) has interpreted the paleodepositional environment of Jeribe Formation as semi-restricted warm lagoon and based observations from his study on the sedimentology and stratigraphy of the Oligocene-Miocene succession in Qayara area near Mosul City.

Al-Abassi (1994; in Ibrahim, 2008) studied Jeribe Formation in Northern Iraq and postulated that the formation can be subdivided into two units; the lower and middle part were deposited in a reef and back reef environments, while the upper part was deposited in a fore reef depositional environment.

Al-Ayobe (2004) has studied Jeribe Formation in three outcrop sections in Northwestern Iraq. He suggested that Jeribe Formation is composed of alternations of seven major facies and the algal boundstone facies is the most important one.

Markaryan (2005) studied Jeribe Formation in a number of fields in Dyala Governorate. Her study revealed that Jeribe Formation has good reservoir properties with an average porosity about 20%, and average permeability about 30md. She examined the porosity types found intraparticle, fracture; channels, vugs and moldic types are all exist in the formation.

Jassim and Al-Gailani (2006), stated that Neogene reservoirs (Euphrates and Jeribe formations) in the Mosul oil fields high contain heavy oil because water washing, biodegradation seal leakage and flushing the reservoir by fresh water. They mentioned also that the oil of Jeribe reservoir in some fields like Najmah, Jawan, Qasab, and Qaiyarah has sulfur content of 0.4 - 7.1%.

Al-Jboury et al. (2007) have studied the stratigraphic and depositional environment of the late-Early Middle Miocene. They have mentioned Jeribe Formation deposited in the Langhian depositional basin. They also have indicated sediments rich in planktonic foraminifera in the lower part of the Jeribe Formation, and shallow water and lagoonal carbonates at the upper part of the formation.

Abdul-Rahman (2007) has studied the successions of the stage Aquitanian–Lower Early Langhian in the well Kor Mor/3. She subdivided the succession into two major sequences of 2nd order which are; major sequence (A) including four 3rd order sequences presenting Ibrahim, Azkand, Anah, Euphrates, and Dhiban formations; major sequence (B) comprising one sequence of 3rd order (B1) relating to Jeribe Formation.

Ibrahim (2008) studied Jeribe Formation from sedimentology and reservoir characterization points of view in two wells of Tawke Oil Field, Kurdistan-Iraq. He concluded that Jeribe Formation belongs to the Miocene Langhian subcycle and composed mainly of limestone and dolomite with thin interbeds of anhydrite. He identified a number of benthonic foraminifera in the formation including *Borelis melo kurdica* the index fossil of Jeribe Formation. He also identified a number of

microfacies within the formation and described the types of porosity existed in the formation including fractures, vugs, interparticles, and intercrystallines.

Aqrawi et al. (2010) have stated that Jeribe Formation probably represents an upward shallowing carbonate ramp sequence. Cycle stacking (ex. in East Baghdad Field) suggests that another sequences present locally at the formation's top.

Al-Ameri et al. (2011) have studied the hydrocarbon in the Middle Miocene Jeribe Formation in a number of oil fields in Dyala District. They have revealed that the oil accumulated in the Jeribe reservoir is originated from the Upper Jurassic-Lower Cretaceous Chia Gara Formation. They also have explored that Jeribe Formation owns an average porosity about 12-27% in the studied oil fields.

The facies, depositional environment and diageneses of Early Middle Miocene Jeribe Limestone Formation have been studied by Al-Dabbas et al. (2012) in selected wells in northern Iraqi oil fields (Ajil, Hamrin, Judaida, and Khashab). They have identified a number of microfacies with variety of diagenetic processes such as compaction, dissolution, cementation, neomorphism, dolomitization, anhydritization, and silicification. They have also determined that the formation deposited in restricted shallow to deep open marine environments.

AL-Hietee (2012) has determined the depositional environment of Jeribe Formation as restricted marine and shallow open marine; in addition to shoal and deep marine environments, this has been made base on studying the formation in Ja-26, Hr-41, and Kz-6 wells.

In Ajeel Oil Field, Gharib (2012) has studied Jeribe and Euphrates formations from a number of wells. He has divided Jeribe Formation using log and microfacies data into two reservoir units separated in the middle part by a marl bed.

The sedimentological and reservoir characteristics of Jeribe Formation have studied by Fadhil (2013) in Allas dome of Hamrin Oil Field / northeastern Iraq. She has recognized four main microfacies within the formation representing extend of depositional environment from semi closed platform to open platform and front slope. Then she has divided Jeribe Formation into two reservoir units (A and B) depending mainly on log data, which have separated by a layer of shale. Later she has noted that Jeribe has porosities ranging between 0 and 33%.

According to Kharajiany (2014), Jeribe Formation in Ashdagh Mountain near Sangaw Town consists of 2m thick grey limestone which is slightly marly and contains *Borelis melo kurdica*.

The Oligocene and Miocene rock have studied by Kharajiany et al. (2014) in Mamlaha anticline near Chamchamal Town. They noticed that the claystone of Fatha Formation overlies Jeribe Formation.

The Tertiary reservoir including Jeribe Formation has studied by Hussein (2015) from a number of wells in Khabbaz Oil Field. The high dispersed shale content was his most noticeable conclusion which has great effect on permeability of the formation.

According to Sissakian et al. (2016), the Langhian Jeribe Formation deposited in shallow marine near shore environment and that depending on the existence of the coquina bed within the formation.

CHAPTER TWO

Lithological Aspect and Shale Content

2.1 Preface

Conventional ways for determining lithology of subsurface beds include examination of the cutting rock samples collected from the shale shaker or more accurately through analysis of the recovered core samples Modern laboratories analyze core samples through different techniques to obtain detailed information about sedimentology, mineralogy, texture, and other lithological issues.

Log data, on the other hand comprises important source of information which can aid in providing continuous image about the lithology of the penetrated beds. Some kinds of log data can be used directly to distinguish the type of lithology and some others through using special cross plots or graphs.

Lithology determination is vital in few log analysis methods especially those which are dealing with porosity determination. Equations of porosity calculation from sonic log and density log data need factors of certain values which depend directly on the matrix or lithology of the examined beds. The same is true with the water saturation equations which beside the resistivity log data also special factors and exponents are needed in the process of water saturation calculation such as cementation factor and tortuosity which their values are depending directly on the lithology of the evaluated bed.

2.2 Microfacies Analysis

The thin sections prepared from the selected cutting rock samples of Jeribe Formation from Ja-49 well were studied optically using transmitted light microscopy.

The classification was proposed by Dunham (1962) for carbonate rocks (Fig.2.1) used terminologies, are mainly, and depended on identification microfacies within the studied thin sections. According to Dunham's classification carbonate lithofacies fell into several distinct lithologic associations ranging from various types of lime mudstone (with less than 10% grains) to wackestone (with more than 10% grains), to the grain supported packstone containing carbonate mud, and grainstone which is grain supported lacking mud. On the other hand Boundstone is defined by Dunham as components, bounded together during deposition (as the case of reefal environments), whereas crystalline lithofacies represented sediments like dolomite with non-recognizable textures.

Porosity types were studied and recognized based upon, the classification of porosity followed by Choquette and Pray (1970) was mainly followed. (Fig.2.2)

The main lithology, microfacies type, porosity type and diagenesis for the studied thin sections of Jeribe Formation in Ja-49 well are listed in the table 2.1. Figures for selected microfacies or selected features as porosity type or diagenesis are shown in the plates 1-3.

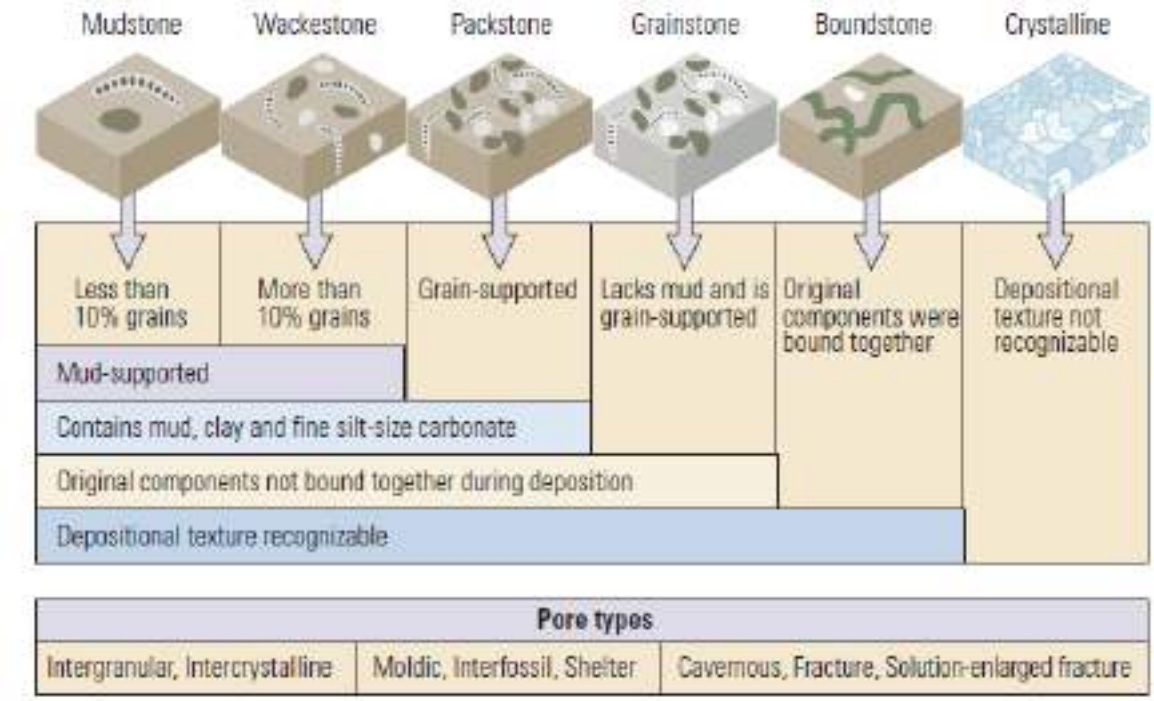

Figure 2.1: Classification of carbonate rock and the pores in each rock type (adapted by Akbar et al., 2001 from Dunham, 1962).

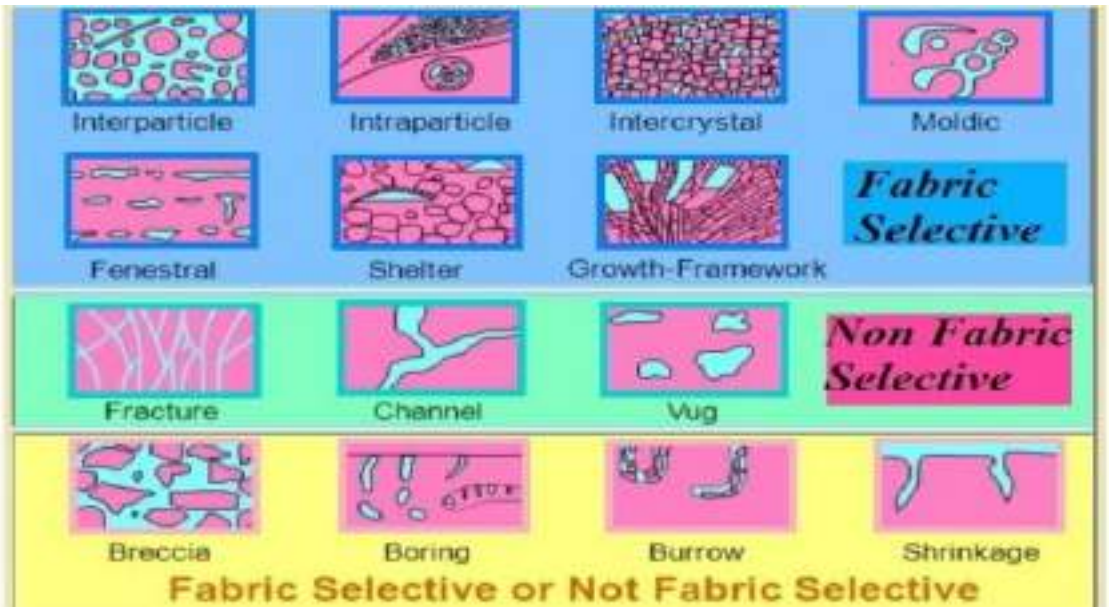

Figure 2.2: Classification of carbonate porosity (after Choqutte and Pray, 1970) Taken from (www.beg.utexas.edu)

Table 2.1: Main lithology, microfacies, pore types, and diagenesis features identified in the studied Jeribe Formation in the well Ja-49.

Sample Depth (m)	Common lithology	Microfacies type	Pore types	Diagenesis
2157	Dolomitic limestone	Algal bearing Wackestone	Interparticle, intraparticle, moldic	Cementation, dissolution
2158	Calcareous dolostone	Wackestone	Microfractures	Cementation
2160	Calcareous dolostone	Wackestone	Microfractures, Interparticle	Dolomitization, cementation
2161	Calcareous dolostone	Wackestone	Microfractures, vugs, intercrystalline	Dolomitization, dissolution
2163	Calcareous dolostone	Packstone / Wackestone	Vugs, intercrystalline, interparticles	Cementation, dissolution
2168	Calcareous dolostone	Packstone / Wackestone	Intraparticle, vugs interparticle, moldic	Cementation, dissolution
2175	Calcareous dolostone	Algal bearing Packstone/ Grainstone	Intraparticle, interparticle, moldic, vugs	Recrystallization, cementation, dissolution
2178	Calcareous dolostone	Wackestone	Microfractures	Cementation
2186	Calcareous dolostone	Wackestone	Microfractures, intercrystalline	Dolomitization
2189	Calcareous dolostone	Quartz Crystals bearing Wackestone	interparticles	Cementation
2194	Dolomitic limestone	Packstone / Wackestone	Intraparticle, interparticle, moldic	Cementation, dissolution
2196	Dolomitic limestone	Wackestone / Packstone	Intraparticle, interparticle,	Cementation
2198	Dolomitic limestone	Wackestone / Packstone	Intraparticle, interparticle, moldic,	Dissolution
2202	Dolomitic limestone	Wackestone / Packstone	Intraparticle, interparticle, microfractures	Cementation
2205	Dolomitic limestone	Wackestone / Packstone	Intraparticle, interparticle, moldic	Cementation, dissolution
2209	Calcareous dolostone	Wackestone	Vugs, channels, intercrystalline	Dissolution
2210	Calcareous dolostone	Wackestone	Vugs, channels, intercrystalline	Dissolution

PLATE – 1

The bar = 100micron

Figure 1: Algal bearing Wackestone Microfacies, A: intraparticle porosity, Depth 2157m

Figure 2: Wackestone Microfacies, A: mostly non-open fractures, Depth 2158m

Figure 3: Wackestone Microfacies, A: dolomite crystals, Depth 2160m

Figure 4: Wackestone Microfacies , A: two sets of fractures filled with Bitumen, Depth 2160

Figure 5: Wackestone Microfacies, A: bitumen filled fractures, B: vug, Depth 2161m

Figure 6: Packstone/Wackestone Microfacies, A: separated vugs, Depth 2163m

PLATE - 1

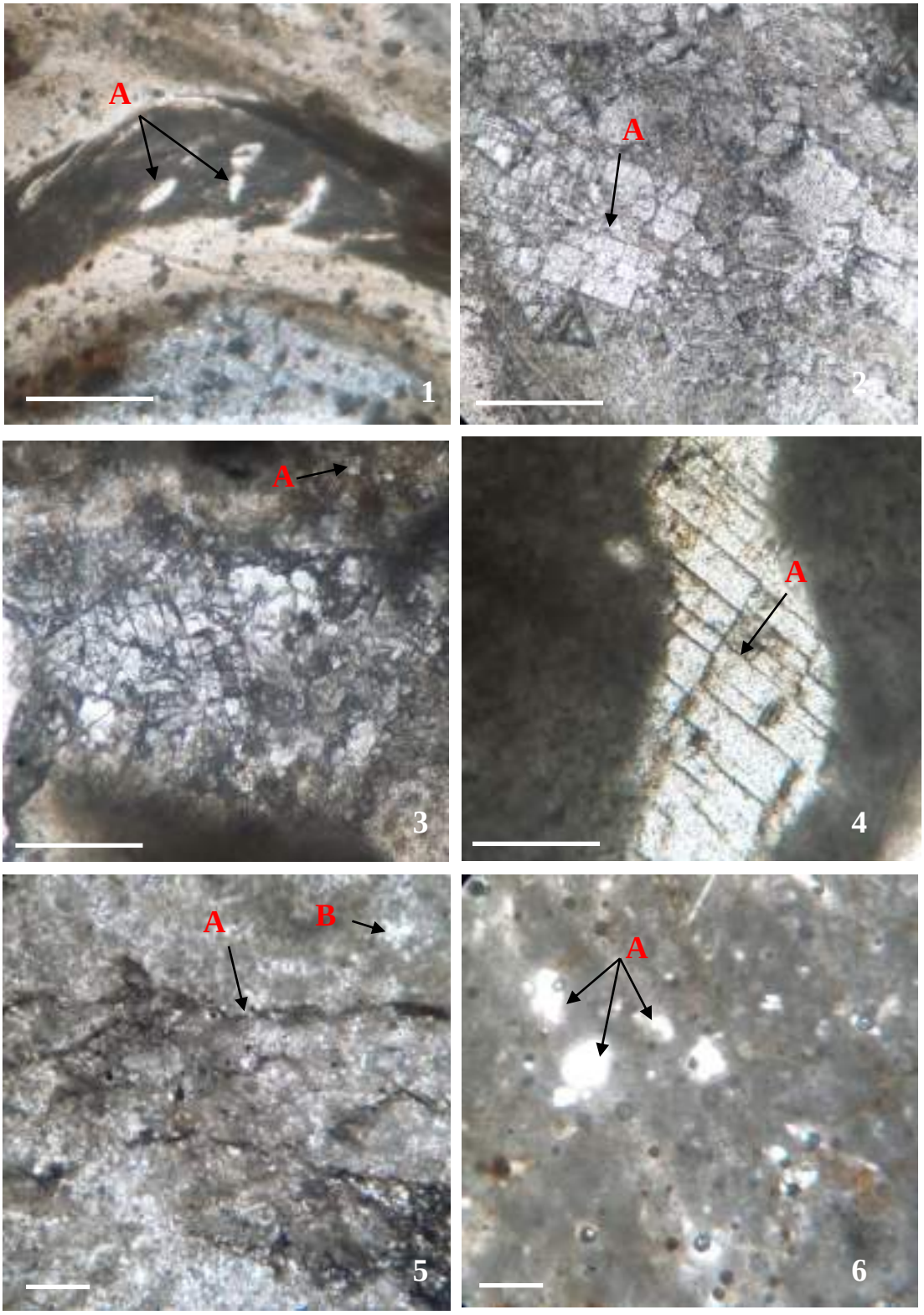

PLATE - 2

The bar = 100micron

Figure 1: Packstone/Wackestone Microfacies , A: intraparticle porosity, Depth 2168m

Figure 2: Algal bearing Packstone/Grainstone Microfacies, Depth 2175m

Figure 3: Algal bearing Packstone /Grainstone Microfacies , A: interparticle porosity, B: intraparticle porosity, C: moldic Porosity Depth 2175m

Figure 4: Algal bearing Packstone/Grainstone Microfacies, A: interparticle porosity, Depth 2175m

Figure 5: Algal bearing Packstone/ Grainstone Microfacies, A: recrystallized formenifera test, Depth 2175m

Figure 6: Algal bearing Packstone/ Grainstone Microfacies, Depth 2175m

PLATE - 2

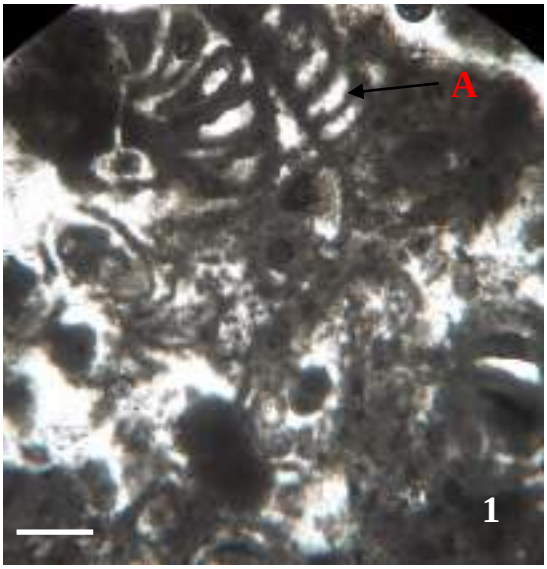

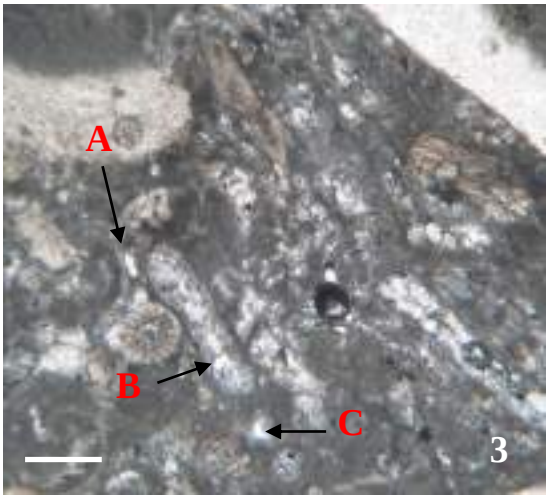

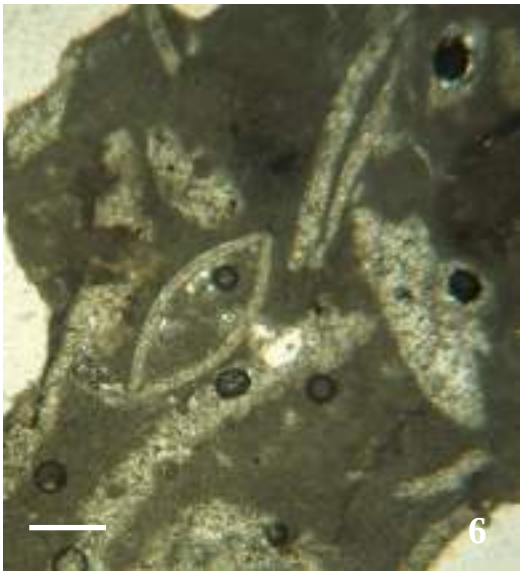

PLATE - 3

The bar = 100micron

Figure 1: Wackestone Microfacies, A: cement filled fracture (closed), B: bitumen filled fracture, Depth 2178m

Figure 2: Wackestone Microfacies, A: bitumen filled fracture, Depth 2186m

Figure 3: Quartz Crystals bearing Wackestone Microfacies, Depth 2189m

Figure 4: Wackestone /Packstone Microfacies , Depth 2202m

Figure 5: Wackestone Microfacies, A & B: vugs, Depth 2209m

Figure 6: Wackestone Microfacies, A: channel filled with bitumen, Depth 2210m

PLATE - 3

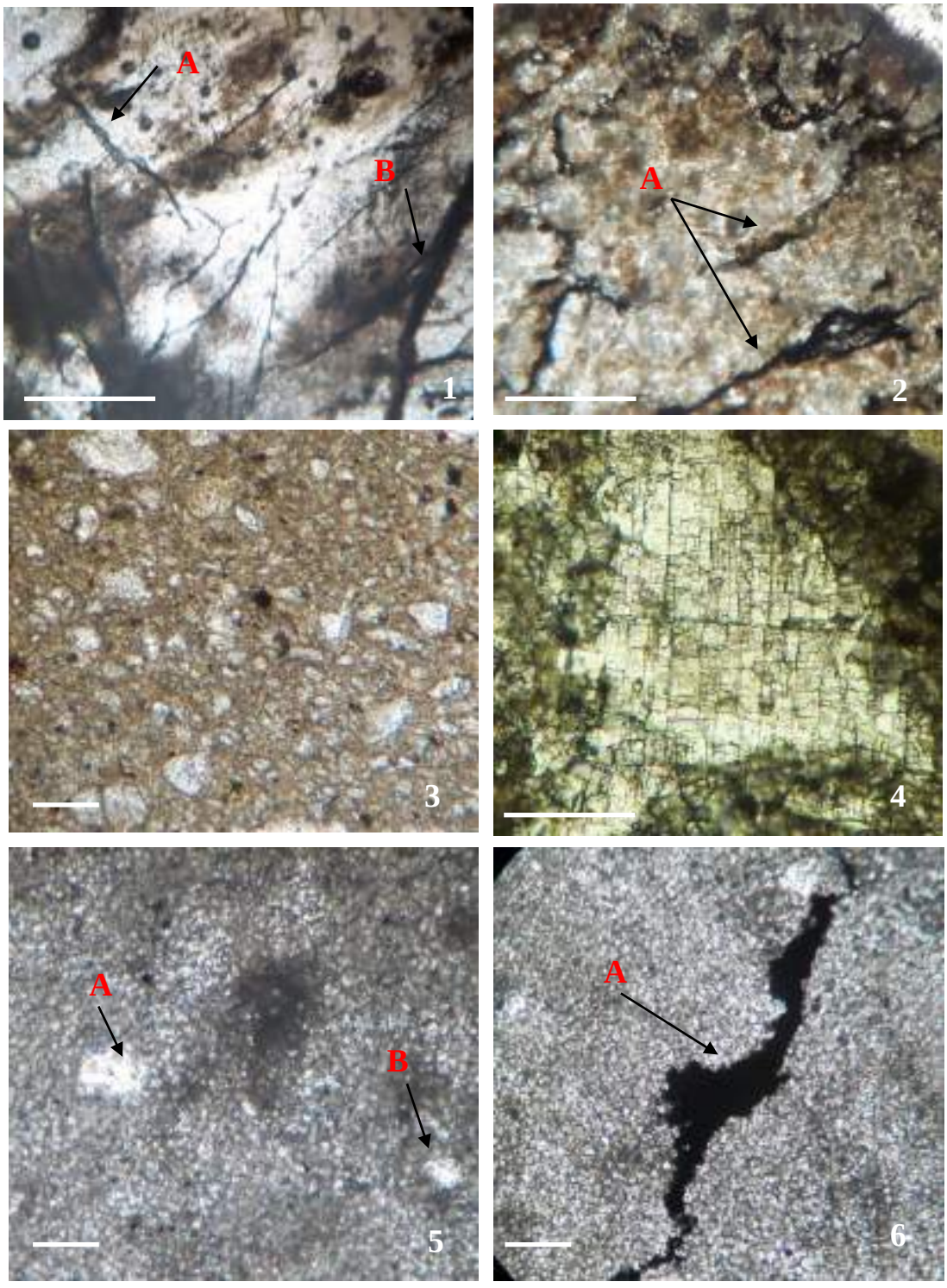

No rock samples obtained from Taza-2 well, but the description of the cored interval from Jeribe Formation between the depths 3255 and 3237m and details of the lithology and microfacies of the mentioned core interval exist in the table 2.2 which was done by Oil Search Company. Figure 2.3 shows the slabed core samples in which anhydrite and anhydritic zones can be recognized easily. The ratios of Ca/Mg (calcimetry) also measured for selected samples of the cored interval from which limestone; dolomitic limestone, calcareous dolostone, and dolostone lithologies can be detected in addition to the general carbonate content.

Table 2.2: Lithology, microfacies, pore types and diagenesis, with the measured calcimetry for the Jeribe Formation in the well Taza-2 (Oil Search Data)

Depth interval (m)	Common lithology	Microfacies Type	Pore types & Diagenesis	Calci-metry (Ca/Mg)
3237	Limestone	Bivalve bearing Wackestone	No visible matrix porosity or fractures, recrytallization, stylolites	59/11
3238	Dolomitic limestone	Bivalve bearing Wackestone	No visible matrix porosity or fractures	41/38
3239	Dolomitic limestone	Wackestone	Recrystallization, microvugs, moldic porosity, no fractures	30/27
3240	Dolomitic limestone	Mudstone/Wackestone	Recrystallization, microvugs	20/29
3241	Calcareous dolostone	Wackestone/Packstone	Vuggy (moldic) porosity, stylolites,	25/30
3242	Calcareous dolostone with nodules of Anhydrites	Mudstone/Wackestone	Dolomitization, poor visible matrix and fracture porosity	30/33
3243	Calcareous dolostone with nodules of Anhydrites	Mudstone/Wackestone	Cementation, poor visible matrix and fracture porosity	35/32

3244	Calcareous dolomite with nodules of Anhydrites	Mudstone/Wackestone	Cementation, poor visible matrix and fracture porosity	25/16
3245	Dolostone/ Anhydrite	Mudstone	Dolomitization, Cementation, poor visible matrix and fracture porosity	16/41
3246	Dolostone	Mudstone/Wackestone	Dolomitization, Cementation, poor visible matrix and fracture porosity	12/27
3247	Dolomitic limestone	Mudstone	Cementation, poor visible matrix and fracture porosity	35/30
3248	Calcareous dolomite, slightly anhydritic	Mudstone	Poor visible matrix and fracture porosity	15/25
3249	Calcareous dolomite, slightly anhydritic	Wackestone	Poor visible matrix and fracture porosity	18/14
3250	Dolomitic limestone	Mudstone/Wackestone	Poor visible matrix or fracture porosity	24/30
3251	Limestone	Wackestone/Packstone	Dolomitization, No visible matrix or fracture porosity	62/20
3252.7	Calcareous dolostone	Mudstone	No visible matrix or fracture porosity	15/16
3253.6	Calcareous dolostone	Mudstone	No visible matrix or fracture	7/13

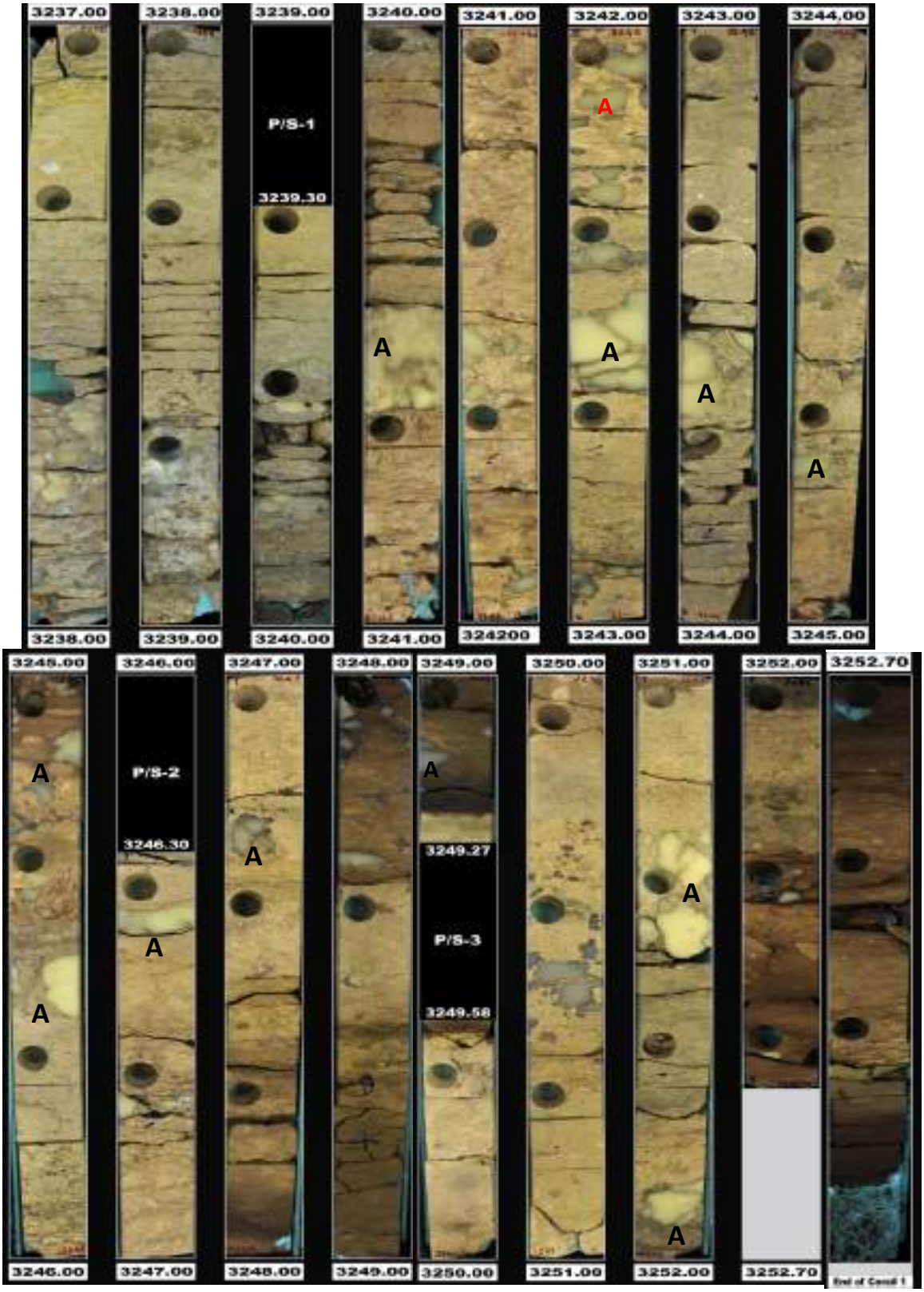

Figure 2.3: The slabbed core samples of Jeribe Formation from the well Taza-2,

A: Anhydrite or anhydritic zones.

2.3 Lithology Determination from Porosity Logs

Generally, lithology determinations were done based on porosity logs. using “crossplots which are a convenient way to explain how various combining of logs respond to lithology and porosity” as “Neutron-Density crossplot and M-N crossplot” the most interesting information can get about the lithology of the studied formation.

2.3.1 Neutron-Density Crossplot

The combined Neutron and the Density logs are the best indicator for lithology identification that they would be useless separately (Rider, 2002).

When a formation consists of only two known minerals in unknown proportions, the combination of density and neutron logs will define the proportions of the two minerals and a better value of porosity（Schlumberger, 1989).

The readings of the density and neutron logs for the studied Jeribe Formation in the two wells of Ja-49, and Taza-2 are listed in the appendix A and plotted on the Neutron-Density crossplot proposed by Schlumberger (1988) for the case of fresh mud drilling fluid for the well Ja-49 (Fig.2.4) and the case of salt mud drilling fluid for the well Taza-2 (Fig.2.5).

The lithology of Jeribe Formation appears to be mostly dolomite and partly dolomitic limestone or limestone. The existence of anhydrite zones in the two wells were observed where sample points of high bulk density and very low neutron porosity values noticed. The sample points related to Lower Fars and Dhiban formations failed in their expected positions within or close to the anhydrite field of the crossplots.

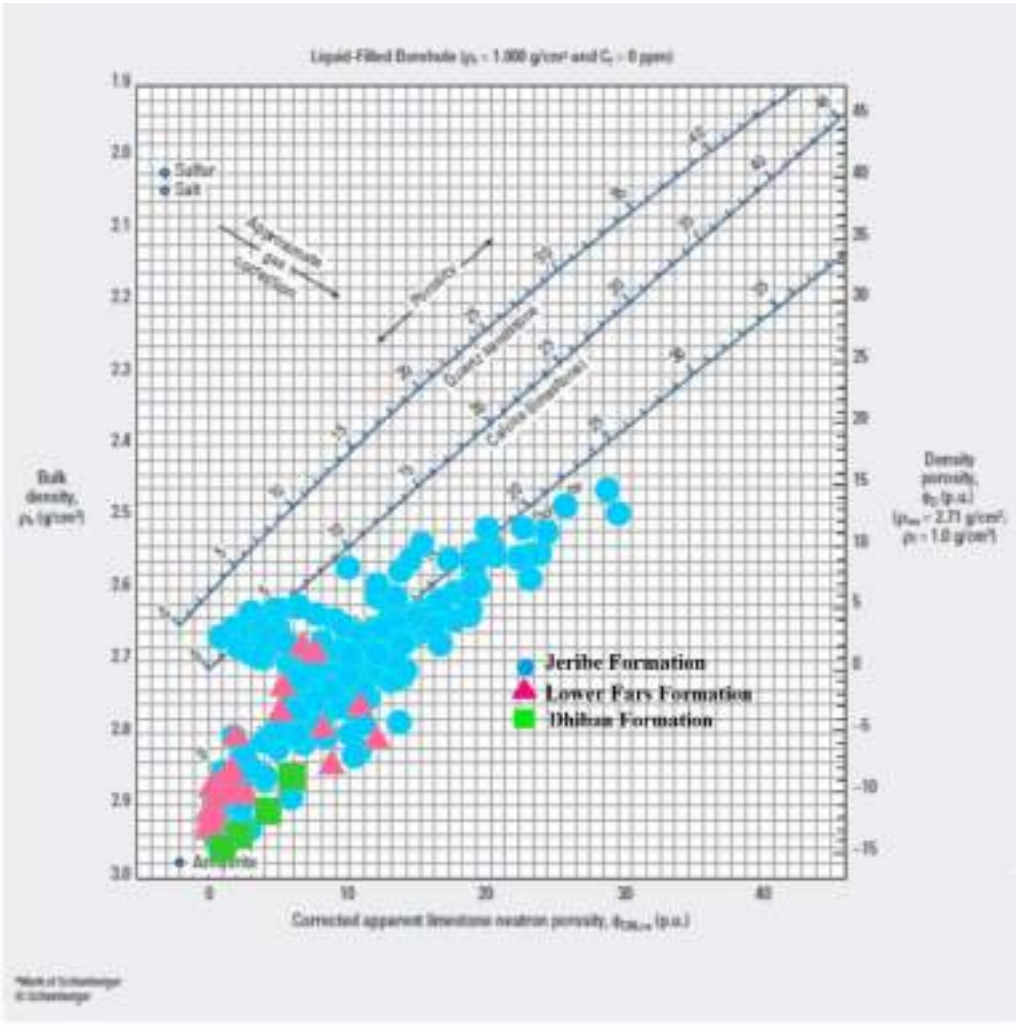

Figure 2.4: Neutron-Density cross plot for Jeribe Formation and the upper most part of Dhiban Formation and the lower most part of Lower Fars Formation in the well Ja-49 (The crossplot after Schlumberger, 1988).

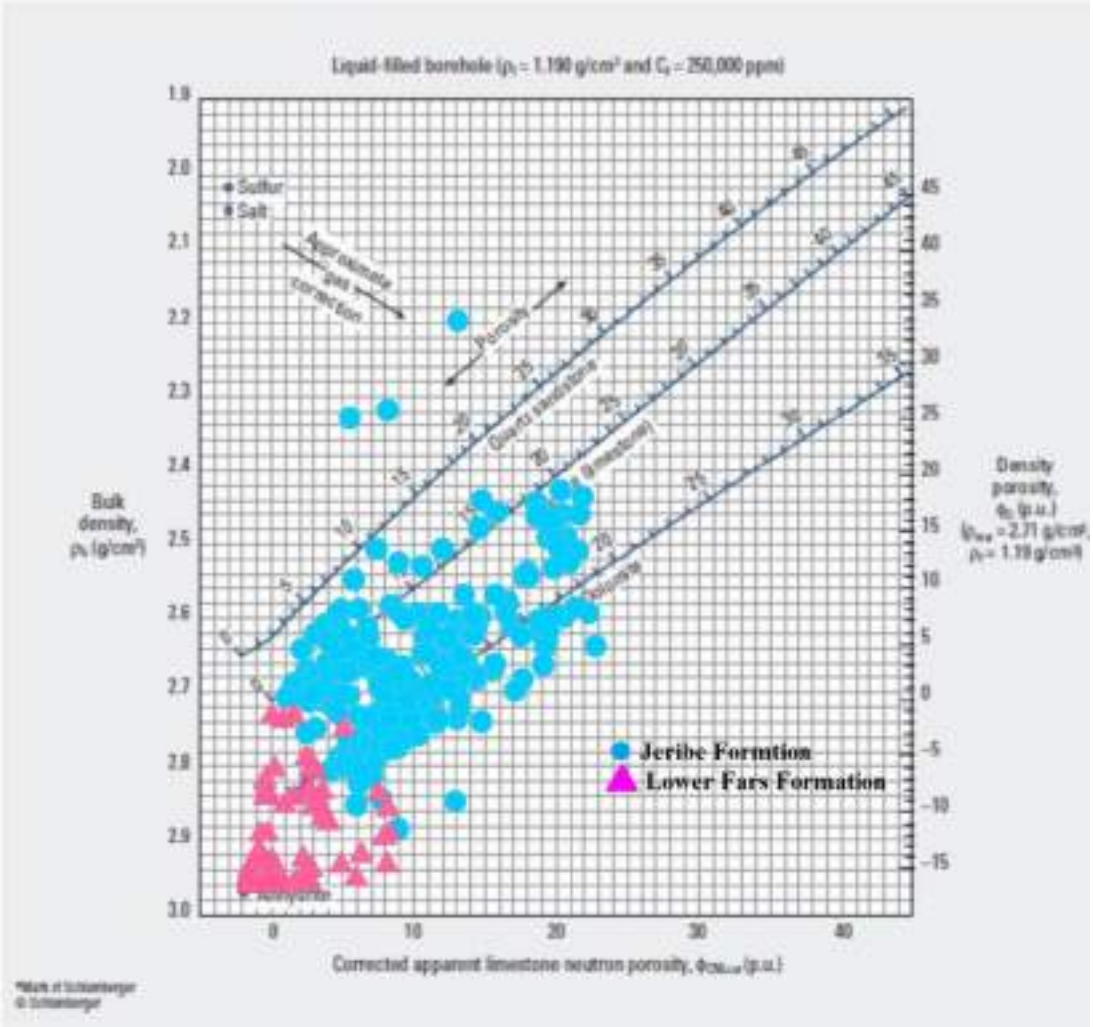

Figure 2.5: Neutron-Density cross plot for Jeribe Formation and the lower most part of Lower Fars Formation in the well Taza-2 (The crossplot after Schlumberger, 1988).

2.3.2 M-N Crossplot

M-N crossplot is helpful in detecting lithology of those logged intervals which are composed of complex mineral mixtures. The advantage of this method on the previously applied method of Neutron -Density crossplot is that sonic log (Δt) data also contribute in this method through calculating the two factors of M and N as shown in the equations Eq.2.1 and Eq.2.2.

$$N = \frac{\Delta_{tf} - \Delta_t}{\rho_b - \rho_{fl}} * 0.01 \quad \text{.....Eq.2.1}$$

$$M = \frac{\emptyset_{Nf} - \emptyset_N}{\rho_b - \rho_{fl}} \quad \text{.....Eq.2.2}$$

Where:

Δt_{fl}: interval transit time in the fluid in the formation

Δt: interval transit time in the formation (from log)

ρ_b: formation bulk density (from log)

ρ_{fl}: fluid density (generally, 1.0 for fresh mud and 1.1 for saline mud)

$\emptyset_{Nf}$: neutron porosity of the fluid in the formation (usually 1.0)

$\emptyset_N$: neutron derived porosity (from log)

The multiplier 0.01 is used to make the M values compatible for easy scaling.

Other advantage of this cross plot is to detect gas filled porosities. When the sample points on the crossplot shift toward the zone of gas as a result of increasing the value of the M factor due to the underestimation of the ΘN values in gas zones. Shale zones are also can be detected when the sample points shift toward the lower part of the crossplot as a result of

decreasing the values of the M factor due to the overestimated ΘN values in shale zones.

The values of M and N for the two studied wells showed in figures 2.6 and 2.7. The lithology for Jeribe Formation is,identified almost the same as appeared in the previously used Neutron - Density crossplot. The dolomite and calcareous dolomite looks to be the dominant litology of the formation. Points spreading in the region of anhydrite are also noticed which were mostly belonging to the formations of Dhiban and L. Fars formation.

An important observation is that the lithology of Jeribe Formation in Taza-2 well is more calcareous in comparison with less calcareous dolostone nature of the formation in Ja-49 well.

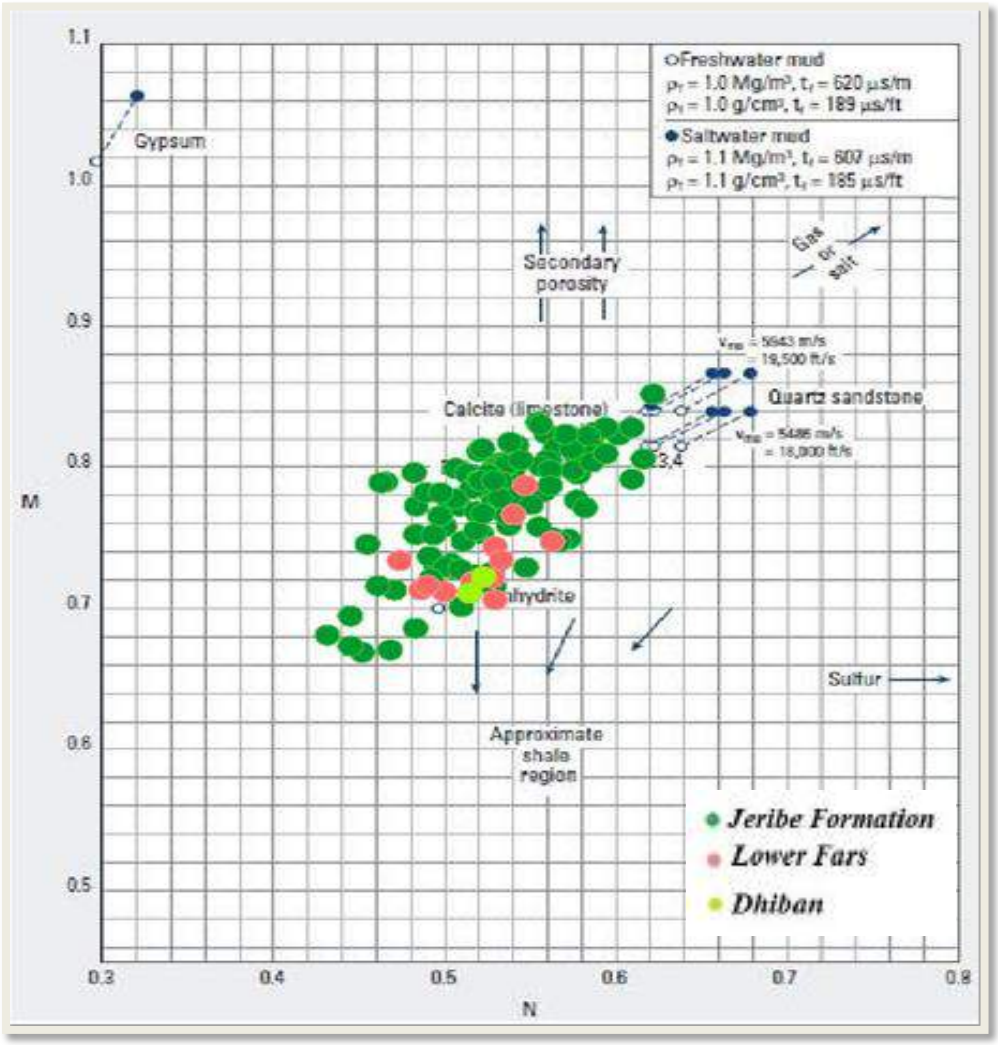

Figure 2.6: M-N Crossplot for lithology identification of Jeribe Formation in Ja-49 well (the crossplot is after Schlumberger, 1998).

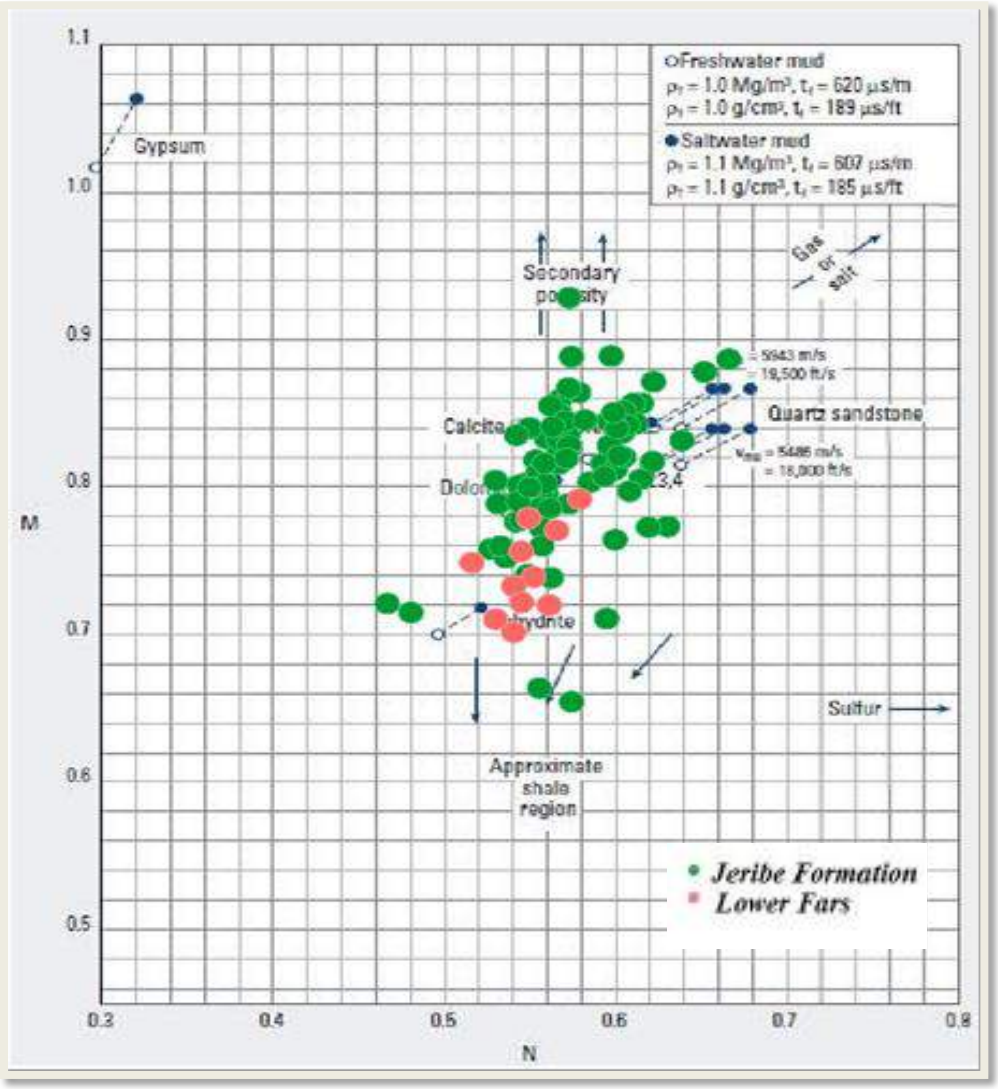

Figure 2.7: M-N Crossplot for lithology identification of Jeribe Formation in Taza-2 well (the crossplot is after Schlumberger, 1998).

2.4 Gamma ray Log

The detector of the gamma ray logging tool responds to the natural radioactivity of the zones which passes through in any drilled wells. The recorded radiation values in API units are mostly emitting from the naturally occurring uranium, thorium and potassium elements which mostly concentrate in the clay minerals and shales. Accordingly, this tool is considered to be the best tool for identifying shale zones and also for numerically calculating shale content values.

As most of the logging tools, the measurements of gamma ray logging tool are affected by several factors such as the logging speed (the bed boundaries will mix when the speed of logging tool is too high or slow). Caving occurring in the wells causes increasing of the drilling mud around the logging tool and lead to dropping the recorded values. Bad borehole conditions also cause lower value measurements of gamma ray (Rider and Kennedy, 2011).

The recorded gamma ray log values of Jeribe Formation in the two studied wells are listed in the appendix A and plotted as curves in the figure 2.8.

The curve of the gamma ray for Jeribe Formation showed in the figure 2.8.There is no obvious variations in their deflections except the values in well Taza-2 are slightly higher than the well Ja-49.

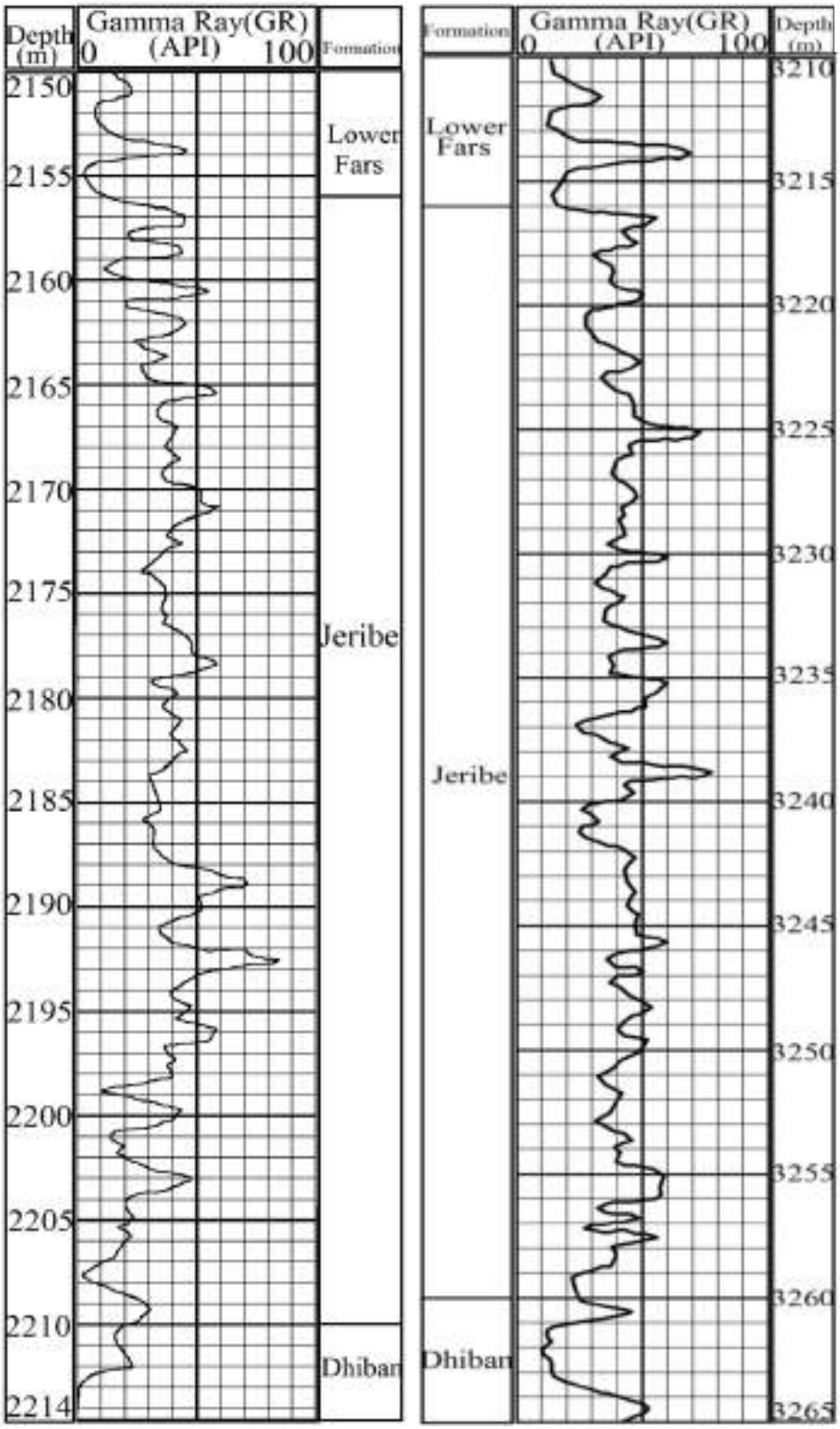

Figure 2.8: Gamma Ray log for Jeribe Formation in Ja-49 and Taza-2 wells. Uppermost part of Dhiban Formation with lowermost part of L. Fars Formation also included.

2.4.1 Shale Volume Calculation

Shale volume calculation is considered as one of the most important applications of gamma ray log.

The recorded gamma ray values in any reservoir are ranging between a minimum value representing a clean horizon and a maximum value representing a shale horizon. Accordingly, the recorded gamma ray values between the minimum and the maximum are representing Shaley horizons containing shale volumes which positively proportion with recorded gamma ray value.

The procedure of calculating shale volume through gamma ray data starts with calculating the gamma ray index (I_{GR}) using the conventional equation Eq.2.3(Asquith and Gibson) 1982.

$$\text{IGR} = \frac{(GRlog - GRmin)}{(GRmax - GRmin)} \quad \text{.....Eq. 2.3}$$

Where:

I_{GR} = Gamma ray index

GR_{log} = Gamma ray reading from log

GR_{min} = Minimum gamma ray reading from log (clean zone)

GR_{max} = Maximum gamma ray reading from log (shale zone)

The maximum gamma ray value has taken from depth 2193m (93 API) and 3239m (77 API) and the minimum value from depth 2154m (3 API) and 3262m (10 API) for Ja-49 and Taza-2 wells, respectively.

The second step in calculating the shale volume is by applying the equation proposed by Larionov (1969) for calculating shale volume in the unconsolidated rocks of Tertiary age (Eq.2.4).

$V_{sh} = 0.083[2^{(3.7*IGR)} - 1.0]$……Eq. 2.4

The calculated volumes of shale for the studied formations in the two studied sections are listed in the appendix B, and their plotted curves are shown in the figure 2.9.

As appears from the plotted shale content curves Jeribe Formation in the studied wells, generally contains less than 40% shale except few narrow horizons (depth intervals 2188-2189m and 2192-2193m in Ja-49 well and in depth intervals 3225-3225.5m, and 3238.5-3239m inTaza-2well). The relatively highest shale content exists in the middle part of the formation.

In order to describe the shaleness of the studied Jeribe Formation; the descriptive classification proposed by Ghorab (2008) on the bases of the percentage of the shale content was followed (table 2.3). Figure 2.9 also shows the zonation of the shaleness on the bases of the Ghorab's classification.

To show the clean, Shaley, and shale zones for Jeribe Formation in the two studied wells, tables 2.4 and 2.5 were prepared. Most part of Jeribe Formation appeared to be Shaley (between 10 and 35% shale content) with only few narrow horizons of shale (more than 35% shale volume). Clean zones of less than 10% shale content are noticed in the lower and upper part of the formation in Ja-49 well, whereas in Taza-2 well no clear and thick clean horizons were observed except about one meter at the last lowermost and uppermost part of the formation near the contact with Dhiban and Lower Fars formations, respectively.

Figure 2.10 drawn as best as can to show the detailed lithology with respect to the gamma ray log readings for Jeribe Formation in the two studied wells..

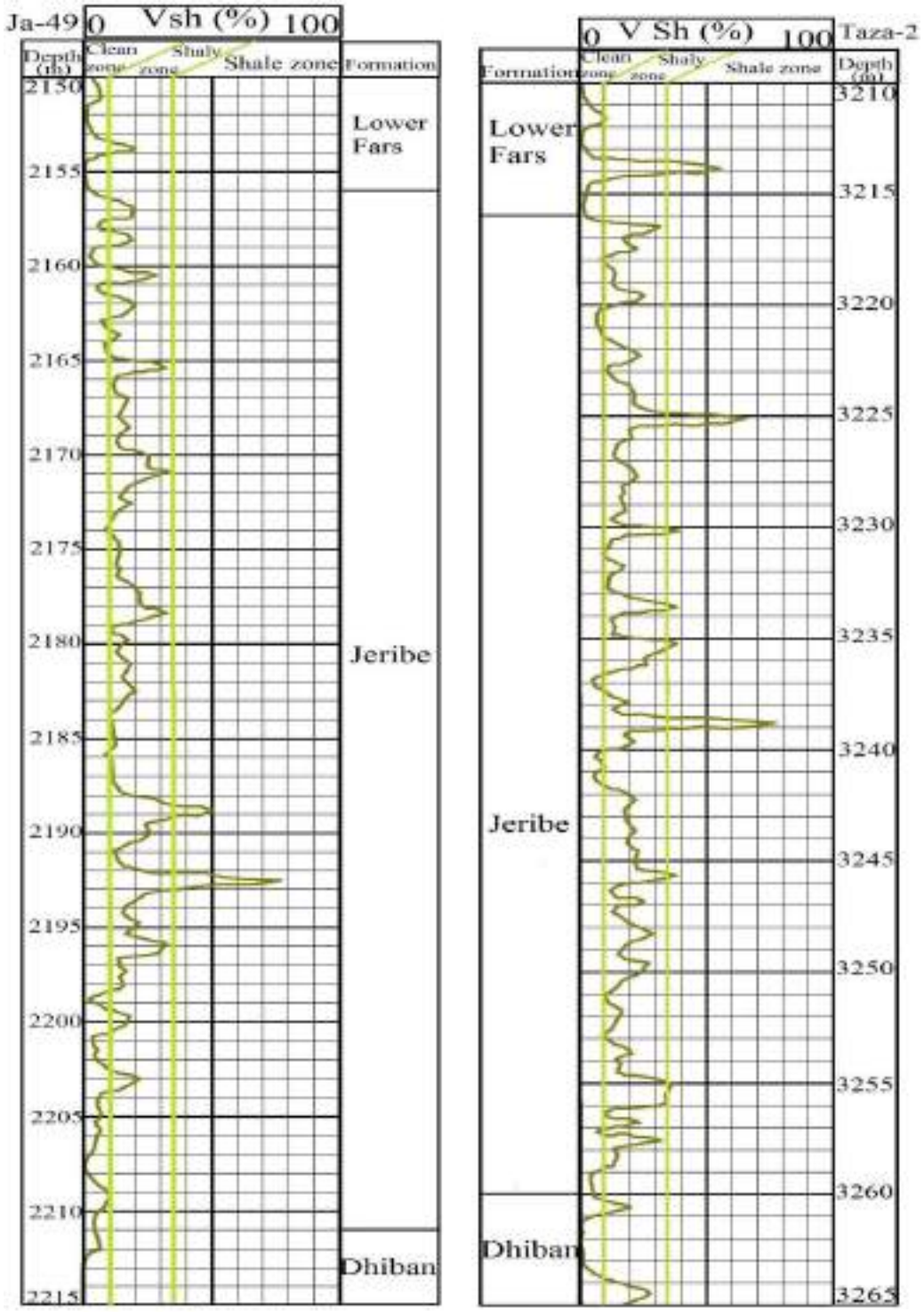

Figure 2.9: Curve plots of the calculated volume of shale and shale content zonations of the studied sections of Ja-49 and Taza -2.

Table 2.3: Classification of shaleness as proposed by Ghorab (2008)

V_{sh} (%)	Zone
⟨10	Clean
10 – 35	Shaley
⟩ 35	Shale

Table 2.4: Shaleness zonation for Jeribe Formation in the studied well of Ja-49.

Well	Depth interval (m)	Shaleness	Depth interval (m)	Shaleness
Ja-49	2156-2156.5	Clean	2184.5-2185.5	Shaley
	2156.5-2157.25	Shaley	2185.5-2186	Clean
	2157.25-2158	Clean	2186-2188.25	Shaley
	2158-2158.5	Shaley	2188.25-2189.25	Shale
	2158.5-2160	Clean	2189.25-2192	Shaley
	2160-2161	Shaley	2192-2193	Shale
	2161-2161.5	Clean	2193-2195.5	Shaley
	2161.5-2162.75	Shaley	2195.5-2196.25	Shale
	2162.75-2163.25	Clean	2196.25-2200.15	Shaley
	2163.25-2170.25	Shaley	2200.15-2202.5	Clean
	2170.75-2171.25	Shale	2202.5-2203.5	Shaley
	2171.25-2178	Shaley	2203.5-2212	Clean
	2178-2178.5	Shale		
	2178.5-2179.5	Clean		
	2179.5-2183.5	Shaley		
	2183.5-2184.5	Clean		

Table 2.5: Shaleness zonation for Jeribe Formation in the studied well of Taza-2

Well	Depth interval (m)	Shaleness
Taza-2	3216-3216.5	Clean
	3216.5-3220	Shaley
	3220-3221	Clean
	3221- 3224.5	Shaley
	3224.5-3225.5	Shale
	3225.5-3235	Shaley
	3235-3235.75	Shale
	3235.75-3236.5	Shaley
	3236.5- 3237.25	Clean
	3237.25-3238.15	Shaley
	3238.15-3239.15	Shale
	3239.15-3240	Shaley
	3240-3241.5	Clean
	3241.5-3254.75	Shaley
	3254.75-3256	Shale
	3256-3258.25	Shaley
	3258.25-3260.25	Clean
	3260.25-3261	Shaley

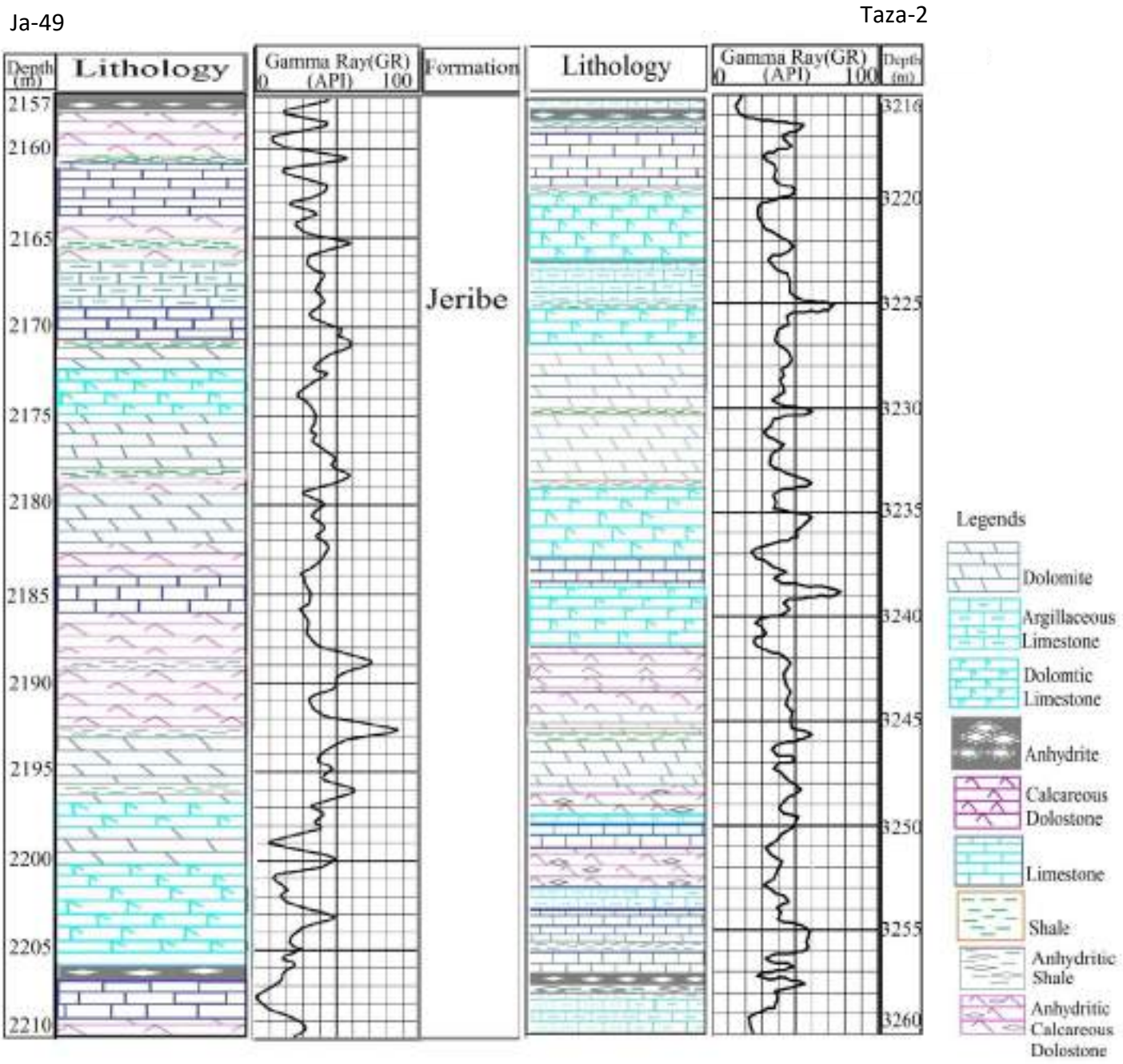

Figure 2.10: Detailed lithology and gamma readings for Jeribe Formation in the two studied wells of Ja-49 and Taza-2.

CHAPTER THREE

Porosity, Permeability, and Reservoir Units

3.1 Preface

A reservoir is a subsurface rock body that has sufficient effective porosity and permeability which usually contains exploitable quantity of hydrocarbon. Reservoir characterization is undertaken to determine its capability to both store and transmit fluid. Characterization deals with the determination of reservoir properties or parameters such as porosity (Φ), permeability (K), fluid saturation and net pay thickness (Ulasi et al., 2012).

Almost all produced oil and gas come from accumulation in the pore space of the reservoir rocks. Porosity is considered as a one of essential parameter of reservoir rock, which can be defined as the ratio of pore space volume to the bulk volume of reservoir rock, or it has defined as a storage capacity of the reservoir. Porosity usually expressed as fraction or percent (Heinemann, 2005). Despite of such an easy definition, porosity can be difficult to estimate especially when discussing the genetic process responsible for the porosity formation. From this corner, two essential types of porosity, primary and secondary can be recognized within the reservoir rocks.

Primary porosity is the original porosity that maintained after deposition. The grain size, shape and sorting of sediment have great effect on its porosity and it tends to decrease with time and depth. A porosity which formed by the effect of formation water and tectonic

forces is known as secondary porosity, of which created right after deposition, the underground water is responsible for dissolution, recrystallization and dolomititation process, while the latter tends to form fracture, stylolite and joints.

In carbonate rocks secondary porosity is normally more important than in siliciclastic sediments, due to the weakness of these minerals and their relatively high solubility. The storage capacity of a reservoir rock always depends on the effective porosity, since it contains the reservoir fluids (Heinemann, 2005). Effective porosity is the amount of mutually interconnected pore spaces present in a rock, which is available for free, fluids and excludes all non-connected porosity including the space occupied by the clay-bound water. The effective porosity is economically important; it is determined by most of the porosity measurements.

3.2 Sonic Log

Sonic logging is an investigation of the elastic properties of the formation through measuring the velocity of compressional waves emitted by the logging tool from a source of acoustic wave and received by pairs of receivers. Sonic log is the record of the time passed by the emitted acoustic wave versus depth. The output of the tool is a record of the interval transit time (Δt) by microsecond per foot which is the time spent by the acoustic wave to travel through one foot of the formation.

The readings of the sonic log (Δt) for Jeribe Formation in the two studied wells listed in the appendix A, and plotted as curves in the figure 3.1.The Δt for a given formation depends upon its lithology and porosity. The speed of sound in a sedimentary rock depends on many parameters

mainly on the rock matrix material (sandstone, limestone, dolomite, etc.), on the distributed porosity, and the nature of the included fluids (Schlumberger, 1989).

As Δt is dependent upon both lithology and porosity; therefore, a formation matrix interval transit time (Δt_{ma}) must be known to derive sonic porosity by Wyllie time average equation (Eq.3.1) (Wyllie et al, 1958: in Asquith and Gibson, 1982).

$$\emptyset_s = \frac{\Delta t_{log} - \Delta t_{ma}}{\Delta t_{fl} - \Delta t_{ma}} \qquad \text{.....Eq. 3.1}$$

Where:

Øs = Sonic porosity (fraction)

Δt_{log}= Interval transit time in the formation (log readings, μsec/ft)

Δt_{fl}= Fluid travel time (filtrate of the drilling mud, μsec/ft)

Δt_{ma}= Interval transit time of formation's matrix (μsec/ft)

As lithology has been detected previously through the optical method and through using the crossplots of N-D and M-N (Chapter two), so the Δtma for calculating sonic porosity can easily be derived from the known Δtma proposed for different lithologies by different authors (Serra,1984; Asquith,1985; Schlumberger,1989; Asquith and Krygowski,2004),(Table 3.1).

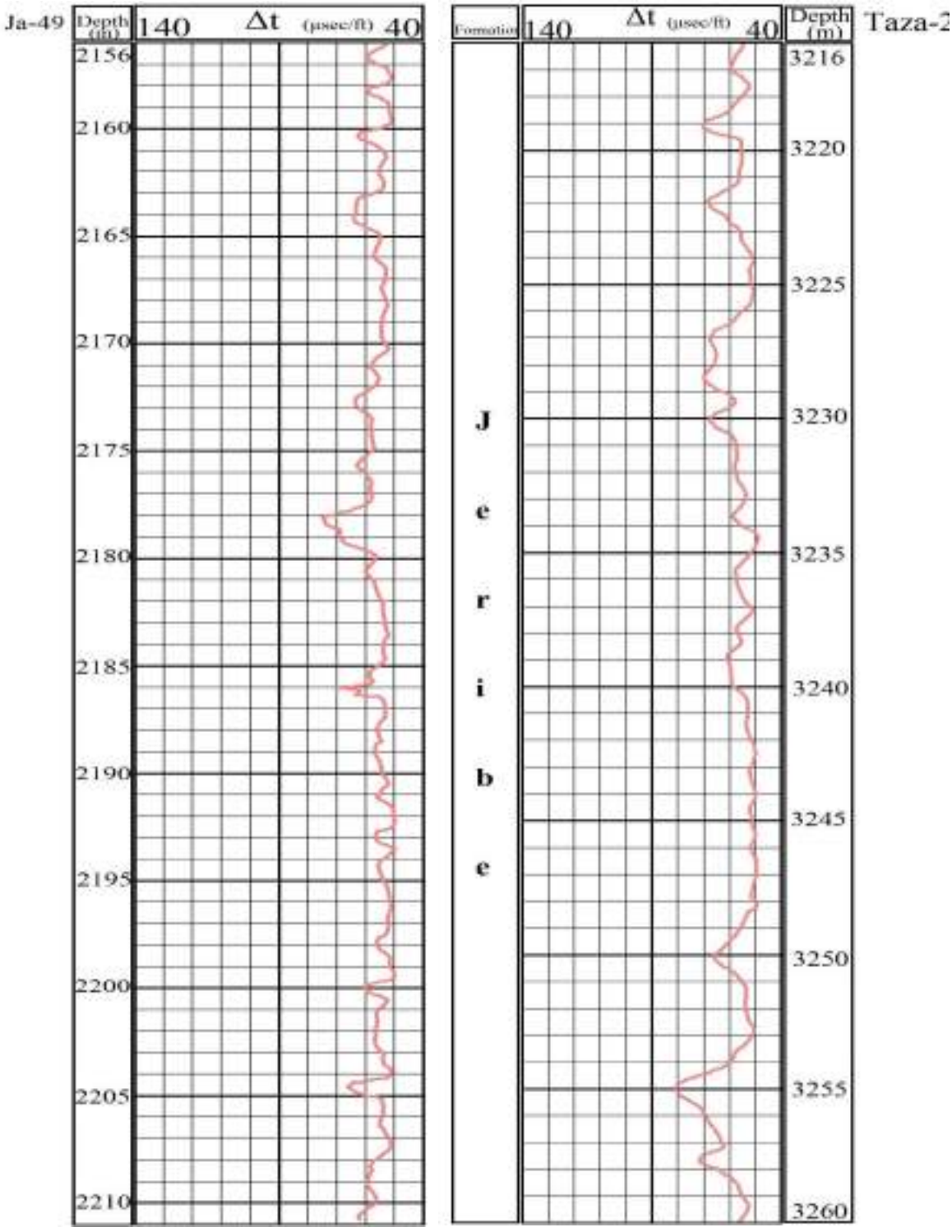

Figure 3.1: Sonic log record (Δt)(Msc/ft) for Jeribe Formation in the two studied wells of Ja-49 and Taza-2.

Table 3.1: Values of the parameters required for calculating porosity using Wyllie's equation (after Asquith and Krygowski, 2004).

Rock type	Δt_{ma} µsec/ft	Δt_{ma} µsec/m	Fluid type	Δt_{fl} µsec/ft	Δt_{fl} µsec/m
Sandstone Θ>0.1	55.5	182	Fresh water mud filterate	189	620
Sandstone Θ<0.1	51.2	168			
Limestone	47.6	156	Salt water mud filtrate	185	607
Dolomite	43.5	143			

Wyllie's equation has been applied for calculating the porosity of Jeribe Formation in the two studied wells using 43.5 µsec/ft as Δt_{ma} (being the lithology dominantly dolomite in both wells), and 189 µsec/ft as Δt_{fl} for Ja-49 well in which fresh water base mud used during drilling, whereas 185 µsec/ft as Δt_{fl} for the case of Taza-2 well because of using salt water base mud during drilling. The calculated values of the sonic porosity (Θs) for Jeribe Formation in both studied wells are listed in the appendix B.

3.3 Density Log

The density tool provides an estimate of the bulk density of the rock by measuring the attenuation of gamma rays between a source and a receiver. Gamma rays are scattered and absorbed in the formation as a function of the electron density of the formation, which is closely related to bulk density (ρb). This is the overall density of a rock including solid matrix and the fluid enclosed in the pore (Rider, 2002). If the formation is saturated with gas or light hydrocarbons, the measured bulk density will be affected, and the computed porosity values become much larger than of reality. The recorded bulk density for the studied Jeribe Formation in both wells are listed in the appendix A and shown as curves in the figure 3.2. In

turn, density is considered related to porosity by a simple equation (Eq. 3.2):

$$\emptyset D = \frac{\rho ma - \rho b}{\rho ma - \rho fl} \text{.....Eq. 3.2}$$

Where:

ØD = density porosity (fraction)

ρma = density of the matrix (gm/cc)

ρfl = fluid density (1.0gm/cc for fresh water mud and 1.1gm/cc for Saline water mud)

ρb = bulk density (log reading, gm/cc)

The determination of porosity from density measurements requires the prior knowledge of lithology and fluid type as for sonic log. The selected value of ρma for calculating density porosity, in this study depends mainly on the determined lithology through the optical examination of the rock samples in addition to the N-D and M-N crossplots (Chapter two). Table 3.2 shows the suggested matrix densities for different lithologies by Asquith and Krygowski (2004).

The calculated porosity from the sonic log, the selected matrix density (ρma) for Jeribe Formation in both studied wells was 2.87 g/cm³ (being the lithology dominantly dolomite), whereas 1.0 and 1.1 g/cm³ values used as fluid density (ρfl) for Ja-49 and Taza-2 wells respectively, depending on the nature of the mud used during drilling the wells. The calculated porosity values from the density log (ϴD) are listed in the appendix B.

Ja-49

Taza-2

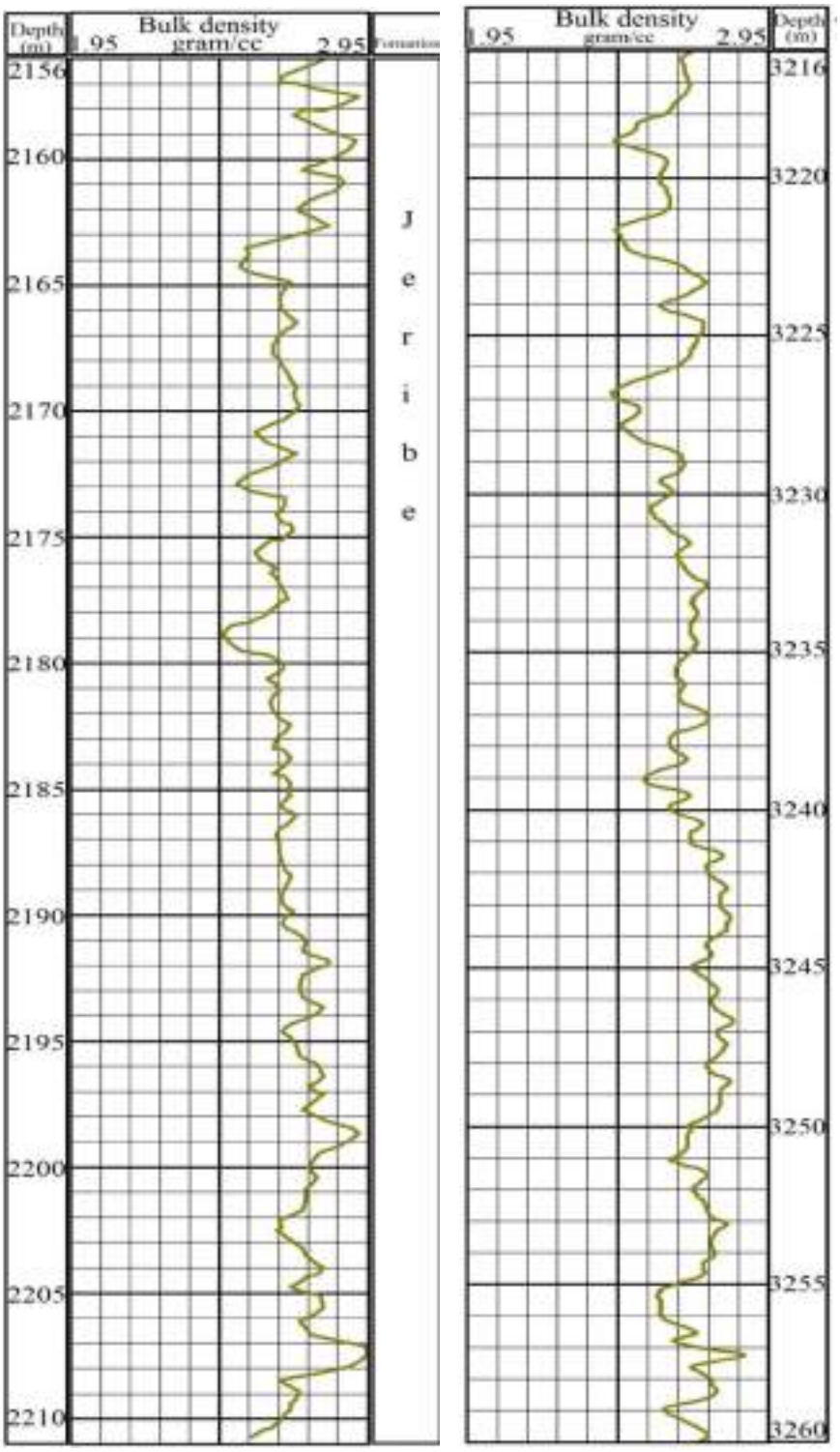

Figure 3.2: The recorded bulk density (ρb) for Jeribe Formation in the studied wells of Ja-49 and Taza-2.

Table 3.2: Matrix densities for different lithologies (after Asquith and Krygowski, 2004)

Lithology	Density (g/cm³)
Sandstones	2.65
Limestones	2.71
Dolomites	2.87
Anhydrite	2.98

3.4 Neutron Log

Historically, Neutron log is considered as the first nuclear logging tool used for estimating porosity in the drilled wells. The basic of the neutron logging is that hydrogen, with its relatively large scattering cross section, and small mass is very efficient in the slowing down of the fast neutrons. So the interaction of high energy source neutrons with a formation can be related to its hydrogen content. As hydrogen in the formation sometimes exists in the pore spaces as water or hydrocarbons, so the correlation with formation porosity can be easily made (Ellis and Singer, 2008).

Like the sonic and the density tools, the neutron tool is sensitive to the lithology of the formation, because the matrix contributes to the slowing and capture of the neutrons. In addition to that, the tool is particularly sensitive to environmental conditions and to the presence of gas, which lowers the hydrogen density of the pore space (Siddiqui et al., 2003).

In this study, the available neutron log of Jeribe Formation has been digitized and the values of the neutron porosity (ϴN) listed in the appendixA.

3.5 Neutron - Density porosity Combination

The combination neutron-density log is a combination of porosity logs which are used to determine porosity. Beside it can be used in determining lithology and detecting gas bearing zones (Asquith and Gibson, 1982). The neutron –density porosity values are slightly affected by changes in lithology; therefore, porosity from a neutron-density log can be calculated mathematically. The root mean square formula is used for determining neutron –density porosity.

$$\Theta_{N\text{-}D} = \frac{\sqrt{\Theta N^2 + \Theta D^2}}{2} \quad \text{..... Eq. 3.3}$$

Whenever a neutron-density log display a density porosity value of less than 0.0 a common value in anhydritic dolomite reservoirs, the following formula should be used to determine neutron-density porosity as proposed by Asquith and Gibson (1982):

$$\Theta_{N\text{-}D} = \frac{\Theta N + \Theta D}{2} \quad \text{.....Eq. 3.4}$$

Appendix B contains the calculated combination neutron-density porosity using the equation Eq. 3.3.

3.6 Correcting Porosity from Shale Impact

The measurement of the true effective porosity will be effected by the presence of shale or clay in the reservoir. This variation in results from the velocity differences between shale and clay and the sand matrix (or carbonate matrix). For porosity correction from shaliness, the fractional shale volume from other logs needs to be estimated (Khan, 1989). This has already done in this study using gamma ray log data (Chapter two).

The diverse characteristic of the shales content has complicated the interpretation of a tool response as the presence of the shale content has a different response to each porosity tool. Shales display low to moderate porosity values on the density porosity log .On the sonic and neutron logs, shales show moderate to relatively high porosity values (Bassiouni, 1994). Whenever shale is present in a formation, all the porosity tools (sonic, density, and neutron) will record too high porosity. This is true in sandstone reservoirs as well as limestone and dolomite reservoirs (Asquith and Gibson, 1982). But permeability was much affected by the presence of very low level of clay mineral in the pore space (Ellis and Singer, 2008) as compared to the porosity. As formation evaluation results will be influenced by the presence of shale, so for addressing this problem the porosity and saturation values must be calculated free from the shale effect.

Shale volumes for Jeribe Formation have been determined in the studied wells (Chapter two), and even the type by which the shales are distributed in the reservoir. So, it is time to correct the calculated and measured porosities (Θs, Θ_D, Θ_N, and $\Theta_{N\text{-}D}$) from shale effect to make their values more reliable.

The equations Eq.3.11-Eq.3.14 are used for correcting the sonic, density, neutron, and combination neutron-density porosities from the effect of shale in this study as shown below:

ΘSonic:

$$\emptyset_{Scorr} = \frac{\Delta tlog - \Delta tma}{\Delta tfl - \Delta tma} - Vsh * \frac{\Delta tsh - \Delta tma}{\Delta tfl - \Delta tma} \ldots\ldots \text{Eq.3.12 (Dresser Atlas,1979)}$$

Where:

$Øs_{corr}$: sonic porosity corrected for shale

Δt_{log}: interval transit time of formation

Δt_{ma}: interval transit time of formation's matrix

Δt_{fl}: interval transit time of fluid

Δt_{sh}: interval transit time of adjacent shale

V_{sh}: volume of shale

ϴDensity:

$$ØDcorr = \frac{\rho ma - \rho b}{\rho ma - \rho fl} - Vsh * \frac{\rho ma - \rho sh}{\rho ma - \rho fl} \ldots\ldots \text{Eq.3.12 (Dresser Atlas,1979)}$$

Where:

$ØD_{corr}$: density log derived porosity corrected for shale

ρ_{ma}: matrix density of formation

ρ_b: bulk density of formation

ρsh: bulk density of adjacent shale

ρ_{fl}:fluid density (1.0 for fresh mud)

V_{sh}: volume of shale

ϴ Neutron:

$$ØNcorr = ØN - (Vsh * ØNsh) \ldots\ldots\ldots\ldots\ldots \text{Eq.3.13 (Dewan,1983)}$$

Where:

$Ø_{N\ corr}$: neutron log derived porosity corrected for shale

$Ø_N$: neutron log derived porosity uncorrected for shale

$Ø_{Nsh}$: neutron porosity for adjacent shale

V_{sh}: volume of shale

Θ Combination of Neutron-Density:

$$\Theta_{N\text{-}Dcorr} = \frac{\emptyset Ncorr + \emptyset Dcorr}{2} \quad \text{.....Eq.3.14}$$

Where:

$\emptyset_{N\text{-}Dcorr}$: neutron-density porosity corrected for shale

$\emptyset_{Ncorr}$: neutron porosity corrected for shale

$\emptyset_{Dcorr}$: density porosity corrected for shale

Figures (3.7 - 3.10) show the curves of the incorrect and corrected porosities of sonic, density, neutron, and combination N-D for Jeribe Formation in the two studied wells. In addition to the effect of shale volume on the porosity magnitude can also be noticed. As the existence of shale always causes an overestimation for the values of the calculated porosities; therefore, a reduction in the porosity values is expected after correction.

The corrected porosity values for Θ_S, Θ_D, Θ_N, and $\Theta_{N\text{-}D}$ are listed in appendix B.

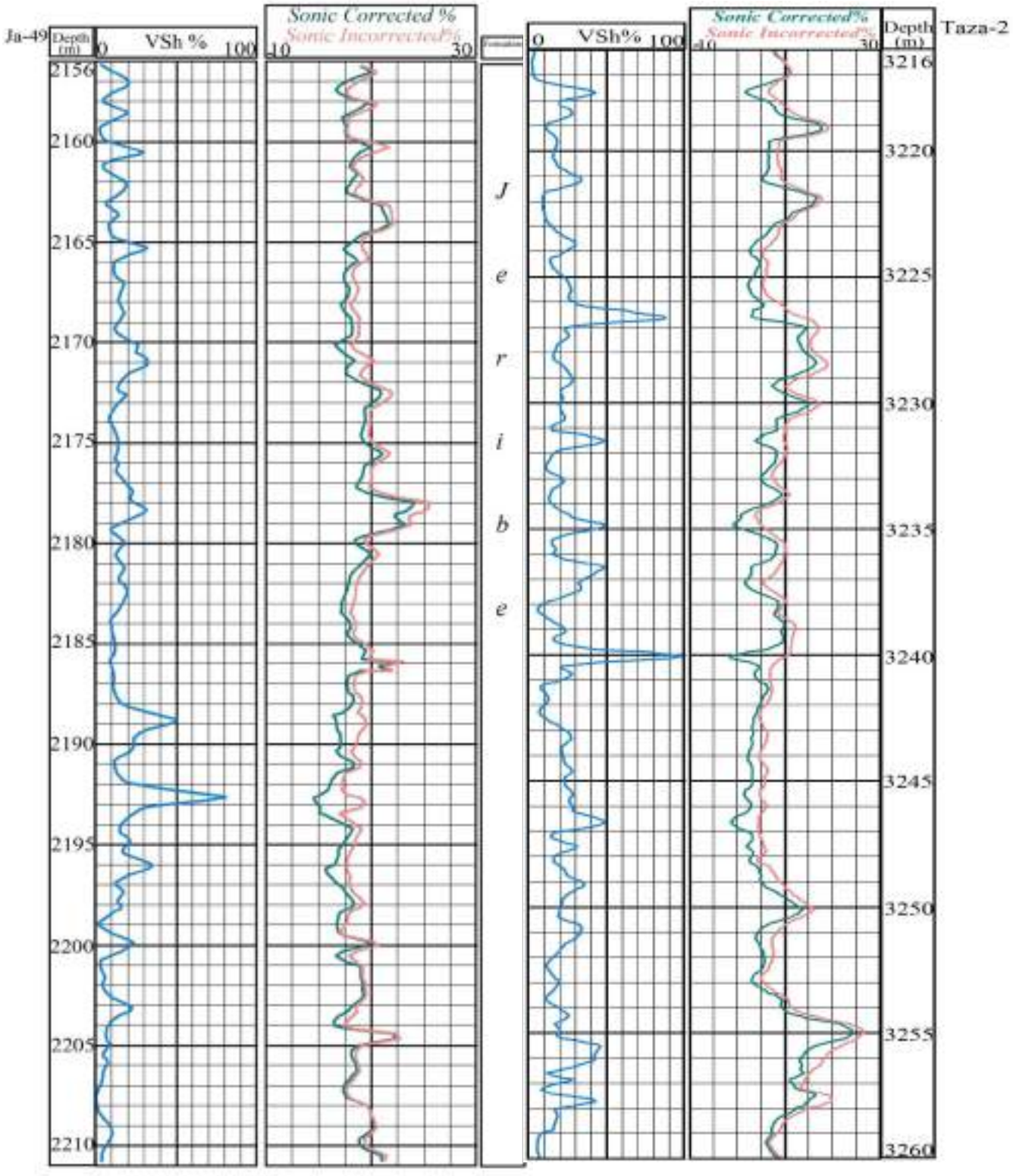

Figure 3.3: Incorrected and corrected sonic porosity from shale content and shale volume curves for the studied Jeribe Formation in Ja-49 and Taza-2 wells.

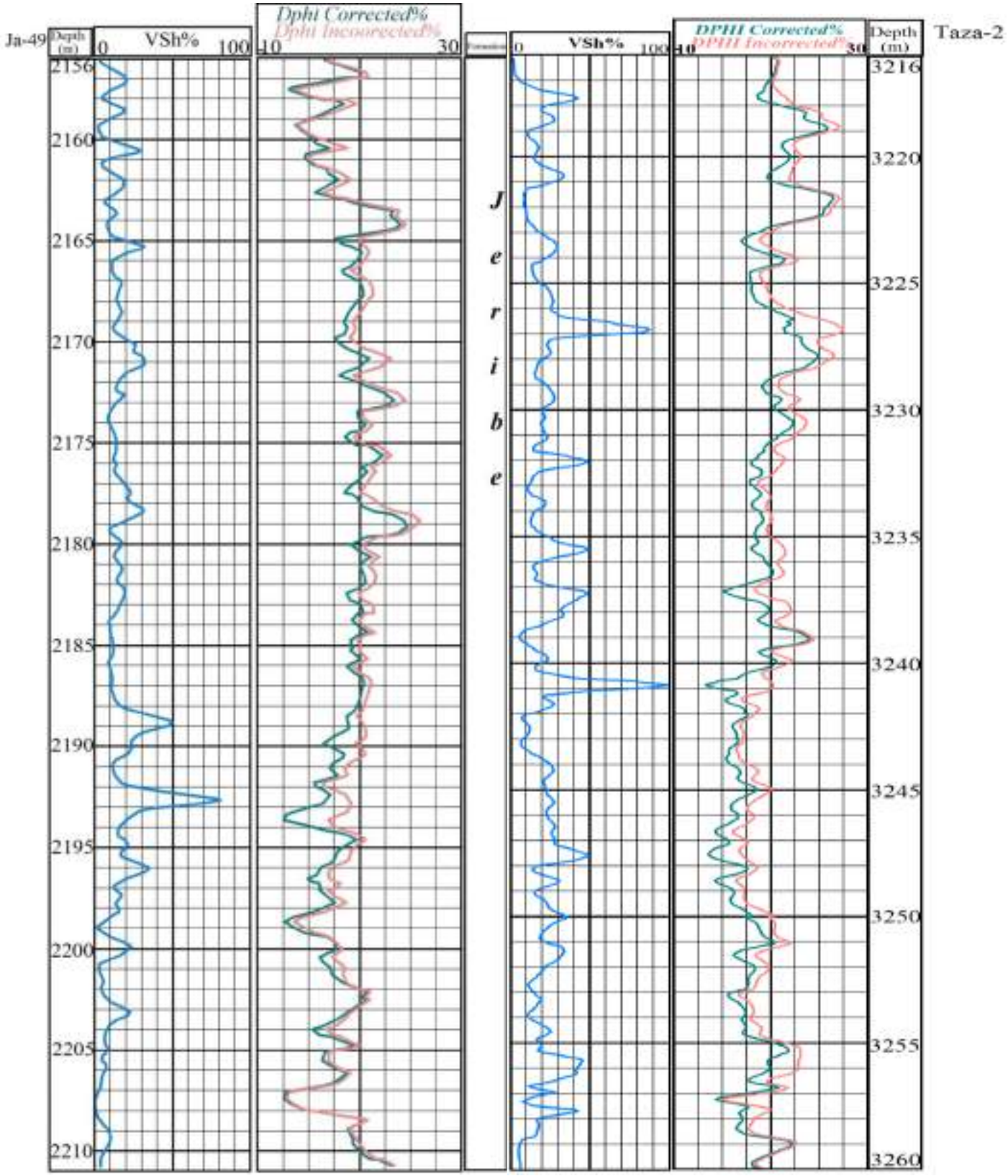

Figure 3.4: Incorrected and corrected Density porosity from shale content and shale volume curves for the studied Jeribe Formation in Ja-49 and Taza-2 wells.

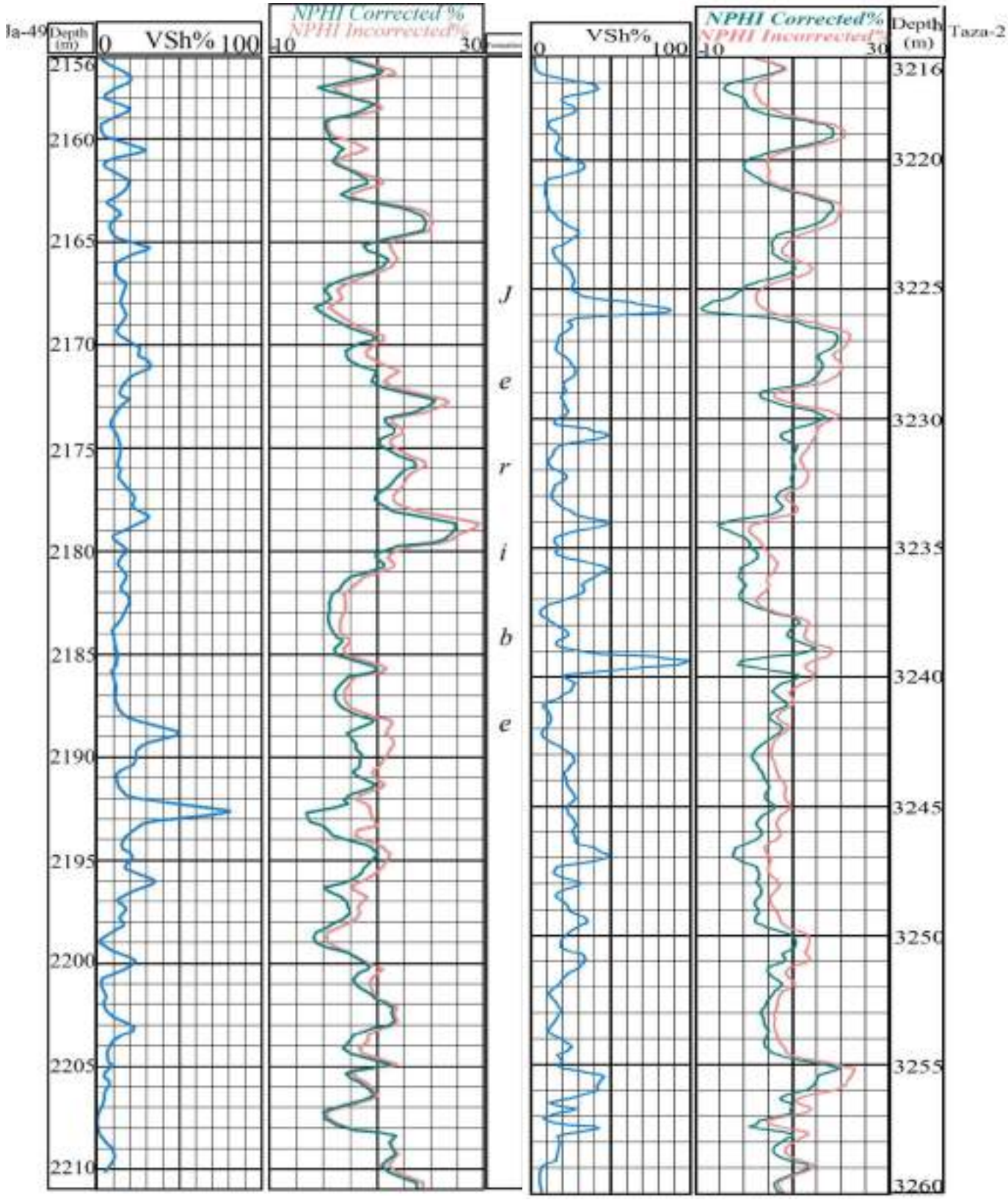

Figure 3.5: Incorrected and corrected Neutron porosity from shale content and shale volume curves for the studied Jeribe Formation in Ja-49 andTaza-2wells.

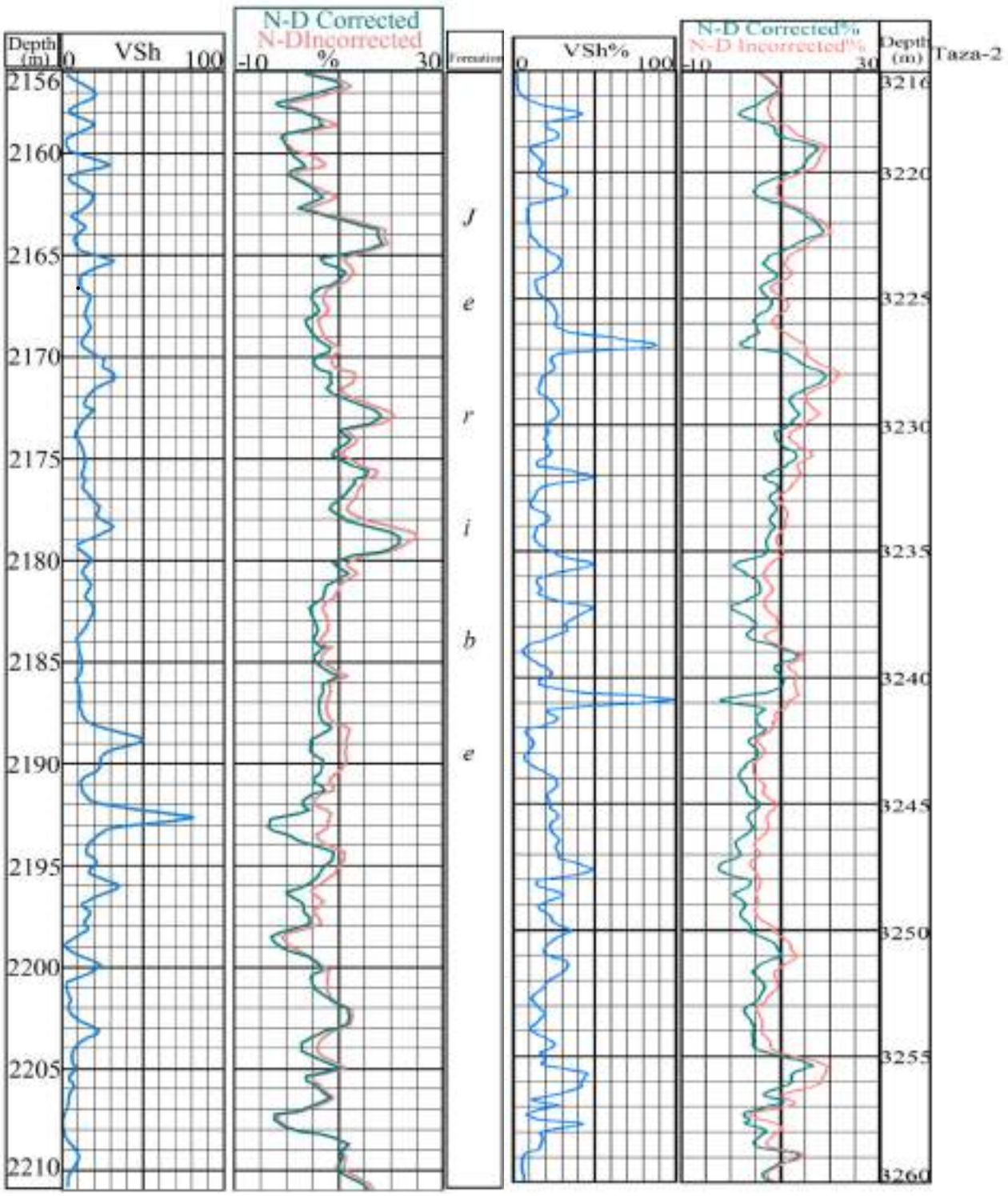

Figure 3.6: Incorrected and corrected N-D porosity from shale content and shale volume curves for the studied Jeribe Formation in Ja-49and Taza-2 wells.

As expected, the reduction occurred to the calculated porosities after correction from shale effect. At each depth the correction was directly proportional with the volume of shale. Comparison between reductions occurred to the different porosities (ΘS, ΘD, and ΘN) shows no obvious difference in reduction intensities between them.

In this study, and for evaluating the porosity of Jeribe Formation, the corrected $\Theta N\text{-}D$ was mainly depended on as it represents the existed primary and secondary porosities in the formation more reliably, whereas the standard proposed by North (1985) for describing ranges of porosities (table 3.3) used in describing the porosities qualitatively.

Table3.3: Description of porosity ranges qualitatively as proposed by North (1985)

Percentage porosity (%)	Qualitative Description
0-5	Negligible
5-10	Poor
10-15	Fair
15-20	Good
20-25	Very Good

The following can be mentioned about the porosity of Jeribe Formation in the two studied wells from the observation of the $\Theta N\text{-}D$ corrected values which shown as curve in figure 3.10:

1. Most parts of the formation have porosities less than 15% (poor porosity).
2. The depth interval between 2172 and 2180m in Ja-49 well is considered being of the highest porosity (good to very good porosity)

in comparison with the other parts of the formation in the both studied wells.

3. The highest porosity value which exceeded 20% (excellent porosity) has been recorded at the depth 2179m in the well Ja-49.
4. The lowest porosity values recorded at those depths were highest shale content exist (e.g. 2192.5m in Ja-49; 3241m in Taza-2).
5. Theoretically, porosity of less than 0% calculated in some depths which either of very high shale content as noticed in the depths 2192.5m in Ja-49 and 3241m in Taza-2 or are anhydritic zones as noticed in the depths 2198.5 and 2207.5m in the well Ja-49.
6. In both studied wells, the porosity is increasing upward and finally decreasing near the top of the formation (near the contact with Lower Fars Formation).

3.7 Secondary Porosity Identification

Porosity can be classified as primary or secondary. Primary porosity forms during deposition of sediments and includes interparticle and intraparticle porosities which also called fabric selective porosity. Secondary porosity is formed after deposition and develops during diagenesis by dissolution, dolomitization, and through production of fractures in the rock. Secondary porosities such as intercrystalline or moldic porosity are also fabric selective porosities, whereas vuggy and fracture secondary porosities are considered as non-fabric selective porosties (Choqutte and Pray, 1970).

Fractures can be observed on cores and also optically through thin section examination from which contribution of fractures in the total

porosity of the reservoir can be detected. Fractures can be characterized as filled, semi-filled and open fractures. Filled fractures do not contribute to the porosity (Heinemann, 2005).

Rocks having both, fractured and intergranular porosity, are called dual (double) porous media.

Fracture can have great effect on total permeability of a rock, but they have very low influence on porosity and saturation or other petrophysical characteristics (Shlumberger, 1989).

Logs are considered as an effective tool for detecting the existence of fractures in the logged formations. The followings are a number of log data observations which are used to determine the possibility of existing fractures in the drilled intervals:

1. Washout and enlarged intervals recorded by caliper log may be due to fracturing (Shlumberger, 1989) (especially when no signs of shale or anhydrites were observed).
2. Drilling time logs are usually recording more rapid penetration in fracture intervals in comparison with unfractured matrix rocks (Ahr, 2007).
3. The larger separation between the resistivity logs is sometimes due to fracture intensity because resistivity device that looks deeper into the formation is less influenced by a fracture than is a shallow reading device (Shlumberger, 1989).
4. SP curve deflection in front of fractured zones has the form of either erratic behavior or some more systematic negative deflection probably due to flow of mud filtrate ions into the formation (Crary et al., 1987).

5. High gamma ray record without indications for high shale content mostly explained as due to deposition of uranium salts along the discontinuity surfaces of a fracture or within the crack itself (Fertl, 1980).
6. Borehole imaging logs are the principle tool for fracture detection especially the acoustic type which is used in wells drilled with oil based mud in which resistivity tool does not work well.
7. Through the comparison between the calculated porosity values using sonic log in a certain depth and that calculated using density or neutron logs for the same depth. As sonic log tool responds only for the fast compressional wave reaches the receiver firstly, therefore the calculated sonic porosity represents mostly the primary matrix porosity (inter and intraparticle porosities). On the other hand, density and neutron logging tools are responding to the bulk electron density and all the existed hydrogens in the formation respectively, therefore their calculated and recorded porosities represent the primary and secondary porosities collectively. Accordingly, in zones having secondary porosity (vugs or fractures), the calculated Θ_S is less than Θ_D, Θ_N, and of course Θ_{N-D}.

In this study, and to evaluate the contribution of secondary porosity in the total porosity of Jeribe Formation in the two studied wells, the equation Eq.3.15 has been applied for calculating the secondary porosity (vugs and fracture porosity) which has computed as the difference between the corrected neutron-density porosity ($\Theta_{N-Dcorr}$) and corrected sonic porosity (Θ_{Scorr}).

$\Theta_{Second} = \Theta_{N\text{-}Dcorr} - \Theta_{Scorr}$ ……Eq.3.15

Where:

Θ_{Second} = Secondary porosity

$\Theta_{N\text{-}Dcorr}$ = Neutron-Density porosity

Θ_{Scorr} = Sonic porosity

The calculated secondary porosity listed in the appendix B and shown as a curve in the figure 3.11.

Figure 3.11, display secondary porosity (either fractures or vugs) contributed in the total porosity of Jeribe Formation in different intervals with different intensities which mostly have not exceeded 5.0% except in few narrow horizons (eg. 3220m and 3223m in Taza-2 well). Generally, secondary porosity in the two studied wells represented and ranged between (2.0 to 3.0%) of the total porosity.

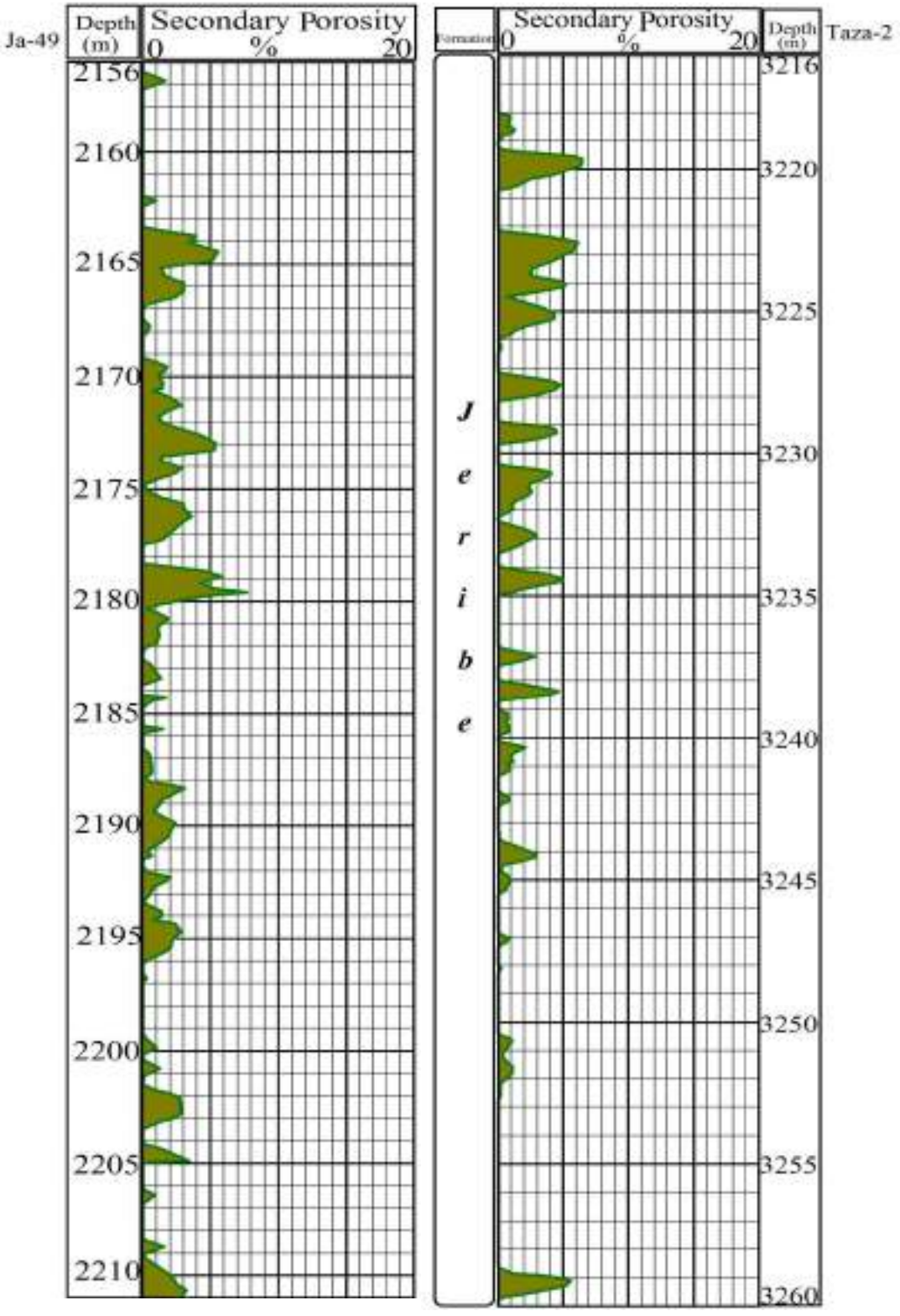

Figure 3.7: Secondary porosity plot for the studied Jeribe Formation in the studied wells of Ja-49 and Taza-2.

3.8 Electrical Micro Imaging (EMI)

Borehole images are electronic pictures of the rocks and fluids encountered by a wellbore. Such images are made by electrical, acoustic, or video devices which have been lowered into the well (Hurley, 2004).

During image logging the formation sampled many times horizontally and at a high rate vertically, to form a dense matrix of measurements in order to create an image. This image is not like a photo made for a core sample in a visible light, it is an image created by computer on geophysical measurements of electrical conductivity or acoustic reflectivity (Rider, 2002).

Electrical borehole images are based on dipmeter technology that has been commercially available since the 1950s. The imaging tools have microresistivity electrodes arranged around the wellbore on pads that are pressed against the borehole wall. The evolutionary trend from dipmeters to borehole images has been from a few electrodes to a complex array of electrodes on multiple pads (Hurley, 2004) (Fig. 3.12).

3.8.1 Data Acquisition

Data acquisition in electrical image logging has been described clearly by Hurley (2004) as follows:

Tools are first run into the hole with the pads closed. At the start of the log run, either four, six, or eight pads are pressed against the borehole wall. The number of pads depends on the logging device which is being used. Electrical current is forced into the rock through the electrodes, and remote sensors measure the current after it interacts with the formation. Raw data include multiple electrode readings, caliper readings from individual pads or pairs of pads, and *x*-, *y*-, and *z*-axis accelerometer and magnetometer readings.

Borehole deviation and pad 1 (tool) orientation are determined from the magnetometers".

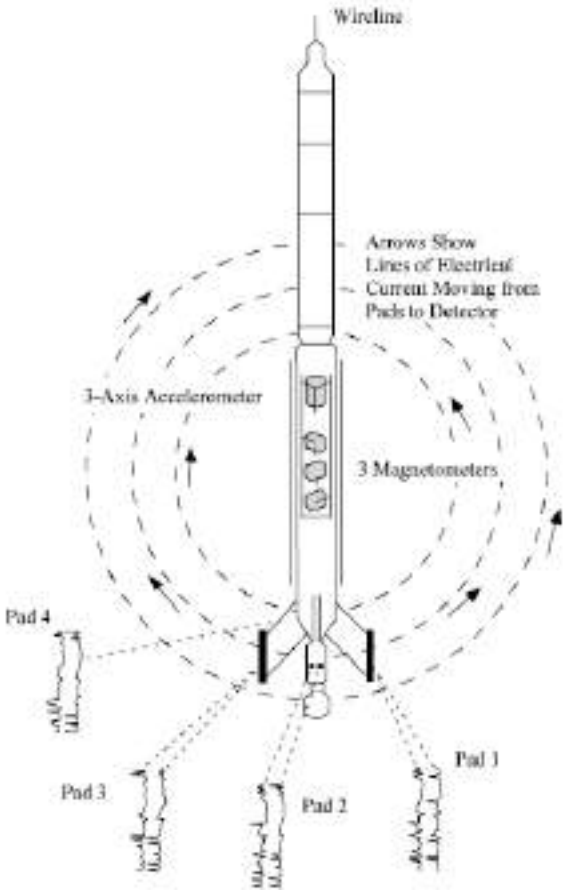

Figure 3.8: Basic principles of electrical dipmeter tools (after Schlumberger, 1983 in Hurley, 2004)

A processed electrical borehole image is basically a map of rock resistivity at the borehole face. Because it is more difficult to examine borehole images in 3-D, it is common to split the borehole along true north, and then unroll the cylinder until it becomes a 2-D view.

Borehole images are created by assigning color maps to different bins or ranges of resistivity values. Colored pixels are then arranged in their proper geometric position around the wellbore. By convention, low-resistivity features, such as shales or fluid-filled fractures, are displayed as dark colors.

High-resistivity features, such as sandstones and limestones, are displayed as shades of brown, yellow, and white (Hurley, 2004).

According to Schon (2015), valuable information which can be derived from Image logging includes:

1. Sedimentation (layring, lamination, dipping, etc.)
2. Pore types in carbonates
3. Fractures, fracture direction and other tectonic elements
4. Stress field

Detecting and orienting fractures and faults are the most important use of borehole images in the area of structural interpretation. Fault plane (especially microfaults) can also be detected and oriented.

Image logging using EMI tool (six pads, 150 electrodes) done for Jeribe Formation in the well Taza-2. Different geological features like lithological characteristics, fractures and vugs (open and closed), porous and dense intervals are identified through the images which have been created by the logging tool along the studied section (Fig. 3.13). The previously determined fractured or vuggy zones depending on Ɵs and ƟN-D have been checked through the EMI log in addition to the other calculated reservoir characteristics like shaleness and porosity. In most of the depth intervals the images supported the previously identified features and acceptable matching observed between them.

Additional observation from the image log is the horizontal or near horizontal nature of the beddings and layers within the Jeribe Formation in the well Taza-2. This is an indication to being the location of the appraisal Taza-2 well on or near the axis line of the Taza anticline and still far from the plunge of the structure (Hydrocarbon accumulation column of less than the closure of the trap, or O/W contact shallower than the depth of the spill plane is expected).

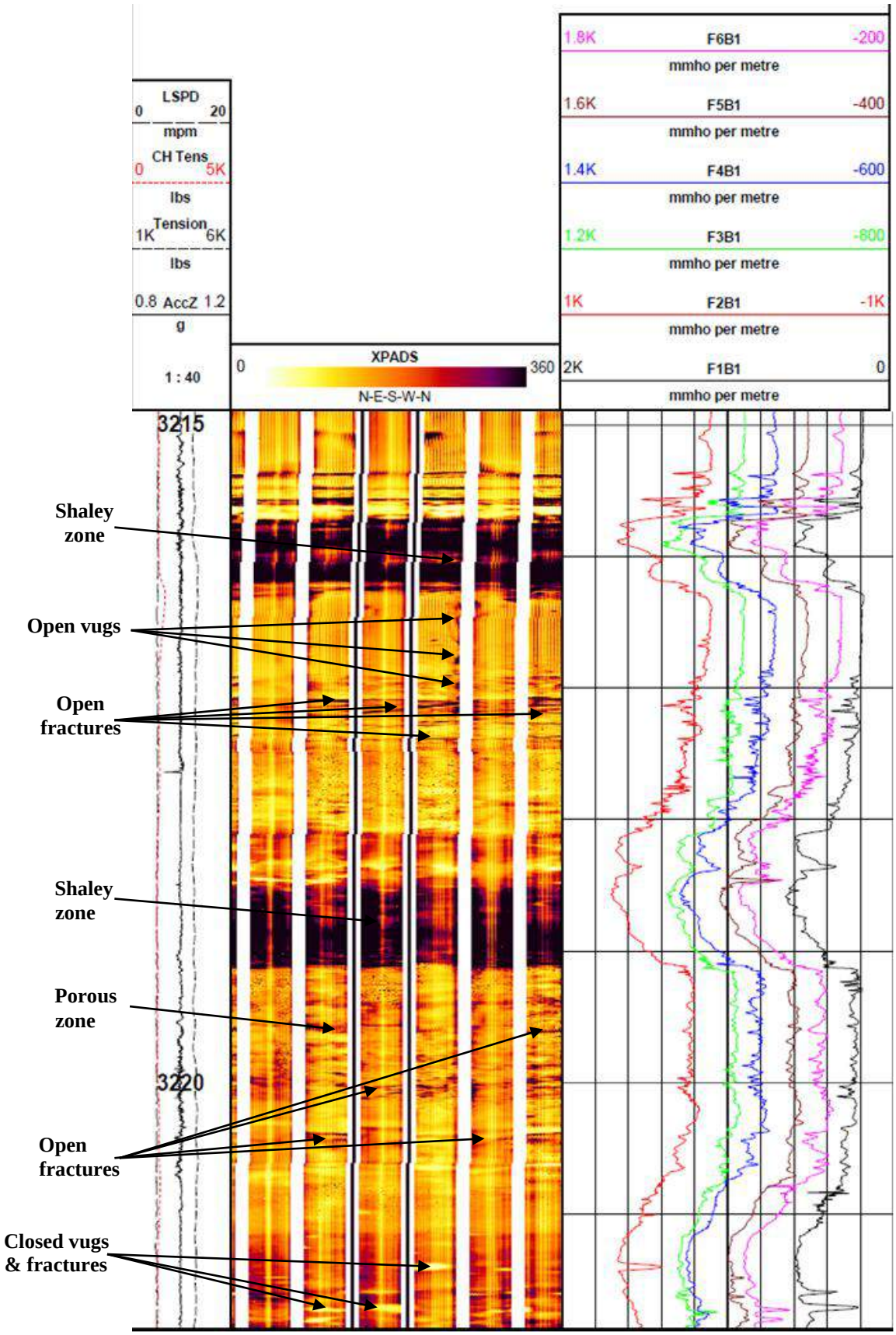

Figure 3.9: Electro Microimaging (EMI) log for Jeribe Formation in the well Taza-2.

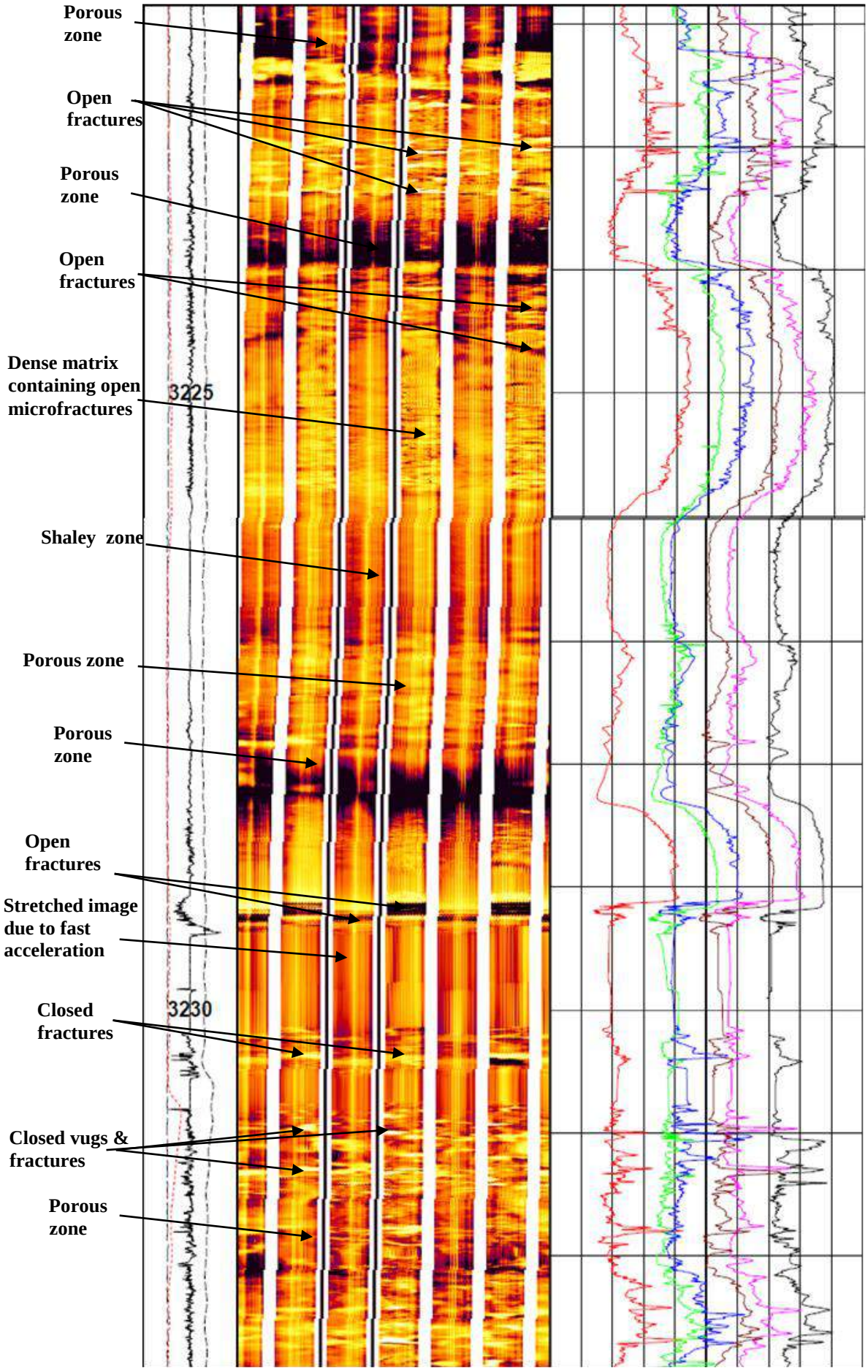
Porous zone
Open fractures
Porous zone
Open fractures
Dense matrix containing open microfractures
3225
Shaley zone
Porous zone
Porous zone
Open fractures
Stretched image due to fast acceleration
3230
Closed fractures
Closed vugs & fractures
Porous zone

continued..

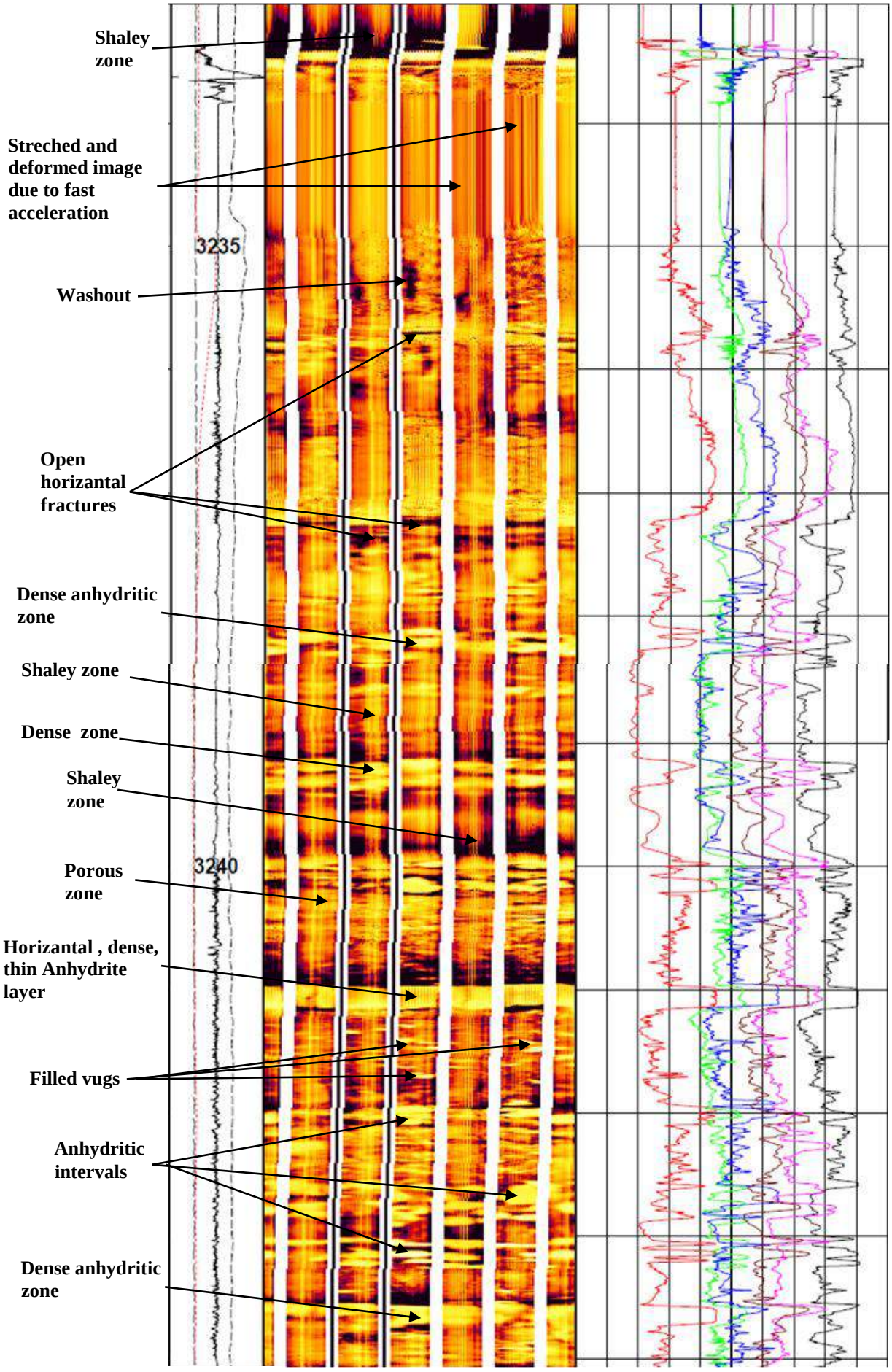
Shaley zone
Streched and deformed image due to fast acceleration
3235
Washout
Open horizantal fractures
Dense anhydritic zone
Shaley zone
Dense zone
Shaley zone
3240
Porous zone
Horizantal , dense, thin Anhydrite layer
Filled vugs
Anhydritic intervals
Dense anhydritic zone

continued..

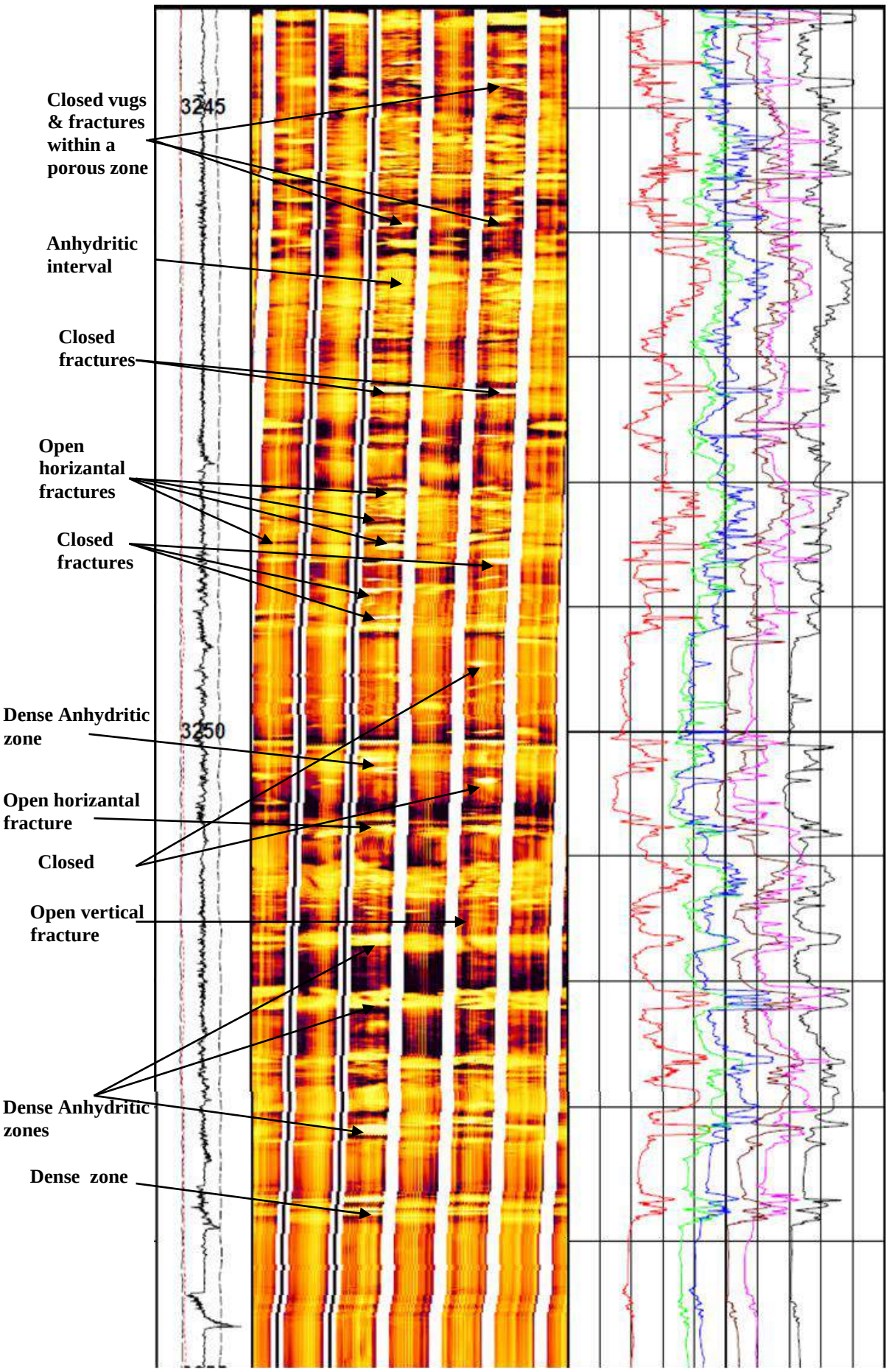
Closed vugs & fractures within a porous zone
3245
Anhydritic interval
Closed fractures
Open horizantal fractures
Closed fractures
Dense Anhydritic zone
3250
Open horizantal fracture
Closed
Open vertical fracture
Dense Anhydritic zones
Dense zone

continued..

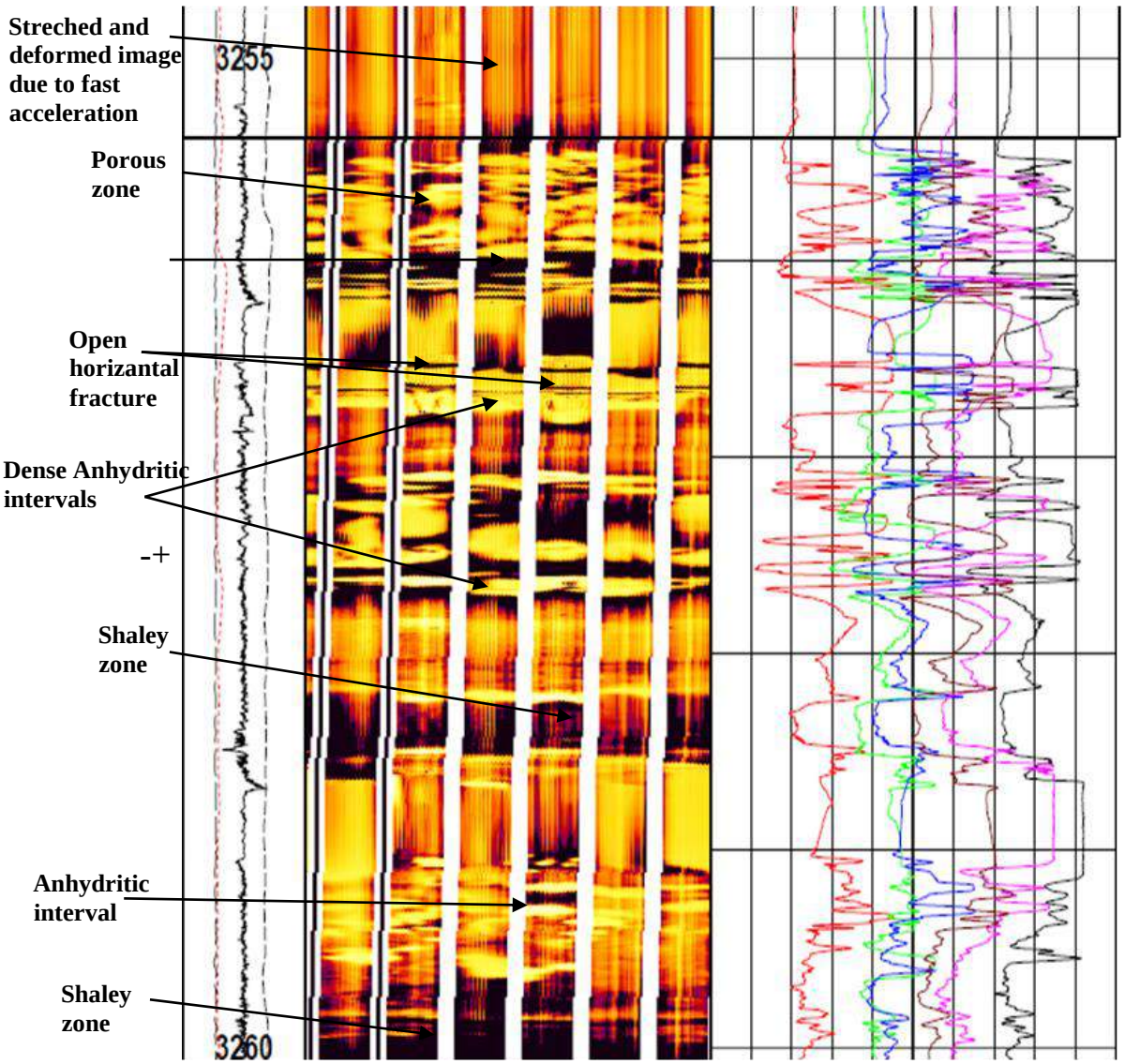

continued..

3.9 Gas Bearing Zone Detection:

In gas-bearing zone an increase in density porosity occurs along with a decrease in neutron porosity, this is called gas effect. Gas in the pores causes the density log to record too high porosity (gas is lighter than oil and water) and the neutron log to record too low porosity "gas has a lower concentration of hydrogen atoms than oil and water" (Asquith and Krygowski, 2004). So, the crossover of the two curves of corrected neutron

and density porosities will aid indirectly in detecting gas zones when clear separation between the two curves occurs with being the value of density porosity higher than the value of the neutron porosity. Figure 3.14 is the plot of the neutron and density porosity crossover curves for Jeribe Formation in the two studied wells of Ja-49 and Taza-2.

The possibility of existing gas filled porosities or low density oil filled porosities are highest in the upper part of Jeribe Formation in Taza-2 well. No obvious indications for gas bearing zones observed in Jeribe Formation in Ja-49well.

3.10 Permeability

Permeability is another important rock parameter for the evaluation of hydrocarbon reservoirs which is originally the ability of the sediment to transport fluid.

Reservoir rocks are formed from grain of solid matter with a different size and shapes and pore spaces which are originate primarily during deposition or as result of diagnesis secondarily. These voids may contain different fluids such as water, oil, or gas; so these pores must be connected to each other to transmit fluid which is important for developing an effective reservoir.

Permeability data can be obtained from well tests, core data analysis and well loggings. Measuring permeability through laboratory tests on cylindrical core samples under reservoir condition and by using the reservoired fluids (or nearly similar fluids) is the most effective method in estimating the permeability of reservoir sediments. Onsite estimation of permeability through different techniques of well testing aids greatly

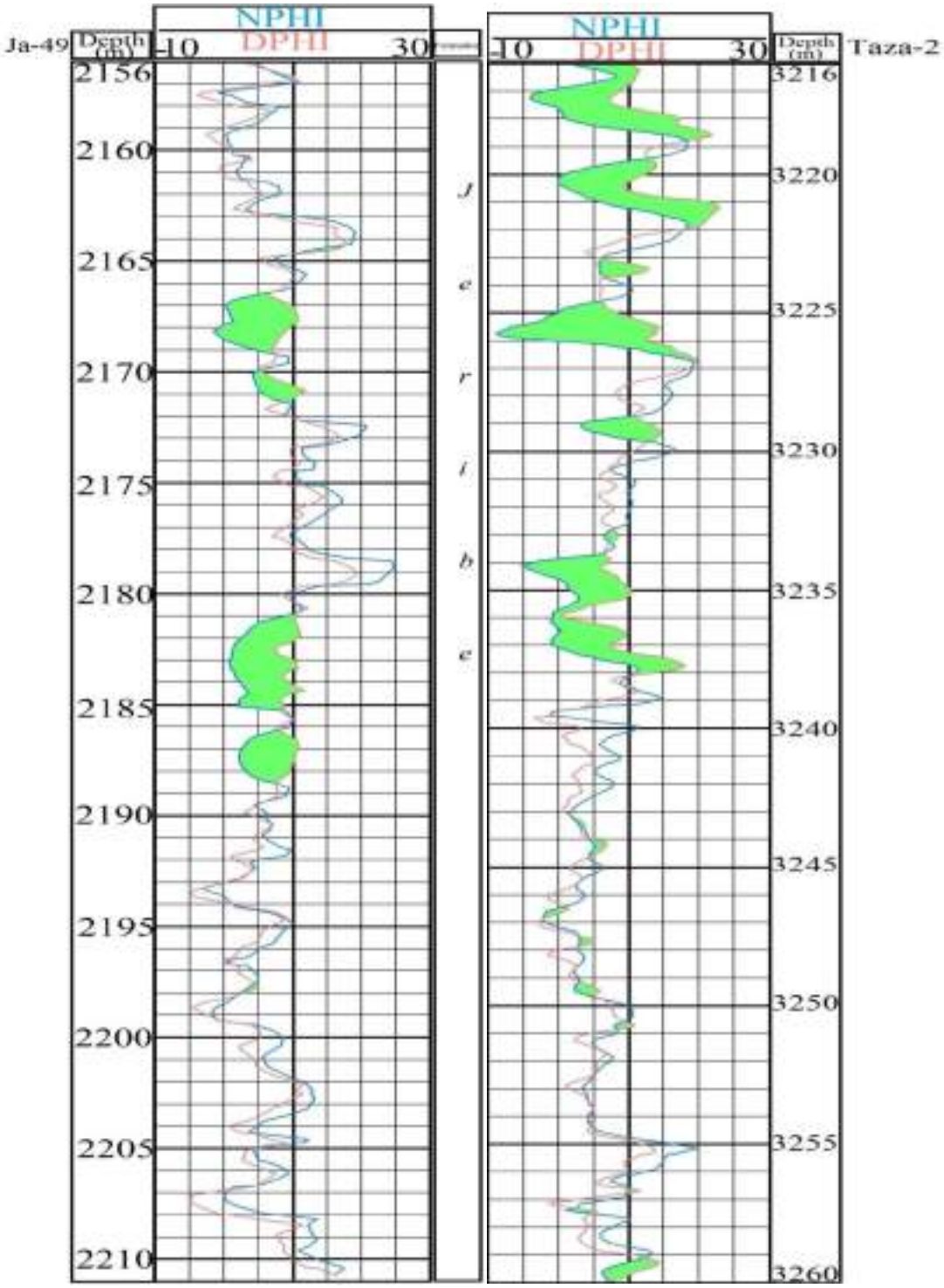

Figure 3.10: Crossover of Neutron and Density porosity curves as appeared in the studied Jeribe Formation in Ja-49 and Taza-2wells.

In predicting the permeability of reservoirs and hence the production capacity of reservoirs.

Data of well logging is helpful mainly in determining the permeable zones within wells without a direct measurement of permeability in millidarcies (except the newly developed NMR logging tools).

In this study, permeability data in millidarcies was available for Jeribe Formation in Taza-2 well through the analysis done for the 18m cored interval of the formation and through the NMR logging done for the whole formation in the well. There was no ability to obtain any kind of direct permeability measurements available for Jeribe Formation in the well Ja-49 either due to confidentiality or due to absence of such data.

Especially for the well Ja-49, traces for permeable zones tried to be followed through examining the helpful logging tools of Caliper (following mudcake formation) and SP (following highly deflected curve zones). The caliper data of Ja-49 well (Fig.3.15) showed no obvious mudcake formation along the section indicating to being the formation of no effective permeability. Even the SP records of the same section (Fig.3.16) showed no great deflection except few horizons in which the SP values exceeded 20millivolts.

Regarding Jeribe Formation in Taza-2 well, the upper part of the formation showed nearly continuous mudcake formation, whereas the lower part of the well appeared to be on gauge indicating to being this part mostly of hard and dense lithology with low permeability. The output of the SP log was of no great benefit in the well Taza-2 and that

due to the low or no deflection of the SP curve because of using salt water base mud during the drilling operation.

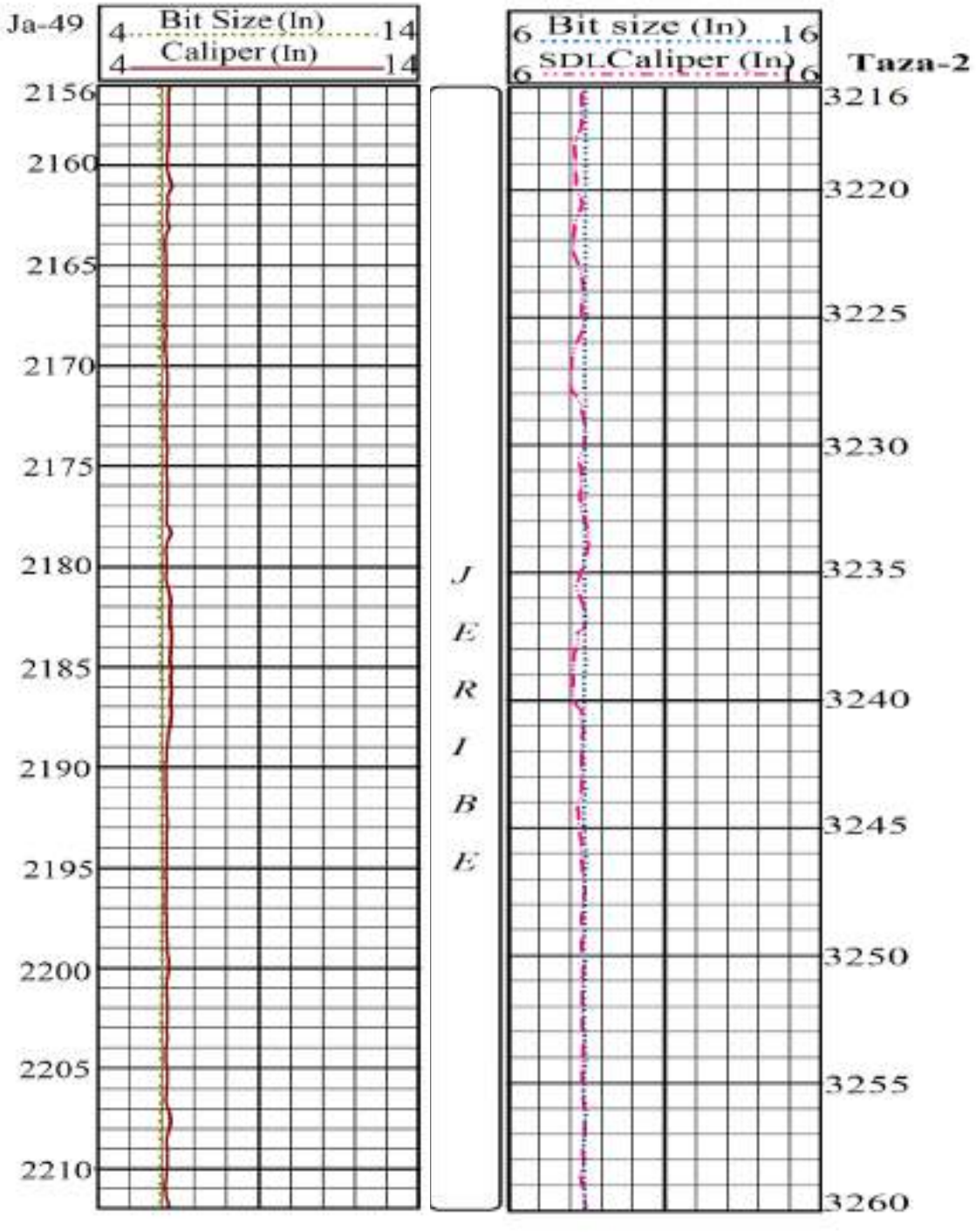

Figure 3.11: Caliper log plot for Jeribe Formation in the two studied wells of Ja-49 and Taza-2.

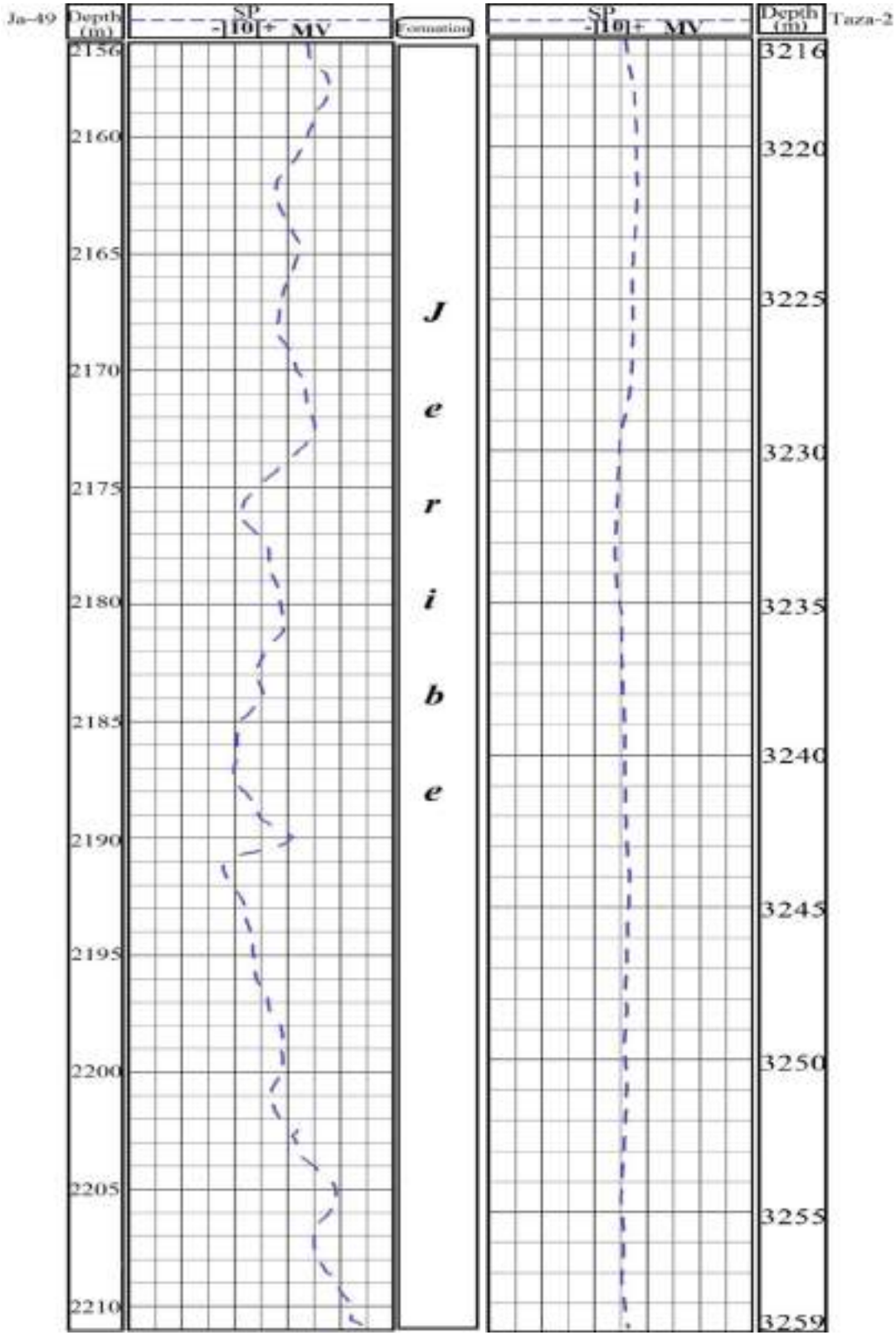

Figure 3.12: SP log plot for Jeribe Formation in both Ja-49 and Taza-2wells.

As an attempt to estimate the permeability of the Jeribe Formation (especially in Ja-49 well) the procedure of adapting the data of the core analysis (porosity and permeability) for measuring the permeability in the non-cored sections for achieving that goal, multilinear regression method was applied in order to formulate a general equation representing the relationship between the permeability values and the different log readings.

The mentioned procedure was applied on the core analysis data and log readings of Jeribe Formation in Taza-2 well and finally the Eq.3.16 formulized as the best representing the relationship between the permeability measured from the core analysis and the log readings at the same depths. (Mohaghehet al., 1997).

$$Log(K) = (-0.069*GR-19.998*\rho_b+0.11*Ø_N+0.31*\Delta_t) \text{ ……...Eq.3.16}$$

Where:

K: Permeability

GR: Gamma Ray

ρb: Bulk Density

ØN: Neutron Porosity

Δt: Interval Transit Time

After being sure that Eq.3.16 is mathematically the best achieved equation for representing the relationship between permeability and the log readings in the cored section of Taza-2 well (Fig.3.17). The same equation applied for calculating permeability in the parts above and below the cored section (non-cored intervals of Jeribe Formation). As there was no chance for formulating a separate equation by the same way for Jeribe Formation in Ja-49 well due to absence of core analysis

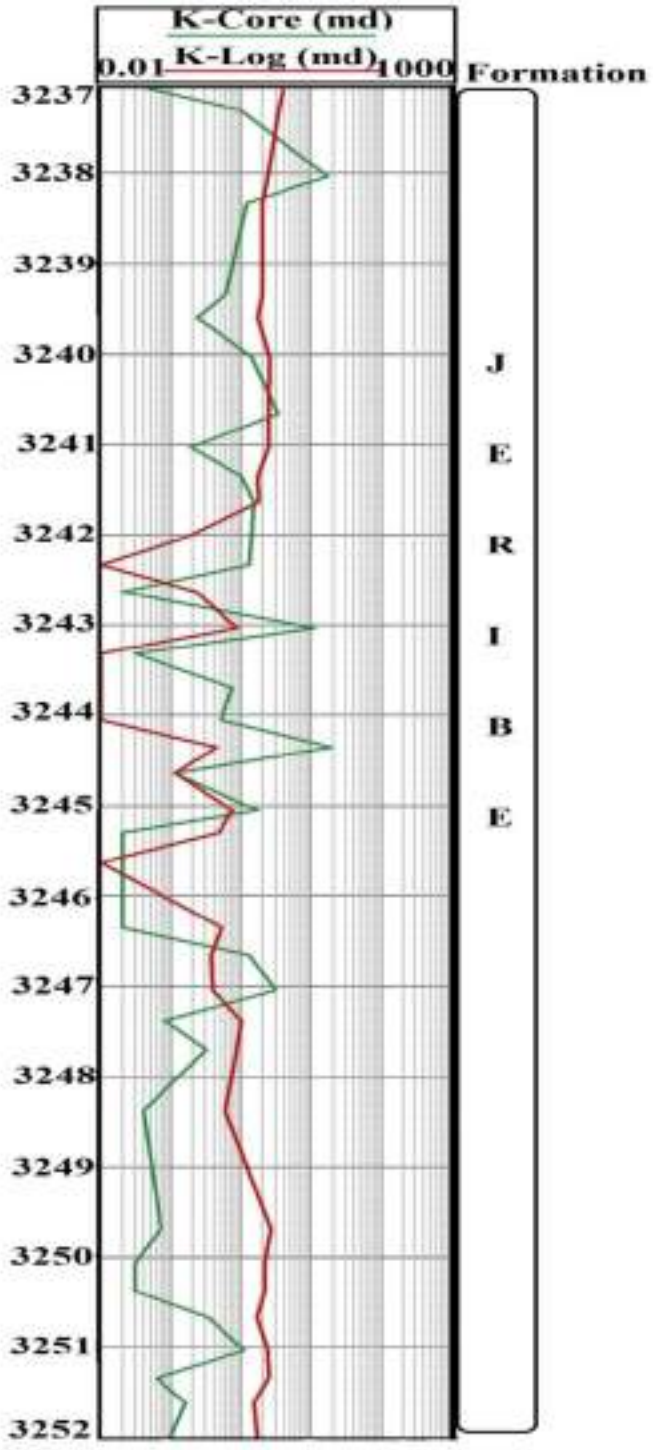

Figure 3.13: Measured permeability from core samples and calculated permeability from log data for the studied Jeribe Formation in Taza-2 well.

The Eq.3.16 applied again for calculating the permeability in Ja-49 well. Definitely, this is not the best way for calculating permeability for Jeribe Formation in Ja-49 well but it is the best which can be achieved in this study, especially the two studied wells are not greatly far from each other and no obvious differences observed in the lithology and microfacies of the Jeribe Formation in the two studied locations.

Finally, the calculated permeability values for Jeribe Formation in the two studied wells are listed in the appendix B and drawn as curves in the figure 3.18. For describing and evaluating permeability in this study qualitatively, the standard proposed by North (1985) (table 3.4) will be depended on.

The following are general notes about the permeability of Jeribe Formation as appears in the figure 3.18:

1. Jeribe Formation in the two studied wells is generally of low permeability (no permeability values higher than 20 millidarcies recorded in both wells). So generally the permeability ranges between poor to moderate permeabilities.
2. No noticeable differences in permeability exist in Jeribe Formation between the two studied wells except few narrow horizons in which lower permeability values calculated in Ja-49 well in comparison with Taza-2 well.
3. Few narrow horizons of permeability 0.0 recorded especially in Ja-49 well which expected to be anhydritic zones.

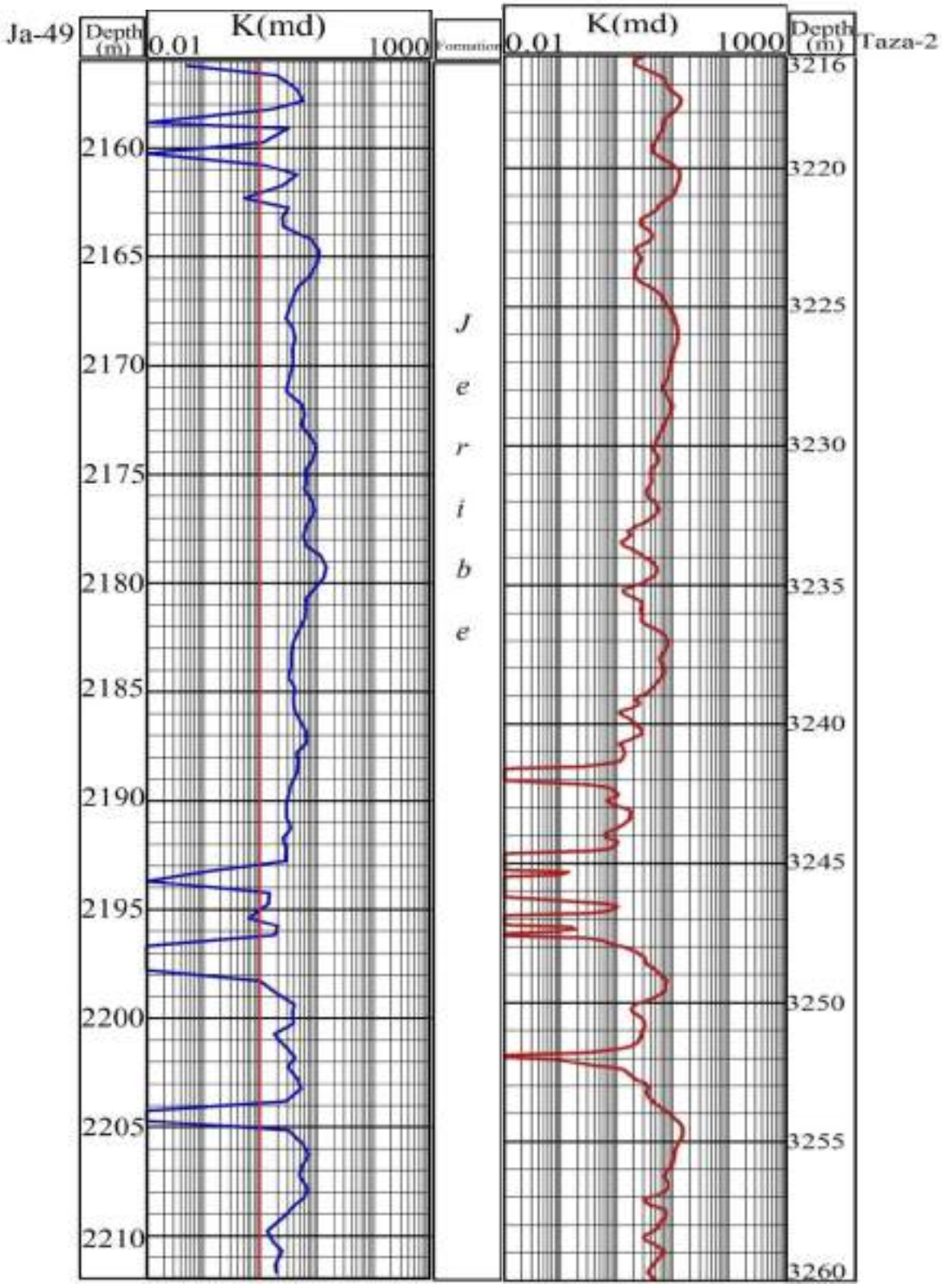

Figure 3.14: Calculated permeability from the log data for the Jeribe Formation in Ja-49 and Taza-2 wells.

Table 3.4: Qualitative description of permeability (after North, 1985)

Qualitative description	K- value (md)
Poor to Fair	1.0 – 15
Moderate	15 – 50
Good	50 – 250
Very good	250 – 1000
Excellent	>1000

3.11 Reservoir Units

In petroleum geology the term reservoir rock represents that element of petroleum system which offers the space for storing fluids. The storage capacity depends mainly on the properties of the grains which form the reservoir rock regarding their mineralogy, shape, size, sorting, and packing in addition to the nature of the cementing materials between the grains. The changes in depositional environment and the later diagenesis occurred (during or after burial) causes heterogeneities in the properties of the reservoir bed. All the mentioned properties have an impact on the porosity and permeability of the reservoir rocks and finally on the storage and production capacity of the reservoirs. Regardless the nature of the reservoired fluid, reservoir beds can be subdivided to units (either vertically or laterally) of different potentiality depending on the variations in the porosity and permeability with taking in consideration the shale content and distribution.

As shaleness, porosity, and permeability have been calculated for Jeribe Formation in the two studied wells, so subdividing the formation

to distinguishable reservoir units was easily done for the two wells of Ja-49 and Taza-2. Three reservoir units are distinguished in this study which nominated from the bottom of the formation to the top as RU-A, RU-B, and RU-C (Figs-3.19 and 3.20).

The tables 3.5 and 3.6 summarize the minimum, maximum, and average values of the mentioned parameters for the distinguished reservoir units of the studied formations and sections. The tables also show the depth interval of each unit within the studied wells.

From the mentioned figures and tables the following observations can be summerized:

1. Jeribe Formation in the two studied wells was subdivided to same number of reservoir units with nearly same reservoir properties.
2. RU-C has the highest thickness (35 and 26m in Ja-49 and Taza-2 respectively) and RU-B has the lowest thickness (about 6.0m in both wells).
3. RU-B is of lower reservoir potentiality, whereas the two units of RU-A and RU-C are nearly of similar reservoir potentiality except the previously detected secondary porosity are concentrated in the RU-C more than RU-A.

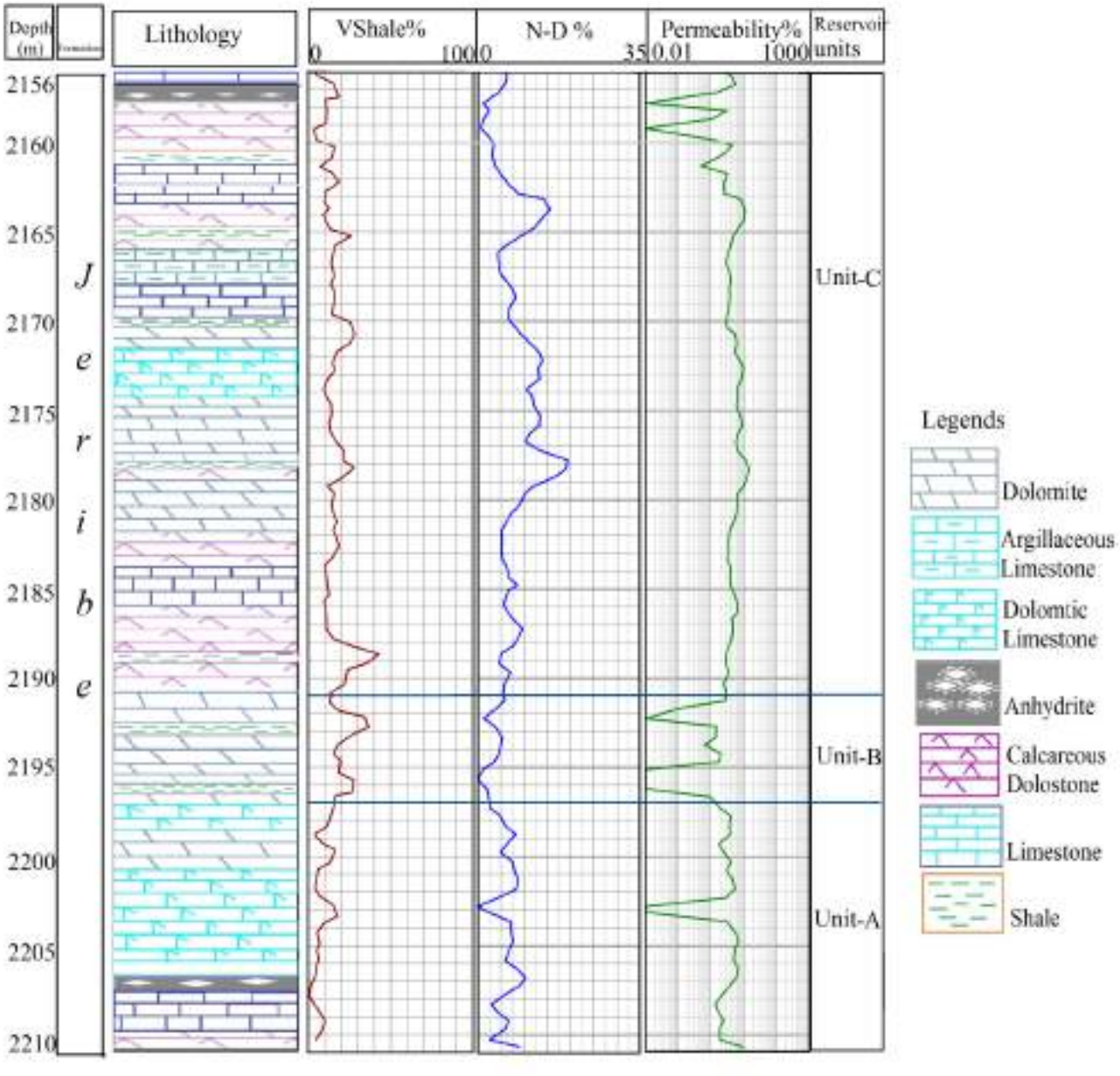

Figure 3.15: Subdivision of the Jeribe Formation into reservoir units on the bases of the porosity, permeability, and volume of the shale in Ja-49well.

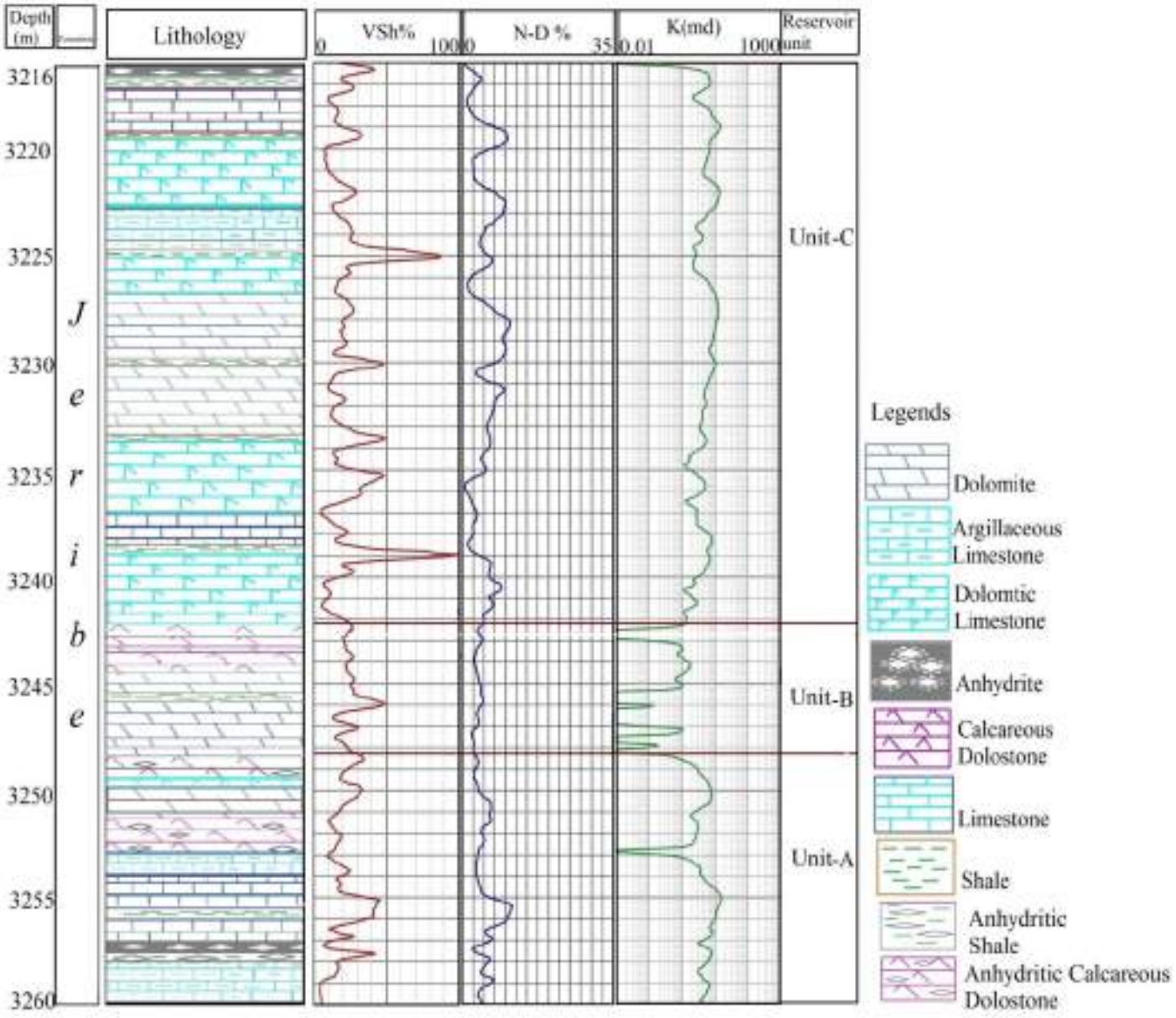

Figure 3.16: Subdivision of the Jeribe Formation into reservoir units on the bases of the porosity, permeability, and volume of the shale in Taza-2 well.

Table3.5: Minimum, maximum, and average values of the porosity,permeability, and shale volume for the distinguished reservoir units for Ja-49well.

Units	Interval (m)	Statistics	Vsh (%)	Porosity (%)	Permeability (md)
Unit C	2156-2191	Min.	1.36	0.73	0.51
		Max.	42.56	19.25	14.35
		Average	15.13	8.16	5.12
Unit B	2191-2197	Min.	14.89	1.14	0.11
		Max.	36.43	5.36	2.01
		Average	22.57	3.23	1.27
Unit A	2197-2011	Min.	0.29	0.28	1.31
		Max.	17.36	10.24	9.21
		Average	7.15	6.35	4.07

Table3.6: Minimum, maximum, and average values of the porosity, permeability, and shale volume for the distinguished reservoir units for Taza-2well.

Units	Interval (m)	Statistics	Vsh (%)	Porosity (%)	Permeability (md)
Unit C	3216-3242	Min.	5.58	0.68	0.05
		Max.	87.63	10.99	13.84
		Average	23.28	5.84	5.58
Unit B	3242-3248	Min.	13.88	2.37	0.04
		Max.	49.16	4.84	1.796
		Average	25.98	3.51	0.82
Unit A	3248- 3260	Min.	5.04	2.32	0.07
		Max.	45.73	11.43	14.93
		Average	21.34	5.23	5.4

CHAPTER FOUR

Saturation and Reservoir Characterization

4.1 Preface

The resistivities of sedimentary rocks are determined by the rock component types and their geometry. The common reservoir framework minerals of quartz, calcite and dolomite can be considered essentially as insulators. The same is true for hydrocarbons in the pore space. The fact that resistivities can be logged in sedimentary rocks is principally due to the conductivities associated with the formation water brine and the cation-exchange capacity of clay minerals within the shales (Doveton, 1994).

When a formation is porous and contains hydrocarbons the overall resistivity will be high. If the same formation contains salt water the resistivity will be low. Depending on this fact, resistivity logs can be used in distinguishing between water bearing and hydrocarbon bearing zones. Additionally, details can be obtained from the data of the resistivity logs about the rate of saturations for the different fluids in the reservoirs and their movability. Such information about the reservoir's fluid content with the petrophysical properties of the reservoir are vital in determining the net to gross reservoir and pay ratios and hence the production capacity of the reservoir.

In this chapter the obtained resistivity log data and the previously determined petrophysical properties, will be used to characterize Jeribe Formation in the studied Ja-49 and Taza-2 wells and evaluate its production capacity.

4.2 Resistivity Logs

The resistivity is the resistance to an electrical current flowage; a resistivity of formation is ability of its constituents to transmit electricity (Rider, 2002).

The conventional resistivity parameters needed to detect the presence of hydrocarbons in reservoirs, such as resistivity of the flushed zone (Rxo) and resistivity of the transition zone (Ri) (which both are related to the invaded zone). In addition to the true resistivity of the uninvaded zone (Rt). The mentioned resistivity values have been obtained for Jeribe Formation in both studied wells through the records of the Micro Spherically Focused Log (MSFL), Shallow Latero Log (LLS), and Deep Latero Log (LLD) tools, respectively.

The records of Rxo, Ri, and Rt are listed in the appendix A and shown as plotted curves together by figure 4.1 for both studied wells.

The way by which the resistivity curves are interpreted and defining high or low values are important for determining the hydrocarbon bearing zones. In such a process attention should be paid for the nature of the used drilling mud as the resistivity of the mud filtrate (Rmf) has a great impact on interpretation of the resistivity output.

Preliminarily, the following notes can be observed through examination of the resistivity record of Jeribe Formation in Ja-49 and Taza-2 wells (Fig.4.1):

1. No separation between the curves of Rxo, Ri, and Rt is an obvious feature in Ja-49 well indicating to possible existence of hydrocarbon filled porosities (fresh water base mud used in drilling this well).

2. In contrast to Ja-49 well, separation between the three curves in Taza-2 well is more noticeable with being the Rxo of the lowest resistivity value due to using salt mud during drilling the well (low Rmf value). So, such a condition also indicates to possible existence of hydrocarbon bearing zone.
3. In the zones where separation occurs between the three curves in Ja-49 well with being the Rt of the lowest value, such conditions indicate to water bearing zones or high water saturation zones (e.g. depths 2176 and 2191.5m).
4. Non separation between the three curves in the well Taza-2 indicates to possible water bearing zones or high water saturation zone (eg. depths 3228.5, 3248, and 3256m).
5. When the values of the three curves together are increasing or decreasing that is due to either decreasing and increasing porosity respectively or due to increasing or decreasing the density of the matrix respectively (change in lithology). For example, at the depth 2334m in Taza-2 well the increasing in the resistivity values of the three curves with remaining separation between them is due to being a hydrocarbon bearing zone with low porosity, whereas decreasing the resistivity of the three curves without separation between them in the depth 2178m in Ja-49 well is an indication to a hydrocarbon bearing zone with high porosity

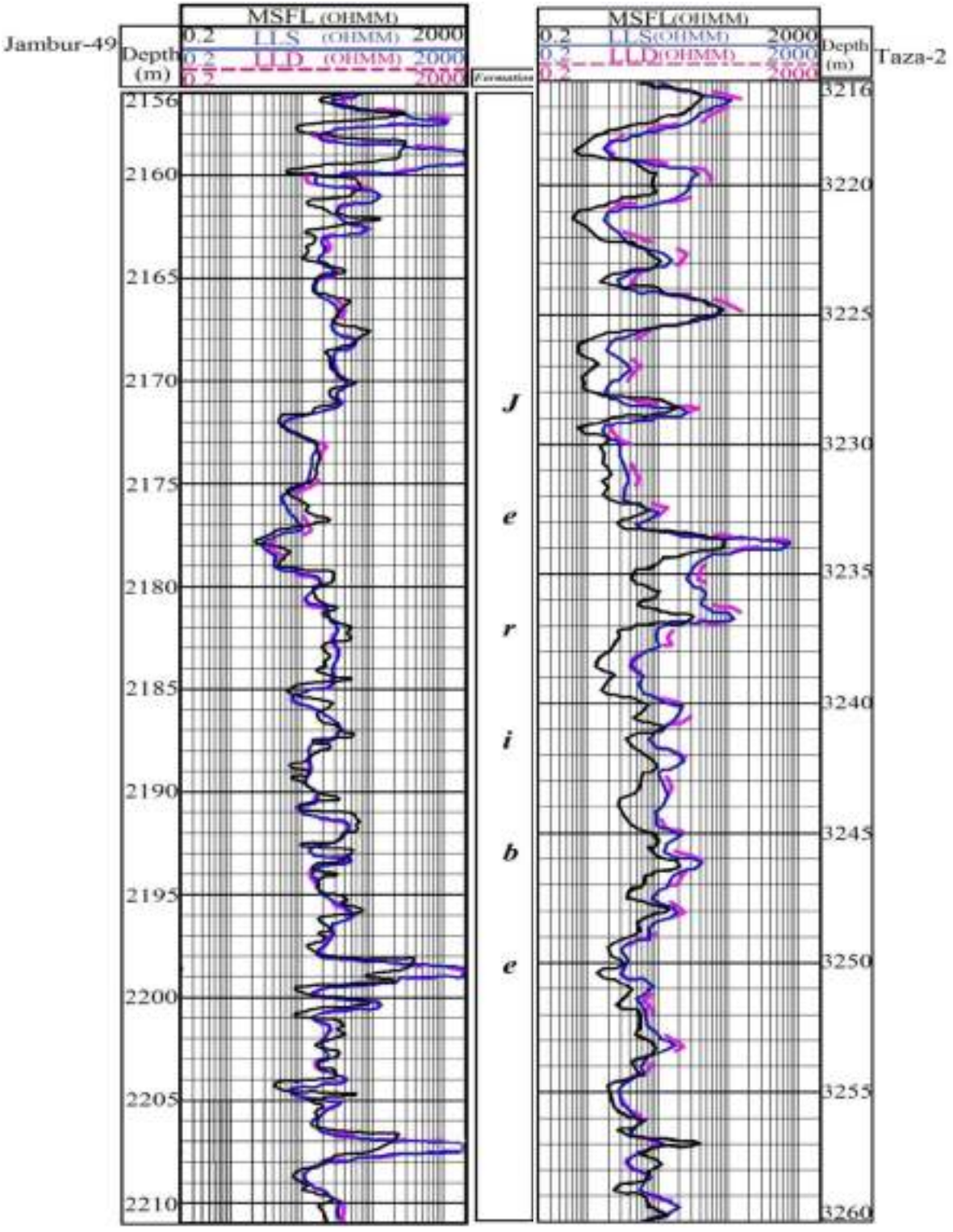

Figure 4.1: LLD, LLS, and MSFL log records for Jeribe Formation in Ja-49 and Taza-2wells.

6. The noticeable increase in the Rt and Ri values at depths 2159, 2199, and 2207m is due to being the zone composed of anhydrite or of anhydritic lithology (high density lithology).

Determining water or hydrocarbon bearing zones using resistivity logs without calculating the saturations of the water or the hydrocarbon consider as incomplete reservoir productivity evaluation process. The equation proposed by Archie (1942; in Asquith and Gibson, 1982) (Eq.4.1) is the most popular equation used by reservoir analysts for calculating water saturations.

$$S_W = \sqrt[n]{\frac{F.Rw}{Rt}} \ldots\ldots\ldots\ldots\ldots\ldots\ldots\ldots \text{Eq. 4.1}$$

Where:

Sw = Water saturation in uninvaded zone

n = Saturation exponent (assumed to be equal to 2.0)

F = Formation resistivity factor

Rw = Resistivity of formation water at formation temperature

Rt = True resistivity of the formation (uninvaded zone)

The same is true with calculating water saturation in the invaded zone of the reservoir based on Archie's assumption also using the Eq.4.2.

$$S_{xo} = \sqrt[n]{\frac{F.Rmf}{Rxo}} \ldots\ldots\ldots\ldots\ldots\ldots\ldots\ldots \text{Eq. 4.2}$$

Where:

Sxo = Water saturation in the invaded zone

n = Saturation exponent (varies from 1.8 to 2.5 but normally equal to 2.0)

F = Formation resistivity factor

Rmf = Resistivity of mud filtrate at formation temperature

Rxo = Resistivity of the flushed zone (shallow resistivity)

Formation resistivity factor (F) in both equations can be related to porosity and expressed by the equation Eq.4.3 as follows:

$F = \sqrt[n]{\frac{a}{\emptyset^m}}$.....Eq.4.3

Where:

F = Formation resistivity factor

n = Saturation exponent (varies from 1.8 to 2.5 but normally equal to 2.0)

a = Tortuosity factor (1.0 for carbonates)

Ø = Porosity

m= Cementation exponent

All the needed factors for calculating water saturations in the invaded and uninvaded zones can be obtained either from known standards (eg. a and n factors) or by logging tools (eg. Ø, Rxo, and Rt) or should be measured or calculated by following certain procedures (e.g. Rmf, m, and Rw).

4.3 Calculation of the Formation Water Resistivity (Rw)

Formation water resistivity (Rw) represents the resistivity value of the water uncontaminated by drilling mud, which saturates the porous formation. Rw can vary widely from well to well in some reservoirs because parameters that affect it include salinity, temperature, fresh water invasion, and changing depositional environment. It is also referred to as connate water or interstitial water.

The sources for Rw are either from catalogs for Rw values for different formations in different oil fields published by oil companies or through

conventional methods for measuring Rw value such as direct measuring of the Rw of sampled reservoir water or through log data especially data of SP log.

As mentioned by Salazar (2007) direct measurement of water resistivity is difficult because fluid samples taken by fluid acquisition tools from the reservoir are often contaminated with mud-filtrate and/or hydrocarbon. In addition to the difficulty in acquiring connate water samples when wells are already in production and water-injection/steam-flood have been applied to enhance production.

In this study, the value of Rw has been measured for the connate water in Jeribe Formation through the data of the SP log for both studied wells. The procedure of calculating Rw from the SP log data has been mentioned in different literatures either through following pure mathematical method or by using special charts. Table 4.1 summarizes the steps for calculating Rw value from data of SP log mathematically. It also considered as synonym for using the special charts for calculating Rw from SP log data, the procedure that has been followed in this study.

Table 4.2 contains the values of the needed factors and parameters for calculating the Rw value in this study which appeared to be 0.18 and 0.05Ωm for Ja-49 and Taza-2 wells, respectively.

4.4 Determination of Cementation Exponent (m)

The calculation of water saturation from resistivity logs requires the determination of cementation factor (m) (which represents the pore system tortuosity) used in Archie's equation. The parameter "m" has levels of variability, especially in heterogeneous reservoirs. Inaccurate estimates of m can cause significant errors in the calculation of water saturation by using

Archie's equation, the difference between log interpretation and production test results have spotted (Rahimi, 2008).

Table 4.1: Mathematical Calculation of Rw from SP, for temperatures in °F (after Western Atlas Logging Services, 1985; in Asquith and Krygowski, 2004)

Identify a zone on the logs that is clean, wet, and permeable. Pick the maximum value for SP in the zone.	
Calculate formation temperature at the depth of the SP value. $AMST$ = Annual Mean Surface Temperature BHT = Bottom Hole Temperature FD = Formation Depth T_f = formation temperature	$T_f = \left(\frac{BHT - AMST}{TD} \times FD\right) + AMST$
Convert R_{mf} from surface (measured) temperature to formation temperature. R_{mf} = R_{mf} at formation temperature R_{mfsurf} = R_{mf} at measured temperature T_{surf} = Measured temperature of R_{mf}	$R_{mf} = \frac{R_{mfsurf}\left(T_{surf} + 6.77\right)}{T_f + 6.77}$
Find the equivalent formation water resistivity, R_{we}, from the SP and R_{mf}. R_{we} = equivalent R_w	$R_{we} = R_{mf} \times 10^{SP/(61+0.133\,BHT)}$
Convert R_{we} to R_w (this value is at formation temperature).	$R_w = \frac{R_{we} + 0.131 \times 10^{\left(\frac{1}{\log(BHT/19.5)}\right)^{1.2}}}{-0.5 \times R_{we} + 10^{\left(\frac{0.0123}{\log(BHT/50.8)}\right)}}$

Table 4.2: Calculated Rw and other parameters for the studied Jeribe Formation in Ja-49 and Taza-2 wells.

Well	SP (mv)	BHT	Rmf @Tm	Rmf @ Tf	Rw (Ωm)
Ja-49	30 @ 2187m	91.6°C @ 2300m	0.462 Ωm @ 55.5°C	0.31 Ωm @ 87.3°C	0.18
Taza-2	9 @ 3233m	108 °C @ 3317m	0.190 Ωm @ 24.0°C	0.06 Ωm @ 105°C	0.05

The value of cementation exponent increases as the degree of connectedness of the pore network diminishes (Tiab and Donaldson, 2004). The cementation exponent does not appear to be related to grain-size, but is controlled by grain shape. Jackson and others (1978;in Doveton,1994) found that the "m" value increased in grain packs as shapes became progressively less spherical. Mendelson and Cohen (1982; in Doveton, 1994) observed that the "m" value was lowest when grains had the same shape and orientation. Generally, the value of "m" ranges between 1.0 and 5.0 and the calculated "Sw" with Archie's equations are highly affected by this level of variability in "m". If fracture is the type of porosity present in the system, the value of "m" will be less than 2.0 and could approach the value of 1.0. If intergranular is the type of porosity in the system the value of "m" is 2.0, whereas in the case of being the system of vugular porosity, the value of "m" becomes much greater than 2.0 (Soto et al., 2011).

There is more than one way for calculating the value of cementation exponent. A value of "m" can be calculated for a core sample, based on laboratory measurements, or from a zone in a well, based on log

measurements of resistivity and porosity, using a transformation of the Archie equation to Eq.4.4 (Doveton, 1994).

$$m = \frac{\log(\frac{Rw}{Rt})}{\log(\emptyset)} \text{.....Eq.4.4}$$

Pickett plot considers as a graphical solution of the Archie's equation by which values of both "Rw" and "m" can be estimated.

The technique of using Pickett plot for estimating the value of "m" needs data of true resistivity (Rt) and porosity (Ø) for certain depths in the reservoir to be plotted on a log-log paper of two or three cycles. The value of the formation water resistivity (Rw) in this technique plays an important role as it determines the resistivity at point of 100% porosity from which the best line connecting between the sample points of the lowest "Rt" values start. Such lowest "Rt" values are more likely to be representing wet resistivity (Ro) (resistivity of the water bearing zones in the reservoir). Accordingly, the slope of the drawn mentioned line will represent cementation exponent (m).

In this study, "m" factor has been calculated for Jeribe Formation in the two wells separately using the mentioned Pickett plot technique as shown in the figures 4.2 and 4.3. As appears from the two mentioned figures, the estimated values for the "m" factor for Jeribe Formation in Ja-49 well is 1.38 and in the well Taza-2 is 1.3. According to Schlumberger (2009) (Fig.4.4) such values reflect contribution of fracture porosity by less than 2% of the total porosity.

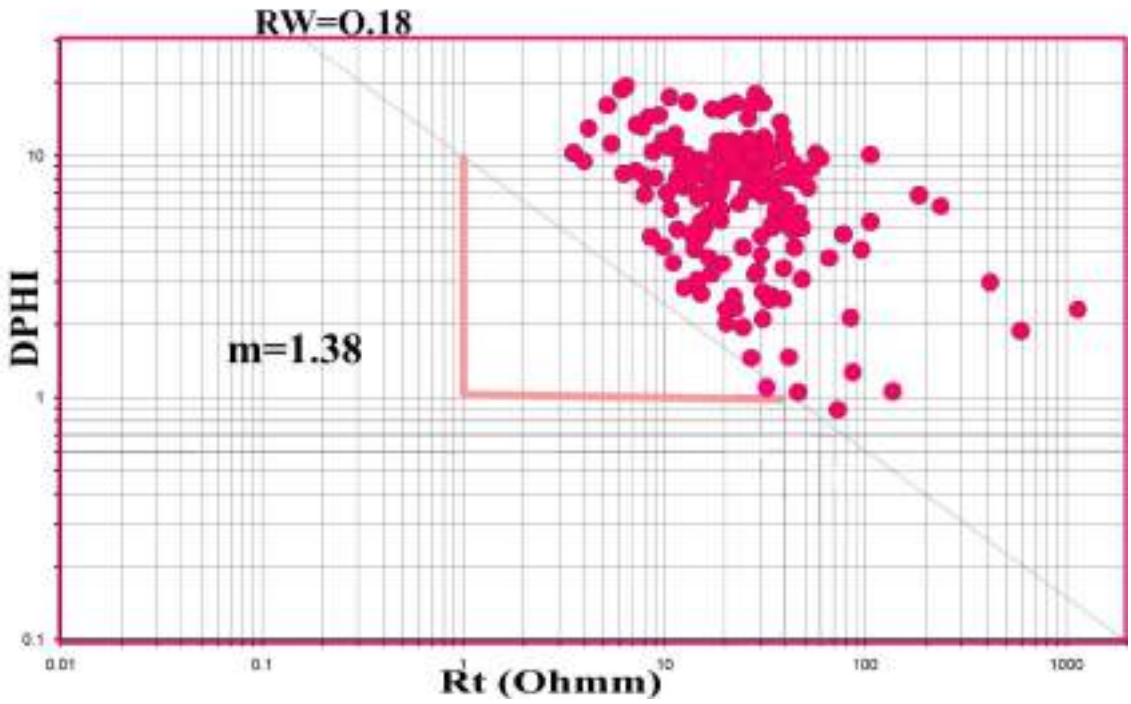

Figure 4.2: Cementation exponent factor (m) from as estimated from Pickett plot for Jeribe Formation in Ja-49well.

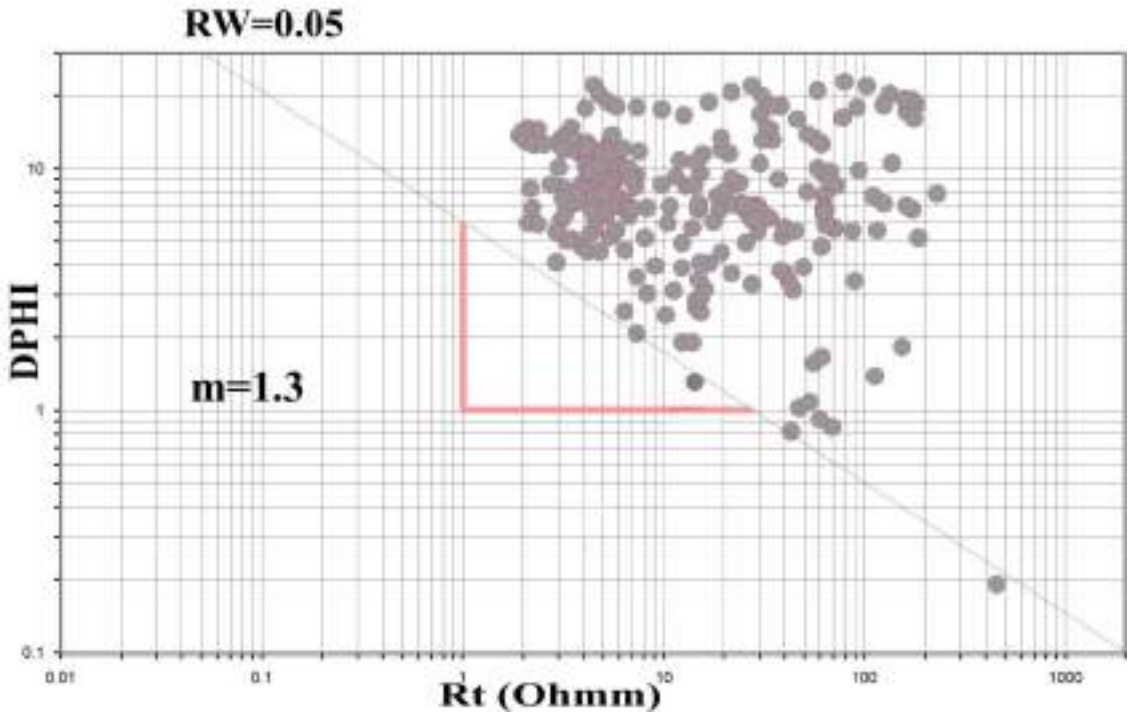

Figure 4.3: Cementation exponent factor (m) from as estimated from Pickett plot for Jeribe Formation in Taza-2well.

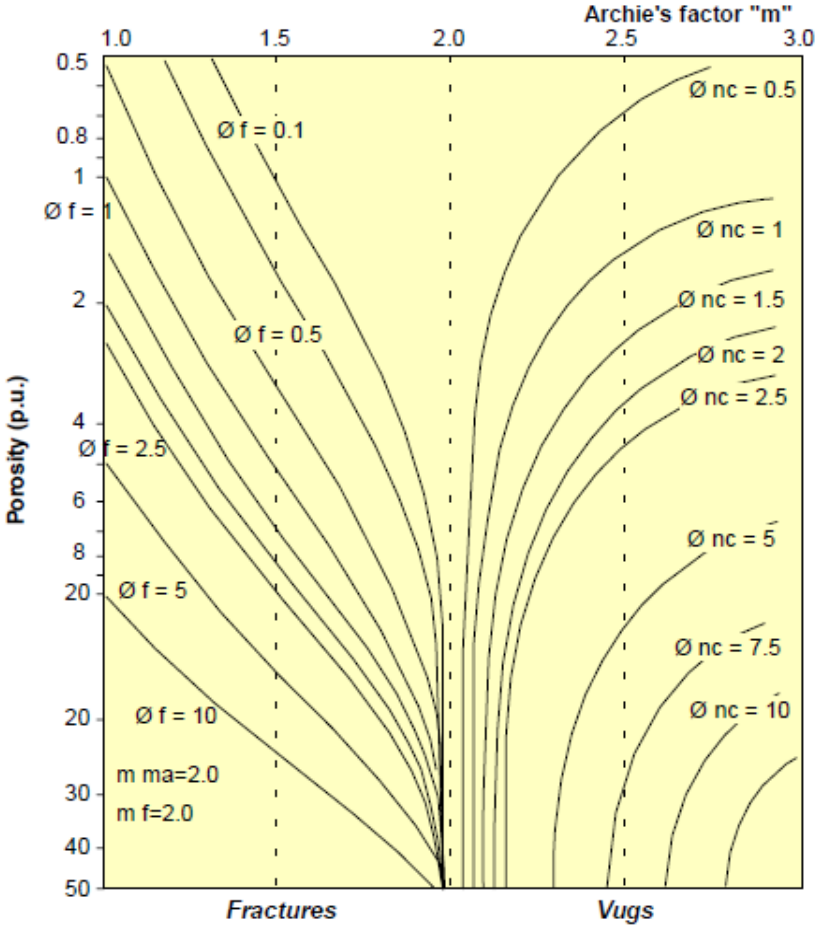

Figure 4.4, Effects of fractures and vugs on Archie's m factor (after Schlumberger, 2009)

4.5 Water Saturation Calculation

Water saturation is the ratio of water volume to pore volume in a rock (Eq.4.5). It is represented as a decimal fraction or as a percentage and has the symbol "Sw" (Asquith and Krygowski, 2004).

$$\text{Water saturation, Sw} = \frac{\text{formation water occupying pores}}{\text{total pore space in the rock}} \ldots\ldots\ldots\ldots \text{Eq. 4.5}$$

It is well known that in any hydrocarbon bearing reservoir the total fluid saturations can be represented as:

Sw + So + Sg = 100% (1.0) Eq.4.6

Zero percentage oil or gas saturation is a common case in water bearing reservoirs but no hydrocarbon bearing reservoirs can be found with zero percentage water saturation because always some water remain in the small capillaries of the reservoir rocks even after full hydrocarbon entrapment. Such remained water within the hydrocarbon occupied reservoir is expressed as irreducible water saturation (S_{wirr}) and its value generally ranges between 5.0 and 40%.

In this study, the equations Eq.4.1 and Eq.4.2 are applied for calculating the water saturation in both uninvaded (Sw) and flushed zones (Sxo) of Jeribe Formation in the two studied wells of Ja-49 and Taza-2. The calculated Sw and Sxo values are listed in the appendix C.

Calculating water saturation is the main step for calculating hydrocarbon saturation (S_h) according to the simple equation of Eq.4.7.

$$S_h = 1.0 - S_w \quad \text{.....Eq.4.7}$$

As commonly not all the hydrocarbons in the reservoirs are movable, so calculating of the movable and residual hydrocarbon saturation (S_{hr}) are vital for best evaluating reserves and production capacity of the reservoirs. For calculating hydrocarbon saturation (Sh) according to the simple equation Eq.4.8 and Eq.9, respectively.

$$\text{Movable Hydrocarbon Saturation (MHS)} = S_{xo} - S_w \quad \text{…….Eq.4.8}$$

$$\text{Residual Hydrocarbon Saturation } (S_{hr}) = 1.0 - S_{xo} \quad \text{……..Eq.4.9}$$

Figure 4.5 shows the water and both residual and movable hydrocarbon saturations for Jeribe Formation in the studied wells of Ja-49 and Taza-2.

The following points can be noticed from the figure 4.5:

1. Jeribe Formation in both studied wells is almost completely contains hydrocarbons with different saturations.

2. RU-C contains the highest hydrocarbon saturation especially in Ja-49 well.
3. There are very narrow water bearing horizons of low porosities which appeared to be of no hydrocarbon saturation or of only residual hydrocarbon saturation (e.g. 2159, 2198, and 2208m in Ja-49; 3218, 3231, and 3236m in Taza-2).
4. Highest movable hydrocarbon saturation exists in those horizons where secondary porosity (fractures or vugs) recorded (e.g. 2163-2164m, 2170-2178m, and 2187-2190m in Ja-49 well; 3222-3223m, 3239-3241m, and 3251-3252m in Taza-2 well).

4.6 Quick Look Methods (QLM)

According to Asquith and Gibson (1982), Quick Look Methods (QLM) in log interpretation are helpful to the geologist because they provide *flags*, or indicators, that point to possible hydrocarbon zones requiring further investigation. The importance of QLM is in their ability to provide information about the nature of the fluids in the pore spaces and the lithology of the reservoirs in a quick and simple way.

Before water saturation is calculated for any zone, it is necessary to scan a log and locate favorable zones that warrant further investigation. This is true not only for potential hydrocarbon-bearing zones, but water-bearing zones as well. This is often referred to as "*scanilizing*" a log (HLS, 2007). There are certain responses that should be looked for, and these responses may indicate whether a zone is water-bearing or hydrocarbon bearing.

Generally, there are three branches for quick look analysis as mentioned by Bateman (1985) which are Compatible overlays of logs, Crossplot of

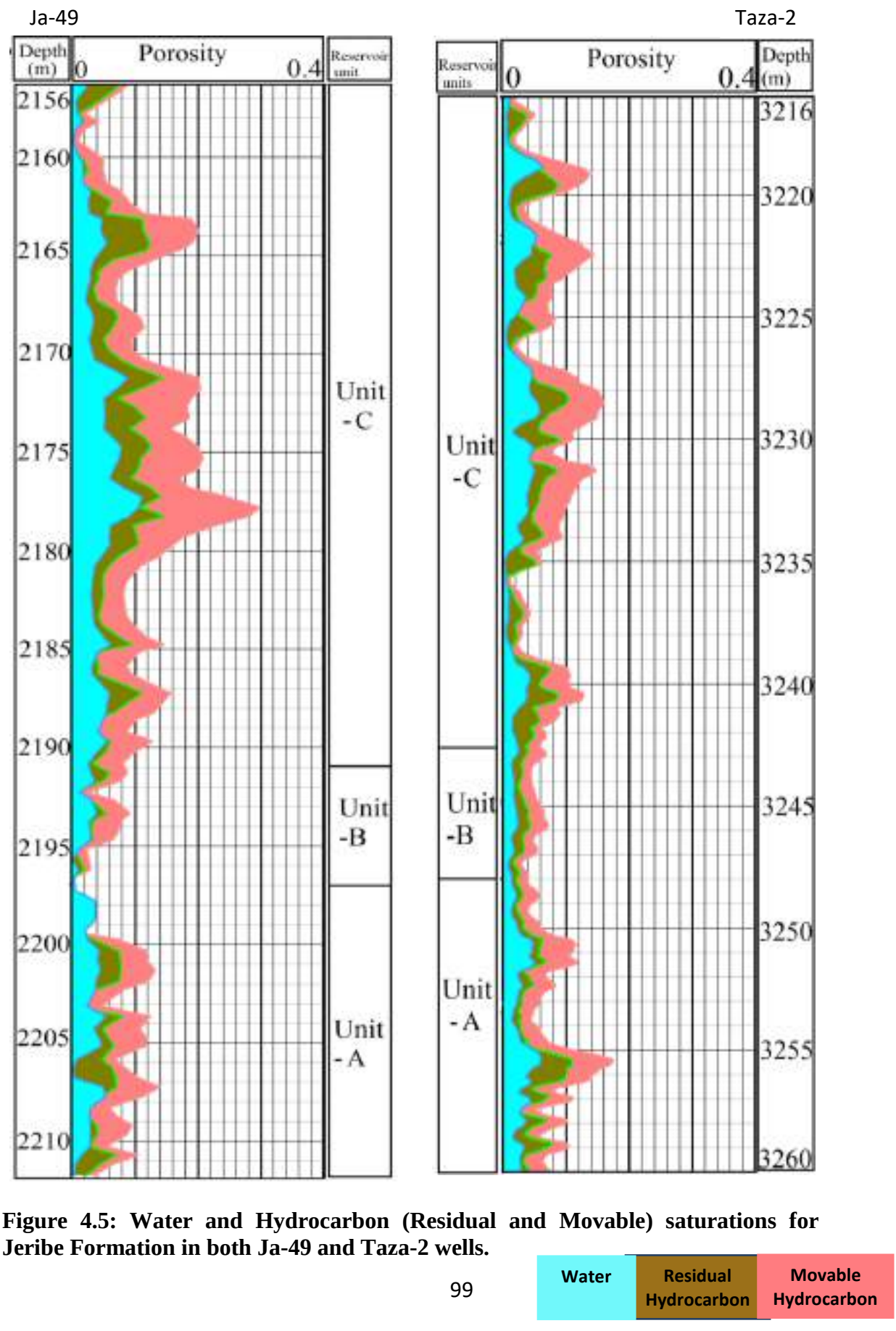

Figure 4.5: Water and Hydrocarbon (Residual and Movable) saturations for Jeribe Formation in both Ja-49 and Taza-2 wells.

selected log readings, and Simple algorithms for calculators. Figures 4.6 and 4.7 show application of two QLM techniques using resistivity log data of Jeribe Formation in the two studied wells, the mentioned techniques are Rwa method and Ro, Rxoo, and Rt compatible overlays methods.

4.6.1 Apparent Formation Water Resistivity (Rwa) method

This technique, as one of the quick look methods in log analysis, mentioned by different authors (Asquith and Gibson, 1982; Bateman, 1985; Schlumberger,1989, Asquith and Krygowski, 2004).

Based on Archie's assumption, the apparent formation water resistivity (Rwa) is equal to true resistivity (Rt) divided by formation factor (F). In any clean water bearing zone (Sw=100%) the wet resistivity (Ro) is equal to Rt and equal to F multiplied by Rw, in such a case also Rwa becomes equal to Rw. So, calculating Rwa along any reservoir aids in detecting water bearing zone by following the zones of the lowest computed Rwa values. In fact, zones of lowest Rwa values will represent either water bearing zone or zones of lowest hydrocarbon saturations. Accordingly, any increase in the Rwa values will positively proportion to the hydrocarbon saturation.

Through following the plotted curve of Rwa (Figs. 4.6 and 4.7) it is so easy to notice zones in which lowest recorded values of Rwa locate. Those zones are expected to be water bearing zones or zones with the lowest hydrocarbon saturation. Accordingly, zones with greater computed Rwa values are zones of higher hydrocarbon saturation.

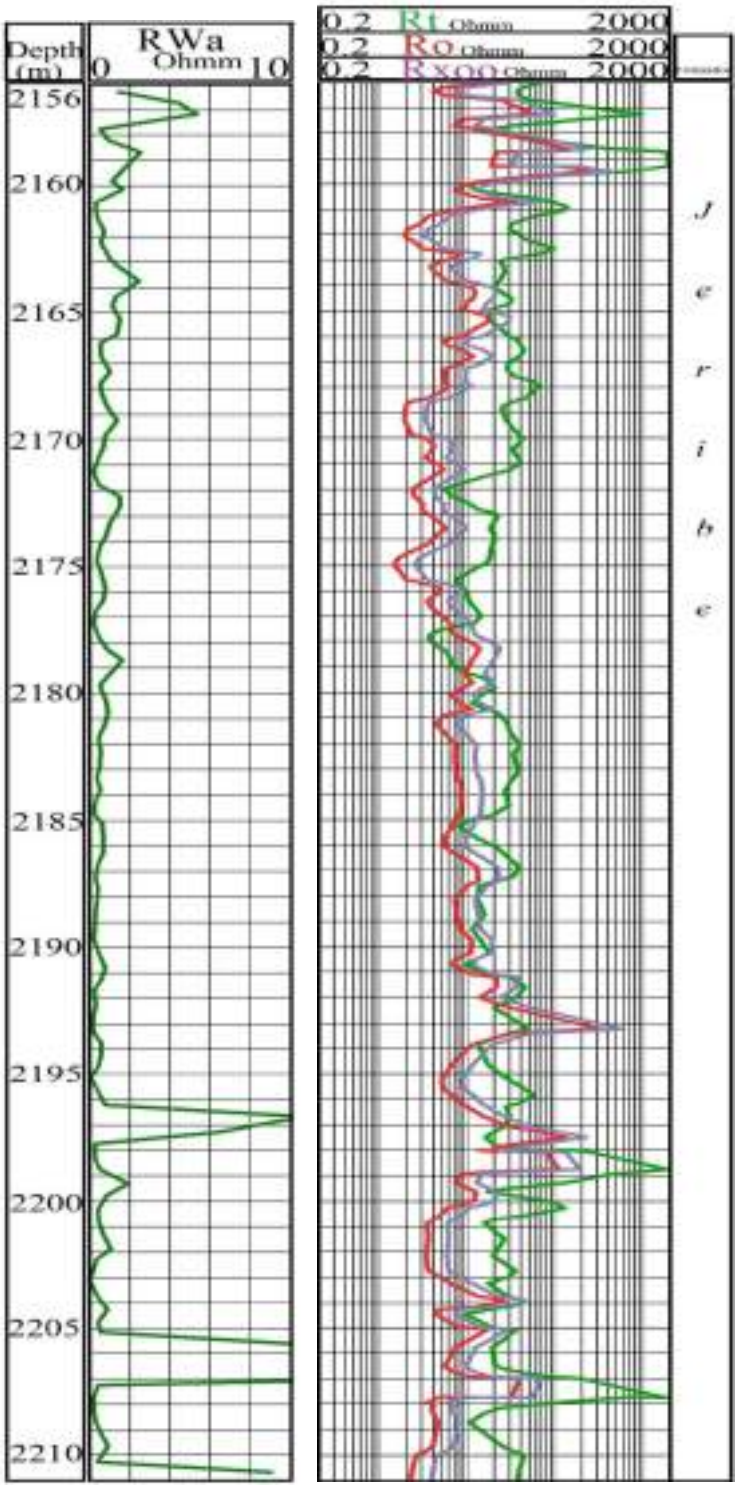

Figure 4.6: Rwa and Ro, Rxoo, and Rt presentation as QLM for determining water and hydrocarbon (residual and movable) bearing zones for Jeribe Formation in Ja-49 well.

4.6.2 Logarithmic Movable Oil Plot Method

In this technique of QLM three curves are plotted on a logarithmic scale and their overlays are followed to detect locations of the water or hydrocarbon bearing zones and also to detect roughly the ratio of the movable hydrocarbons. The needed curves for applying this technique are drawn from values of wet resistivity (Ro), resistivity of flushed zone full of mud filtrate (Rxoo), and true resistivity of the uninvaded zone (Rt) recorded, in this study, by the LLD logging tool.

For calculating Ro values, which is the resistivity of the water bearing uninvaded zone, the simple equation of Ro= F.Rw is applied, whereas F multiplied by Rmf used for calculating Rxoo. As shown in the figures 4.6 and 4.7, the Ro curve is mostly of the lower resistivity value due to being the reservoir water of saline nature and conductive. On the other hand, the Rt curve shows higher resistivity values in most of the zones and becomes close or of the same value with Ro in few zones.

As a QLM, any separation between the Ro and Rt curves is an indication to hydrocarbon bearing zones, whereas non separation cases are due to existance of water bearing zone. The space between the two curves is proportion to the ratio of the hydrocarbon saturation. The benefit of plotting Rxoo curve with the two curves of Ro and Rt is to show preliminarily the ratio between the residual and the movable hydrocarbons. The space between Ro and Rxoo represents the residual hydrocarbons, whereas the space between the Rxoo and Rt represents the movable hydrocarbons.

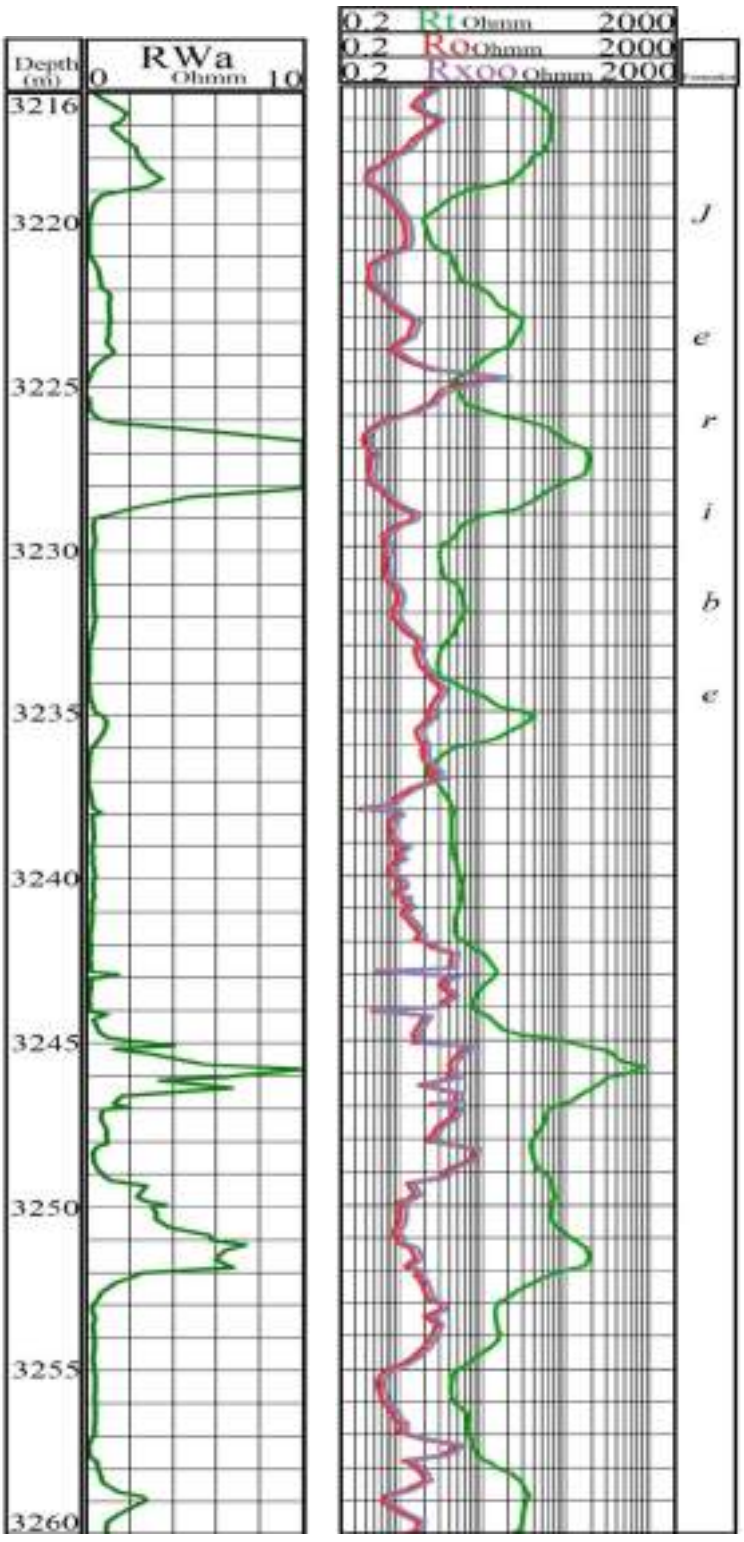

Figure 4.7: Rwa and Ro, Rxoo, and Rt presentation as QLM for determining water and hydrocarbon (residual and movable) bearing zones for Jeribe Formation in Taza-2well.

By comparing the two figures of 4.6 and 4.7 with the previously drawn 4.5 figure the following points can be observed:

1. Most but not all the depth intervals show the same result about the containing fluids and their relative saturations.
2. The separation between Ro and Rxoo in the well Taza-2 is so little due to being the resistivity of the formation water (Rw) and the resistivity of the mud filtrate (Rmf) after correction to formation temperature is very close (Rw=0.05, Rmf=0.06).
3. The intervals of high Rwa values showed high recorded Rt values (and vise versa) indicating to the workable of the Rwa technique in detecting hydrocarbon bearing zones in this study (e.g. depth intervals 2156-2158m in Ja-49 well; 3225-3230m in Taza-2 well).
4. Zones of high recorded Rt values are not necessarily zones of high hydrocarbon saturations. Zones of low porosity and zones of dense lithology both are showing high recorded Rt values.
5. The high difference between the resistivity of the formation water and the resistivity of hydrocarbons may result in high separation between the calculated Ro and the recorded Rt curves regardless to the water or hydrocarbon saturations ratio.

4.7 Nuclear Magnetic Resonance (NMR) Log:

Magnetic resonance imaging instruments are commonly used as diagnostic tools in medicine today, but nuclear magnetic resonance (NMR) is also extensively used by the oil industry in wireline logging, as part of its quest for permeability.

The first NMR logging tool was developed by Brown and Gamson of Chevron Research and the first log was run in 1960 (Akkurt et al, 2008).

4.7.1 Basics of NMR Logging

Before a formation is logged with an NMR tool, the protons in the formation fluids are randomly oriented. When the tool passes through the formation, the tool generates magnetic fields that activate those protons. First, the tool's permanent magnetic field aligns, or polarizes, the spin axes of the protons in a particular direction. Then the tool's oscillating field is applied to tip these protons away from their new equilibrium position. When the oscillating field is subsequently removed, the protons begin tipping back, or relaxing, toward the original direction in which the static magnetic field aligned them (Fukushima and Roeder, 1981 in Coates et al., 1999).

Specified pulse sequences are used to generate a series of so-called spin echoes, which are measured by the NMR logging tool and are displayed on logs as spin-echo trains (Coates et al., 1999).

NMR tool measures the amplitude of the spin echoes as a function of time. Because the spin echoes are measured over a short time, an NMR tool travels no more than a few inches in the well. The initial amplitude of the spin-echo train is proportional to the number of hydrogen nuclei associated with the fluids in the pore (Coates et al., 1999).

4.7.2 Important Parameters Measured During the NMR Logging

The following are the most important parameters that are measured by the NMR tool or calculated by the analysts during analyzing the output of the tool:

Longitudinal relaxation time (T1)*:* The time required to align the hydrogen nuclei along the direction of the applied magnetic field **(**Freedman and Heaton, 2004).

Wait time (Polarizing time) (Tw): The time that the hydrogen nuclei are exposed to the static magnetic field. During the wait time, the nuclear magnetization grows exponentially towards its equilibrium value (*M*o). The porosity and the types and volumes of fluids determine *Mo*. If too short a wait time is used, NMR total porosities will underestimate true formation porosities. Long wait times, and therefore, reduced logging speeds are required in formations containing low viscosity oil or gas **(**Freedman and Heaton, 2004).

Transverse relaxation times (T2): Times representing the rate of decay of the NMR signal. The wide range of decay times in sedimentary rocks is generally due to broad distributions of pore sizes (Fig.4.8). It is customary to fit the measured NMR signals to a sum of about 30 decaying single-exponential signals each with amplitude, *A*(*T*2), and associated decay time *T*2. For bulk crude oils, the *T*2 distribution reflects the molecular composition of the oil. That is, each *T*2 in the distribution is inversely proportional to a microscopic constituent viscosity of a particular constituent molecule (Freedman et al., 2001). The longer *T*2s in a crude oil *T*2 distribution correspond to signals from mobile molecules, whereas the short *T*2s are associated with signals from larger molecules (Fig.4.9) and by defining appropriate *T*2 cut-offs, the *T*2 distribution can be partitioned into bound water and free water **(**Freedman and Heaton, 2004) (Fig.4.10).

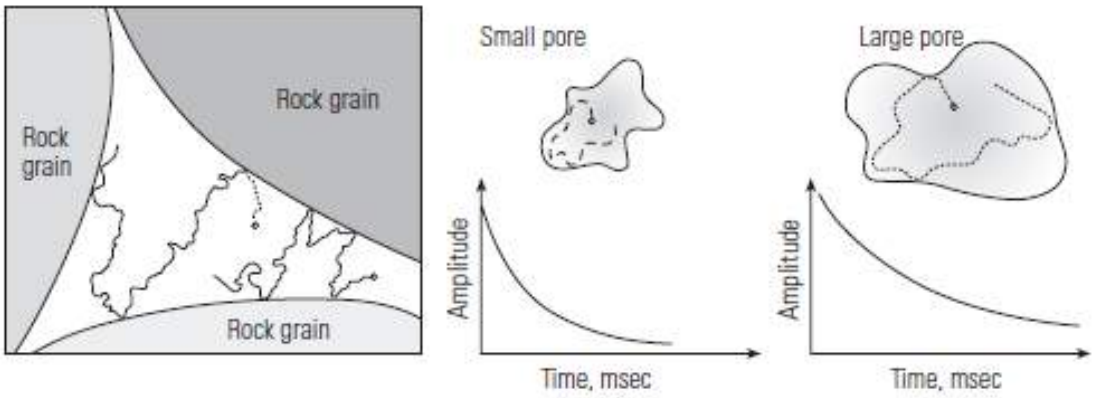

Figure 4.8: The notion of grain relaxation and the role of small and large pores in the decay time of the relaxation curve (after Ellis and Singer, 2008).

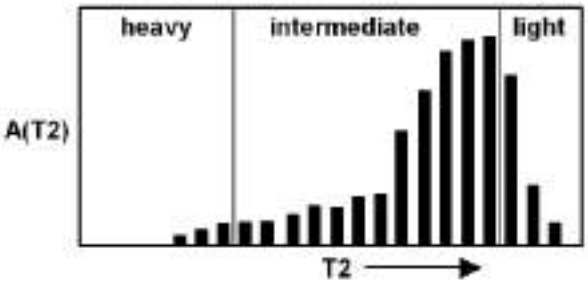

Figure 4.9: A plot of a typical *T*2 distribution of a bulk crude oil. The Broad distribution of *T*2 values reflects the broad distribution of Molecular sizes (after Freedman and Heaton, 2004).

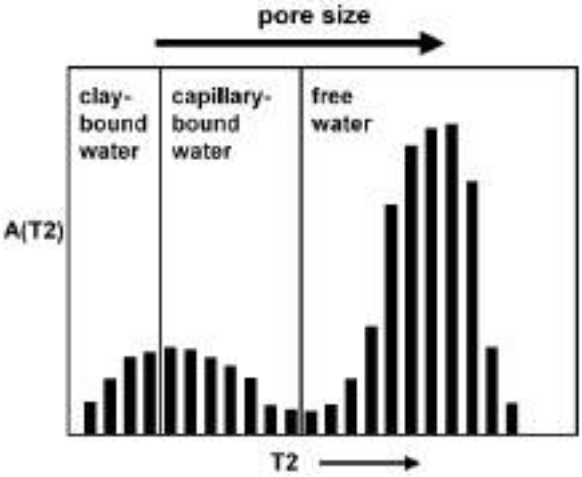

Figure 4.10: Schematic plot of a typical *T*2 distribution for a water-saturated rock. The distribution can be partitioned into free and bound water using empirically determined *T*2 cutoffs (after Freedman and Heaton, 2004).

Diffusion constant (D): is the molecular diffusion constant of the fluid molecule. Small lightweight molecules like methane and ethane are relatively mobile in the gas phase and have molecular diffusion coefficients (*D*) that are typically about an order of magnitude greater than those of water molecules (Freedman and Heaton, 2004). In contrast, intermediate- to high-viscosity crude oils have molecular diffusion coefficients that are much smaller than those of water (Fig.4.11).

Inter-echo spacing (TE): is the time between the individual echoes in an echo train (Coates et al., 1999).

Hydrogen Index (HI): is a measure of the density of hydrogen atoms in the fluid (Coates et al., 1999).

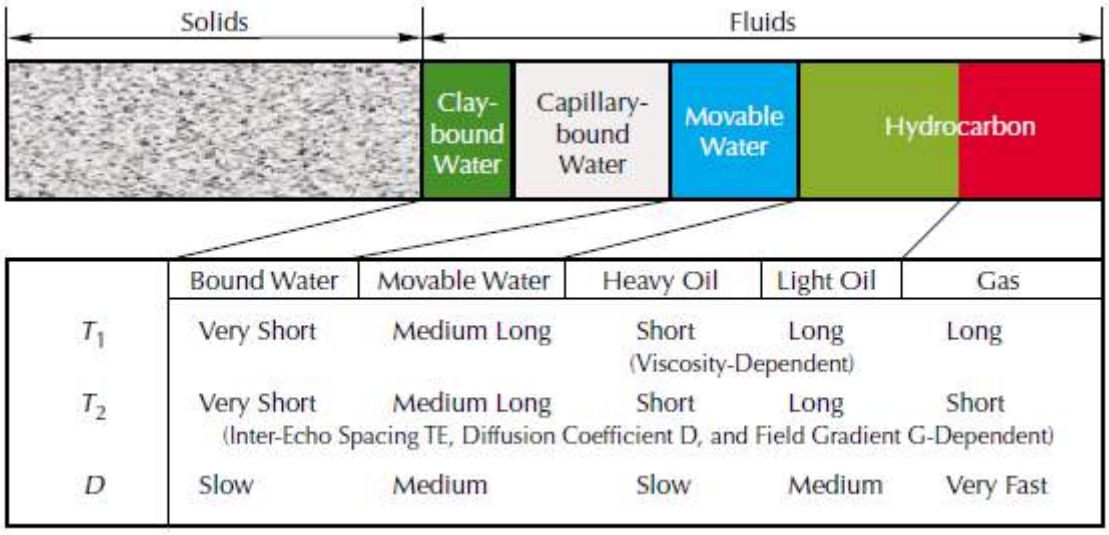

Figure 4.11: The typical qualitative values of T1, T2, and D for different fluid types and rock pore sizes demonstrate the variability and complexity of the T1 and T2 relaxation measurements (after Coates et al., 1999).

4.7.3 Magnetic Resonance Imaging Logging (MRIL):

Magnetic Resonance Imaging Logging (MRIL), introduced by NUMAR in 1991(Coates et al., 1999) and was the first commercial pulsed NMR tool. Permeability can be estimated for reservoirs by using this log in addition to its other applications such as getting information about:

- quantities of the fluids in the rock
- properties of these fluids
- free and bound fluid porosity
- sizes of the pores that contain these fluids

Earlier generation of NMR logging tools were unable to see water in the micro-pores, and because this water was associated most often with clays,

the porosity measured by these earlier tools was often characterized as being an "effective porosity." Whereas modern MRIL logging tools can see essentially all the fluids in the pore space, and the porosity measurement made by these tools is thus characterized as being a "total-porosity" measurement.

Many formulas are in use for determining permeability from NMR measurements. The two most commonly used are the Coates equation and the Schlumberger-Doll Research (SDR) equation According to the Coates equation,

$$K = [\frac{\Theta}{C}]^4[\frac{FFI}{BVI}]^2 \text{ ....……..Eq.4.10}$$

Where:

K = Permeability

Θ = Porosity

C = Variable that is dependent on the processes that created the formation

BVI = Bulk Volume Irreducible

FFI = Free Fluid Index (can be expressed as Θ – BVI)

4.7.4 MRIL of Jeribe Formation in Taza-2:

Figure 4.12 is the output of the MRIL done for Jeribe Formation in the Taza-2 well. The output includes information about the permeability along the formation and the ratio of the fluids within the micropores, as a bound fluid, and as free fluid within the total measured porosity. The T2 time as milliseconds with the logarithmic mean of the recorded T2 also plotted in the same column.

The permeability measured by the MRIL showed that most parts of the Jeribe Formation are of very low permeability (negligible permeability).

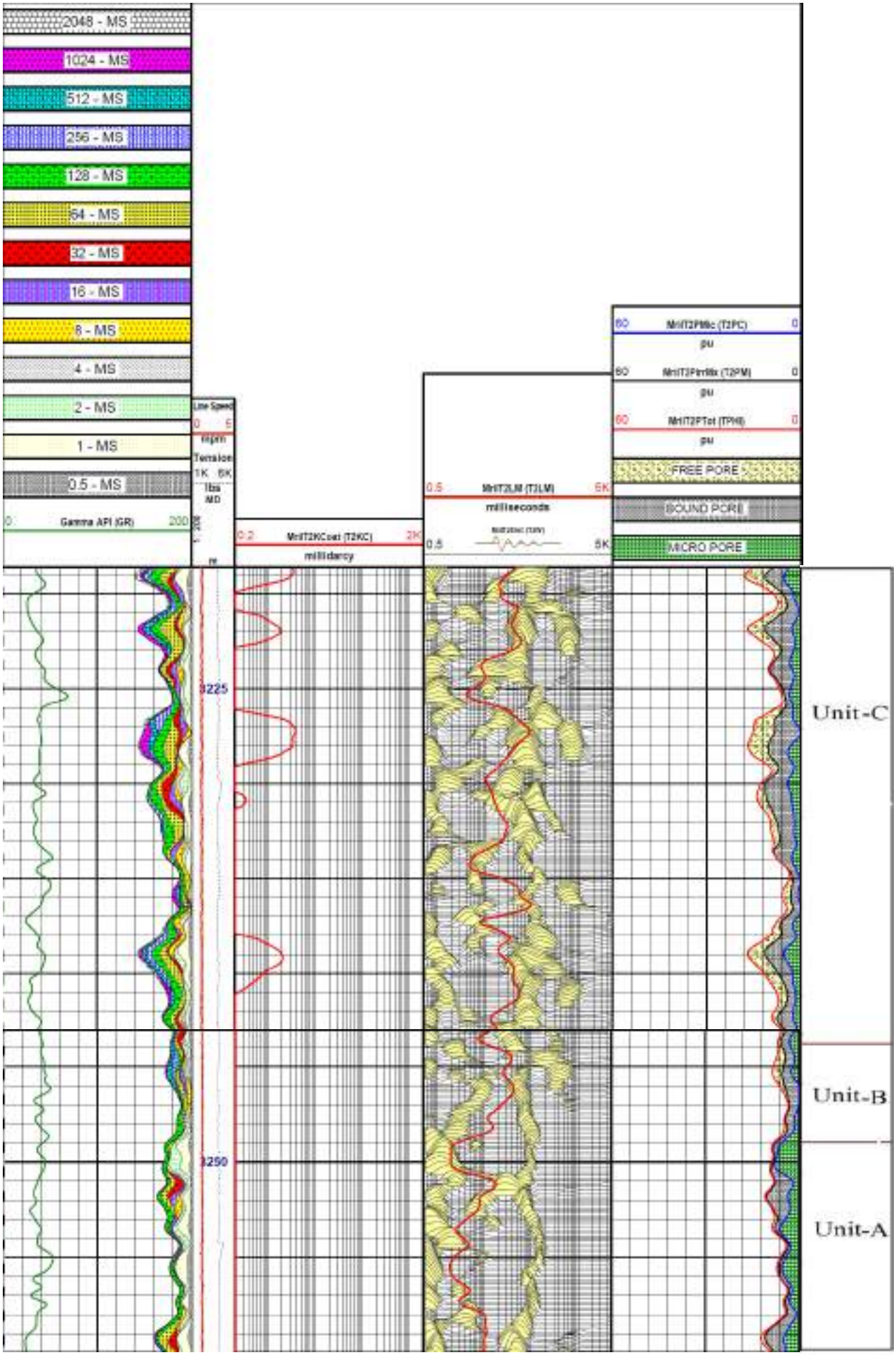

Figure 4.12: The output of the MRIL done for Jeribe Formation in Taza-2 well (Oil Search log).

The indicated permeable zones by the MRIL tool can be easily observed on the log which in the best cases did not exceed 4md (poor permeability). Most detected relatively permeable zones concentrated at the upper part of the formation (determined RU-C unit).

On the other hand, the measured porosity by the MRIL tool revealed that the Jeribe Formation in the well Taza-2 is almost of upward gradually increasing porosity, with no zones reaching 20% or more porosity (18% is the maximum measured porosity). As noticed in the measured permeabilities, the RU-C unit showed the highest porosities, whereas the RU-B appeared to be of the lowest porosity interval. The reservoir unit RU-A looked to own porosities ranging between 4.0 and 12%,

Most of the pores containing free movable fluid have been recorded by the MRIL tool within the RU-C unit. As expected, the highest free fluid containing intervals are also the highest permeable intervals. The units of the RU-A and RU-B both showed, no and very low free fluid content. As ratios, most of the lower part of the formation (RU-A and RU-B) contain highest ratio of non movable fluids within the micropores, whereas the upper part of the formation (RU-C) showed that non movable fluid as bound fluid comprises the highest ratio of fluids within the pore spaces. The three types of the distinguished fluids within the pore spaces and their ratios also can be noticed through observing the T2 curves as recorded time in milliseconds and as amplitude of the appeared curves.

In addition to the gamma ray record, the track #1 in the figure 4.12 contains the partial porosities of each fluid decay component in the Jeribe Formation. The T2 time from 0.5 to 2.0ms represents the decay time for the fluid existing in the micropores, whereas T2 between 1.0 and 256ms represents decay time for bounded fluids in the pore spaces. Free fluids within

the pores are of more than 256ms decay time. Appearance of wider spectra of decay times in any interval depends on the nature and ratio of the existed fluids in addition to their type of existence either within the micropores, or as bounded fluids, or as free fluids within the pore spaces.

As noted, no significance difference can be seen between the measured porosity by the MRIL for Jeribe Formation in the well Taza-2 and the calculated Θ_{NDcorr} using the conventional logs of neutron and density.

Regarding permeability, the determined high, low and non permeable zones using both techniques of MRIL and the multiple linear regressions are almost similar but the difference is in being the calculated values of the permeability in millidarcies relatively higher when calculated by the second mentioned technique.

In this study, the evaluation of the Jeribe Formation in both wells will be continued depending on the measured porosity and permeability as done in chapter three.

4.8 Bulk Volume Water (BVW)

Bulk Volume Water (BVW) in log analysis can be defined as the fraction of rock volume that is occupied by water and mathematically is expressed as the product of formation's water saturation (Sw) and its porosity (Ø) (Eq.4.11).

$$BVW = S_w * Ø \quad \text{.....Eq.4.11}$$

The term of Bulk Volume Hydrocarbon (BVH) also used to define the fraction of rock volume which occupied by hydrocarbons and can be expressed as:

$$BVH = Ø * (1-Sw) \quad \text{..... Eq.4.12}$$

Accordingly the sum of BVW and BVH is equal to the total porosity (Ø).

As grain size decreases, the diameters of pore throats within the reservoir will decrease, resulting in higher capillary pressures. This condition implies a reservoir in which a substantial amount of water may be trapped and unable to move. Therefore, when a reservoir is determined to be at irreducible water saturation, values for bulk volume water (BVW) may be used to estimate the average grain size of that reservoir (HLS,2007). Table 4.3 shows the relationship between BVW values at irreducible water saturation condition and the grain sizes in clastic rocks and the type of porosity in carbonate rocks.

The presence of clay minerals in a reservoir also has an impact on values of irreducible water saturation (Swirr) and bulk volume water (BVW). As the volume of clay minerals in a reservoir (Vsh) increases, both Swirr and BVW will increase because of the inclination of clay to trap interstitial formation water (HLS, 2007).

BVW values for Jeribe Formation have been calculated in both studied wells and listed in the appendix C.

For getting benefit from the calculated BVW, in this study, for detecting zones at irreducible water saturation, Buckles plot depended on which is a graph of porosity versus water saturation in which points of equal BVW values form hyperbolic lines across the plot. Zones at irreducible water saturation condition are zones from which water free hydrocarbon can be produced. Figures 4.13 and 4.14 show the distribution of the sample points related to the identified reservoir units of Jeribe Formation in the wells Ja-49 and Taza-2, respectively. Sample points related to zones being at irreducible

water saturation condition are concentrating around a single hyperbolic line (same BVW value), whereas zones of producible water show scattering of the sample points around more than one hyperbolic line (different BVW values).

Table 4.3: BVW at irreducible water saturation as a function of grain size and type of carbonate porosity (after Asquith, 1985, partially modified from Fertl and Vercellino, 1978)

Grain Size (millimeters)		**Bulk Volume Water (BVW)**
coarse	1.0 to 0.5 mm	0.02 to 0.025
medium	0.5 to 0.25 mm	0.025 to 0.035
fine very	0.25 to 0.125mm	0.035 to 0.05
fine	0.125 to 0.0625 mm	0.05 to 0.07
silt	< 0.0625mm	0.07 to 0.09
Carbonate Porosity		**Bulk Volume Water (BVW)**
Vuggy		0.005 to 0.015
Vuggy & Intercrystalline (intergranular)		0.015 to 0.025
Intercrystalline (intergranular)		0.025 to 0.04
Chalky		0.05

As observed in the figures 4.13 and 4.14, the reservoir unit RU-B showed the closest distribution of the sample points to a single hyperbolic line which means this reservoir unit may produce hydrocarbons (if there are hydrocarbons in the unit) with the lowest quantity of water. On the other hand, the reservoir unit RU-C seems to be the highest heterogeneous unit as its sample points scattered around more than three or four hyperbolic lines. Production in such a reservoir unit will accompanied by a large quantity of water, Reservoir unit RU-A in Ja-49 well appears to be more homogeneous than in Taza-2 well and that from the way by which its sample points distributed, (the sample points are less scattered than in Taza-2well).

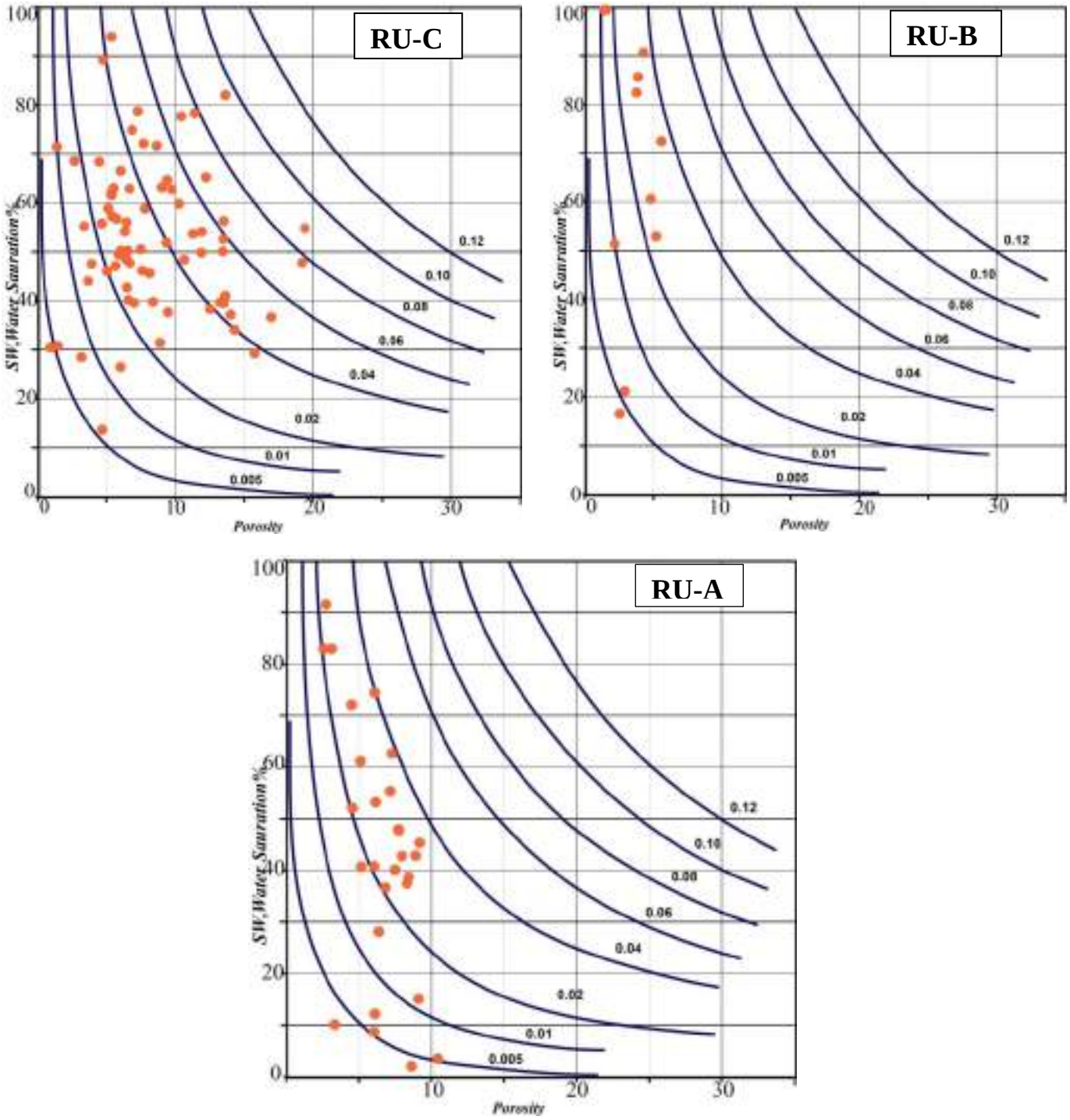

Figure 4.13: Ø versus Sw on Buckles plot to show the BVW values for the reservoir units of the studied Jeribe Formation in Ja-49 well.

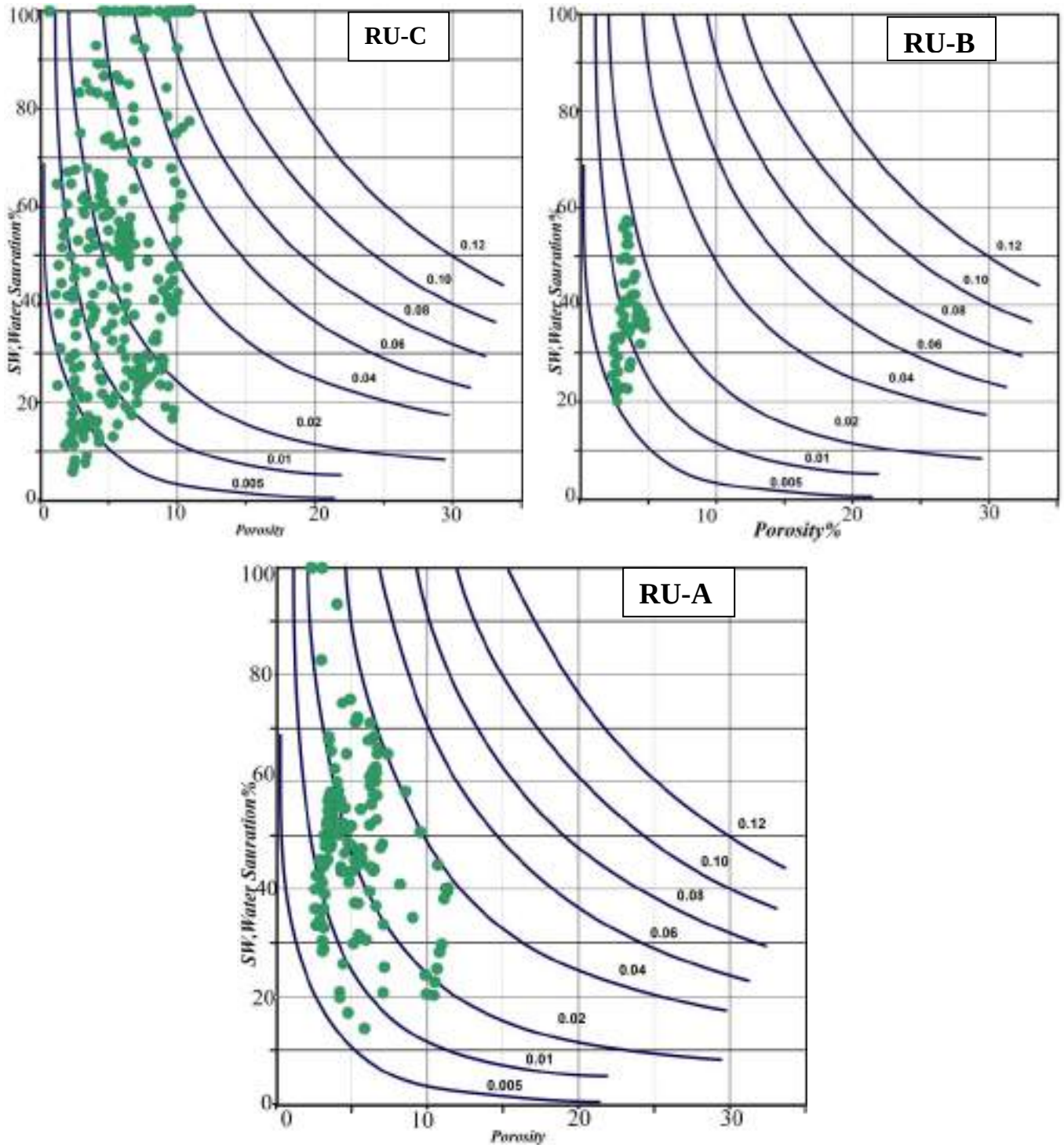

Figure 4.14: Ø versus Sw on Buckles plot to show the BVW values for the reservoir units of the studied Jeribe Formation in Taza-2well.

4.9 Movable Hydrocarbon Index (MHI)

Water saturation of the uninvaded zone (Sw) and flushed zone (Sxo) can be used as an indicator of hydrocarbon moveability. If the value of Sxo is much larger than Sw, then hydrocarbons in the flushed zone have probably been moved or flushed out of the zone nearest the borehole by the invading drilling fluids.

The ratio method for identifying hydrocarbon moveability bases on the difference between water saturations in the flushed zone (Sxo) and the uninvaded zone (Sw). When the water saturation in the uninvaded zone from of Archie's equation (Eq.4.1) is divided by the water saturation in the flushed zone (Eq.4.2), the Eq.4.13 results which is representing MHI:

$$\frac{Sw^2}{Sxo^2} = \left[\frac{Sw^2}{Sxo}\right] = \frac{F*\frac{Rw}{Rt}}{F*\frac{Rmf}{Rxo}} = \frac{\frac{Rw}{Rt}}{\frac{Rmf}{Rxo}} = \frac{\frac{Rxo}{Rt}}{\frac{Rmf}{Rw}} \dots\dots\dots\dots\dots\dots \text{Eq. } 4.13$$

Where:

F = formation factor

Sxo = water saturation, flushed zone

Sw = water saturation, uninvaded zone

Rt = resistivity, uninvaded zone (deep reading log)

Rxo= resistivity, flushed zone (shallow reading zone)

Rmf = resistivity of mud filtrate

Rw = resistivity of formation water

When Sw is divided by Sxo (Eq.4.13), formation factor (F) will be cancelled out which means it is no longer necessary to know porosity or a value for the cementation exponent (m) to determine water saturation.

Schlumberger (1972) reports that if the ratio of Sw/Sxo is 1.0 or greater, no hydrocarbons are moved during invasion, this is true regardless of

whether or not the zone contains hydrocarbons. Whenever the ratio of Sw/Sxo is less than 0.7 for sandstone and less than 0.6 for limestone, movable hydrocarbons are indicated. If carbonate reservoir has a MHI less than 0.6, hydrocarbons are present and the reservoir has enough permeability so that hydrocarbons have been moved during the invasion process by mud filtrate (Asquith, 1985).

Calculated MHI values for Jeribe Formation in the studied Ja-49 and Taza-2 wells are listed in the appendix C and shown as curves in the figure 4.8. In the same figure, the MHI value of 0.6 used as a cutoff value for separating zones of movable hydrocarbons from zones of non- movable hydrocarbons (due to being Jeribe Formation of carbonate nature).

The following points are general notes about the calculated MHI values which represent effective movable hydrocarbon zones for Jeribe Formation as appears in the figure 4.15:

1. Although almost all parts of Jeribe Formation contains hydrocarbons but not all the parts contain effective movable hydrocarbons and hence productivity.
2. Jeribe Formation in Ja-49 well contains more horizons of movable hydrocarbons than the Jeribe Formation in Taza-2well.
3. The reservoir units of RU-A and RU-B in Taza-2 well are nearly of no effective movable hydrocarbons.
4. RU-B is of the least movable hydrocarbons among the identified three reservoir units in this study.
5. Thickest continuous intervals of movable hydrocarbon in both wells exceed 4.0m, randomly.

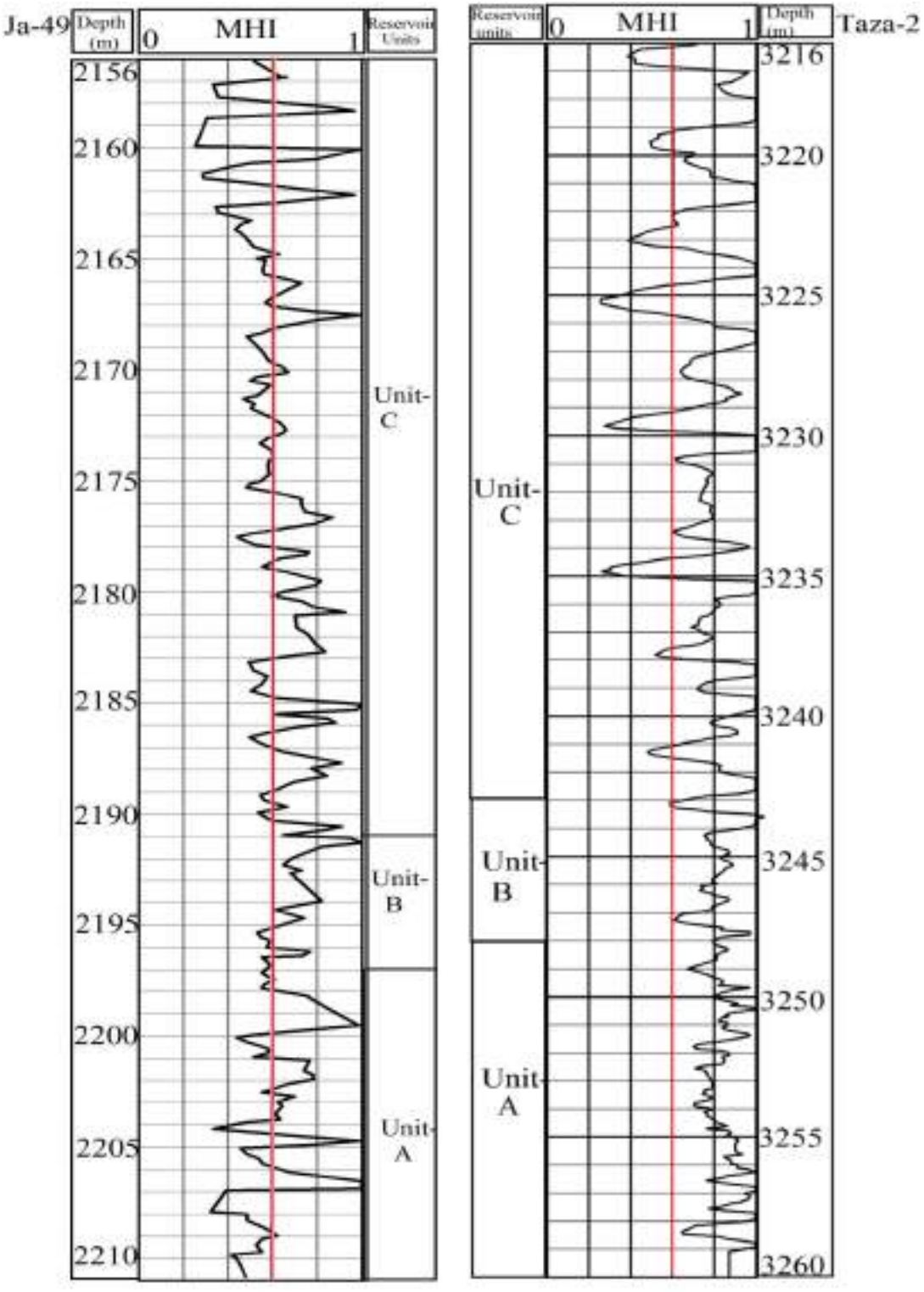

Figure 4.15: Movable Hydrocarbon Index (MHI) curve for the studied Jeribe Formation in Ja-49 and Taza-2wells. The red line represents 0.6 MHI value separating movable hydrocarbon zones (≤0.6) from non movable hydrocarbon zones (>0.6).

4.10 Rock Fabric / Petrophysical Relationship

Pittman (1992) and Kolodizie (1980) both in Lucia (1999) have published petrophysical relationships between interparticle porosity, permeability, and capillary pressure. Although they applied their tests on siliciclastics (interparticle porosity), but it can be applied also for carbonates. They conclude that pore-throat size measured at 35% mercury saturation gives the best relationship to porosity and permeability according to the equation Eq.4.14.

$$\text{Log}(R35) = 0.255 + 0.565\log(k) - 0.523\log(Ø) \quad \text{.....Eq.4.14}$$

Where:

R35 = Pore throat size calculated at 35% mercury saturation

K = Permeability in md

Ø = Porosity in fraction

The equation Eq.4.14 plotted in a figure proposed by Lucia (1999) connecting between the porosity and permeability to distinguish three petrophysical classes of rock fabrics (Fig.4.16) which based initially on the classification of carbonate rocks proposed by Dunham (1962).

The three classes distinguished by Lucia (1999) in figure 4.16 are permeability fields of certain particle size and sorting. The field of class 1 includes: (1) grainstones, (2) dolomitized grainstones, and (3) large crystalline dolostones, which may be dolograinstones, grain dominated dolopackstones or mud dominated dolostones (Fig. 4.17).

Three rock fabrics make up the class 2 field including (1) grain dominated packstones, (2) fine to medium crystalline grain dominated

dolopackstones, and (3) medium crystalline mud dominated dolostones.

Regarding the class three, two rock fabrics make up this class which is (1) mud-dominated fabrics (mud dominated packstone, wackestone, and mudstone) and (2) fine crystalline mud dominated dolostones.

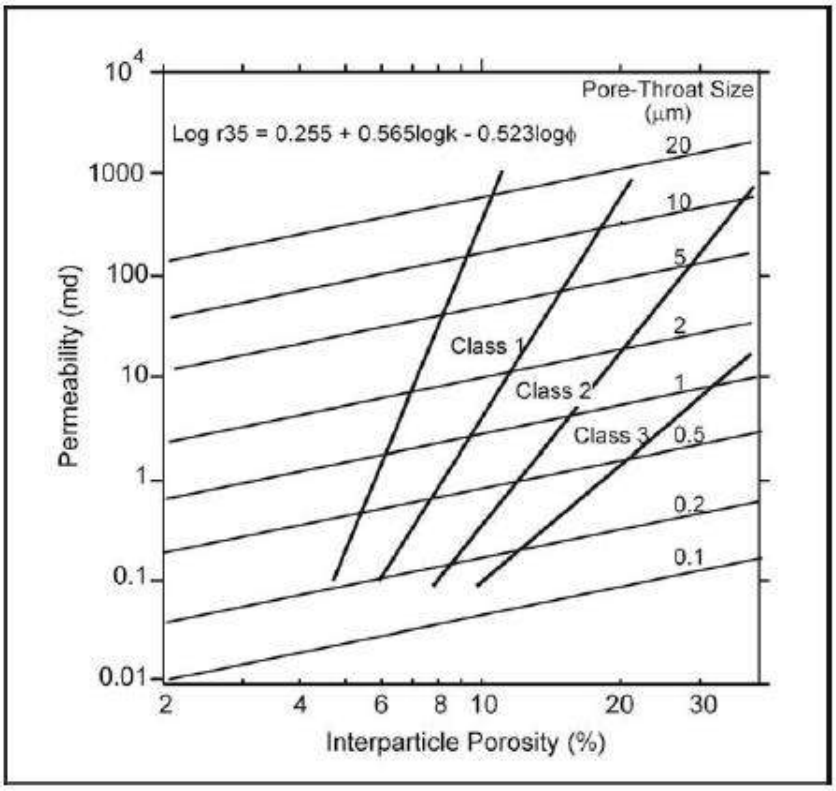

Figure 4.16: Comparison of petrophysical class fields and pore throat sizes versus interparticle porosity and permeability (after Lucia, 1999).

According to Lucia (1999) it is apparent that, within a petrophysical class, pore throat size decreases as interparticle porosity decreases. The eight basic rock fabrics defined by Lucia (1999) constrained to specific petrophysical class fields and not to a specific pore throat size. Therefore, there is no direct link between pore size and rock fabrics in carbonate rocks.

The pore throat size values shown in the figure 4.16 can be expressed qualitatively according to the table 4.4 proposed by Lucia (1999), and which will be used in this study.

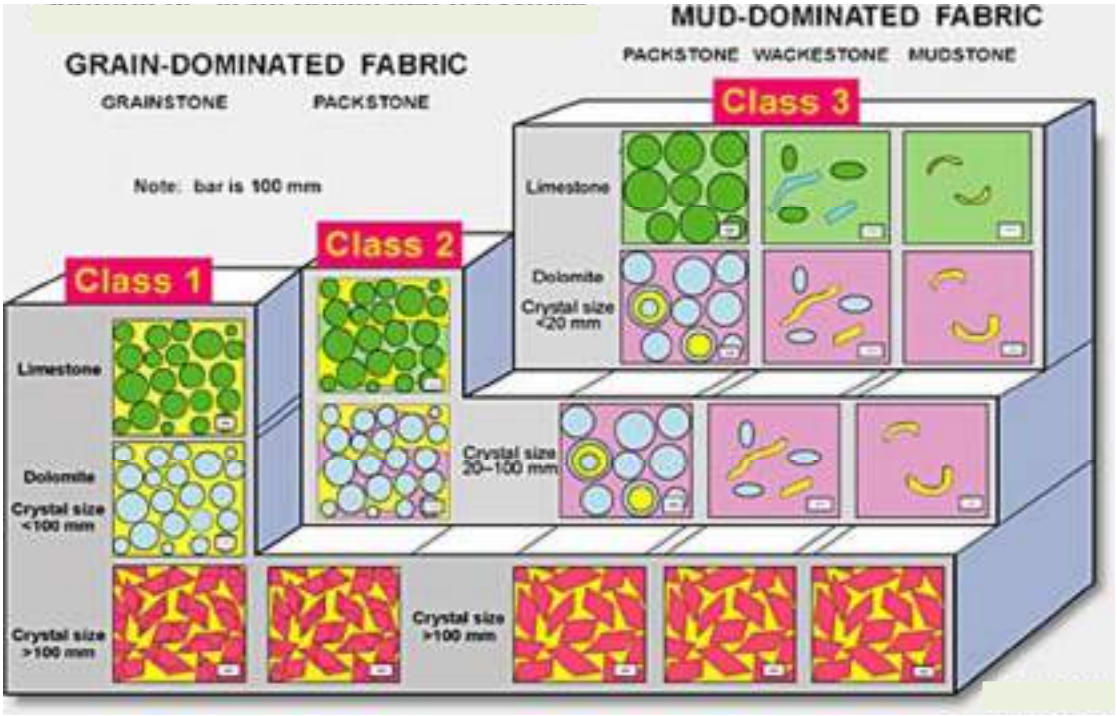

Figure 4.17: A block diagram illustrating the relationship between rock fabrics and petrophysical classes proposed by Lucia (1999).

Table 4.4: Qualitative classification of pore types depending on pore throat sizes (after Lucia, 1999)

Pore throat Size (µm)	Pore Type
< 0.2	Nano
0.2 - 0.5	Micro
0.5 – 2	Meso
2 – 10	Macro
10 – 50	Mega

As an attempt to identify the type of the petrophysical rock fabrics existing in the determined reservoir units of Jeribe Formation and the dominated pore throat sizes in each unit, sample points representing

porosity and permeability values have been plotted on the crossplot proposed by Lucia (1999) as shown in the figures 4.18 and 4.19 for the Wells Ja-49 and Taza-2 respectively.

Reservoir unit RU-A of Jeribe Formation appeared to be composed mainly of rock fabric class 2 in Ja-49 well, whereas it composes of class 1 and 2 in the well Taza-2 with being the pore throats mostly of sizes between 0.5 and 1.0 µm (micro to meso pore type) in both wells. Regarding the reservoir unit RU-B, it showed large similarity in both wells as it appeared to be composed mainly of class 3 with pore sizes ranging between 0.1 and 0.5µm (nano to micro pore type). Finally, the reservoir unit RU-C in Ja-49 well composes almost completely of rock fabric class 2, whereas in Taza-2 well composes of both class 1 and 2. The pore throat sizes of the sediments in the reservoir unit RU-C ranges between 0.5 and 1.0µm (meso pore type) in the well Ja-49 with being relatively of wider range (between 0.5 and 2.0µm) in Taza-2 well.

As conclusion, the reservoir unit RU-C showed the best reservoir properties from the pore throat size point of view and hence of highest permeability among the three identified reservoir units. By contrast, reservoir unit RU-B showed the lowest reservoir properties with the narrowest pore throat sizes due to being composed mainly of wackestones and mudstones.

The properties of the reservoir unit RU-A is closer to the reservoir unit RU-C than RU-B as both are composing of the same rock fabric but the former is of relatively narrower pore throat sizes (lower permeability than RU-C).

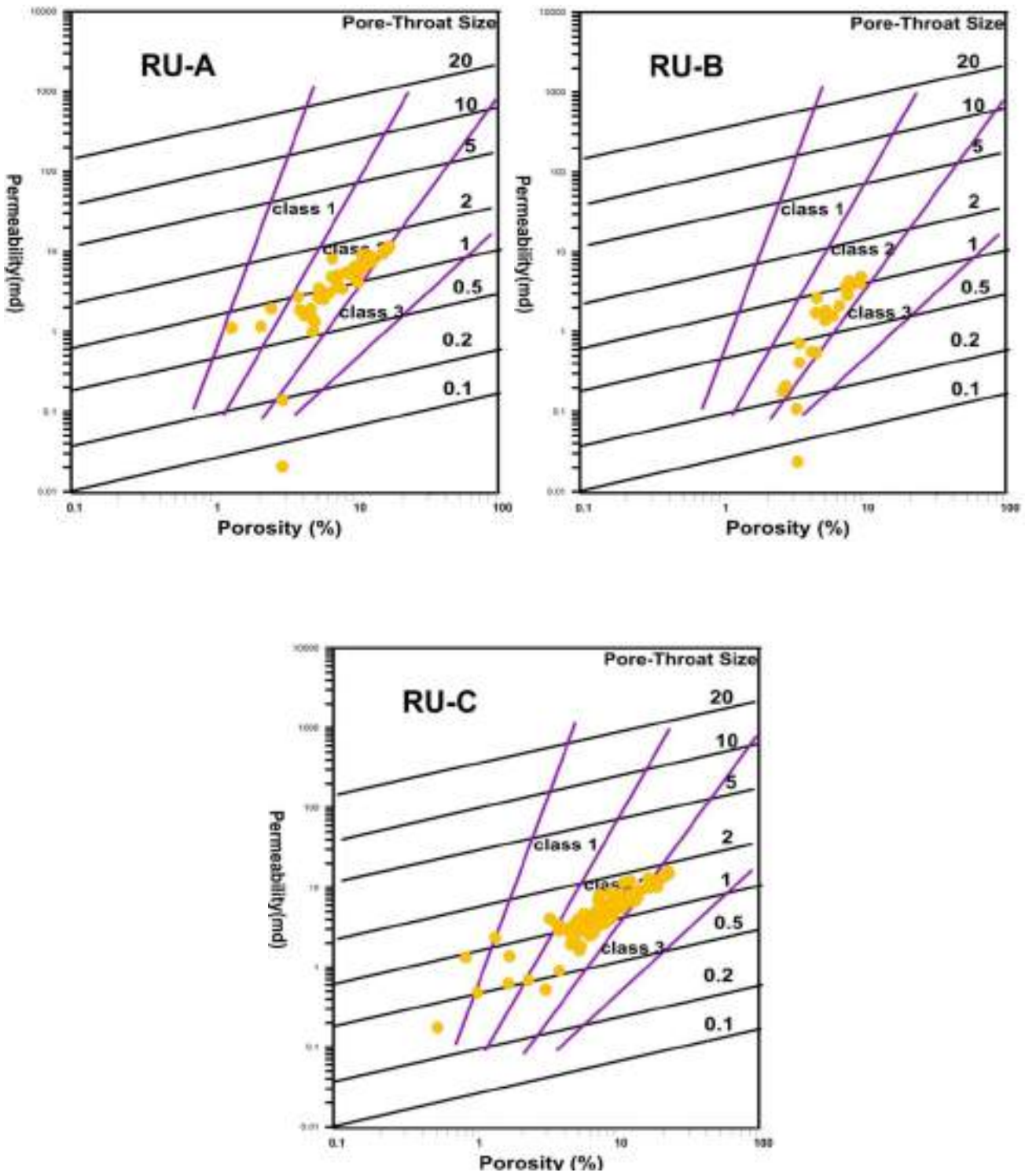

Figure 4.18: Porosity- permeability cross plot, shows the pore throat size and petrophysical rock fabric classes of reservoir units A, B and C in Ja-49 well.

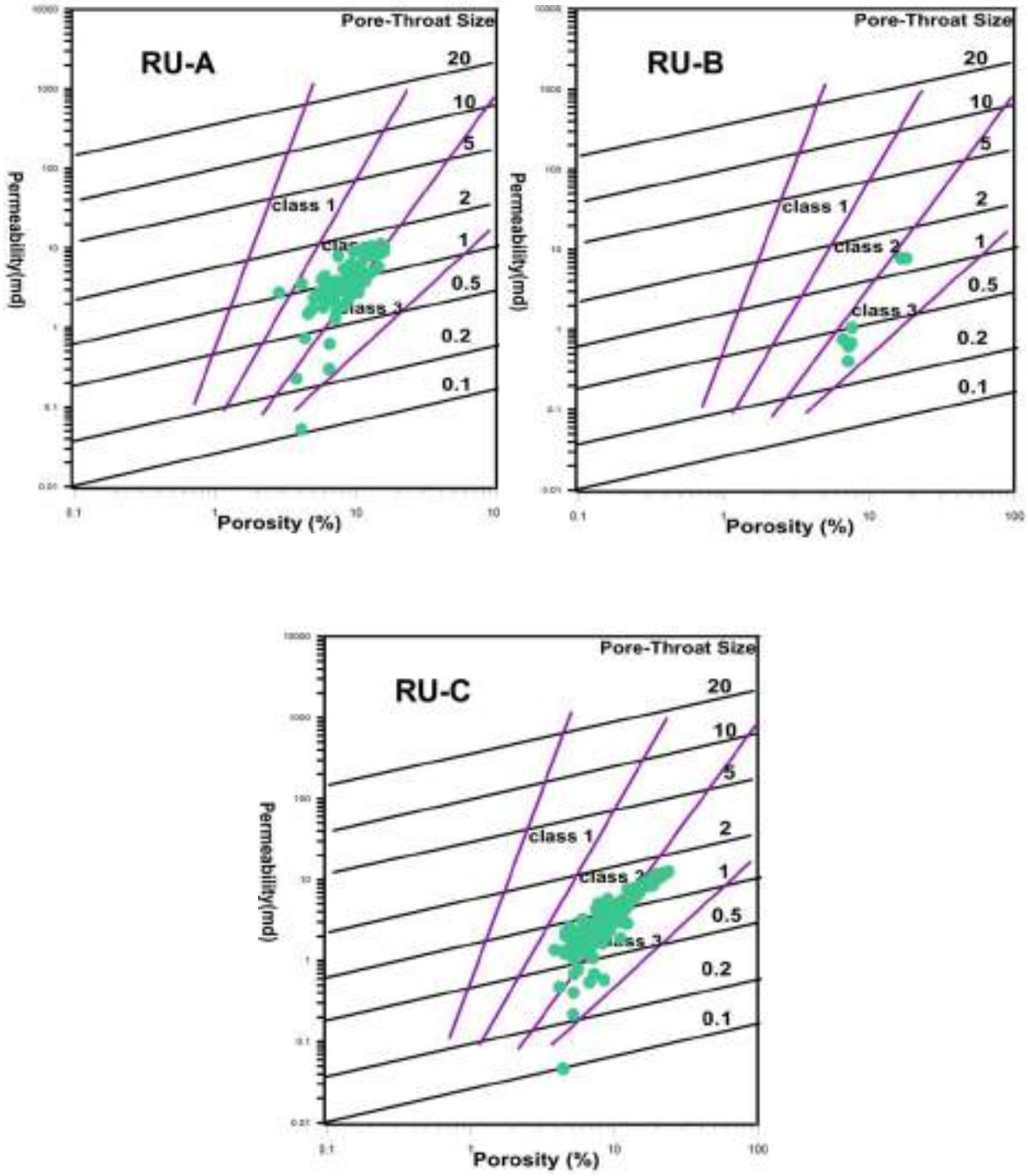

Figure 4.19: Porosity- permeability cross plot, shows the pore throat size and petrophysical rock fabric classes of reservoir units A, B and C in Taza-2 well.

4.11 Fluid Flow within Jeribe Formation

The relationship between Ɵ and K (taking pore throat size in consideration) can also tell about the effectiveness of fractures in flowing the fluids out of the reservoir rock. Such a relationship is arranged through a crossplot combining between the values of porosity and permeability with existing of contour lines representing iso K/Ɵ ratios (Humbolt, 2006) and values for the expected ranges of pore throat sizes in microns.

According to Rivas et al. (2014), the technique of R35 proposed by Winland in the year 1972 is behind the idea of the mentioned crossplot above. The measured Ɵ and K values through core analysis with capillary pressure data are the requested data for applying this technique and developing an empirical relationship between porosity, air permeability, and the pore throat size equivalent to a mercury non-wetting phase of 35% (R35).

Figure 4.20 shows the pattern of distribution for the sample points representing Ɵ and K values obtained from the core analysis test done for selected plugs from the cored sample of Jeribe Formation in the well Taza-2 between depths 3237 and 3253.6m. Flow through connected pores within the matrix of the rocks and through open fractures looks to be the way by which Jeribe Formation in Taza-2 can produce fluids. Additional conclusion is the relatively wide range of pore throat sizes for the connected pores or the opening of the fractures (generally between < 0.2 and >2.0 micron, between nano and macro type of pore throats).

On the other hand, the same technique applied on the log derived porosity and permeability for the complete thickness of Jeribe Formation in the both studied wells.

Figures 4.21- 4.23 show the distribution of the sample points for the distinguished reservoir units of Jeribe Formation in this study. Most of the sample points also indicated to flow ability through connected pores within the matrix and through open microfractures existed in the formation. According to the pattern of the distribution, RU- C in the well Ja-49 looks to be containing higher rate of effective open fractures or connected vugs among the distinguished reservoir units. As a clarification, when low calculated porosity values showed relatively high permeability, that is an indication to the possibility of being fractures or connected vugs the main providers of avenues for fluids to flow out of the reservoir.

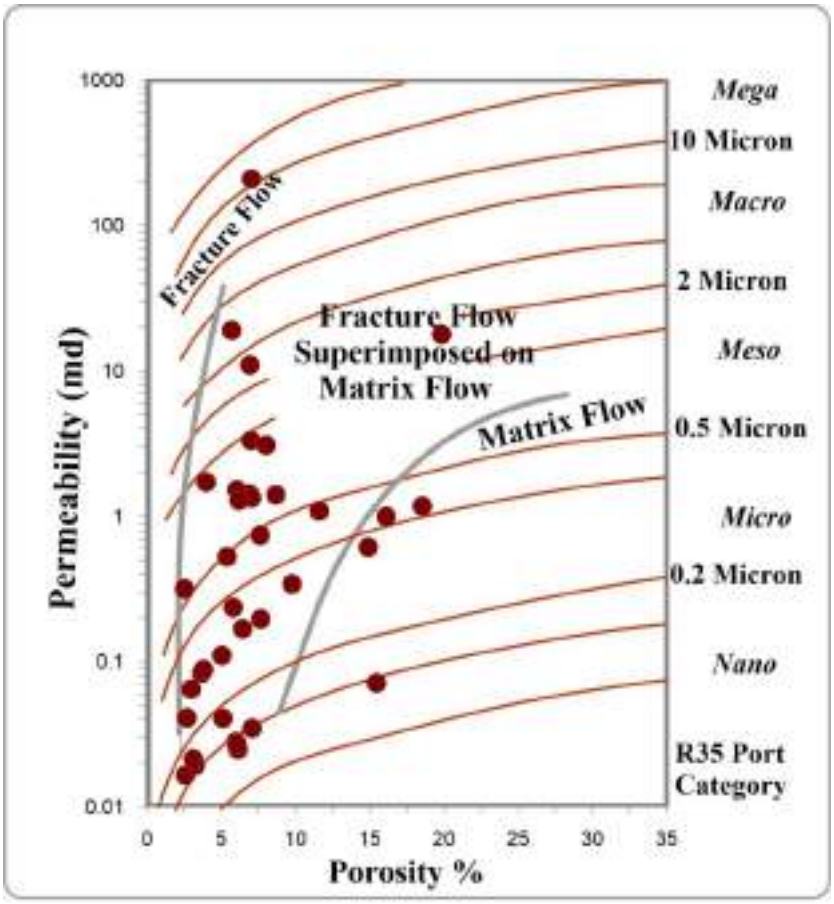

Figure 4.20: Porosity- Permeability cross plot for showing type of fluid flow in Jeribe Formation in the well Taza-2 (Data of core analysis for the cored interval of the formation between depths 3237 and 3253.6m

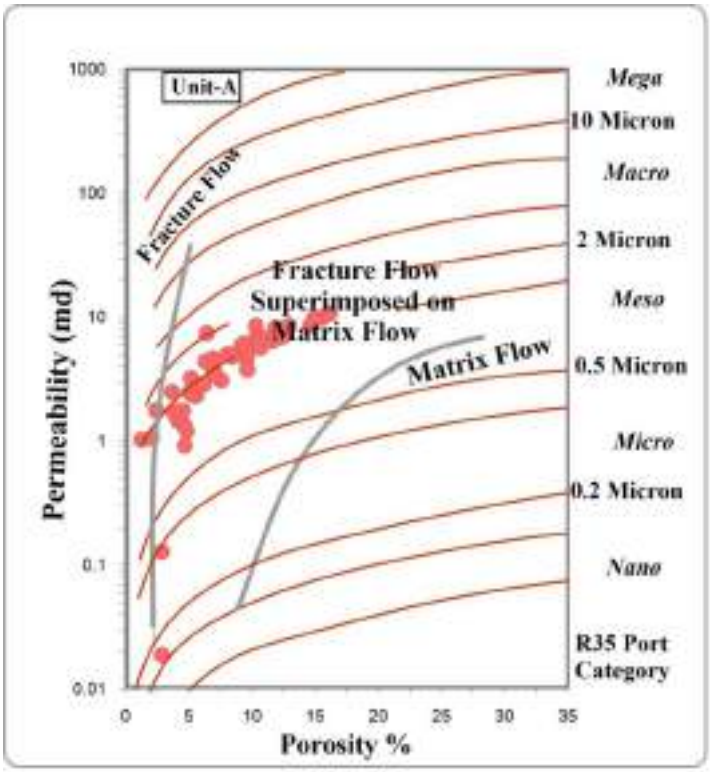

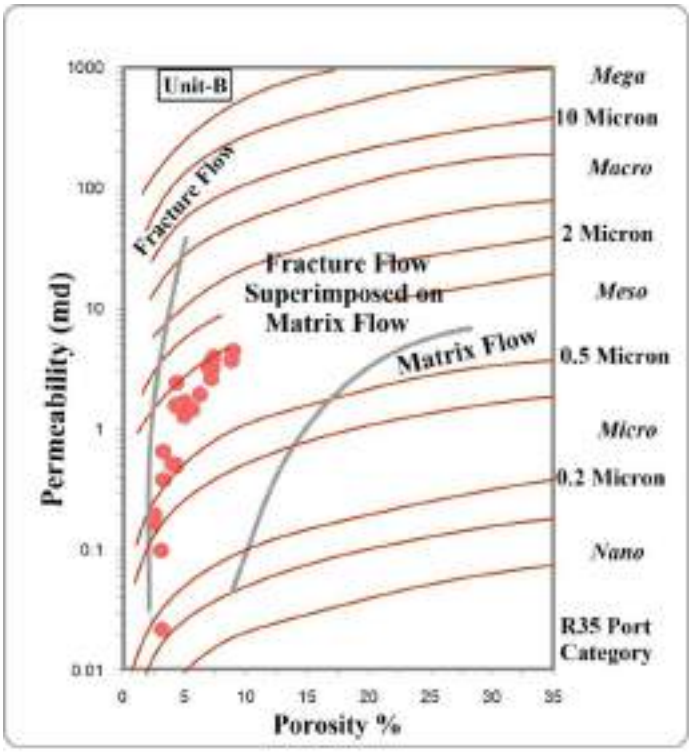

Figure 4.21: Porosity- Permeability cross plot for showing type of fluid flow in the reservoir unit RU-A and RU-B of Jeribe Formation in the Ja-49 well.

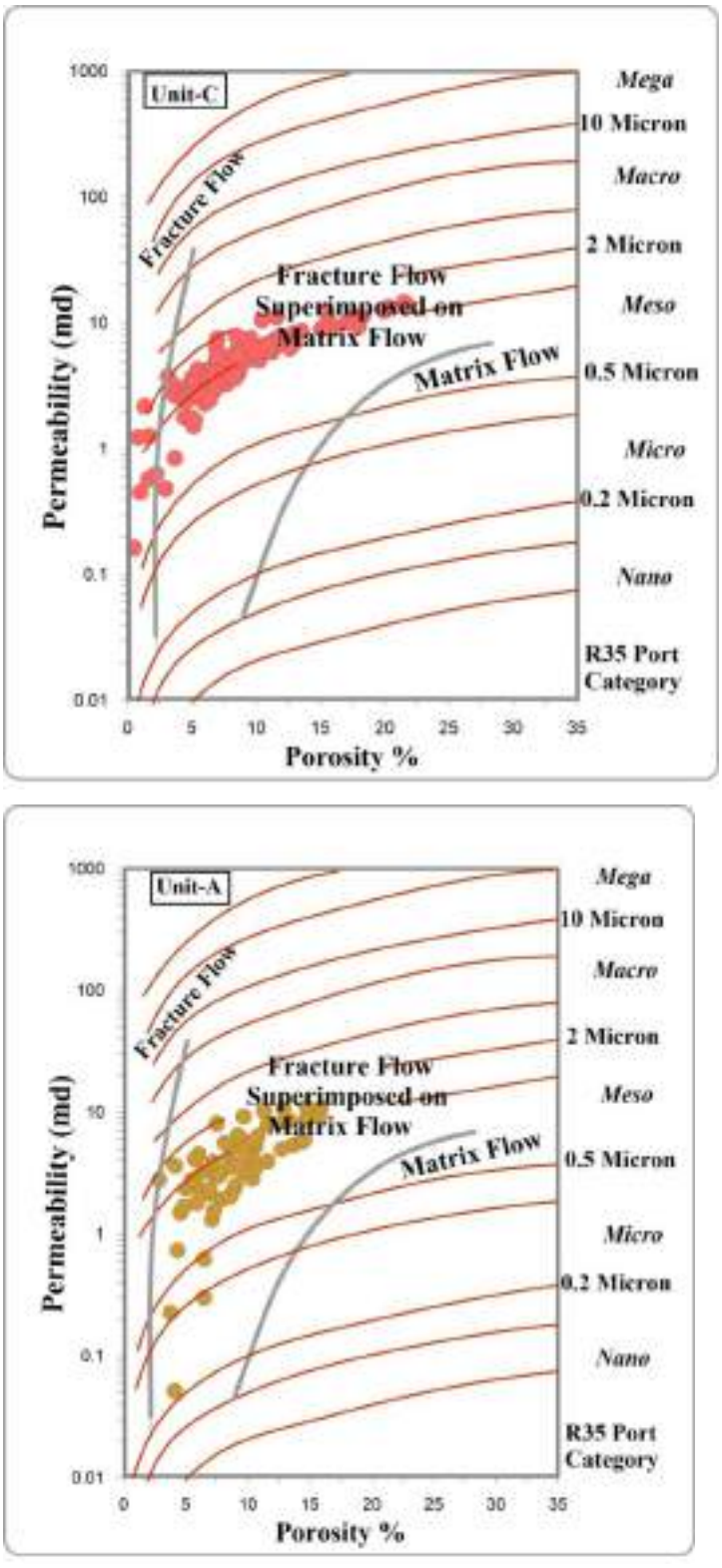

Figure 4.22: Porosity- Permeability cross plot for showing type of fluid flow in the reservoir unit RU-C (Ja-49) above, and reservoir unit RU-A (Taza-2) below, of Jeribe Formation.

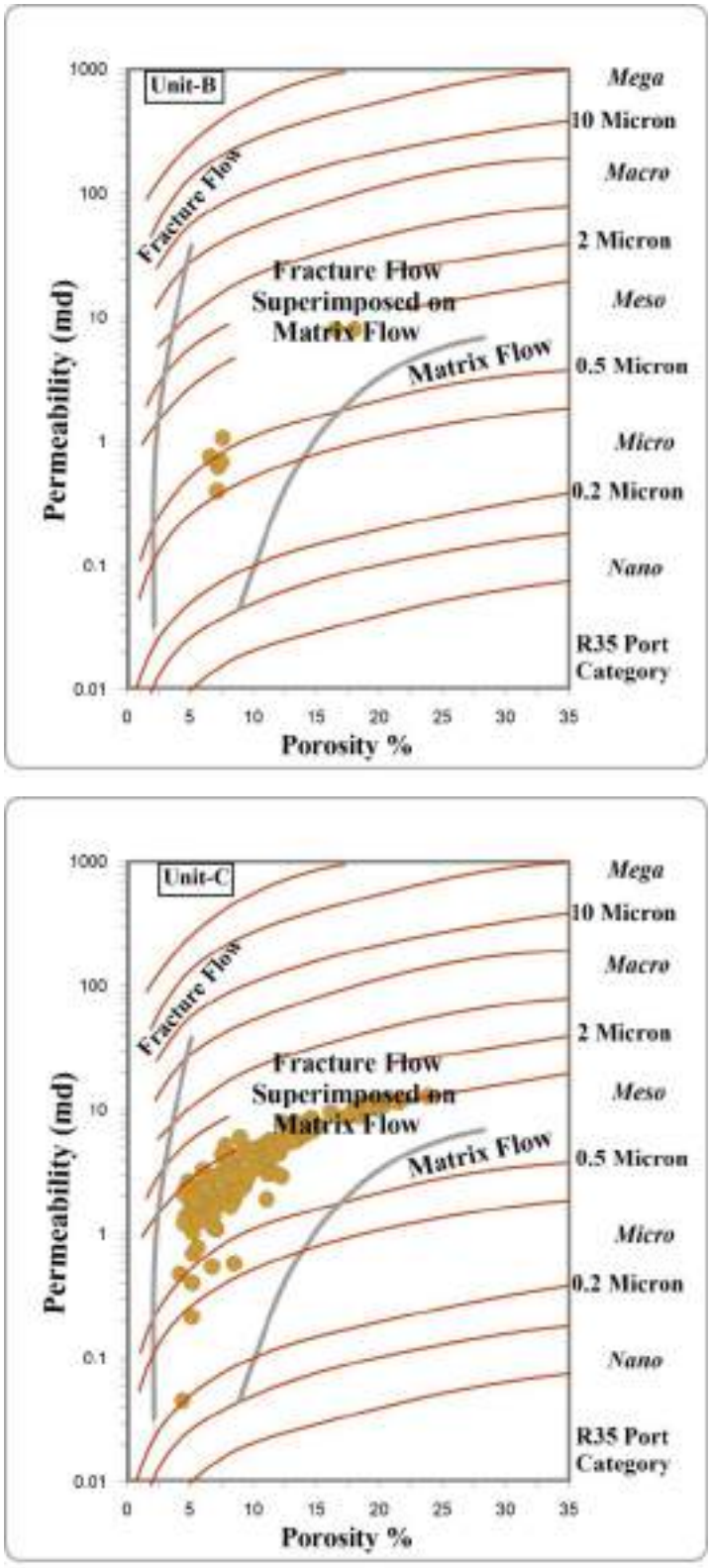

Figure 4.23: Porosity- Permeability cross plot for showing type of fluid flow in the reservoir unit RU-B and RU-C of Jeribe Formation in the Taza-2 well.

4.12 Estimation of Flow Zone Indicator (FZI)

Flow Zone Indicator (FZI) is a "unique and useful value to quantify the flow character of a reservoir and one that offers a relationship between petrophysical properties at small scale, such as core plugs, and large scale, such as well bore level" (Al-Dhafeeri and Nasr-El-Din, 2007; in Chatterjee et al., 2013).

Amaefule et al. (1993) designated FZI as a unique parameter that varies inversely with tortuosity, shape factor and grain surface area, which are the critical factors determining the flow in the rock. Therefore, the FZI value discriminates the pore geometry of facies into flow zones, in which a high FZI value indicates that the rock exhibits coarse, well-sorted grains and lower shape factor. In the same manner, a low FZI value represents a rock constituent of fine and poorly sorted grained (Teh et al., 2011).

According to Amaefule et al. (1993), FZI can be expressed in terms of the Reservoir Quality Index (RQI) and Normalized porosity (Øz) as shown in Eq.4.15.

$$FZI = \frac{RQI}{\emptyset_z} \quad \text{..... Eq.4.15}$$

Where:

FZI = Flow Zone Indicator in µm

RQI = Reservoir Quality Index

Øz = Normalized Porosity Index (pore volume to matrix volume ratio)

For calculating RQI and Øz , equations Eq.4.16 and Eq.4.17 are formulated by Amaefule et al. (1993).

$$RQI = 0.0314\sqrt{\frac{K}{\emptyset_e}} \text{.....Eq.4.16}$$

$$Ø_z = \frac{ø_e}{1-ø_e} \text{..... Eq.4.17}$$

Where:

RQI = Reservoir Quality Index

Øz = Normalized Porosity Index

Øe = Effective porosity in fraction

K = Permeability in md

Zones of certain FZI values represent zones of characteristic Hydraulic Flow Units (HFU). The flow unit can be defined as a reservoir zone that has lateral and vertical continuity with the same porosity, permeability and bedding characteristic (Hear et al., 1984; in Baker et al, 2013).

Based on equation Eq.4.15, for any hydraulic unit, a log-log plot of RQI versus Øz yield a straight line with a slope of 1.0, each flow unit will have a separate FZI value where each FZI value refers to a unique hydraulic flow unit having similar pore throat characteristic (Tiab and Donaldson, 2004).

The calculated FZI values for Jeribe Formation in Ja-49 and Taza-2 wells are listed in the appendix C.

Normal probability index used as a preliminary method to distinguish between the variable FZI populations or groups and that through following the changes occurred to the slope of the distributed FZI values(Figs. 4.24 and 4.25). Four distinguishable FZI intervals identified representing four unique hydraulic units with different RQI versus Øz relationship in each of the two studied wells (Figs. 4.26 and 4.27).

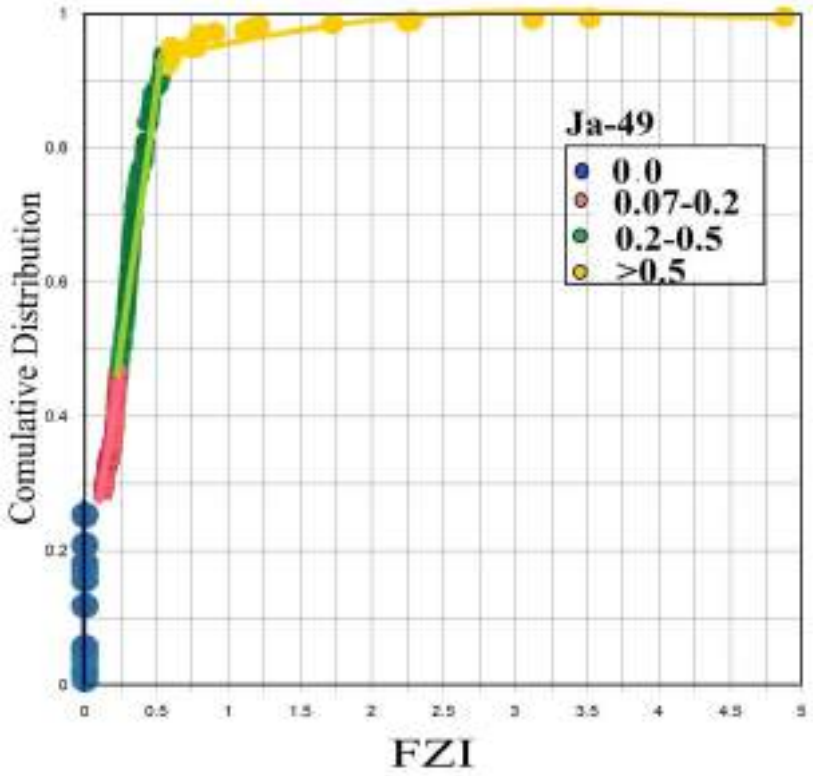

Figure 4.24: Normal probability analysis for the calculated Flow Zone Indicator values for Ja-49well.

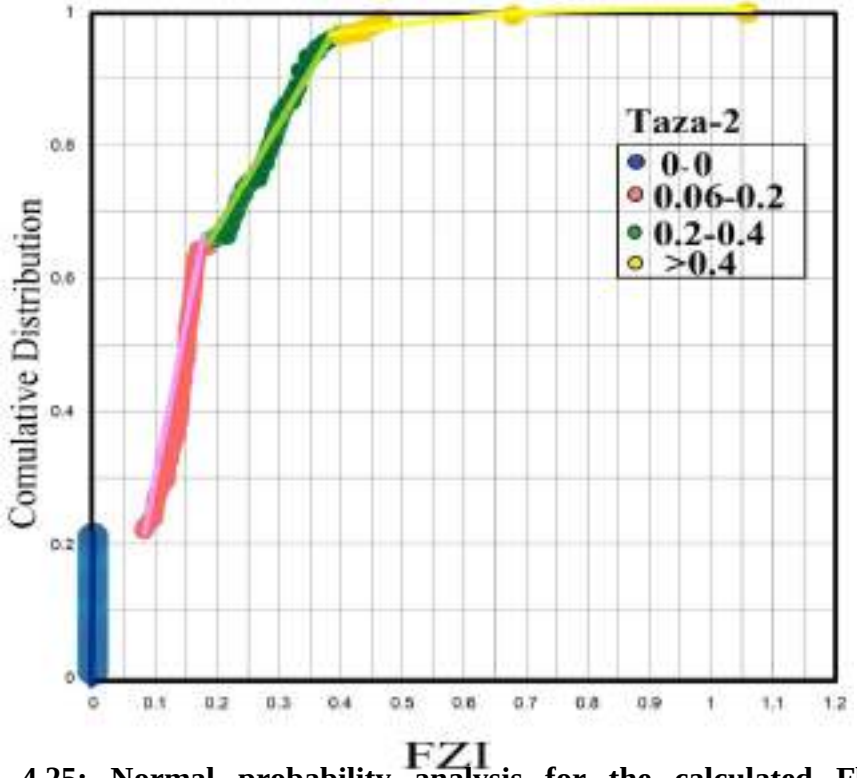

Figure 4.25: Normal probability analysis for the calculated Flow Zone Indicator values for Taza-2 well.

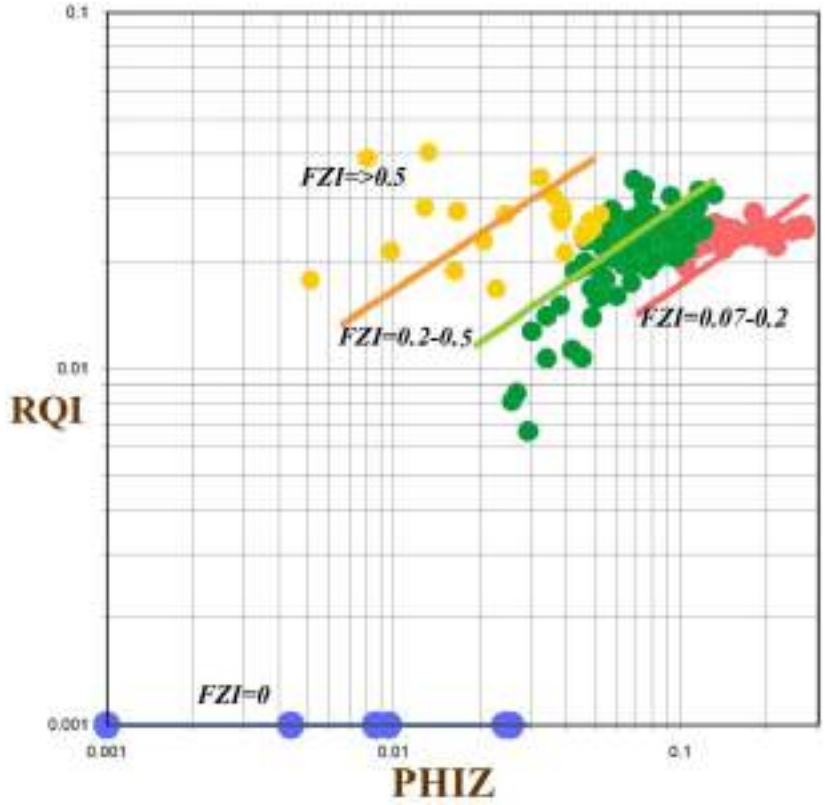

Figure 4.26: RQI versus Øz plot for the studied Jerbi Formation in Ja-49 well with the ranges of the clustered FZI values.

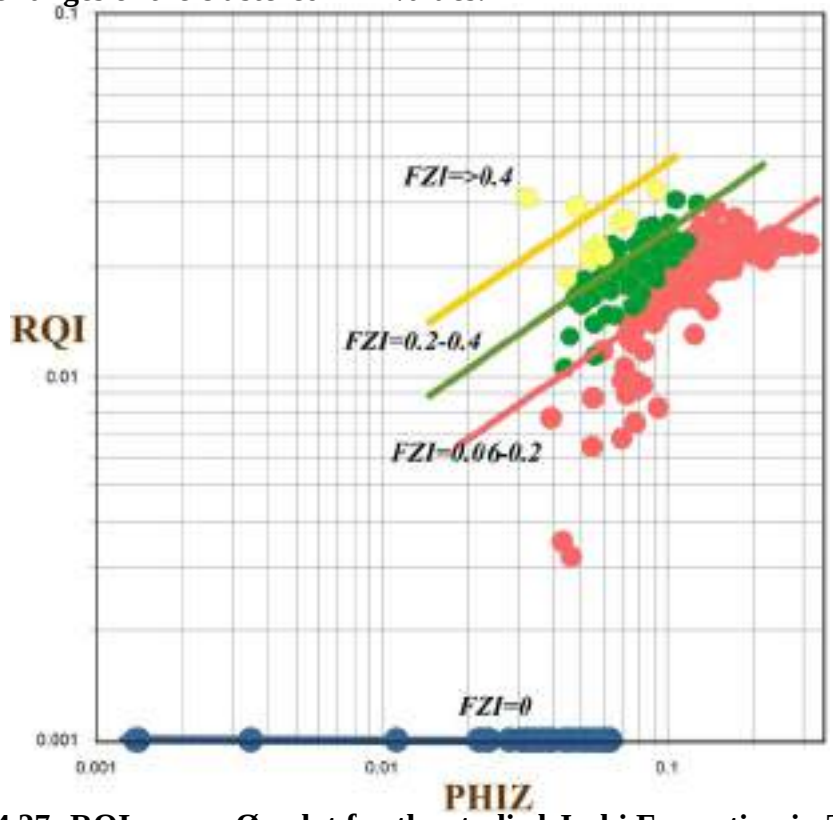

Figure 4.27: RQI versus Øz plot for the studied Jerbi Formation in Taza-2 well with the ranges of the clustered FZI values.

Table 4.5 shows the ranges and averages of the calculated FZI units and the distinguished hydraulic flow units for Jeribe Formation in the wells Ja-49 and Taza-2. The relatively low values of the FZI are an indication to non- effective hydraulic flow zones or zones of low fluid movability which mostly is due to low permeability.

Table 4.5: Range and average of the calculated FZI and the hydraulic units distinguished for the studied Jeribe Formation in Ja-49 and Taza-2wells.

Well	FZI range	Average FZI	Hydraulic Unit
Ja-49	0.0	0	HU-1
	0.07-0.2	0.14	HU-2
	0.2-0.5	0.31	HU-3
	>0.5	1.23	HU-4
Taza-2	0.0	0	HU-1
	0.06-0.2	0.14	HU-2
	0.2-0.4	0.26	HU-3
	>0.4	0.52	HU-4

4.13 Net to Gross Reservoir and Pay Ratios

It is well known that most of the time not all parts of any formation defined as reservoir can contain appreciable fluid volume or can produce hydrocarbons economically. Accordingly, terms such as gross and net thicknesses are used in characterizing reservoirs for better evaluating reserves and production capacity of reservoirs.

In this study, the *gross thickness* represents the thickness of the studied Jeribe Formation from the top to the bottom including even the non-reservoir rocks such as shales, anhydrites, dense dolomitic zones, etc. The *net reservoir*

thickness is that fraction of the gross thickness that subjected to defined cutoffs of shaleness, porosity, and permeability. The *net pay thickness*, on the other hand, is that portion of the net thickness that subjected additionally to the saturation cutoff. Finally, the *net production thickness* represents that portion of the net pay thickness which subjected to the MHI cutoff for being sure about the productivity of the intervals. Accordingly, ratios of each of the last three mentioned parameters can be calculated in comparison with the gross thickness.

The expected net to gross ratios are ranges from 1.0 (100%) to 0.0 (0.0%) for each types of the mentioned net to gross reservoir, pay, or production ratios.

In order to measure the net to gross ratios in this study, the necessary cutoffs of shaleness, porosity, permeability, and water saturation tried to be determined following dependable procedures.

The shaleness cutoff of 35% believed to be acceptable for separating shale zones (of very low permeability) from Shaley zones (may be of appreciable porosity and permeability). The selected value of 35% shaleness for separating shale from Shaley zones has been explained in chapter two of this study.

Regarding permeability cutoff, the value of 1.0md is most acceptable by different authors (Peters, 2001; Law et al., 2001; Tiab and Donaldson, 2004 ; Darling, 2005; and Parnell et al., 2010) to be used for separating zones of effective capacity for fluid transmission from those zones which are incapable producing fluids (zones of less than 1.0md permeability).

As certain value of porosity may be of different values of permeability depending on the type of porosity and the ratio of the effective to total

porosity, so porosity cutoff should be determined depending on the relationship between the calculated porosities and the measured permeabilities, Figure 4.28 shows the crossplot of the porosity versus permeability used for determining the porosity cutoff for Jeribe Formation in Taza-2 well from the laboratory measurements of porosity and permeability done for the cored samples of the formation. As shown in the figure 4.28, the porosity value used as cutoff is the one with 1.0md permeability which appeared to be 11% porosity. Due to absence of core sample analysis data of Jeribe Formation in Ja-49 well, the same 11% porosity value has been used as cutoff in this well also. Accordingly, the values of 35%, 11%, and 1.0md are the cutoffs of shaleness, porosity and permeability, respectively used in this study for measuring the net reservoir thickness and calculating N/G reservoir ratio for Jeribe Formation in both wells of Ja-49 and Taza-2.

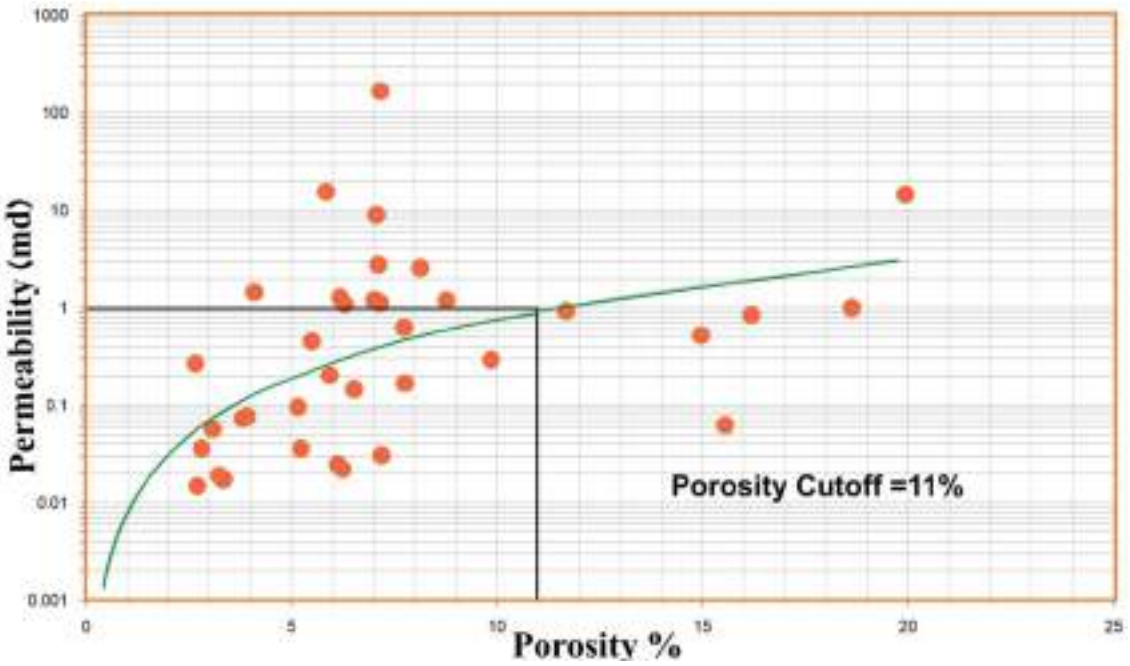

Figure 4.28: Porosity cutoff measurement for Jeribe Formation using porosity versus permeability crossplot for the core data analysis of Taza-2 well.

For distinguishing the hydrocarbon pay zones from water pay zones within the previously determined net reservoir intervals, water saturation cutoff measured for Jeribe Formation in both studied wells as shown in the figures 4.29 and 4.30.

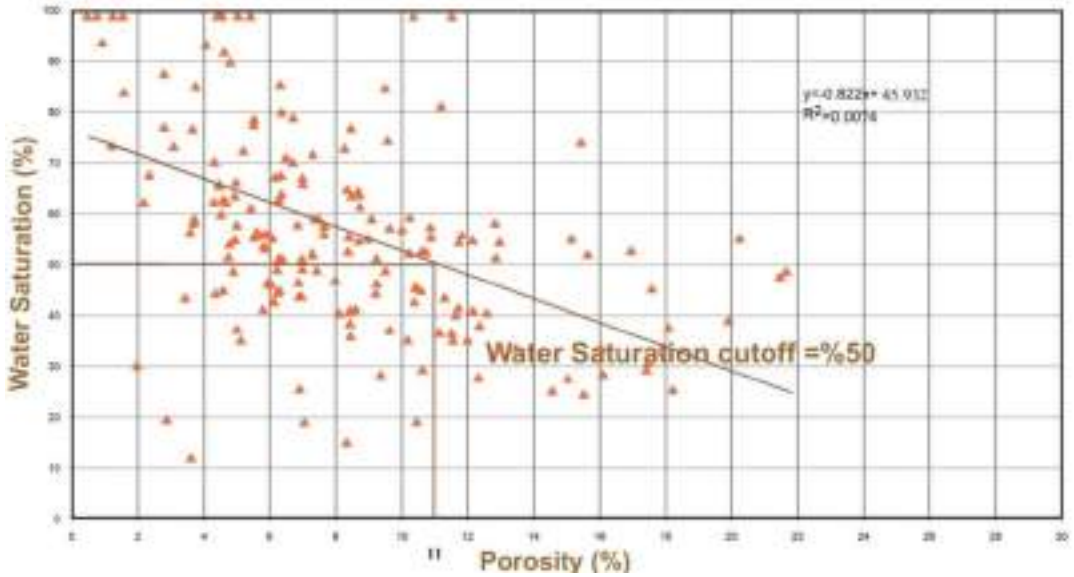

Figure 4.29: Water saturation cutoff determination for Jeribe Formation in Ja-49 well using porosity versus water saturation crossplot.

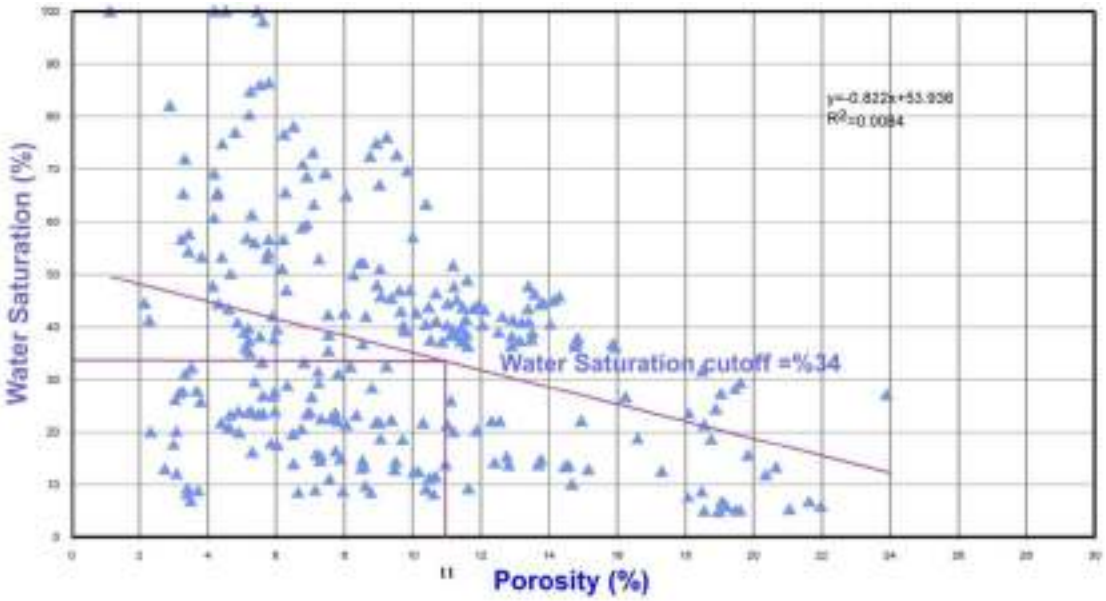

Figure 4.30: Water saturation cutoff determination for Jeribe Formation in Taza-2 well using porosity versus water saturation crossplot.

The mentioned two figures are crossplots of water saturation versus porosity as measured from the log data for Jeribe Formation in the two studied wells with paying attention to the determined porosity cutoff value (11%). The saturation cutoff values for Jeribe Formation in Ja-49 well appeared to be 50% and in Taza-2 well 34%. So zones of higher water saturation than the determined cutoff values consider being non- payable zones due to either absence of hydrocarbons or due to the high volume of the water accompanied the produced hydrocarbons.

As not necessarily all the reservoir hydrocarbons have ability of movement (even with being of high saturations) so distinguishing zones of effective movable hydrocarbons within the payable intervals is vital for calculating N/G production ratio for Jeribe Formation and determining zones for perforation and production in the two studied wells. For this purpose the MHI value of 0.6 used as cutoff for separating zones of effective movable hydrocarbons (zones of ≤0.6 MHI) from zones of immovable or non-effective movable hydrocarbons (zones of >0.6 MHI). Tables 4.6 and 4.7 contain the measured gross thickness of Jeribe Formation in the studied wells and the measured net reservoir, net pay, and net production thicknesses in addition to the calculated N/G reservoir, pay, and production ratios

Table 4.6: Measured N/G reservoir, pay, and production ratios for the studied Jeribe Formation in Ja-49 well.

Reservoir Units	Gross Thickness (m)	Net Reservoir Thickness (m)	Net Pay Thickness (m)	Net Production Thickness (m	N/G Reservoir %	N/G Pay %	N/G Production %
C	35	10	5.75	2.75	29	16	7.0
B	6.0	0.40	0.0	0.0	6.0	0.0	0.0
A	14	3.60	0.85	0.30	26	6.0	2.0
Total	55	14	6.60	3.05	61	22	9.0

Table 4.6: Measured N/G reservoir, pay, and production ratios for the studied Jeribe Formation in Taza-2 well.

Reservoir Units	Gross Thickness (m)	Net Reservoir Thickness (m)	Net Pay Thickness (m)	Net Production Thickness (m	N/G Reservoir %	N/G Pay %	N/G Production %
C	27	11.25	4.45	2.25	42	16	8.3
B	5.0	0.0	0.0	0.0	0.0	0.0	0.0
A	12	2.35	0.90	1.0	20	7.5	8.3
Total	44	13.60	5.35	3.35	62	23.5	16.6

The following observations can be summarized, from the data in the tables 4.5 and 4.6:

1. Reservoir unit RU-C is of the best reservoir potentiality among the distinguished units, whereas the unit RU-B is of the least reservoir potentiality.

2. RU-B in Taza-2 well is completely no payable and consequently non producible unit.
3. The N/G reservoir and pay ratio of Jeribe Formation is almost similar in the two studied wells.
4. The N/G production of Jeribe Formation is higher in Taza-2 than in Ja-49 well.

Figures 4.31 and 4.32 are comprehension figures showing all the applied cutoffs for measuring the net to gross values exhibited in the tables 4.5 and 4.6. From those two figures, the locations of the effective reservoir, payable, and producible zones of Jeribe Formation within the two studied wells can be seen, which will be very helpful in determining best locations for perforation and production. A comparison between the calculated MHI and the FZI values can also be done in the figures 4.31 and 4.32.

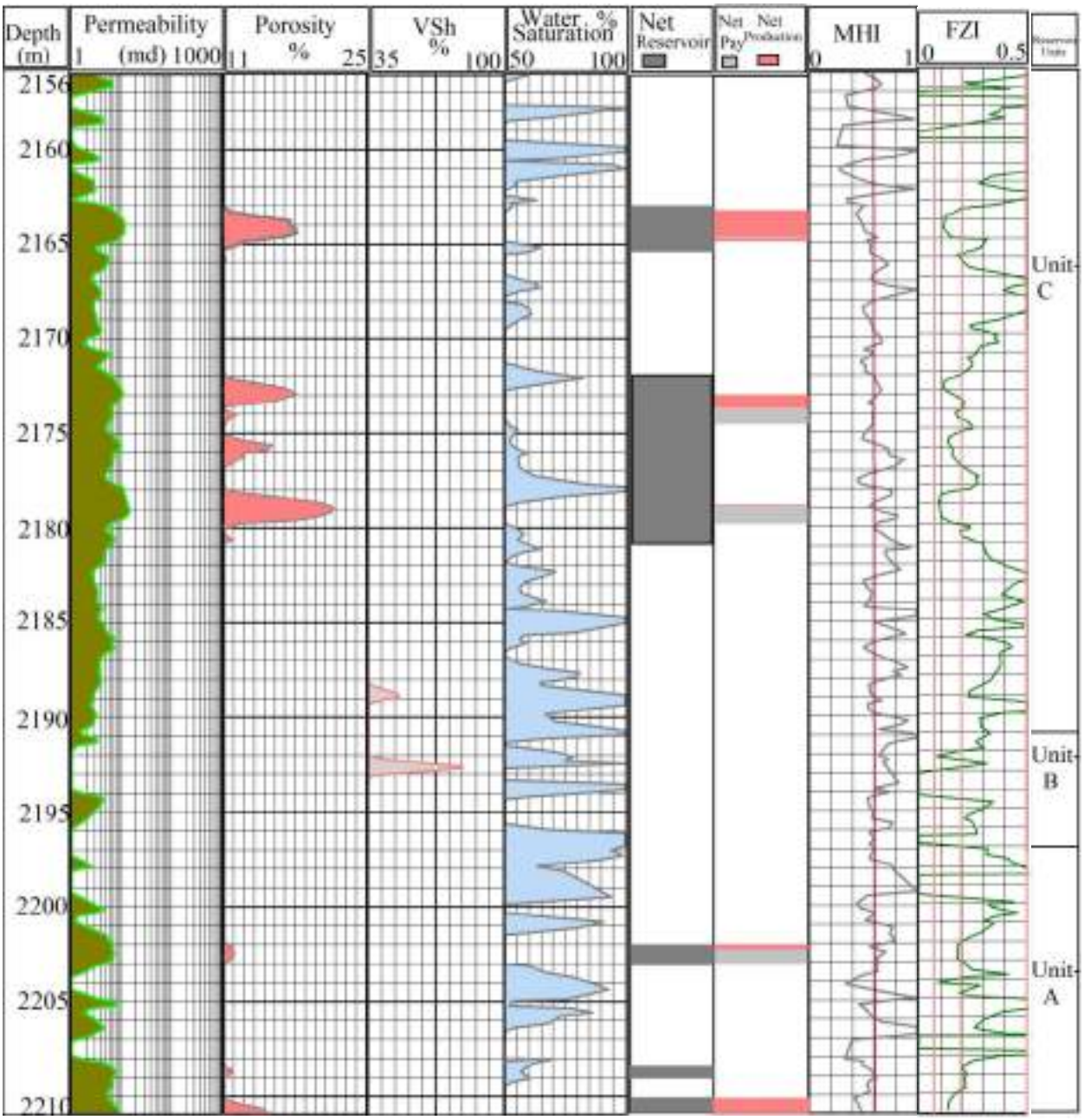

Figure 4.31: Net reservoir, pay, and production with the used cutoffs for the studied Jeribe Formation in the well Ja-49.

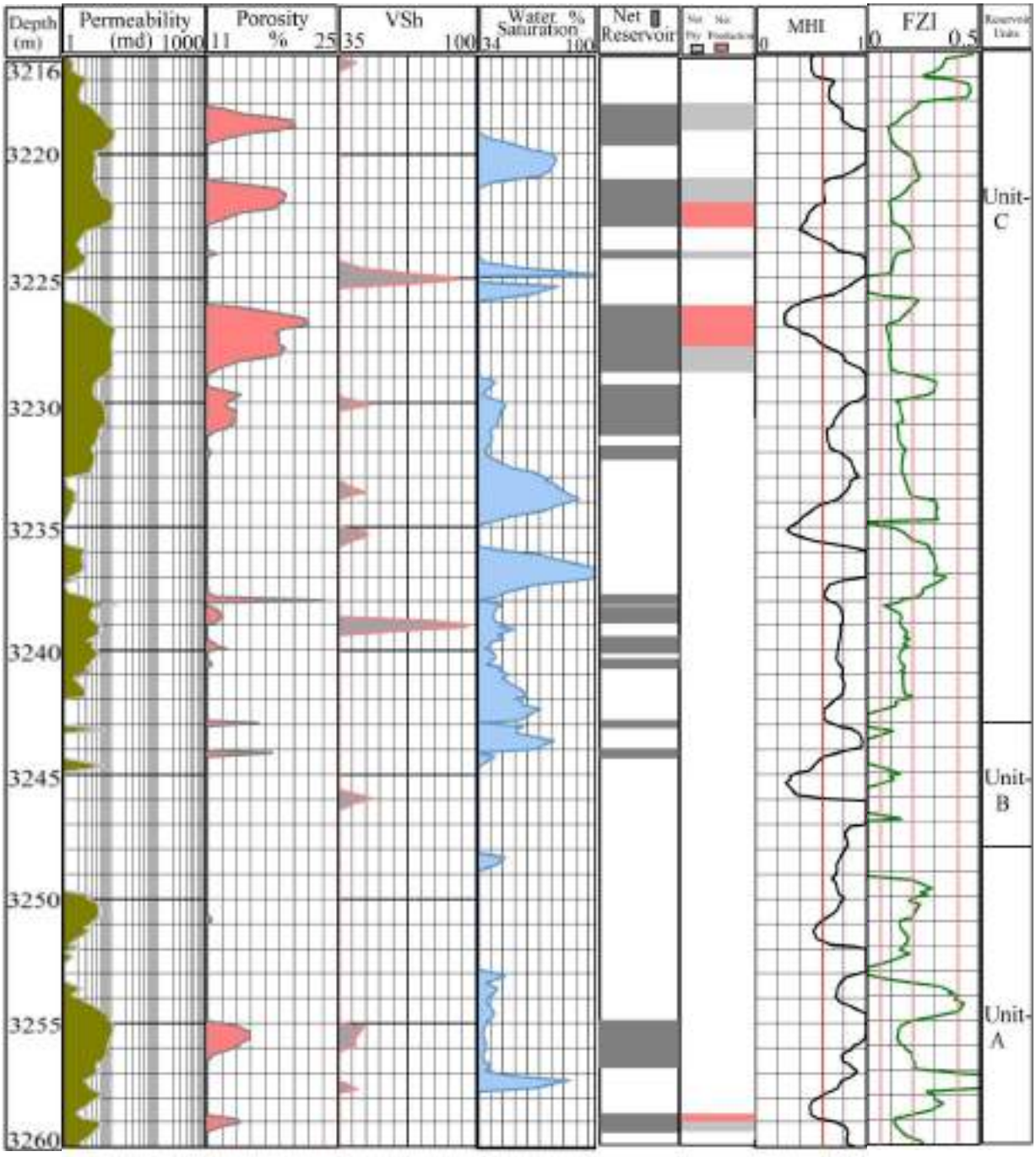

Figure 4.32: Net reservoir, pay, and production with the used cutoffs for the studied Jeribe Formation in the well Taza-2.

CHAPTER FIVE

Conclusions and Recommendations

5.1 Conclusions

From all the previous chapters of this study the following points can be summarized as conclusions:

1. Jeribe Formation in the two studied locations is of around 50m in thickness and comprises mainly of Dolostone and calcareous dolostone and secondly of limestone and dolomitic limestone, interbeded with thin horizons of anhydrite or anhydritic zones.
2. The formation is mostly consists of Wackestone and Mudstone Microfacies with less contribution of Packstone Microfacies and lesser contribution of Grainstone Microfacies.
3. Most parts of Jeribe Formation in the studied wells are Shaley containing less than 35% of shale with being the middle part of the formation relatively of the highest shale content.
4. The porosity is generally fair (less than 15%) and increases upward, and finally decreases near the contact with the Lower Fars Formation. Only few horizons in the formation are of porosity more than 15% and that in the well Ja-49.
5. Secondary porosity (either fractures or vugs) in the two studied wells is generally representing about 2.0 to 3.0% of the total porosity in the formation.
6. There is possibility for existing gas or low density oil filled porosities in the upper part of Jeribe Formation in Taza-2 well with indication for such possibility in Ja-49 as well.

7. Generally, and depending on the multilinear regression method, by taking benefit from the core analysis and log data in calculating permeability, the permeability ranges between poor to moderate (less than 20md).
8. Jeribe Formation in the two wells of Ja-49 and Taza-2 can be subdivided to three distinguishable units on the bases of shale content, porosity, and permeability with being the upper unit (RU-C) of the highest thickness and being the middle unit (RU-B) of the least thickness and least reservoir quality.
9. Almost all parts of the Jeribe Formation in the two studied wells contain hydrocarbons but with different saturations.
10. The relatively low value of the determined cementation factor for Jeribe Formation is an indication for contribution of the fractures (as secondary porosities) in the total porosity of the formation.
11. Highest movable hydrocarbons exist in the determined reservoir unit RU-C of the formation with being the highest in the fractured horizons.
12. A portion of the accumulated hydrocarbons exist in micropores within the matrix which definitely not easy to be produced by conventional ways of production.
13. The expected hydrocarbon production from Jeribe Formation in the two studied wells is being associated with an appreciable value of water especially production from the reservoir unit RU-C and that mostly due to the heterogenitic nature of the formation.
14. Jeribe Formation in the well Ja-49 contains more movable hydrocarbon horizons than in the well Taza-2.

15. The pore throat sizes in the sediments of the Jeribe Formation are highest in the RU-C unit (between 0.5 and 2.0 μm) and lowest in the reservoir unit RU-B (between 0.1 and 0.5 μm).
16. The fluid flow within Jeribe Formation in the studied two wells is through avenues created by connected pores within the rock matrix and through open fractures and vugs.
17. Four flow zone indicators can be distinguished in Jeribe Formation in Ja-49 and Taza-2 wells indicating to four unique hydraulic flow units.
18. From the 55m of the Jeribe Formation in Ja-49 well, only about 3m (09%) can be considered as commercially and naturally productive. Additional 3-4m of payable thickness can be changed to commercially productive by enhancing production through fracturing and increasing permeability.
19. Jeribe Formation in Taza-2 well has almost the same naturally productive thickness (3.35m, 16.6%) from the gross 44m thickness of the formation. With enhancing production by fracturing additional 5-6m may be added to the commercially productive thickness.

5.2 Recommendations

To evaluate Jeribe Formation as best as can be in the two studied fields of Jambour and Taza, the following points are highly recommended:

1. Applying the modern methods of reservoir characterization on Jeribe Formation in highest number of the drilled wells in the two fields (especially, in Jambour Field in which large number of wells have been drilled). Highest number of control points always results to more accurate conclusions.
2. Being Taza Field a new discovered field in the region, and till writing this thesis only three wells have been drilled, (Taza-1 is a discovery well drilled in the crest of the structure, whereas Taza-2 and Taza-3 are appraisal wells), so combining the data of those three wells will too much support in preliminarily detecting the properties and potentiality of Jeribe Formation in the field.
3. Studying Jeribe Formation from reservoir characterization point of view in the fields of Kor Mor and Pulkhana which both are the closest fields to Jambour and Taza, is vital for better understanding the regional heterogeneties occurred to the formation.
4. Evaluating Jeribe Formation in the newly logged or relogged wells in Jambour Field and comparing the results with the old log data will be very helpful in following the changes occurred in the dynamic properties of the field due to the long periods of production or due to any production enhancement operations done for the field.

Appendices

Appendix A

Table A.1: well log data Ja-49 well

Depth (m)	GR (API)	Δt (μs/ft)	ρb (g/cc)	PHIN (%)	Caliper (IN)	MSFL (Ω.m)	LLD (Ω.m)	LLS (Ω.m)
2150.00	14.07	54.53	2.76	5.33	6.15	47.04	51.14	73.42
2150.35	17.10	55.66	2.68	7.80	6.13	27.11	20.59	63.71
2150.60	20.34	55.19	2.67	6.89	6.13	35.18	15.59	57.41
2150.95	23.37	54.25	2.73	5.52	6.22	60.69	20.47	51.26
2151.14	20.99	52.83	2.79	2.27	6.30	80.89	45.87	45.74
2151.28	16.23	52.17	2.86	0.96	6.20	97.58	130.34	40.43
2151.52	10.38	52.45	2.91	0.51	6.20	138.64	277.61	34.74
2151.96	6.91	53.11	2.87	0.51	6.22	170.06	348.78	30.73
2152.23	6.91	54.25	2.90	0.77	6.22	130.39	231.92	27.94
2152.53	8.86	55.19	2.87	1.36	6.22	88.74	125.97	25.90
2152.75	11.45	55.94	2.84	2.01	6.20	63.00	74.95	24.49
2152.86	14.27	56.79	2.87	2.92	6.17	40.89	48.08	22.50
2153.29	26.60	61.23	2.83	8.92	6.17	25.38	26.91	22.11
2153.65	46.08	59.62	2.80	12.05	6.15	29.78	16.13	23.91
2153.81	46.08	55.00	2.75	10.87	6.24	26.23	13.94	26.09
2153.97	40.23	51.89	2.78	8.33	6.26	10.99	56.25	29.51
2154.16	28.11	51.13	2.87	2.02	6.17	8.33	748.13	32.76
2154.36	9.49	51.13	2.91	0.84	6.20	9.17	3519.44	36.38
2154.52	2.78	50.94	2.90	0.39	6.22	13.81	5278.59	41.16
2154.79	1.92	50.94	2.91	0.39	6.20	23.14	6320.06	46.58
2155.01	2.35	50.85	2.92	0.39	6.20	57.26	8036.06	53.20
2155.34	4.29	50.85	2.90	0.52	6.20	145.33	9704.66	61.95
2155.63	6.46	51.13	2.88	1.04	6.20	241.37	11457.25	70.76
2155.91	9.05	52.36	2.85	1.63	6.20	277.67	9086.72	84.00
2156.15	14.68	55.85	2.80	4.89	6.20	334.44	3383.82	95.06
2156.42	27.01	59.25	2.66	9.84	6.20	350.81	361.21	108.57
2156.59	35.45	59.06	2.65	12.84	6.17	323.70	81.05	120.53
2156.91	45.41	55.94	2.71	13.49	6.17	285.40	48.34	137.70
2157.10	46.49	52.74	2.78	7.04	6.17	208.24	37.17	151.42

2157.27	44.32	51.42	2.88	1.83	6.22	130.17	43.37	171.63
2157.57	30.69	50.94	2.92	2.48	6.30	76.95	56.71	189.02
2157.84	19.00	52.83	2.86	4.05	6.17	43.22	106.25	204.25
2158.03	18.78	58.68	2.80	10.24	6.20	39.02	236.12	235.73
2158.49	44.53	59.43	2.74	10.82	6.17	33.41	590.37	266.87
2158.66	44.31	58.40	2.70	10.11	6.17	21.24	1104.69	293.36
2158.96	30.89	51.70	2.80	6.52	6.22	26.84	406.19	338.36
2159.25	12.93	51.42	2.89	1.38	6.13	59.25	43.67	372.41
2159.36	11.19	51.13	2.91	0.73	6.11	121.34	14.44	359.20
2159.58	12.27	52.08	2.89	0.86	6.11	225.33	17.14	326.97
2159.88	18.77	55.00	2.85	1.84	6.13	169.79	30.28	286.45
2160.43	53.18	60.00	2.78	5.23	6.13	63.89	185.12	255.60
2160.53	56.21	62.83	2.75	8.16	6.13	20.90	1138.38	223.86
2160.64	53.39	59.72	2.73	6.86	6.13	9.47	2000.71	195.99
2160.91	31.53	54.91	2.86	4.12	6.13	14.26	1137.47	175.00
2161.11	18.32	52.64	2.87	2.36	6.17	32.29	366.44	153.26
2161.24	17.46	53.96	2.84	3.01	6.13	72.89	65.94	132.96
2161.38	20.27	55.00	2.79	7.05	6.13	183.91	11.53	115.31
2161.98	44.08	55.94	2.75	10.77	6.13	276.97	11.98	99.09
2162.19	44.29	55.00	2.71	10.96	6.11	241.24	38.87	86.86
2162.41	42.99	54.06	2.76	7.71	6.15	212.47	95.37	76.08
2162.77	34.33	53.30	2.82	4.97	6.11	102.76	120.40	62.36
2162.98	23.29	54.91	2.76	5.69	6.11	27.41	119.89	52.10
2163.12	22.42	59.62	2.74	9.27	6.13	8.50	72.91	45.30
2163.53	36.71	62.83	2.67	16.38	6.15	10.80	39.20	40.44
2163.66	38.00	63.49	2.63	18.46	6.15	33.25	30.48	35.45
2163.91	30.86	63.49	2.54	19.96	6.17	63.17	35.92	31.69
2164.10	26.10	64.06	2.55	20.22	6.17	61.56	45.48	28.02
2164.29	25.66	61.23	2.52	19.70	6.17	49.54	66.00	25.01
2164.64	29.99	57.55	2.54	15.08	6.13	24.68	86.63	21.91
2164.81	34.75	55.19	2.57	13.58	6.15	15.61	43.67	19.94
2165.27	58.34	55.66	2.69	12.21	6.15	22.48	23.61	17.98
2165.38	56.61	56.51	2.67	12.73	6.13	33.36	25.72	15.91
2165.60	47.30	57.36	2.66	13.19	6.13	86.23	24.53	15.34
2165.95	33.88	56.23	2.65	13.78	6.17	63.52	22.52	16.44
2166.17	32.79	54.72	2.66	12.61	6.15	26.82	20.48	19.50
2166.52	32.79	53.40	2.69	10.52	6.15	14.10	22.05	23.14
2166.79	36.47	52.64	2.71	7.98	6.17	13.32	28.38	27.73

2166.96	42.31	53.40	2.70	5.70	6.17	15.40	31.15	31.98
2167.18	42.31	53.77	2.67	3.75	6.17	13.60	26.10	37.61
2167.39	40.36	54.53	2.65	2.51	6.15	11.69	19.13	43.82
2167.61	39.06	54.25	2.63	3.03	6.15	12.15	16.32	50.53
2167.94	37.11	53.68	2.63	3.42	6.28	11.13	18.25	58.28
2168.10	39.06	52.17	2.65	1.80	6.17	12.39	21.72	66.54
2168.32	41.22	53.02	2.66	0.89	6.13	19.39	26.72	75.31
2168.56	42.95	53.96	2.68	2.19	6.15	31.54	32.90	89.34
2168.86	39.48	54.91	2.69	3.95	6.15	30.18	37.03	105.99
2169.14	35.59	54.62	2.71	6.75	6.13	18.81	40.73	129.38
2169.27	33.85	54.62	2.70	11.12	6.20	15.75	40.35	158.12
2169.49	35.80	54.62	2.71	11.25	6.26	14.53	36.38	187.59
2169.92	47.05	53.58	2.72	9.88	6.24	17.86	30.67	220.45
2170.12	52.90	52.36	2.70	7.99	6.24	30.06	27.34	261.54
2170.50	51.60	53.58	2.67	8.06	6.28	44.89	29.22	307.45
2170.71	57.00	56.42	2.64	8.97	6.28	42.92	39.24	361.30
2170.88	58.52	58.68	2.57	9.88	6.26	37.55	53.33	420.58
2171.12	58.30	56.89	2.61	11.90	6.24	33.66	60.01	508.52
2171.26	54.62	55.57	2.66	14.12	6.28	30.19	53.77	644.76
2171.50	46.61	54.91	2.71	12.49	6.26	28.38	46.68	757.93
2171.94	39.46	56.60	2.67	11.19	6.28	43.46	34.49	865.68
2172.29	36.65	59.43	2.63	13.27	6.26	77.28	29.54	1017.64
2172.43	37.95	62.74	2.58	22.72	6.28	81.23	30.70	1231.59
2172.59	44.44	63.77	2.55	23.37	6.26	65.63	31.90	1531.69
2172.73	43.14	63.11	2.51	22.27	6.20	55.70	34.10	1851.99
2173.05	36.86	59.62	2.55	18.82	6.17	42.13	39.56	3445.99
2173.27	33.18	58.11	2.63	15.04	6.15	28.43	46.73	3935.00
2173.68	27.33	57.55	2.67	12.63	6.13	22.53	51.90	4286.06
2173.90	26.68	57.83	2.67	12.76	6.13	24.66	39.11	4705.76
2174.12	31.01	57.74	2.64	14.78	6.13	25.03	31.33	5370.68
2174.36	34.04	57.45	2.66	14.78	6.15	27.59	34.84	6061.61
2174.58	35.55	57.36	2.69	12.44	6.15	33.39	35.81	6925.47
2174.85	37.28	58.40	2.70	12.44	6.17	42.70	30.19	8047.97
2175.07	37.50	60.57	2.66	14.13	6.15	54.01	19.24	9185.15
2175.45	36.84	62.08	2.62	16.15	6.15	37.50	12.24	10377.2
2175.67	35.11	63.02	2.57	18.76	6.15	25.20	7.60	113815
2175.83	34.46	62.17	2.59	19.08	6.13	25.09	5.45	12338.32
2176.02	37.92	58.68	2.64	17.46	6.15	28.16	5.88	11406.14

2176.32	35.76	58.02	2.62	16.41	6.13	26.42	7.28	10246.45
2176.46	35.75	58.02	2.64	15.50	6.13	16.98	9.39	8954.09
2176.81	41.81	58.11	2.65	14.79	6.15	13.32	13.09	7904.03
2177.36	49.17	57.55	2.67	13.16	6.15	8.01	19.29	6977.12
2177.52	48.95	60.38	2.68	12.97	6.17	4.88	21.59	6341.36
2177.74	47.00	65.38	2.66	13.81	6.17	5.03	19.16	5442.43
2177.93	48.95	73.58	2.64	14.73	6.20	5.90	19.16	4806.74
2178.23	56.95	74.06	2.60	17.40	6.20	7.87	18.98	4322.61
2178.34	57.82	72.45	2.55	22.74	6.15	10.53	18.63	3713.79
2178.47	56.52	69.81	2.49	28.93	6.15	14.11	17.77	3276.53
2178.72	49.81	68.40	2.46	28.15	6.17	16.71	16.95	1995.16
2179.21	30.76	68.77	2.48	25.22	6.17	16.40	13.90	1763.25
2179.32	29.67	64.62	2.52	23.92	6.17	17.29	11.24	1603.53
2179.42	30.54	57.36	2.56	21.90	6.15	17.88	8.36	1430.84
2179.89	42.44	56.23	2.61	16.42	6.17	17.30	7.77	1288.93
2180.02	42.87	57.08	2.67	12.45	6.13	16.42	8.76	1138.96
2180.49	35.73	60.00	2.61	13.24	6.17	15.68	9.87	1006.70
2180.62	35.29	58.02	2.64	12.84	6.17	13.11	10.65	872.95
2180.76	37.24	56.42	2.65	9.59	6.15	8.96	12.12	771.58
2181.17	42.87	55.66	2.63	7.70	6.13	6.38	13.26	669.15
2181.33	42.65	54.91	2.62	6.40	6.22	6.79	13.34	602.63
2181.71	37.88	54.25	2.63	5.03	6.26	8.31	10.25	503.15
2181.87	38.53	53.77	2.65	3.79	6.20	10.65	6.26	428.15
2182.09	43.08	53.68	2.69	3.99	6.15	12.00	3.99	360.84
2182.26	45.02	53.40	2.67	3.99	6.17	11.53	3.54	290.08
2182.47	45.24	53.02	2.65	4.06	6.17	14.10	4.21	242.17
2182.83	42.64	52.74	2.64	3.47	6.15	20.80	5.21	204.07
2183.29	38.31	52.08	2.63	3.08	6.11	19.22	6.09	168.77
2183.53	34.63	52.83	2.66	3.08	6.13	9.37	6.45	139.58
2183.72	30.51	53.58	2.69	3.08	6.22	5.09	6.89	115.38
2183.86	28.35	53.68	2.67	3.73	6.22	3.47	10.64	98.18
2184.05	30.29	53.02	2.63	4.71	6.20	2.55	17.35	85.11
2184.32	30.72	53.30	2.67	4.97	6.22	2.81	18.55	70.37
2184.60	32.24	54.34	2.69	3.67	6.30	5.28	15.96	61.59
2184.92	34.40	56.60	2.68	4.06	6.20	6.15	13.44	52.88
2185.25	34.18	58.49	2.69	10.71	6.20	5.25	11.32	46.29
2185.52	33.31	57.36	2.65	11.69	6.22	4.84	11.32	40.53
2185.71	30.28	66.79	2.71	10.91	6.22	7.15	12.45	34.48

2185.82	27.90	61.51	2.68	5.96	6.22	18.21	18.15	29.62
2186.07	29.85	63.77	2.65	4.98	6.20	27.96	23.81	26.93
2186.34	31.79	56.89	2.64	4.46	6.17	27.18	28.27	27.68
2186.56	33.09	53.68	2.65	3.87	6.17	20.04	28.96	31.91
2186.77	32.87	53.11	2.65	3.87	6.15	14.50	26.70	37.13
2187.21	32.00	53.11	2.66	4.40	6.24	14.93	29.37	43.22
2187.37	33.73	53.58	2.67	5.50	6.26	15.66	32.31	50.78
2187.64	35.68	55.19	2.69	7.33	6.17	17.97	30.82	59.65
2188.11	45.63	55.28	2.68	12.35	6.22	27.41	27.77	70.10
2188.24	52.34	54.34	2.66	12.80	6.20	20.97	25.98	81.59
2188.73	70.30	55.57	2.66	11.50	6.20	23.09	24.78	97.72
2188.84	71.17	56.42	2.68	12.87	6.20	30.78	27.00	115.93
2188.95	69.87	56.42	2.70	13.20	6.20	41.81	26.25	136.24
2189.09	65.97	55.57	2.67	12.35	6.20	46.73	15.01	164.71
2189.28	58.40	54.72	2.66	11.90	6.20	44.89	8.15	186.23
2189.44	53.85	54.06	2.68	10.85	6.20	48.22	7.20	210.70
2189.69	50.17	53.30	2.70	10.27	6.17	32.69	8.93	245.27
2190.09	50.17	52.36	2.73	9.10	6.17	20.34	12.92	296.53
2190.37	47.57	53.11	2.74	9.36	6.17	20.98	17.29	358.27
2190.64	37.82	55.28	2.73	10.27	6.22	23.62	21.06	433.14
2190.86	33.49	54.91	2.75	11.38	6.30	23.71	26.29	508.89
2191.07	33.93	53.58	2.82	10.73	6.17	21.29	32.35	598.04
2191.43	36.09	50.94	2.81	6.75	6.20	19.50	33.25	716.28
2191.84	42.58	50.19	2.78	6.36	6.17	17.73	27.18	841.76
2191.97	49.72	50.00	2.73	7.93	6.17	25.21	17.94	970.48
2192.22	66.60	51.13	2.72	8.71	6.22	40.36	12.18	1129.28
2192.60	85.86	55.28	2.73	8.71	6.13	20.04	11.62	1046.27
2192.65	86.30	56.23	2.75	9.56	6.11	7.69	12.54	898.69
2192.82	80.67	55.19	2.80	10.02	6.11	6.66	13.03	772.02
2193.06	62.27	49.62	2.78	6.37	6.13	8.71	12.79	663.04
2193.20	55.12	49.25	2.74	5.98	6.13	16.51	11.63	564.20
2193.55	47.76	51.89	2.71	7.48	6.13	26.00	11.10	475.56
2193.96	40.83	55.47	2.68	9.43	6.13	22.70	12.52	408.64
2194.23	38.67	54.62	2.66	10.87	6.13	18.51	15.78	361.18
2194.45	39.53	53.77	2.69	12.37	6.17	16.73	15.79	307.26
2194.61	45.37	53.30	2.71	11.59	6.13	18.14	14.77	269.09
2194.83	47.54	52.45	2.72	10.74	6.13	24.53	10.77	224.70
2195.21	42.34	51.79	2.75	9.70	6.13	33.90	8.59	189.32

2195.35	41.47	51.23	2.78	8.00	6.11	45.14	9.91	156.56
2195.46	42.99	51.13	2.80	6.18	6.15	38.12	16.69	129.48
2195.92	60.08	51.13	2.79	5.20	6.11	18.75	34.62	107.06
2196.06	60.73	51.70	2.77	6.31	6.11	20.19	46.33	89.38
2196.19	58.78	52.17	2.75	8.14	6.13	21.40	41.57	78.26
2196.52	46.88	51.79	2.78	7.36	6.15	15.76	34.09	66.58
2196.87	35.19	52.08	2.80	6.45	6.15	13.04	24.59	55.59
2196.98	34.75	53.02	2.77	6.84	6.17	9.81	15.24	46.41
2197.28	41.68	54.91	2.73	6.06	6.17	7.20	26.29	38.37
2197.39	42.33	56.13	2.81	4.04	6.17	9.47	40.53	33.28
2197.77	36.91	54.72	2.90	2.41	6.13	12.62	21.00	27.77
2197.88	37.78	53.11	2.92	0.78	6.15	9.25	13.10	22.96
2198.02	40.16	51.79	2.89	0.52	6.15	9.51	14.58	19.72
2198.18	39.94	51.23	2.85	1.11	6.13	12.05	17.43	17.92
2198.31	34.09	50.57	2.82	2.61	6.13	14.36	18.43	19.69
2198.89	9.85	49.25	2.79	4.69	6.17	21.24	23.43	23.57
2199.02	9.41	50.94	2.77	7.43	6.15	31.54	30.08	27.44
2199.38	28.24	58.77	2.75	9.91	6.15	19.40	40.29	33.49
2199.68	44.47	59.72	2.78	11.01	6.17	9.19	48.32	41.26
2199.87	49.67	53.68	2.76	10.04	6.17	23.02	44.36	51.82
2200.03	47.72	51.89	2.74	8.80	6.17	52.84	33.01	65.07
2200.33	40.57	54.06	2.74	8.80	6.15	59.55	27.05	76.47
2200.74	13.51	55.66	2.73	9.39	6.15	62.37	25.56	89.87
2200.93	12.21	55.66	2.70	10.24	6.28	59.48	27.32	107.65
2201.17	13.94	55.66	2.68	11.67	6.17	48.90	24.61	137.80
2201.36	17.19	56.42	2.65	12.65	6.13	37.01	22.60	168.18
2201.61	20.87	56.42	2.66	13.69	6.15	33.68	20.36	195.80
2201.91	16.32	56.60	2.64	13.17	6.15	18.23	17.82	227.93
2202.07	17.19	55.85	2.67	13.82	6.13	24.71	34.04	267.82
2202.32	20.86	54.25	2.73	12.91	6.20	50.51	136.05	323.62
2202.64	31.47	53.58	2.74	11.09	6.26	45.24	669.34	394.99
2202.86	42.07	54.25	2.77	8.29	6.24	37.70	1605.26	464.06
2203.11	49.00	52.74	2.80	8.35	6.24	22.67	925.75	561.12
2203.30	47.05	51.13	2.78	6.73	6.28	13.85	111.32	672.23
2203.49	38.39	50.28	2.75	7.18	6.28	22.22	30.78	797.22
2203.79	28.86	52.83	2.72	13.70	6.26	24.66	17.39	945.81
2204.22	23.02	65.09	2.69	12.53	6.24	17.37	16.60	1111.36
2204.55	21.93	65.85	2.72	6.53	6.28	17.02	44.75	1356.61

2204.82	24.53	55.47	2.79	5.23	6.26	23.18	105.92	1687.29
2204.93	28.85	53.96	2.80	6.34	6.28	35.98	84.51	1908.97
2205.12	24.52	53.68	2.79	7.97	6.26	40.76	30.79	2040.33
2205.34	18.03	54.34	2.76	9.40	6.28	45.89	14.18	1785.87
2205.53	17.38	54.91	2.72	9.93	6.26	67.39	15.31	1563.14
2205.69	24.30	53.77	2.74	8.75	6.20	45.97	20.35	1317.10
2205.91	24.95	53.30	2.76	6.47	6.17	21.24	25.85	1109.78
2206.13	20.41	51.70	2.80	1.85	6.13	18.95	23.75	917.47
2206.34	17.37	50.94	2.94	0.61	6.22	22.35	21.74	744.27
2206.59	17.16	51.70	2.95	0.87	6.26	24.60	19.49	615.30
2206.83	15.21	53.11	2.93	2.96	6.20	19.34	21.08	508.73
2207.27	6.98	55.00	2.89	5.89	6.15	21.29	26.27	412.77
2207.51	2.65	57.17	2.83	10.32	6.17	16.67	27.84	334.85
2207.73	2.43	57.83	2.78	13.51	6.17	12.22	18.80	276.85
2207.98	4.81	58.02	2.65	12.28	6.15	13.93	17.87	237.78
2208.33	9.57	58.77	2.72	13.19	6.11	21.38	28.99	189.24
2208.52	15.19	59.25	2.71	13.97	6.13	50.33	39.98	144.98
2208.69	20.39	58.30	2.69	13.06	6.22	210.79	42.74	115.37
2208.96	27.75	56.13	2.69	12.02	6.22	355.38	30.98	91.81
2209.28	31.21	56.51	2.67	13.72	6.20	315.49	14.26	77.36
2209.45	31.21	58.68	2.65	15.93	6.17	182.80	7.88	64.57
2209.69	27.96	60.38	2.62	18.54	6.17	92.55	8.02	55.98
2209.88	24.71	62.08	2.60	18.54	6.13	131.73	14.84	48.07
2210.13	19.30	61.60	2.56	16.98	6.09	77.64	29.52	40.90
2210.26	17.13	59.25	2.56	14.31	6.17	11.88	28.24	34.80
2210.48	15.61	57.74	2.59	11.96	6.17	9.30	22.12	30.17
2210.75	15.40	56.79	2.69	10.01	6.13	22.16	19.58	26.16
2211.03	15.61	55.00	2.75	7.53	6.09	60.70	16.66	22.46
2211.62	19.94	51.42	2.91	4.21	6.17	27.46	15.92	16.89
2211.95	21.23	51.23	2.94	2.19	6.17	9.59	19.30	15.51
2212.11	19.28	51.23	2.96	1.02	6.15	9.74	36.40	16.58

Appendix B

Well Log Derived Porosities, Permeability, and Shale Volume.

Table B.1: well log derived Porosity, Permeability, and Shale volume - Ja- 49 well

Depth (m)	Vsh%	ØS %	ØS corr%	ØN %	ØN Corr%	ØD %	ØD corr %	N-D corr%	Øf %	K-log (md)
2156.10	3.27	8.48	8.11	4.89	4.40	3.52	3.08	3.74	0.00	3.02
2156.43	8.36	10.82	9.88	9.84	8.62	11.29	10.2	9.42	0.00	6.65
2156.68	12.62	10.69	9.24	12.84	10.94	11.75	10.0	10.52	1.27	6.52
2156.84	19.49	8.55	6.31	13.49	10.57	8.74	6.17	8.37	2.05	3.81
2157.22	20.36	6.34	4.01	7.04	3.99	4.56	1.88	2.94	0.00	0.48
2157.49	18.64	5.43	3.30	1.83	-0.97	-0.66	-3.10	0.00	0.00	0.00
2157.66	9.96	5.11	3.97	2.48	0.99	-2.63	-3.93	0.00	0.00	0.00
2157.82	4.79	6.41	5.86	4.05	3.33	0.51	-0.12	1.60	0.00	0.57
2158.34	4.71	10.43	9.89	10.24	9.53	3.87	3.25	6.39	0.00	4.33
2158.50	18.80	10.95	8.79	10.82	8.00	7.12	4.64	6.32	0.00	4.06
2158.61	18.63	10.23	8.10	10.11	7.31	9.32	6.87	7.09	0.00	4.50
2158.83	10.07	5.63	4.47	6.52	5.01	3.64	2.31	3.67	0.00	0.84
2159.02	2.71	5.43	5.12	1.38	0.97	-1.11	-1.46	0.00	0.00	0.00
2159.18	2.18	5.24	4.99	0.73	0.40	-2.27	-2.5	0.00	0.00	0.00
2159.51	2.51	5.89	5.60	0.86	0.48	-0.88	-1.20	0.00	0.00	0.00
2159.87	4.70	7.90	7.36	1.84	1.13	1.09	0.47	0.80	0.00	1.24
2160.11	26.3	11.34	8.31	5.23	1.27	4.81	1.33	1.30	0.00	2.16
2160.47	29.5	13.25	9.90	8.16	3.73	6.43	2.55	3.14	0.00	3.76
2160.63	26.59	11.14	8.09	6.86	2.87	7.59	4.09	3.48	0.00	3.28
2160.82	10.41	7.83	6.64	4.12	2.56	0.75	-0.62	0.97	0.00	0.45
2161.04	4.54	6.28	5.76	2.36	1.68	-0.06	-0.66	0.51	0.00	0.16
2161.23	4.23	7.19	6.70	3.01	2.38	1.45	0.89	1.63	0.00	1.26
2161.69	5.27	7.90	7.29	7.05	6.26	4.11	3.42	4.84	0.00	2.83
2161.96	18.45	8.55	6.43	10.77	8.00	6.32	3.89	5.95	0.00	2.71
2162.16	18.62	7.90	5.76	10.96	8.17	8.29	5.84	7.01	1.24	3.16
2162.43	17.64	7.25	5.23	7.71	5.06	6.09	3.77	4.42	0.00	1.78

2162.67	11.96	6.73	5.36	4.97	3.18	2.84	1.27	2.22	0.00	0.63
2162.84	6.497	7.83	7.09	5.69	4.72	5.74	4.88	4.80	0.00	3.05
2163.05	6.13	11.08	10.37	9.27	8.35	7.14	6.32	7.34	0.00	5.48
2163.33	13.38	13.28	11.75	16.38	14.37	10.50	8.74	11.55	0.00	7.52
2163.49	14.20	13.73	12.11	18.46	16.33	12.59	10.7	13.53	1.42	8.64
2163.74	10.05	13.73	12.58	19.96	18.45	17.81	16.48	17.47	4.88	11.24
2164.04	7.729	14.12	13.24	20.22	19.06	17.00	15.98	17.52	4.28	11.47
2164.42	7.53	12.18	11.31	19.70	18.57	18.97	17.98	18.28	6.96	11.30
2164.74	9.60	9.65	8.55	15.08	13.64	17.81	16.55	15.09	6.54	8.93
2164.85	12.21	8.03	6.63	13.58	11.75	15.84	14.23	12.99	6.36	6.97
2165.15	31.87	8.35	4.70	12.21	7.43	9.58	5.38	6.41	1.71	3.01
2165.43	29.93	8.94	5.50	12.73	8.24	10.51	6.53	7.41	1.90	3.79
2165.56	21.02	9.52	7.11	13.19	10.04	11.32	8.55	9.30	2.18	5.05
2165.83	11.70	8.74	7.40	13.78	12.02	11.90	10.36	11.19	3.79	5.91
2166.19	11.09	7.70	6.43	12.61	10.94	10.97	9.51	10.23	3.79	5.04
2166.46	11.09	6.80	5.52	10.52	8.86	9.58	8.12	8.49	2.96	3.88
2166.62	13.24	6.28	4.76	7.98	6.00	8.31	6.56	6.28	1.52	2.64
2166.87	17.14	6.80	4.83	5.70	3.13	9.12	6.86	5.00	0.16	2.52
2167.09	17.14	7.06	5.09	3.75	1.18	10.51	8.26	4.72	0.00	2.94
2167.31	15.76	7.57	5.77	2.51	0.15	11.91	9.83	4.99	0.00	3.69
2167.47	14.89	7.38	5.67	3.03	0.80	12.60	10.64	5.72	0.04	4.01
2167.74	13.6	6.99	5.43	3.42	1.38	12.61	10.81	6.10	0.66	4.02
2168.04	14.89	5.95	4.25	1.80	-0.44	11.68	9.72	4.64	0.39	2.89
2168.18	16.36	6.54	4.66	0.89	-1.57	10.98	8.83	3.63	0.00	2.65
2168.40	17.61	7.19	5.17	2.19	-0.45	10.29	7.97	3.76	0.00	2.70
2168.72	15.17	7.83	6.09	3.95	1.67	9.48	7.48	4.58	0.00	3.13
2169.13	12.70	7.64	6.18	6.75	4.85	8.55	6.87	5.86	0.00	3.27
2169.54	11.69	7.64	6.30	11.12	9.36	9.13	7.59	8.48	2.17	4.09
2169.76	12.83	7.64	6.17	11.25	9.32	8.67	6.98	8.15	1.98	3.80
2169.92	20.82	6.93	4.54	9.88	6.76	7.97	5.3	6.00	1.45	2.29
2170.28	26.10	6.08	3.09	7.99	4.08	9.25	5.81	4.95	1.85	1.77
2170.55	24.84	6.93	4.08	8.06	4.33	10.64	7.37	5.85	1.77	2.77
2170.63	30.37	8.87	5.39	8.97	4.41	12.27	8.27	6.34	0.95	3.98
2170.77	32.07	10.43	6.75	9.88	5.07	16.10	11.8	8.48	1.72	6.10
2171.04	31.82	9.20	5.55	11.90	7.13	14.01	9.2	8.48	2.93	5.00
2171.29	27.83	8.29	5.10	14.12	9.94	10.99	7.33	8.64	3.54	3.97
2171.53	20.45	7.83	5.49	12.49	9.42	8.68	5.98	7.70	2.21	3.28
2171.78	15.16	9.00	7.26	11.19	8.92	10.53	8.53	8.73	1.46	4.84

2172.08	13.35	10.95	9.42	13.27	11.27	12.97	11.1	11.24	1.82	7.05
2172.62	14.16	13.22	11.59	22.72	20.60	15.29	14.2	17.01	5.42	9.89
2172.76	18.73	13.93	11.78	23.37	20.56	17.15	4.68	17.62	5.84	10.52
2172.95	17.7	13.47	11.44	22.27	19.61	19.00	16.7	18.14	6.69	10.98
2173.27	13.48	11.08	9.53	18.82	16.79	17.15	1537	16.09	6.55	9.26
2173.44	11.31	10.04	8.74	15.04	13.34	12.97	11.48	12.41	3.67	7.08
2173.55	8.30	9.65	8.70	12.63	11.38	10.65	9.56	10.47	1.77	6.18
2173.74	7.99	9.84	8.93	12.76	11.56	10.77	9.71	10.64	1.71	6.37
2174.04	10.13	9.78	8.62	14.78	13.26	12.51	11.7	12.22	3.60	6.91
2174.28	11.79	9.57	8.23	14.78	13.01	11.24	9.8	11.35	3.11	6.14
2174.58	12.68	9.52	8.07	12.44	10.53	9.73	8.06	9.30	1.23	5.19
2174.83	13.74	10.23	8.66	12.44	10.37	8.92	7.11	8.74	0.08	5.09
2175.10	13.88	11.72	10.13	14.13	12.05	11.12	9.29	10.67	0.54	6.75
2175.37	13.47	12.76	11.22	16.15	14.13	13.44	11.6	12.90	1.68	8.35
2175.62	12.42	13.41	11.99	18.76	16.89	16.11	14.48	15.69	3.70	10.04
2175.86	12.04	12.83	11.45	19.08	17.28	14.72	13.13	15.21	3.76	9.34
2176.03	14.15	10.43	8.81	17.46	15.33	12.29	10.42	12.88	4.07	6.94
2176.22	12.80	9.97	8.51	16.41	14.49	13.22	11.5	13.01	4.50	7.11
2176.44	12.80	9.97	8.51	15.50	13.58	12.52	10.83	12.21	3.70	6.75
2176.84	16.78	10.04	8.11	14.79	12.27	11.83	9.6	10.94	2.83	6.03
2177.25	22.63	9.65	7.05	13.16	9.76	10.78	7.80	8.79	1.73	4.78
2177.50	22.44	11.59	9.02	12.97	9.60	9.97	7.02	8.31	0.00	5.35
2177.72	20.78	15.03	12.65	13.81	10.70	11.13	8.40	9.55	0.00	7.55
2177.83	22.44	20.67	18.10	14.73	11.36	12.41	9.45	10.41	0.00	10.54
2178.07	30.31	21.00	17.52	17.40	12.85	14.27	10.28	11.57	0.00	11.12
2178.32	31.28	19.89	16.31	22.74	18.05	17.05	12.9	15.49	0.00	12.19
2178.64	29.84	18.08	14.66	28.93	24.45	20.07	16.14	20.30	5.64	13.26
2178.86	23.20	17.11	14.45	28.15	24.67	21.81	18.75	21.71	7.26	13.84
2179.19	10.00	17.37	16.22	25.22	23.72	20.65	19.3	21.53	5.30	14.52
2179.43	9.44	14.51	13.43	23.92	22.50	18.68	17.43	19.97	6.53	12.43
2179.60	9.89	9.52	8.39	21.90	20.41	16.82	15.52	17.97	9.58	9.21
2179.76	17.23	8.74	6.77	16.42	13.84	13.69	11.42	12.63	5.86	6.27
2180.12	17.55	9.33	7.31	12.45	9.82	10.56	8.25	9.04	1.72	4.90
2180.31	14.41	10.95	9.29	11.93	9.77	11.49	9.59	9.68	0.38	6.24
2180.63	12.79	11.35	9.87	13.24	11.32	13.93	12.24	11.78	1.91	7.64
2180.77	12.53	9.97	8.54	12.84	10.97	12.54	10.88	10.93	2.38	6.50
2181.10	13.72	8.87	7.30	9.59	7.53	11.84	10.03	8.78	1.48	5.25
2181.23	17.54	8.35	6.34	7.70	5.07	12.65	10.34	7.71	1.36	4.72

2181.51	17.38	7.83	5.84	6.40	3.79	13.23	10.94	7.37	1.52	4.58
2181.86	14.12	7.38	5.76	5.03	2.91	13.00	11.14	7.03	1.26	4.46
2182.05	14.54	7.83	5.39	3.79	1.61	11.61	9.70	5.66	0.26	3.62
2182.30	17.70	6.99	4.96	3.99	1.33	9.76	7.43	4.38	0.00	2.61
2182.54	19.18	6.80	4.60	3.99	1.11	10.45	7.93	4.52	0.00	2.64
2182.84	19.35	6.54	4.32	4.06	1.15	11.50	8.95	5.05	0.73	2.91
2183.14	17.38	6.34	4.35	3.47	0.86	12.54	10.25	5.56	1.21	3.32
2183.44	14.39	5.89	4.24	3.08	0.92	12.78	10.88	5.90	1.66	3.46
2183.66	12.13	6.41	5.02	3.08	1.26	11.27	9.67	5.47	0.45	3.39
2183.85	9.87	6.93	5.79	3.08	1.60	9.76	8.46	5.03	0.00	3.35
2184.18	8.79	6.99	5.98	3.73	2.42	10.81	9.65	6.03	0.05	3.99
2184.26	9.76	6.57	5.42	4.71	3.25	13.01	11.72	7.49	2.07	4.57
2184.39	9.93	6.736	5.59	4.97	3.47	10.93	9.61	6.54	0.95	3.89
2184.75	10.77	7.44	6.21	3.67	2.05	9.53	8.11	5.08	0.00	3.44
2185.02	12.00	9.00	7.62	4.06	2.26	10.23	8.65	5.46	0.00	4.30
2185.54	11.88	10.30	8.94	10.71	8.93	9.65	8.09	8.51	0.00	5.41
2185.68	11.35	9.52	8.21	11.69	9.98	11.63	10.1	10.05	1.83	5.96
2185.87	9.75	16.00	14.88	10.91	9.44	8.73	7.44	8.44	0.00	7.93
2186.08	8.57	12.37	11.39	5.96	4.67	10.24	9.10	6.89	0.00	6.48
2186.36	9.53	13.93	12.84	4.98	3.55	11.74	10.49	7.02	0.00	7.50
2186.55	10.55	9.20	7.99	4.46	2.88	12.33	10.9	6.91	0.00	5.39
2186.77	11.26	6.99	5.70	3.87	2.18	11.86	10.3	6.28	0.58	4.07
2187.17	11.14	6.60	5.32	3.87	2.20	11.52	10.05	6.13	0.80	3.78
2187.45	10.66	6.60	5.38	4.40	2.80	11.05	9.65	6.22	0.84	3.72
2187.64	11.62	6.93	5.59	5.50	3.76	10.59	9.06	6.41	0.81	3.70
2187.86	12.76	8.03	6.57	7.33	5.41	9.78	8.10	6.76	0.19	3.96
2188.05	15.38	8.29	6.52	9.61	7.30	9.43	7.40	7.36	0.83	3.92
2188.18	19.67	8.09	5.84	12.35	9.40	10.24	7.65	8.53	2.68	4.03
2188.32	25.56	7.44	4.51	12.80	8.97	11.17	7.81	8.39	3.87	3.67
2188.81	48.19	8.29	2.76	11.50	4.27	11.29	4.95	4.61	1.85	2.71
2189.16	49.60	8.87	3.19	12.87	5.43	10.13	3.61	4.52	1.33	2.63
2189.35	47.50	8.87	3.43	13.20	6.07	9.09	2.8	4.46	1.03	2.37
2189.63	41.63	8.29	3.52	12.35	6.10	10.48	5.0	5.56	2.04	2.80
2189.84	31.93	7.70	4.04	11.90	7.10	11.18	6.98	7.04	2.99	3.27
2190.23	27.04	7.25	4.15	10.85	6.80	10.25	6.69	6.75	2.59	2.92
2190.47	23.52	6.73	4.03	10.27	6.74	9.09	5.99	6.37	2.33	2.44
2190.72	23.52	6.08	3.39	9.10	5.57	7.70	4.60	5.09	1.70	1.51
2190.91	21.25	6.60	4.17	9.36	6.17	7.00	4.21	5.19	1.02	1.69

2191.13	14.09	8.09	6.48	10.27	8.16	7.59	5.73	6.95	0.46	3.35
2191.32	11.49	7.83	6.52	11.38	9.65	6.54	5.03	7.34	0.82	3.27
2191.48	11.73	6.93	5.58	10.73	8.97	2.60	1.05	5.01	0.00	1.29
2191.83	13.00	5.11	3.62	6.75	4.80	3.18	1.47	3.14	0.00	0.10
2192.08	17.33	4.59	2.60	6.36	3.76	4.92	2.64	3.20	0.59	0.02
2192.27	23.12	4.46	1.81	7.93	4.46	7.24	4.2	4.33	2.51	0.51
2192.43	42.53	5.24	0.36	8.71	2.33	8.29	2.69	2.51	2.14	0.17
2192.71	79.71	8.09	1.03	8.71	-3.25	7.48	-3.00	0.00	1.04	0.00
2193.12	80.80	8.74	0.51	9.56	-2.56	6.20	-4.41	0.00	0.52	0.00
2193.31	67.60	8.03	0.28	10.02	-0.12	3.88	-5.00	0.00	0.00	0.00
2193.52	36.63	4.20	0.09	6.37	0.87	4.81	-0.00	0.44	0.43	0.00
2193.80	28.35	3.94	0.69	5.98	1.73	6.78	3.05	2.39	1.69	0.00
2194.01	21.41	5.76	3.30	7.48	4.26	8.64	5.82	5.04	1.74	1.70
2194.18	16.09	8.22	6.38	9.43	7.02	9.92	7.80	7.41	1.03	3.98
2194.34	14.63	7.64	5.96	10.87	8.67	11.19	9.26	8.97	3.00	4.49
2194.70	15.20	7.06	5.31	12.37	10.08	9.57	7.57	8.83	3.51	3.73
2195.08	19.46	6.73	4.50	11.59	8.67	8.30	5.73	7.20	2.70	2.62
2195.40	21.22	6.15	3.71	10.74	7.55	7.83	5.04	6.30	2.58	1.95
2195.62	17.16	5.69	3.73	9.70	7.12	6.44	4.18	5.65	1.92	1.47
2195.92	16.54	5.31	3.41	8.00	5.52	4.70	2.5	4.03	0.61	0.52
2196.11	17.63	5.24	3.22	6.18	3.54	3.78	1.45	2.50	0.00	0.00
2196.30	33.92	5.24	1.35	5.20	0.12	4.24	-0.2	0.00	0.00	0.00
2196.52	34.70	5.63	1.65	6.31	1.11	5.17	0.6	0.86	0.00	0.00
2196.77	32.38	5.95	2.24	8.14	3.28	6.21	1.9	2.62	0.37	0.19
2197.01	20.67	5.69	3.32	7.36	4.25	5.05	2.3	3.30	0.00	0.38
2197.29	12.44	5.89	4.46	6.45	4.57	3.66	2.0	3.30	0.00	0.66
2197.53	12.21	6.54	5.14	6.84	5.00	5.17	3.56	4.29	0.00	1.58
2197.86	16.68	7.83	5.9	6.06	3.55	7.38	5.18	4.37	0.00	2.43
2198.10	17.15	8.68	6.71	4.04	1.46	3.32	1.06	1.26	0.00	1.03
2198.29	13.56	7.70	6.16	2.41	0.38	-1.44	-3.21	0.00	0.00	0.00
2198.48	14.02	6.60	4.99	0.78	-1.33	-2.83	-4.67	0.00	0.00	0.00
2198.78	15.62	5.69	3.90	0.52	-1.82	-0.97	-3.02	0.00	0.00	0.00
2199.03	15.48	5.31	3.53	1.11	-1.21	1.12	-0.91	0.00	0.00	0.00
2199.25	11.83	4.85	3.50	2.61	0.83	2.63	1.07	0.95	0.00	0.00
2199.47	1.78	3.94	3.74	4.69	4.42	4.02	3.78	4.10	0.36	1.47
2199.87	1.66	5.11	4.92	7.43	7.18	5.41	5.19	6.19	1.26	2.84
2200.15	8.74	10.49	9.49	9.91	8.60	6.46	5.30	6.95	0.00	4.63
2200.31	18.76	11.14	8.99	11.01	8.20	4.60	2.13	5.17	0.00	3.24

2200.47	23.07	6.99	4.35	10.04	6.58	5.76	2.7	4.65	0.30	1.33
2200.80	21.38	5.76	3.31	8.80	5.59	6.92	4.1	4.85	1.54	1.21
2201.13	15.91	7.25	5.43	8.80	6.41	6.81	4.71	5.57	0.13	2.33
2201.51	2.89	8.35	8.02	9.39	8.95	7.51	7.12	8.04	0.01	5.02
2201.75	2.49	8.35	8.07	10.24	9.86	9.02	8.68	9.28	1.20	5.76
2201.89	3.03	8.35	8.00	11.67	11.22	10.06	9.66	10.44	2.43	6.19
2202.03	4.13	8.87	8.40	12.65	12.03	12.03	11.48	11.76	3.36	7.04
2202.16	5.51	8.87	8.24	13.69	12.86	11.22	10.49	11.68	3.44	6.60
2202.44	3.83	9.00	8.56	13.17	12.60	12.03	11.52	12.06	3.50	7.22
2202.79	4.13	8.48	8.01	13.82	13.20	10.53	9.98	11.59	3.58	6.43
2203.01	5.50	7.38	6.75	12.91	12.09	7.74	7.01	9.55	2.80	4.55
2203.12	10.38	6.93	5.74	11.09	9.53	6.93	5.56	7.55	1.81	3.11
2203.47	16.97	7.38	5.43	8.29	5.74	5.54	3.31	4.53	0.00	1.76
2203.72	22.48	6.34	3.77	8.35	4.98	3.69	0.73	2.86	0.00	0.13
2204.13	20.82	5.24	2.85	6.73	3.60	4.85	2.1	2.86	0.00	0.02
2204.37	14.45	4.66	3.00	7.18	5.02	6.24	4.34	4.68	1.67	0.92
2204.89	9.04	6.41	5.37	13.70	12.34	8.10	6.9	9.63	4.25	3.78
2204.97	6.38	14.84	14.10	12.53	11.57	9.84	8.99	10.28	0.00	8.50
2205.22	5.93	15.36	14.67	6.53	5.64	7.98	7.20	6.42	0.00	7.46
2205.35	7.02	8.22	7.42	5.23	4.18	4.15	3.23	3.70	0.00	2.50
2205.57	9.04	7.19	6.15	6.34	4.98	3.81	2.61	3.80	0.00	1.72
2205.79	7.02	6.99	6.19	7.97	6.91	4.50	3.58	5.25	0.00	2.37
2206.17	4.43	7.44	6.94	9.40	8.74	5.90	5.31	7.03	0.08	3.70
2206.42	4.20	7.83	7.35	9.93	9.29	8.10	7.54	8.42	1.07	4.80
2206.61	6.93	7.06	6.26	8.75	7.71	7.06	6.14	6.93	0.66	3.45
2206.80	7.21	6.73	5.90	6.47	5.39	5.67	4.71	5.06	0.00	2.49
2207.10	5.32	5.63	5.02	1.85	1.05	3.70	2.99	2.02	0.00	1.07
2207.23	4.20	5.11	4.63	0.61	-0.02	-3.96	-4.5	0.00	0.00	0.00
2207.51	4.12	5.63	5.16	0.87	0.25	-4.42	-4.96	0.00	0.00	0.00
2207.83	3.45	6.60	6.21	2.96	2.44	-3.14	-3.5	0.00	0.00	0.00
2208.08	0.99	7.90	7.78	5.89	5.74	-0.82	-0.95	2.39	0.00	1.78
2208.19	0.08	9.39	9.40	10.32	10.33	2.31	2.32	6.33	0.00	4.41
2208.38	0.13	9.84	9.86	13.51	13.53	4.75	4.76	9.15	0.00	5.88
2208.70	0.43	9.97	9.92	12.28	12.21	11.59	11.53	11.87	1.94	8.19
2209.06	1.70	10.49	10.30	13.19	12.93	7.88	7.65	10.29	0.00	6.81
2209.25	3.44	10.82	10.42	13.97	13.46	8.58	8.1	10.79	0.36	6.92
2209.47	5.32	10.17	9.56	13.06	12.26	9.39	8.6	10.48	0.91	6.47
2209.82	8.50	8.68	7.70	12.02	10.75	9.74	8.62	9.68	1.98	5.30

2210.15	10.24	8.94	7.76	13.72	12.18	10.55	9.20	10.69	2.92	5.67
2210.37	10.24	10.43	9.25	15.93	14.39	11.71	10.3	12.38	3.12	7.02
2210.64	8.60	11.59	10.61	18.54	17.25	13.11	11.97	14.61	4.00	8.57
2210.91	7.10	12.76	11.95	18.54	17.47	14.61	13.67	15.58	3.62	9.88
2211.18	4.90	12.43	11.88	16.98	16.24	16.70	16.05	16.15	4.27	10.72
2211.38	4.11	10.82	10.34	14.31	13.69	16.70	16.16	14.93	4.58	9.84
2211.51	3.59	9.78	9.37	11.96	11.42	14.85	14.37	12.90	3.53	8.53
2211.65	3.51	9.13	8.73	10.01	9.48	9.63	9.167	9.32	0.59	6.10

Appedix C

Well Log derived Saturation.

Table C.1: well log derived saturation Ja-49 well

Depth	Sw (%)	Sxo (%)	ROS (%)	MOS (%)	BVW	BVH	MHI	FZI
2156.10	0.59	1.14	-0.135	0.55	0.022	0.015	0.52	0.726
2156.80	0.29	0.45	0.549	0.16	0.027	0.067	0.64	0.254
2156.79	0.19	0.29	0.708	0.10	0.020	0.085	0.67	0.210
2156.89	0.15	0.25	0.749	0.10	0.013	0.071	0.61	0.232
2157.16	0.20	0.59	0.405	0.40	0.006	0.024	0.33	0.421
2157.27	-	-	-	-	-	-	-	0.000
2157.50	-	-	-	-	-	-	-	0.000
2157.70	1.11	3.12	-2.120	2.01	0.018	-0.002	0.36	1.152
2158.14	0.68	0.80	0.202	0.11	0.044	0.020	0.86	0.379
2158.32	0.52	0.53	0.465	0.02	0.033	0.030	0.97	0.373
2158.50	0.19	0.31	0.689	0.12	0.014	0.057	0.62	0.327
2158.66	0.12	0.40	0.600	0.28	0.005	0.032	0.31	0.395
2159.37	-	-	-	-	-	-	-	0.000
2159.52	-	-	-	-	-	-	-	0.000
2159.72	-	-	-	-	-	-	-	0.000
2159.91	1.46	5.77	-4.773	4.31	0.012	-0.004	0.25	4.812
2160.06	2.50	2.35	-1.354	-0.14	0.033	-0.020	1.06	3.061
2160.52	0.74	0.93	0.069	0.19	0.023	0.008	0.80	1.058
2160.69	0.44	0.88	0.121	0.44	0.015	0.019	0.50	0.844
2160.88	0.95	2.37	-1.367	1.42	0.009	0.001	0.40	2.182

2161.17	1.48	5.22	-4.223	3.74	0.008	-0.002	0.28	3.455
2161.35	0.85	2.94	-1.939	2.09	0.014	0.002	0.29	1.662
2161.54	0.55	1.16	-0.158	0.61	0.027	0.022	0.47	0.472
2161.75	0.54	0.82	0.175	0.29	0.032	0.027	0.65	0.335
2162.12	0.44	0.46	0.542	0.02	0.031	0.039	0.97	0.280
2162.49	0.45	0.73	0.266	0.28	0.020	0.024	0.61	0.431
2162.66	0.63	1.81	-0.814	1.18	0.014	0.008	0.35	0.735
2162.91	0.52	1.47	-0.471	0.95	0.025	0.023	0.35	0.496
2163.26	0.53	1.05	-0.050	0.52	0.039	0.035	0.50	0.342
2163.44	0.37	0.82	0.183	0.45	0.043	0.073	0.45	0.194
2163.68	0.34	0.79	0.210	0.45	0.046	0.089	0.43	0.160
2163.84	0.30	0.65	0.350	0.35	0.052	0.123	0.46	0.119
2164.08	0.31	0.64	0.358	0.33	0.055	0.121	0.49	0.120
2164.45	0.26	0.50	0.501	0.24	0.047	0.136	0.52	0.110
2164.77	0.28	0.45	0.554	0.17	0.042	0.109	0.63	0.136
2164.96	0.34	0.64	0.359	0.30	0.044	0.086	0.53	0.154
2165.05	0.65	1.14	-0.140	0.49	0.041	0.023	0.57	0.314
2165.54	0.60	1.07	-0.074	0.48	0.044	0.030	0.56	0.281
2165.70	0.47	0.83	0.172	0.36	0.044	0.049	0.57	0.226
2165.89	0.37	0.56	0.438	0.19	0.042	0.070	0.66	0.181
2166.09	0.36	0.49	0.511	0.13	0.036	0.066	0.73	0.193
2166.52	0.36	0.57	0.431	0.20	0.031	0.054	0.64	0.229
2166.70	0.45	0.75	0.251	0.30	0.028	0.034	0.60	0.304
2166.95	0.56	0.98	0.022	0.42	0.028	0.022	0.57	0.424
2167.14	0.63	1.05	-0.049	0.42	0.030	0.017	0.60	0.501
2167.37	0.64	0.82	0.184	0.17	0.032	0.018	0.79	0.514
2167.52	0.56	0.54	0.457	-0.02	0.032	0.025	1.04	0.433
2167.74	0.47	0.58	0.422	0.11	0.028	0.033	0.81	0.393
2168.11	0.46	0.76	0.243	0.30	0.021	0.025	0.60	0.509
2168.32	0.57	1.03	-0.032	0.46	0.021	0.016	0.55	0.711
2168.48	0.60	1.23	-0.226	0.63	0.022	0.015	0.49	0.681
2168.65	0.61	1.20	-0.203	0.60	0.028	0.018	0.50	0.541
2169.28	0.54	0.96	0.038	0.42	0.032	0.027	0.56	0.377
2169.57	0.41	0.71	0.290	0.30	0.035	0.050	0.58	0.235
2169.75	0.41	0.66	0.337	0.25	0.033	0.048	0.62	0.241
2169.85	0.47	0.73	0.275	0.25	0.028	0.032	0.65	0.304
2170.10	0.49	0.74	0.264	0.24	0.024	0.025	0.67	0.361
2170.29	0.42	0.79	0.213	0.37	0.024	0.034	0.53	0.347

2170.48	0.45	0.91	0.092	0.45	0.029	0.035	0.50	0.367
2170.68	0.42	0.70	0.297	0.29	0.035	0.049	0.59	0.288
2171.14	0.39	0.73	0.274	0.34	0.033	0.052	0.54	0.260
2171.30	0.42	0.89	0.106	0.48	0.036	0.050	0.47	0.225
2171.50	0.57	1.09	-0.092	0.52	0.044	0.033	0.52	0.245
2171.71	0.65	1.29	-0.292	0.64	0.057	0.030	0.50	0.245
2172.15	0.82	1.37	-0.369	0.55	0.092	0.020	0.60	0.196
2172.52	0.53	0.82	0.177	0.29	0.091	0.079	0.65	0.117
2172.69	0.46	0.69	0.306	0.24	0.081	0.095	0.66	0.113
2172.84	0.38	0.59	0.412	0.21	0.069	0.112	0.65	0.110
2173.05	0.34	0.59	0.413	0.25	0.055	0.106	0.58	0.124
2173.30	0.39	0.71	0.292	0.32	0.048	0.076	0.54	0.167
2173.58	0.46	0.78	0.225	0.32	0.048	0.057	0.59	0.206
2173.90	0.45	0.75	0.246	0.30	0.048	0.058	0.60	0.204
2174.17	0.42	0.72	0.285	0.30	0.051	0.071	0.58	0.170
2174.43	0.44	0.76	0.242	0.32	0.050	0.063	0.58	0.180
2174.70	0.52	0.88	0.116	0.37	0.048	0.045	0.59	0.229
2174.99	0.55	1.01	-0.009	0.45	0.048	0.039	0.55	0.250
2175.12	0.53	1.06	-0.063	0.53	0.057	0.050	0.50	0.209
2175.28	0.52	1.07	-0.071	0.55	0.067	0.062	0.49	0.171
2175.52	0.53	0.85	0.153	0.32	0.083	0.074	0.62	0.135
2175.79	0.56	0.76	0.236	0.21	0.085	0.067	0.73	0.137
2176.07	0.59	0.81	0.193	0.22	0.076	0.053	0.73	0.156
2176.38	0.55	0.74	0.261	0.19	0.072	0.058	0.75	0.155
2176.62	0.55	0.64	0.364	0.08	0.068	0.054	0.87	0.168
2176.91	0.56	0.71	0.287	0.15	0.061	0.048	0.79	0.190
2177.32	0.62	1.19	-0.189	0.57	0.055	0.033	0.52	0.240
2177.51	0.74	1.68	-0.677	0.94	0.061	0.022	0.44	0.278
2177.63	0.86	1.84	-0.844	0.99	0.082	0.014	0.46	0.265
2177.87	1.01	1.93	-0.931	0.92	0.105	-0.001	0.52	0.272
2178.19	1.00	1.31	-0.311	0.31	0.116	0.000	0.76	0.235
2178.29	0.75	0.99	0.007	0.24	0.116	0.039	0.75	0.152
2178.48	0.56	0.89	0.109	0.33	0.113	0.090	0.63	0.100
2178.85	0.49	0.89	0.114	0.39	0.107	0.110	0.56	0.090
2179.07	0.48	0.73	0.266	0.25	0.104	0.111	0.66	0.094
2179.49	0.40	0.48	0.516	0.09	0.079	0.121	0.82	0.099
2179.69	0.33	0.42	0.580	0.09	0.060	0.120	0.79	0.103
2179.98	0.41	0.63	0.367	0.22	0.052	0.074	0.65	0.153

2180.16	0.56	0.94	0.062	0.38	0.050	0.040	0.59	0.233
2180.27	0.58	0.88	0.119	0.30	0.056	0.041	0.66	0.235
2180.40	0.55	0.75	0.249	0.20	0.065	0.053	0.73	0.189
2180.67	0.58	0.74	0.261	0.16	0.063	0.046	0.79	0.197
2180.91	0.64	0.70	0.305	0.05	0.057	0.031	0.93	0.252
2181.06	0.58	0.83	0.171	0.25	0.045	0.032	0.70	0.294
2181.59	0.53	0.74	0.259	0.22	0.039	0.035	0.71	0.311
2181.87	0.50	0.66	0.343	0.16	0.035	0.035	0.76	0.331
2182.32	0.57	0.72	0.278	0.15	0.032	0.024	0.79	0.419
2182.70	0.71	0.85	0.153	0.14	0.031	0.013	0.84	0.528
2182.91	0.66	1.01	-0.007	0.34	0.030	0.015	0.66	0.507
2183.15	0.59	1.18	-0.182	0.60	0.030	0.021	0.50	0.448
2183.50	0.56	1.09	-0.089	0.53	0.031	0.024	0.51	0.412
2183.77	0.57	0.98	0.016	0.42	0.033	0.026	0.58	0.383
2183.93	0.62	1.09	-0.094	0.48	0.034	0.021	0.57	0.428
2184.14	0.67	1.21	-0.211	0.54	0.034	0.017	0.55	0.483
2184.46	0.57	1.12	-0.120	0.55	0.034	0.026	0.51	0.397
2184.76	0.50	0.81	0.190	0.31	0.037	0.038	0.61	0.303
2185.05	0.72	0.70	0.298	-0.02	0.047	0.018	1.02	0.346
2185.29	1.16	1.19	-0.186	0.03	0.059	-0.008	0.98	0.482
2185.48	1.18	1.96	-0.959	0.78	0.064	-0.010	0.60	0.483
2185.68	0.78	0.92	0.084	0.14	0.066	0.019	0.85	0.269
2185.87	0.58	0.65	0.350	0.07	0.058	0.043	0.89	0.216
2186.09	0.56	0.79	0.215	0.22	0.047	0.037	0.72	0.330
2186.31	0.59	1.00	-0.001	0.42	0.040	0.029	0.59	0.411
2186.52	0.52	1.04	-0.039	0.52	0.036	0.034	0.50	0.430
2186.79	0.47	0.87	0.132	0.40	0.033	0.036	0.54	0.374
2187.14	0.50	0.79	0.212	0.29	0.031	0.032	0.63	0.377
2187.47	0.56	0.69	0.305	0.14	0.034	0.027	0.80	0.378
2187.69	0.68	0.75	0.252	0.07	0.042	0.020	0.91	0.366
2187.94	0.81	1.04	-0.045	0.24	0.052	0.012	0.77	0.348
2188.26	0.80	0.94	0.057	0.14	0.054	0.014	0.85	0.332
2188.53	0.73	1.04	-0.037	0.31	0.053	0.020	0.70	0.289
2188.85	0.64	1.03	-0.029	0.39	0.055	0.030	0.62	0.232
2189.12	0.66	1.20	-0.200	0.54	0.055	0.029	0.55	0.227
2189.39	1.04	1.84	-0.844	0.81	0.048	-0.002	0.56	0.497
2189.68	1.08	1.62	-0.621	0.54	0.049	-0.004	0.67	0.506
2189.91	1.03	1.91	-0.912	0.89	0.046	-0.001	0.54	0.491

2190.00	0.78	1.44	-0.438	0.65	0.044	0.012	0.55	0.379
2190.27	0.67	1.12	-0.119	0.45	0.047	0.024	0.60	0.282
2190.54	0.71	0.78	0.222	0.07	0.048	0.020	0.91	0.286
2190.69	0.86	1.03	-0.032	0.17	0.055	0.009	0.84	0.286
2190.94	1.13	1.75	-0.750	0.62	0.057	-0.007	0.65	0.319
2191.08	1.04	1.09	-0.091	0.05	0.054	-0.002	0.95	0.327
2191.29	0.65	0.59	0.411	-0.07	0.045	0.024	1.11	0.292
2191.47	0.44	0.53	0.466	0.10	0.032	0.041	0.82	0.264
2191.83	0.49	0.68	0.321	0.19	0.025	0.025	0.72	0.302
2192.05	0.72	1.06	-0.060	0.34	0.022	0.009	0.68	0.173
2192.28	0.78	1.20	-0.201	0.42	0.025	0.007	0.65	0.079
2192.51	0.75	1.02	-0.022	0.28	0.032	0.011	0.73	0.237
2192.64	1.38	2.02	-1.022	0.64	0.035	-0.010	0.68	0.314
2193.15	-	-	-	-	-	-	-	0.000
2193.48	-	-	-	-	-	-	-	0.000
2193.63	-	-	-	-	-	-	-	0.000
2193.89	4.99	6.08	-5.081	1.09	0.022	-0.017	0.82	0.000
2194.30	1.46	2.40	-1.401	0.94	0.035	-0.01	0.61	0.000
2194.67	0.80	1.07	-0.075	0.28	0.040	0.010	0.74	0.343
2195.10	0.60	0.98	0.018	0.39	0.044	0.030	0.61	0.287
2195.32	0.46	0.87	0.130	0.41	0.042	0.048	0.53	0.226
2195.52	0.41	0.75	0.247	0.34	0.036	0.052	0.55	0.211
2195.68	0.41	0.70	0.304	0.29	0.030	0.042	0.59	0.244
2195.99	0.41	0.72	0.283	0.31	0.026	0.037	0.57	0.260
2196.18	0.46	0.60	0.399	0.14	0.026	0.030	0.77	0.267
2196.38	0.68	0.92	0.080	0.24	0.027	0.3	0.74	0.269
2196.44	1.04	1.88	-0.882	0.84	0.026	-0.01	0.55	0.000
2196.66	-	-	-	-	-	-	-	0.000
2196.82	2.17	3.66	-2.658	1.49	0.019	-0.01	0.59	0.000
2197.14	1.06	1.91	-0.909	0.85	0.028	-0.01	0.55	0.318
2197.44	0.94	1.55	-0.552	0.61	0.031	0.002	0.61	0.313
2197.63	0.99	1.75	-0.752	0.76	0.033	0.000	0.56	0.411
2197.82	0.88	1.60	-0.601	0.72	0.038	0.005	0.55	0.426
2198.18	0.63	0.83	0.169	0.20	0.028	0.016	0.76	0.512
2198.34	0.74	0.96	0.044	0.21	0.009	0.003	0.78	2.215
2198.50	-	-	-	-	-	-	-	0.000
2198.62	-	-	-	-	-	-	-	0.000
2199.06	-	-	-	-	-	-	-	0.000

2199.30	-	-	-	-	-	-	-	0.000
2199.52	1.90	1.91	-0.915	0.02	0.018	0.009	0.99	0.000
2199.93	0.94	1.79	-0.786	0.84	0.039	0.002	0.53	0.439
2200.06	0.43	0.99	0.015	0.55	0.027	0.035	0.44	0.323
2200.21	0.26	0.55	0.451	0.29	0.018	0.051	0.47	0.343
2200.52	0.36	0.62	0.379	0.26	0.018	0.033	0.57	0.456
2200.70	0.63	1.08	-0.077	0.44	0.030	0.017	0.59	0.344
2200.91	0.91	1.76	-0.756	0.85	0.044	0.004	0.52	0.307
2201.07	0.80	1.04	-0.036	0.24	0.044	0.011	0.77	0.345
2201.56	0.48	0.64	0.360	0.16	0.038	0.042	0.74	0.284
2201.72	0.45	0.57	0.425	0.13	0.042	0.051	0.78	0.242
2201.93	0.43	0.55	0.448	0.12	0.045	0.059	0.78	0.207
2202.15	0.42	0.63	0.373	0.21	0.049	0.068	0.67	0.182
2202.51	0.41	0.74	0.265	0.33	0.047	0.069	0.55	0.178
2202.69	0.36	0.51	0.493	0.15	0.043	0.078	0.70	0.177
2202.94	0.36	0.57	0.430	0.21	0.041	0.075	0.62	0.178
2203.13	0.49	0.76	0.235	0.27	0.047	0.048	0.65	0.205
2203.50	0.60	0.98	0.024	0.38	0.045	0.030	0.61	0.247
2203.73	0.67	1.05	-0.050	0.38	0.030	0.015	0.63	0.413
2203.87	0.78	1.64	-0.642	0.86	0.022	0.006	0.48	0.227
2204.16	0.89	2.65	-1.650	1.76	0.025	0.003	0.33	0.087
2204.31	0.93	1.81	-0.814	0.88	0.043	0.003	0.51	0.284
2204.71	0.75	0.54	0.457	-0.21	0.073	0.024	1.39	0.185
2204.90	0.53	0.68	0.321	0.15	0.054	0.048	0.78	0.249
2205.04	0.52	1.14	-0.142	0.62	0.033	0.031	0.45	0.493
2205.32	0.78	1.59	-0.589	0.81	0.029	0.008	0.49	0.670
2205.50	0.86	1.60	-0.597	0.74	0.033	0.005	0.54	0.535
2205.72	0.73	1.32	-0.315	0.58	0.038	0.014	0.56	0.381
2206.11	0.68	1.01	-0.006	0.33	0.048	0.023	0.68	0.302
2206.52	0.53	0.42	0.584	-0.12	0.045	0.039	1.28	0.258
2206.66	0.44	0.29	0.711	-0.15	0.031	0.039	1.54	0.298
2206.86	0.38	0.38	0.622	0.00	0.019	0.031	1.00	0.414
2206.94	0.31	0.78	0.218	0.48	0.006	0.014	0.39	1.105
2206.95	-	-	-	-	-	-	-	0.000
2207.55	-	-	-	-	-	-	-	0.000
2207.65	-	-	-	-	-	-	-	0.000
2207.89	0.69	2.11	-1.113	1.43	0.016	0.008	0.32	.105
2208.01	0.63	1.30	-0.302	0.67	0.040	0.023	.49	0388

2208.29	0.60	1.23	-0.228	0.63	0.055	0.037	049	0.50
2208.63	0.57	1.00	0.000	0.43	0.067	0.052	0.57	0.194
2208.98	0.60	0.97	0.033	0.37	0.062	0.041	0.62	0.223
2209.10	0.53	0.96	0.040	0.43	0.057	0.051	0.55	0.208
2209.38	0.46	0.88	0.124	0.41	0.049	0.056	0.53	0.211
2209.72	0.38	0.68	0.321	0.30	0.036	0.060	0.55	0.217
2209.85	0.30	0.72	0.278	0.42	0.032	0.075	0.41	0.191
2210.01	0.28	0.64	0.356	0.36	0.035	0.089	0.44	0.167
2210.39	0.26	0.56	0.444	0.30	0.037	0.109	0.46	0.141
2210.81	0.25	0.52	0.481	0.27	0.039	0.117	0.48	0.136
2211.04	0.29	0.56	0.436	0.28	0.047	0.115	0.51	0.133

REFERNECES

[1] Abdul Rahman, N.A., "Sedimentological and Petrophysical Properties study of Stratigraphic Succession for (Aquitanian-Lower Early Langhian)Stage in Well KorMor/ 3 at Kirkuk Area", *M.Sc.thesis*, University of Mosul, Mosul, Iraq, (2007).

[2] Ahr, W. M., Geology of Carbonate Reservoirs (The Identification, Description, and Characterization of Hydrocarbon Reservoirs in Carbonate Rocks), John Wiley & Sons, inc., publication, New Jersey, 277p, (2007).

[3] Akkurt, R., Bachman, H. N., Crary, S., Decoster, E., Heaton, N., Hurliman, M. D., Loovestiin, W. J., Mardon, D., and White, J., Nuclear Magnetic Resonance come out of its Shell, Oilfield Review, Vol. 20, No.4, pp 4-23.(2009).

[4] Al-Ameri T. K., Zumberg , J., and Markarian Z. M. "Hydrocarbons In the Middle Miocene Jeribe Formation Dyala Region, NE Iraq", Journal of Petroleum Geology, vol.34 (2), 199-216 (2011)

[5] Al-Ayobe Nawrast Sabah,"Microfacies and Modeling of Jeribe Formation (EarlyMiddle Miocene) Northwest of Iraq", M.Sc.thesis, Basra University, Basra, Iraq, (2004).

[6] Al-Dabbas, M. A., Al-Sagri, K. E. A., Al-Jassim, J. A., and Al-Jwaini, Y. S. "Sedimentological and diagenetic study of the Early Middle Miocene Jerib Limestone Formation in selected wells from Iraq northern oilfields (Ajil; Hamrin; Jadid; Khashab)"Journal of Baghdad for Science, Vol.10, 10 (2012)

[7] AL-Hietee, S. A. A., "Facies architecture and Sequence Stratigraphy of the Lower and Middle Miocene, Kirkuk area, North Iraq", M.Sc.thesis, Baghdad University,Baghdad, Iraq. (2012)

[8] Al-Juboury A. L., Al-Tarif, A. M., and Al-Eisa, M. "Basin analysis of the Burdigalian and Early Langhian successions, Kirkuk Basin, Iraq", Geological Society,London, v. 285, 53-68. (2007)

[9] Al-Mehaidi, K., "prudent Oil Field Development, Iraq". (2009)

[10] Amaefule, J. O., Altunbay, M., Tiab, D., Kersey, D. G. and Keelan, D. K. "Enhanced Reservoir Description: Using core and log data to identify hydraulic (flow) Units and predict permeability in Uncored Intervals/Wells", *68th Annual Tech. Conf.*

And Exhibit. Houston, TX Paper SPE26435, (1993).

[11] Amin, D. H. M. " Biostratigraphy of Garagu Formation in selected wells from Northern Iraqi Oil Fields" *M.Sc.thesis*, (unpublished), University of Baghdad, Baghdad, Iraq.134,(1989).

[12] Aqrawi, A. A. M., Goff, J. C., Horbury, A. D., , and Sadooni, F. N., "*Petroleum Geology of Iraq"*, Scientific press Lt Po box 21, Beaconsfield, Bucks HP9 1NS, UK,(2010).

[13] Archie, G.E., "The Electrical Resistivity Log as an Aid in Determining Some Reservoir Characteristics", Trans. AIMS, v.146, (1942).

[14] Asquith, G. B., "*Handbook of log evaluation techniques for carbonate Reservoirs"* AAPG, Tusla, Oklahoma USA, (1985).

[15] Asquith, G. B., and Gibson, C. R., *Basic Well Analysis for Geologist*, The American Association of Petroleum Geologists, Tusla, Oklahoma .USA,(1982).

[16] Asquith, G., and Krygowski, D. "chapter 1: Basic relationship of well log Interpretation", in *Basic Well Log Analysis*, AAPG Methods in exploration 16, Tusla, Oklahoma, (2004).

[17] Baker, H. A., AL-Jawad, S. N., and Murtadha, Z. I., "Permeability Prediction in Carbonate Reservoir Rock Using FZI" , Iraqi Journal of Chemical and Petroleum Engineering, Vol.14 No.3 pp. 49- 54(2013)

[18] Bassiouni, Z., "*Theory, Measurement, and Interpretation of Well Logs"*, Society of Petroleum Engineers, Richardson, Texas, (1994).

[19] Bateman, R. M, *Open-Hole Log Analysis and Formation Evaluation*, 137 Newbury Street, Boston. (1985).

[20] Beiranvand , B., Kamali, M.R" Petrophysical Evaluation and Determination of Rock Types in a Carbonate Reservoir in SW Iran with Interpretation of Petrography and Geophysical Well Logs" *Iranian Int. J. Sci.* 5(2): 203-221. (2004).

[21] Bellen, R.C Van. M., Dunnington. H.V and Wetyzel, R and Morton, D, *Lexiquestratigraphique International*, Asie, Fscicule 10a, Iraq, Paris, (1959).

[22] Buday, T., " Volume I: Stratigraphy and Paleontology" in the *Regional Geology of Iraq*, Dar Al-Kutib publishing house, University of Mosul, Iraq, 133, (1980).

[23] Buday, T., and Jassim, S. Z. " VolumeII: Tectonic, Magmatism, and

Metamorphism “in The *Regional Geology of Iraq*, Dar Al-Kutib publishing house, University of Mosul Iraq, (1987).

[24] Chatterjee, R., Manoharan, K, and Mukhopdhyay, M., , Petrophysical and mechanical properties of cretaceous sedimentary rocks of Cauvery basin, Eastern Continental Margin of India, J. Ind. Geophys. Union, Vol.17, No. 4, pp. 349-359, (2013)

[25] Choquette, P.W., and Pray, L.C. "Geological Nomenclature and Classification of Porosity in Sedimentary Carbonates" AAPG Bulletin Vol.54, 207-250, (1970).

[26] Coates, G. R., Xiao, L., and Prammer, M. G.,“NMR Logging Principles and Applications”, Halliburton Energy Services, Houston, (1999).

[27] Crary, S., Boyeldieu, C., Brown, S.,” Fracture Detection With Logs”, The Technical Review. V. 35, no. 1, pp. 23-34.(1987).

[28] Darling, T. “*Well logging and Formation Evaluation”*, Elsevier, Amsterdam. (2005)

[29] Dewan, J. T. (1983) *Essential of modern open-hole log interpretation*, Tulsa, Oklahoma, penn well publishing company.

[30] Doveton, J.H., “Geological log interpretation”, SEPM Short Course Notes No. 29, USA (1994).

[31] Dresser Atlas, “Log interpretation charts” Houstone.Dresser Industries,Inc (1979).

[32] Dunham, R.J. "Classification of carbonate rocks according to depositional

[33] Ellis, d. V., and Singer, J. M. *Well Logging for Earth Scientists*, Second Edition, Springer (2008).

[34] Fadhil T. D., "Sedimentological and Reservoir Characterization forJeribe Formation at Alass Dome/North HamrinOil Field", *M.Sc.thesis*, (unpublished) University of Tikrit, Tikrit, Iraq.134,(2013).

[35] Fertl, W. H., “Evaluation of Fractured Reservoirs Using Geophysical Well Logs”, SPE Symposium on Unconventional Gas Recovery held in Pittsburgh, Pennsylvania.(1980).

[36] Freedman, R. and Heaton, N., “ Fluid Characterization using Nuclear Magnetic Resonance Logging Petrophysics”, vol. 45, no. 3, pp 241-250.(2004).

[37] Freedman, R., Lo, S., Flaum, M., Hirasaki, G.J., Matteson, and Sezginer, A., “A new NMR method of fluid characterization in reservoir rocks”: Experimental confirmation and simulation results: SPE Journal, vol. 6, no. 4, pp. 452–464. (2001).

[38] Gharib, A. F., "Sedimentological and Reservoir Characterization of Euphrates and JeribeFormations in Selected Wells in Ajeel Oil Field/Northern Iraq", *M.Sc.thesis*, (unpublished) University of Tikrit, Tikrit, Iraq. (2012).

[39] Ghorab, M., Ramadan, A.M., and Nouh, A.Z. "The relation between shale Origin (source or nonsource) and its type for Abu Roash formation at Wadi-El Naturn Area, south of Western Desert, Egypt," *Australian Journal of Basic Applied Sciences*, Vol. 2, No. 3, 360-371. (2008).

[40] Hambolt, A., "Genetic pore typing as a means of characterizing reservoir flow units": Sanandres, Sunflower field, Terry county, Texas, *MSc thesis* (unpublished), Texas A&M University, 175p. (2006)

[41] Heinemann,Z. E, "Fluid Flow in Porous Media", (Volume 1 of Text BookSeries), University of Montan, Leobon, (2005)

[42] HLS, Basic Log Interpretation, Log Interpretation Seminar, New Delhi, 106p. (2007)

[43] Hurley, Neil, Borehole Images; in Asquith, G. and Krygowski, D., Basic Well Log Analysis: AAPG Methods in Exploration 16, p. 151–163. (2004).

[44] Hussein,S.H., "Characterization of the Tertiary Reservoirs in Khabbaz Oil Field, Kirkuk Area, Northern Iraq" *MSc thesis* University of Sulaimani, Iraq,(2015).

[45] Ibrahim, D. M., Sedimentology and reservoir characteristics of Jeribe Formation (Middle Miocene) in Tawke Oil Field, Zakho, Kurdistan Region - Iraq, *MSc thesis* (unpublished), Salahaddin University, 122p.(2008).

[46] Jassim, S. Z. and Buday, T. Latest Eocene-Recent Megasequence AP11, in Jassim, S. Z., and Goff, J. C. (eds) *Geology of Iraq*. Dolin, Prague and Moravian Museum, Czech Republic, 169-184. (2006).

[47] Khan, M. N., *Introduction to Wire line Log Interpretation*, Oil and GasDevelopment Cooperation.135,(1989).

[48] Khan.N , Zhu.P.M & Konaté. A. A., "Petrophysical Parameters Estimation Using Geophysical Well Log Data of Indus Sub-Basin Area, Pakistan" vol. 5, No.4, (2013)

[49] Kharajiany, S. O. A., "Occurrence of Eraly and Middle Miocene Rocks Euphrates, Dhiban, and Jeribe Formation in Ashdagh Mountain, Sangaw area, Sulaimania Vicinity , NE Iraq", Iraqi Bulletin of Geology and Minig, Vol.10, No.1: 21- 39. (2014).

[50] Kolodzie, S. "Analysis of Pore Throat Size and Use of Waxman-Smits

Equation to Determine OOIP in Spindle Field", Colorado, SPE (9382), (1980).

[51] Larionov, W. W., "*RadiometrijaSkwaschin*, NedraVerlag", Moscow. (1969).

[52] Lawa, F. A., "Biostratigraphy and Depositional Environments of the Oligocene-Miocene Sediments in the Mosul -Qaiyarah Area, North Iraq", Unpublished Report,DGS. Lib No.180 Baghdad/Iraq, (1989).

[53] Law, A. , Megson, J. and Pye, M., *"* Low Permeability Reservoirs": introduction, Petroleum Geoscience, Vol. 7, No.1, pp. 2-2 (2001).

[54] Lucia,F.J, "*Carbonate Reservoir Characterization".* Austin, Texas. (1999)

[55] Markaryan, Z.M., "Hydrocarbon generation, migration pathways and their accumulation of the Jeribi Formation in NE Iraq", *M.Sc.thesis*, (unpublished), university of Baghdad, Baghdad, Iraq, (2005).

[56] Martin, A. J. (Jeff). Solomon, S. T., and Hartmann D. J., Characterization of Petrophysical Flow Units in Carbonate Reservoir, Reply: AAPG Bulletin, Vol. 83, No. 7, pp.1164-1173. (1999).

[57] Mohagheh, S., Balan, B., and Ameri, S (1997) "Permeability determination from well log data", SPE, 170-174.

[58] Moradi ,S, Moeini ,M ,Ghassem al-Askari,M,K, Mahvelati, E,H "Determination of Shale Volume and Distribution Patterns and Effective Porosityfrom Well Log Data Based On Cross-Plot Approach For Shaly Carbonate Gas Reservoir",Earth and Environmental Science 44(2016).

[59] North, F. K., *Petroleum Geology,* Allen and Unwin Inc. (1985).

[60] Oil Search, "Kurdistan Investor Field Trip (Kurdistan Region Overview)", Oil Search Limited, (2014).

[61] Parnell, J. , Taylor, C.W., Thackrey, S. , Gordon R., Osinski, S., and Lee, L., "Permeability data for impact breccias imply focussed hydrothermal fluid flow", Journal of Geochemical Exploration, Vol. 106, Issues 1–3, pp. 171-175 (2010).

[62] Peters, E.J., "*Advanced Petrophysics"*, University of Texas, USA. (2001).

[63] Pittman, F. D. "Relationship of Porosity and Permeability to Various Parameters Derived from Mercury Injection-Capillary Pressure Curve for Sandstone",AAPG Bulletin, V.76,.No.2 (February 1992), 191-198. (1992).

[64] Prazak, J., "Stratigraphy and Paleontology of the Miocene of the Western

Desert, W. Iraq", Manuscript report, GUESURV, Baghdad, (1974).

[65] Rahimi, M., and Hassani-giv, M., "New Correlations for Porosity Exponent in Carbonate Reservoirs of Iranian Oil Fields in Zagros Basin", JUST 34(2), 1-7, (2008).

[66] Rider, M., "*The Geological Interpretation of Well Logs"* Second Edition, Rider French Consulting Ltd., Aberdeen and Sutherland, (2002).

[67] Rider, M., and Kennedy, M., *the Geological Interpretation of Well Logs*.

[68] Rivas, J., Busnego, H., Bejarano, C. and Meza, R., Modeling of Pore Throat Radio using Pittman Modified Equation for Carabobo Area in the Faja Petrolífera del Orinoco. Heavy Oil (Latin America Conference and Exhibition), Venezuela, (2014).

[69] Salazar, J. M., Wang, G. L., Torres-Verdín, C., and Lee, H. J.," Combined simulation and inversion of SP and resistivity logs for the estimation of connate water resistivity and Archie's cementation exponent" SPWLA 48th Annual Logging Symposium, Texas, USA. (2007).

[70] Schlumberger (1972) *Log Interpretation / Charts*: Huston, Schlumberger Well Services, Inc, Vol.1. (2011)

[71] Schlumberger, "*Log Interpretation Principles/Applications"*, Sguard Land, Texas, (1989).

[72] Schlumberger, "*Log interpretation chart"*, Schlumberger Educational Services, U.S.A (1988).

[73] Schlumberger "*Log Interpretation Charts"*,Sguard Land, Texas, (2009).

[74] Schon, J., Basic Well Logging and Formation Evaluation (1st Edition). Bookboon,com. 179p, (2015).

[75] Serra, O., *Fundamentals of well – log interpretation.* Singapore,(1984).

[76] Siddiqui, S., Hughes, G.W., Sadler, R.K. and Khamees, A.A., "A Density-Based Imaging Technique to Supplement FMI Images for Sedimentary Facies Modeling," SCA paper No. 2003- 58, presented at the SCA Symposium held in Pau, France (2003).

[77] Sharland,P.R., Archer,R., Casey,D.M., Davies,R.B., Hall,S.H., Heward,A.P., Horbury,A.D. and Simmons,M.D "Arabian Plate Sequence Stratigraphy", *GeoArabia* . Manama, Bahrain,(2001).

[78] Sissakian, V. K., Karim, S. A., Al-Kubaisyi, K. N., Al-Ansari, N., and Knutsson, S., The Miocene Sequence in Iraq, a review and discussion, with emphasize on the

stratigraphy, paleoecology and economic potential, Journal of Earth Sciences and Geotechnical Engineering, 6 (3): 271-317. (2016).

[79] Soto, R.B., Martin, C., Perez, O., and Durray, A., "A new reservoir classification based on pore types improves characterization", ACIPET, TEC-86(2011).

[80] Teh, W.J., Willhite, G.P., Doveton, J.H., and Tsau, JS, Improved Predictions of Porosity from Microresistivity Logs in a Mature Field through Incorporation of Pore Typing, SPE-149506-PP(2011).

[81] Tiab D. and Donaldson E.C., Petrophysics – Theory and Practice of Measuring Reservoir Rock and Fluid Transport Properties, 2nd Ed., Boston: Gulf Publishing Co. (2004).

[82] Ulasi, A.I, Onyekuru,S.O and Iwuagwu,C.J., Petrophysical evaluation of uzek well using well log and core data, Offshore Depobelt, Niger Delta, Nigeria Pelagia Research Library Vol.3 (5):2966-2991(2012).

[83] Van Golf-Racht, T.D., fundamentals of fractured reservoir, Engineering, Developments in Petroleum Science, 12, Elsevier, Amsterdam, 709p, (1982).

.

خلا صة

تم تقييم تكوين الجريبي (المايوسين الأوسط) مكمنيا في البئر Ja-49 و البئر Taza-2, الواقعتين ضمن حقلي جمبور و تازة على التوالي في كوردستان / شمال العراق. أعتمد في أنجاز الدراسة على الشرائح التى تم أحضارها من النماذج الصخرية (الفتات و اللباب) مع البيانات المسجلة بواسطة المجسات البئرية المختلفة سواء التقليدية منها أو الحديثة, بالأضافة الى النتائج المختبرية للفحوصات التي أجريت على النماذج الصخرية من اللباب.

تراوح سمك تكوين الجريبي بين ٥٥ مترا في بئر Ja-49 و ٤٤ مترا في بئر Taza-2 متكونا صخاريا من حجر الدولومايت بصورة رئيسية ومن الحجر الدولومايتى الجيرى بصورة ثانوية بالأضافة الى وجود أنطقة نحيفة من الصخور الأنهايدراتية. كما ان التكوين من الناحية السحنية يتشكل غالبا من الحجر الواكي و الحجر الطينى بالأضافة الى القليل من الحجر المرصوص و الحبيبي. أن معظم أجزاء التكوين أظهرت طبيعة سجيلية و ذلك بأحتوائها على نسبة لم تتجاوز غالبا٣٥% من السجيل المتناثر. المسامية المحتسبة لتكوين الجريبي في بئري الدراسة و بصورة عامة لم تتجاوز ١٥% بأستثناء بعض الأنطقة القليلة التي سجلت فيها مسامية تجاوزت ٢٠%. أن المسامات الثانوية الناتجة من الكسور الدقيقة او الفجوات المفتوحة قد شكلت بحدود ٢-٣% من المسامية الكلية للتكوين. النفاذية المحتسبة رياضيا للتكوين أعتمادا على طريقة التعدد الخطي التكراري و بأستخدام معطيات المجسات و نتائج الفحص المختبري قد أظهرت أن التكوين ذو نفاذية فقيرة الى معتدلة (أقل من ٢٠ ملليدارسي).

تم تقسيم التكوين الى ثلاث وحدات مكمنية أعتمادا على التباين في المحتوى السجيلي, المسامية, و النفاذية. و قد لوحظ بأن الوحدة المكمنية RU-C في الجزء العلوي من التكوين هي الوحدة الأكثر سمكا و ذي المواصفات المكمنية الأحسن من بين الوحدات الثلاث. بينت

الدراسة ان معظم أجزاء تكوين الجريبي يحتوى على الهايدروكاربونات و لكن بنسب تشبعية متباينة و بكفاءات حركية مختلفة. و قد لوحظ وجود بعض هذه الهايدروكاربونات في مسامات مجهرية دقيقة غير قابلة للأنتاج بالطرق التقليدية.

أن أختبار حجم الماء الكلي بينت بان انتاج الهايدروكاربونات من معظم أجزاء التكوين سوف يصاحبه نسب متفاوتة من الماء.

ان أحجام الأعناق بين المسامات في ترسبات الجريبى أظهرت قيمها العليا ضمن الوحدة المكمنية RU-C متراوحا بين ٠.٥ و ٢.٠ مايكرونا بينما أقل القيم تم أحتسابها ضمن الترسبات التابعة للوحدة المكمنية RU-B و التي تراوحت بين ٠.١ و ٠.٥ مايكرونا. كما أظهرت الدراسة أيضا ان جريان الموائع ضمن التكوين يتم من خلال المسامات المترابطة الموجودة في أرضية التكوين و كذلك الكسور الدقيقة و الفجوات المفتوحة .

اربع أنطقة جريان دالة ممثلة لأربع وحدات هايدرولوكية مختلفة تم تمييزها في تكوين الجريبي في هذة الدراسة معبرة عن قدرات حركية متباينة لسريان الموائع في التكوين.

أن حسابات نسب سمك المكمن الصافي الى الكلي , سمك العطاء الصافي الى الكلي, و سمك المنتج الصافي الى الكلي كانت ٦١%, ٢٢%, و ٠٩% في بئر **Ja-49** على التوالي, بينما كانت ٦٢%, ٢٢%, و ١٦.٦% في بئر**Taza-2** على التوالي أيضا.

دراسة الخواص المكمنية لتكوين الجريبي (مايوسين الأوسط) في آبار مختارة من كوردستان / شمال العراق

رسالة
مقدمة الى مجلس كلية العلوم
في جامعة السليمانية كجزء من متطلبات
نيل شهادة ماجستير في علوم
الجيولوجي
(جيولوجيا النفط)

من قبل

آسوس صديق عبدالله

بكلوريوس جيولوجي (٢٠٠٨)، جامعة السليمانية

باشراف

د. دلير حسين بابان

استاذ مساعد

جمادي الثاني ١٤٣٨ **مارس ٢٠١٧**

پوختە

لەم توێژینەوەیەدا کۆگای ماوەی مایۆسینی ناوەڕاست کە پێکهاتەی جیرێبی لەخۆی دەگرێ لە هەردوو بیری جەمبوری -٤٩ و تازە -٢ لە کێڵگەی جەمبورو تازە دا لەڕووی تایبەتمەندیەکانی کۆگای نەوتیەوە خوێندنەوەی بۆ کراوە.

جۆری داتای بەکارهاتوو بریتین لە نموونەی بەردی براو لە جۆری جیاوازی ئاسای و تۆماری هاوچەرخ وهەروەها نموونەی بەردی کرۆکیش. ئەستوری پێکهاتەی جیرێتی لە دەوروبەری ٥٥م لە جەمبور وە ٤٤م لە تازە . لەڕووی لیسۆلۆجی یەوە دەرکەوت کە پێکهاتەی جەمبور بە شێوەیەکی سەرەکی پێکهاتووە لە دۆلستۆن و کە لکاریەس دۆلستۆن وە بەڕێژەی دووەمی بریتین لە بەردە قسڵی لەگەڵ ئاسۆی باریك لە ئەنهایدرایت .

لەڕووی راسەکردنی مایکرۆنەیشسەوە جیرێتی بەرشێوەیەکی سەرەکی لە واکستۆن و مەدستۆن لەگەڵ بوونی ڕێژەیەکی کەم لە پاکستۆن و گرەین ستۆن .

بوونی سروشتی شەیل لە زۆربەی بەشی پێکهاتەی جیرێبی کە بەڕێژەی کەمتر ٣٥٪ لە جۆری شەیلێ پەرش و بلاّو پیشان دەدرێت .

بڕی کونیلەکان کەمتر ١٥٪ جگە لەچەند بەشێکی کەم کە بڕی کونیلەکان زیاترن ٢٠٪ کە ٣٪-٢ کونیلەکان دووەمین لەجۆری (ڤەگ و شکان یان درزن) .

بڕی دەلاّندن بۆ پێکهاتەی جیرێبی کە هەژمارکراوە بە بەکارهێنانی گونجاوترین هاوکێشەی multi linear regression بە بڕی (٢٠ میلی دراسی کە لە پۆلی زۆر لاواز بۆ ناوەند هەژمار دەکرێ . بەپشت بەستن بە هەریەك لە کونیلەو دەلاّندن و بڕی شەیلێ تەواوی ئەو بڕگانە لە چوار چێوەی توێژینەوەکەن و بۆ سێ یەکەی کۆگەی لە هەردوو بیری دراسەکراو، دابەشکراون.

لە کاتێکدا یەکەی کۆگەی –C - لە بەشی سەرەوەی پێکهاتەی جیرێبی بە ئەستورترین و باشترین تایبەتمەندی کۆگە لەنێو سێ پەکەکەدا هەژمار دەکرێت . پێکهاتەی جیرێتی بوونی هایدرۆکاربۆن نیشان دەدات لەگەڵ جیاوازی لە تێربوونی و توانای جولاّنەوەی دا . بەشێك لەیەکەی کۆگەی هایدرۆکاربۆن لەنێو کونیلەی زۆر بچوکن هەر لەبەر ئەمەیە کە بەرهەم هێنانیان پێویستی بە زیاتر ڕێگای ئاسای بەرهەمهێنان دەبێت . قەبارەی گشتی هەژمارکراوی ئاو ئەگەری بەرهەمهێنانی هایدرۆکاربۆن نیشان دەدات لەگەڵ بوونی قەبارەیەکی دیاری ئاو لە زۆربەی بەشەکانی پێکهاتەکەدا .

تیرەی گەرووی کونیلەکان لەسێدیمێنتی پێکهاتەی جیرێتی لەیەکەی کۆگای –C- بەرزە لەنێوان ڕێژەی (0.5-2mN مایکرۆمیترە) لە کاتێکدا لەیەکە کۆگەی –B- (مایکرۆمیترە 0.1-0.5) .

جولّەی شلە لەڕێگەی کونیلەی پێکەوە بەستراو لەناو ماتریکس دا یان لەڕێگەی درزی بچوکی کراوە یان لەڕێگەی ڤەگەوە نیشان دەدرێت . چواریەکەی هایدرۆلیکی لەمیانەی دیاریکردنی چوار ناوچەی جولّەی شلەکان لەپێکهاتەی جیرێبی دا ، هەژمارکراوە.بەهەژمارکردن بۆ پوختەی پێدان بۆ تەواوی بڕی پێدان و ڕێژەی بەرهەمهێنان ئەوە نیشان دەدات کەبیری جەمبوری – ٤٩ بە هەرسێ ڕێژەی ٩٪ ، ٢٢٪ ، ٦١٪ و هەروەها بیری تازە-٢- بەڕێژەی بەپێی ڕیزبەندی ٦٢٪ ، ٢٣.٥٪ ، ١٦.٦٪ .

تایبەتمەندییەکانی کۆگای نەوتی پێکهاتەکانی ماوەی مایوسینی ناوەراست جێرێبی لە بیرە نەوتەکانی کوردستان /باکوری عێراق

نامەیەکە
پێشکەشکراوە بە ئە نجومەنی کۆلێجی
زانست لە زانکۆی سلێمانی وەك بەشێك لە پێداویستیەکانی
بە دە ستهێنانی بروانامەی ماستەر
لە زانستی جیۆلۆجی
(جیۆلۆجی نەوت)

لەلایەن

ئاسۆس صدیق عبدالله

بە کالوریۆس لە جیۆلۆجی (٢٠٠٨)،زانکۆی سلێمانی

بە سەر پە رشتی

د.دلێر حسین بابان

پرۆفیسۆری یاریدەدەر

ڕە شەمێ ٢٧١٦ **مارس ٢٠١٧**